

We are committed to providing [accessible customer service](#).

If you need accessible formats or communications supports, please [contact us](#).

Nous tenons à améliorer [l'accessibilité des services à la clientèle](#).

Si vous avez besoin de formats accessibles ou d'aide à la communication, veuillez [nous contacter](#).

ASSESSMENT REPORT

on the

WESTERN BEAR PROPERTY

Birch-Uchi Subprovince

Red Lake Mining Division

RED LAKE, ONTARIO

NTS 52L 09 NAD 83 Zone 15N E406700 N5636400

Lat. 50° 52' 18.27" Long. -94° 19' 33.63"

for

TRILLIUM GOLD MINES INC.

2.12.21



T.N.J. Hughes, P. Geo

Contents

SUMMARY	i
1.0 INTRODUCTION	1
2.0 PROPERTY DETAILS.....	2
2.1 Location & Access	2
2.2 Topography & Vegetation.....	3
2.3 Claim Status.....	4
3.0 HISTORY.....	11
3.1 Government & Institutional.....	11
3.2 Industry Exploration.....	12
4.0 REGIONAL GEOLOGY	13
4.1 Regional Quaternary Geology.....	24
5.0 PROPERTY GEOLOGY	27
6.0 DEPOSIT TYPES	30
7.0 RESULTS.....	35
8.0 CONCLUSIONS	44
9.0 RECOMMENDATIONS.....	45
10.0 REFERENCES	47
11.0 STATEMENT OF QUALIFICATIONS.....	51

APPENDIX

Western Bear Airborne Geophysical Survey Logistics Report as a separate file
Sydney Lake –(Western Bear)-(Leo) geophysics report as a separate file

Table of Figures

Figure 1 Regional Location map	2
Figure 2 Western Bear DTM	3
Figure 3 Land tenure.....	9
Figure 4 Claim map with flight lines	10
Figure 5 Generalized tectonic map of the western Uchi Subprovince	13
Figure 6 Schematic map, Western Superior Province.....	14
Figure 7 Major tectonic assemblages	15
Figure 8 Geology of the centre-west Uchi Subprovince	16
Figure 9 Regional residual magnetic intensity data	17
Figure 10 Regional Geology 2.....	21
Figure 11 Regional Geology 3.....	22
Figure 12 Quaternary Geology.....	24
Figure 13 Western Bear Property Geology.....	28
Figure 14 Plan View – Western Bear survey block.....	35
Figure 15 Regional and TGM residual magnetic data	36
Figure 16 Regional residual magnetic data and TMI vertical gradient data	37
Figure 17 Regional residual magnetic data with TGM RTP data	38
Figure 18 Interpretation I.....	39
Figure 19 Interpretation II.....	40
Figure 20 Diagramme of a simple shear	41
Figure 21 PGW recommended primary and secondary targets	43

List of Tables

Table 1 Claims.....	4
---------------------	---

SUMMARY

The Western Bear project, located approximately 37 km west south-west of the town of Red Lake, Northern Ontario is the focus of a multi-disciplinary project targeting precious and base metals within western Uchi subprovince.

The property is underlain by several Neoproterozoic to Late Archean intrusions and intrusive gneiss complexes, the Atikaki Batholith, Onnie-Detour stock and the Sydney Lake – Rainfall Lake Dome, a large regional gneiss and intrusive complex. Geophysical and limited outcrop data indicate the presence of thin, modified, relict mafic to ultramafic supracrustal sequences and a single mafic to ultramafic metamorphosed Late Archean intrusion.

On the 12th October, 2020, Precision GeoSurveys Inc. of Langley, B.C. flew a high resolution helicopter-borne aeromagnetic survey for Trillium Gold Mines Inc. over the contiguous 105 claim Western Bear block..

The survey was flown at 100 metre line spacing at a heading of 090°/270°; tie lines were flown at 1000 metre spacing at a heading of 000°/180°. A total of 237.4 line km was flown, over an of 21.6 km².

Results outline an approximately one 1km x 1 km intrusion underlying the epicentre of the property, adjacent to a major north-south deformation zone, tentatively defined as a sinistral ductile shear. The intrusion may lie within a rhomb graben feature formed contemporaneously with the ductile shear. Greenstone terrane is identified as a south-east extension to that around Telescope Lake to the north-west, plus a number of partially preserved bodies within the Sydney Lake – Rainfall Lake dome and the Atikaki batholith.

A separate report on the results of the survey is provided as an appendix – auth. E. Mueller-Markham, Vice-President and Senior Consulting Geologist for Paterson, Grant and Watson Ltd. The report provides a comprehensive, detailed analysis of the survey and results, with interpretation and recommendations for further work.

The property has received no known systematic work. Recommended is property-wide mapping, focussing on structural and metamorphic geology, and alteration assemblages, with grid geochemical sampling employing lithogeochemical and soil or humus sampling. For the mafic-ultramafic unit, every effort should be made to obtain a representative suite for lithogeochemical analysis. There should be focus on target areas recommended by Mueller-Markham and Hughes in their respective reports.

The co-ordinate system used in the report is UTM, NAD 83 Zone 15N. All units in this report are metric unless otherwise stated.

1.0 INTRODUCTION

This report covers an examination of an October 2020 high resolution airborne magnetic survey over the Western Bear property, Red Lake region, northwest Ontario, a review of the regional geology and geophysics, the exploration history, and property geology.

Based on these studies and assessments, a number of areas on the property were identified as favourable for ground follow-up.

Recommendations are made, with a budget provided.

2.0 PROPERTY DETAILS

2.1 Location & Access

The Property is located approximately 37 km west south-west of Red Lake, and 76 km west north-west of Ear Falls, north-west Ontario, within the Telescope Lake and Leano Lake map areas, Red Lake Mining Division, (Fig. 1), and with property epicentre at UTM Zone 15N NAD83 co-ordinates E406700 N5636400. Claims are located on the old map sheet G-1807, Leano Lake.

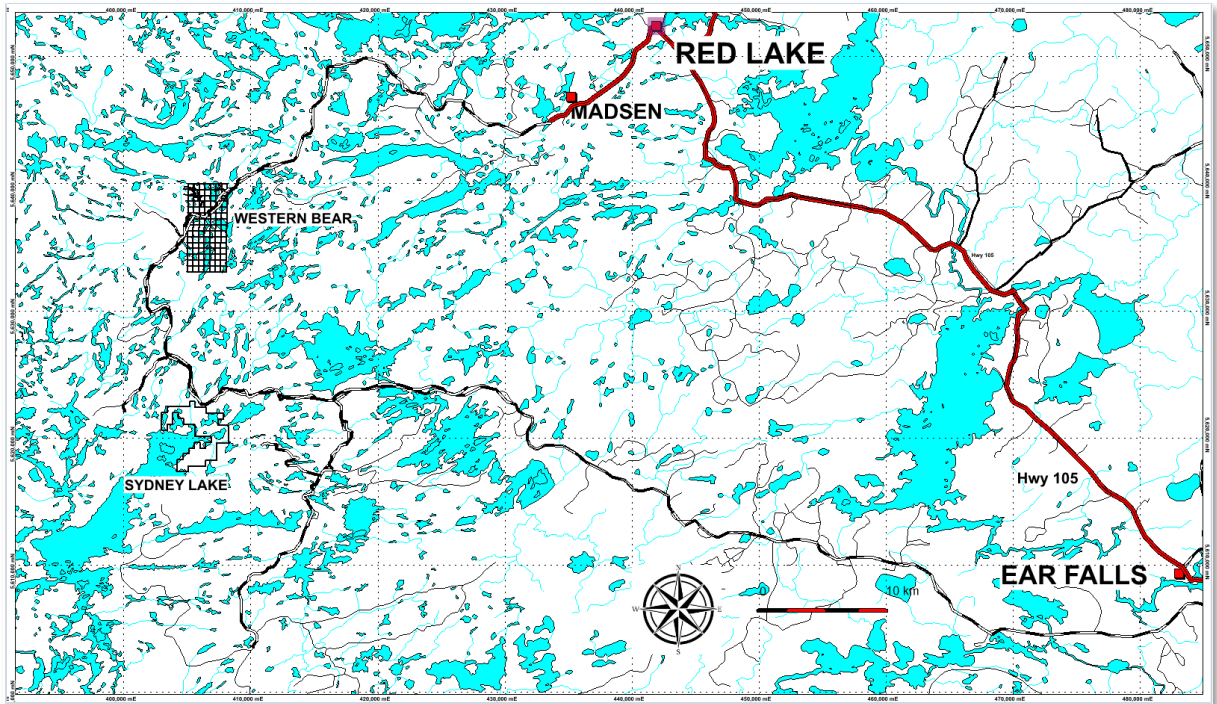


Figure 1 Regional Location map

Access

South from Red Lake, along Hwy. 618, past Madsen, then taking the Suffel lake and Iriam lake roads west, south and south-west, a distance of approximately 48 km. Iriam lake road passes through the north and north-centre of the property.

Alternatively, west from Ear Falls on Hwy. 804, past Manitou Falls along the Longlegged Lake road, past English River road, west and north along Irian lake road, reaching the west boundary of the property, a distance of some 120 km.

2.2 Topography & Vegetation

The property is located in boreal forest, with significant modification by fires and in the north of the property, clear-cutting. Today, it's largely covered by second growth poplar, pine, alders and spruce. The physiography is uneven, with elevations from 400 m. asl to 430 m on some partly exposed ridges. A large fire burnt much of the region in the late 70's. The 2021 fire did not affect the property, this based on a government map showing the extent of the regional fire.

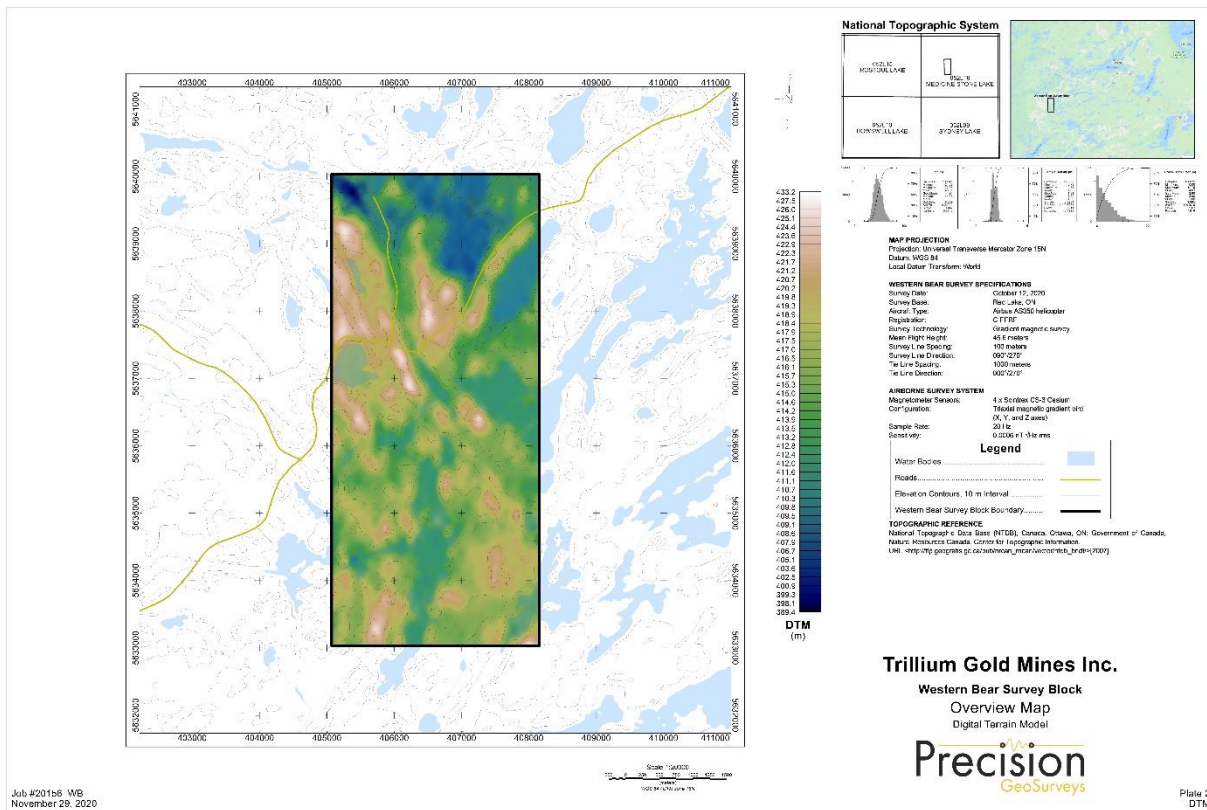


Figure 2 Western Bear DTM

2.3 Claim Status

The Western Bear property consists of 105 contiguous single-cell mining claims covering an area of 2141.16 ha. The claim numbers are shown in Figure 2 and listed in Table 1. All claims that were flown. Below, **Table 1 Western Bear claims**

Tenure Number	Township / Area	Holder	No of cells	Area_Ha
560628	TELESCOPE LAKE AREA	(100) Canadian Shield Developments Corp.	1	20.379
560629	TELESCOPE LAKE AREA	(100) Canadian Shield Developments Corp.	1	20.379
560630	TELESCOPE LAKE AREA	(100) Canadian Shield Developments Corp.	1	20.379
560631	TELESCOPE LAKE AREA	(100) Canadian Shield Developments Corp.	1	20.379
560632	TELESCOPE LAKE AREA	(100) Canadian Shield Developments Corp.	1	20.379
560633	TELESCOPE LAKE AREA	(100) Canadian Shield Developments Corp.	1	20.379
560634	TELESCOPE LAKE AREA	(100) Canadian Shield Developments Corp.	1	20.379
560635	TELESCOPE LAKE AREA	(100) Canadian Shield Developments Corp.	1	20.381
560636	TELESCOPE LAKE AREA	(100) Canadian Shield Developments Corp.	1	20.381
560637	TELESCOPE LAKE AREA	(100) Canadian Shield Developments Corp.	1	20.381
560638	TELESCOPE LAKE AREA	(100) Canadian Shield Developments Corp.	1	20.381
560639	TELESCOPE LAKE AREA	(100) Canadian Shield Developments Corp.	1	20.381
560640	TELESCOPE LAKE AREA	(100) Canadian Shield Developments Corp.	1	20.381
560641	TELESCOPE LAKE AREA	(100) Canadian Shield Developments Corp.	1	20.381
560642	TELESCOPE LAKE AREA	(100) Canadian Shield Developments Corp.	1	20.383
560643	TELESCOPE LAKE AREA	(100) Canadian Shield Developments Corp.	1	20.383
560644	TELESCOPE LAKE AREA	(100) Canadian Shield Developments Corp.	1	20.383
560645	TELESCOPE LAKE AREA	(100) Canadian Shield Developments Corp.	1	20.383
560646	TELESCOPE LAKE AREA	(100) Canadian Shield Developments Corp.	1	20.383

560647	TELESCOPE LAKE AREA	(100) Canadian Shield Developments Corp.	1	20.383
560648	TELESCOPE LAKE AREA	(100) Canadian Shield Developments Corp.	1	20.383
560649	TELESCOPE LAKE AREA	(100) Canadian Shield Developments Corp.	1	20.385
560650	TELESCOPE LAKE AREA	(100) Canadian Shield Developments Corp.	1	20.385
560651	TELESCOPE LAKE AREA	(100) Canadian Shield Developments Corp.	1	20.385
560652	TELESCOPE LAKE AREA	(100) Canadian Shield Developments Corp.	1	20.385
560653	TELESCOPE LAKE AREA	(100) Canadian Shield Developments Corp.	1	20.385
560654	TELESCOPE LAKE AREA	(100) Canadian Shield Developments Corp.	1	20.385
560655	TELESCOPE LAKE AREA	(100) Canadian Shield Developments Corp.	1	20.385
560656	TELESCOPE LAKE AREA	(100) Canadian Shield Developments Corp.	1	20.387
560657	TELESCOPE LAKE AREA	(100) Canadian Shield Developments Corp.	1	20.387
560658	TELESCOPE LAKE AREA	(100) Canadian Shield Developments Corp.	1	20.387
560659	TELESCOPE LAKE AREA	(100) Canadian Shield Developments Corp.	1	20.387
560660	TELESCOPE LAKE AREA	(100) Canadian Shield Developments Corp.	1	20.387
560661	TELESCOPE LAKE AREA	(100) Canadian Shield Developments Corp.	1	20.387
560662	TELESCOPE LAKE AREA	(100) Canadian Shield Developments Corp.	1	20.387
560663	TELESCOPE LAKE AREA	(100) Canadian Shield Developments Corp.	1	20.388
560664	TELESCOPE LAKE AREA	(100) Canadian Shield Developments Corp.	1	20.388
560665	TELESCOPE LAKE AREA	(100) Canadian Shield Developments Corp.	1	20.388
560666	TELESCOPE LAKE AREA	(100) Canadian Shield Developments Corp.	1	20.388
560667	TELESCOPE LAKE AREA	(100) Canadian Shield Developments Corp.	1	20.388
560668	TELESCOPE LAKE AREA	(100) Canadian Shield Developments Corp.	1	20.388
560669	TELESCOPE LAKE AREA	(100) Canadian Shield Developments Corp.	1	20.388
560670	TELESCOPE LAKE AREA	(100) Canadian Shield Developments Corp.	1	20.39

560671	TELESCOPE LAKE AREA	(100) Canadian Shield Developments Corp.	1	20.39
560672	TELESCOPE LAKE AREA	(100) Canadian Shield Developments Corp.	1	20.39
560673	TELESCOPE LAKE AREA	(100) Canadian Shield Developments Corp.	1	20.39
560674	TELESCOPE LAKE AREA	(100) Canadian Shield Developments Corp.	1	20.39
560675	TELESCOPE LAKE AREA	(100) Canadian Shield Developments Corp.	1	20.39
560676	TELESCOPE LAKE AREA	(100) Canadian Shield Developments Corp.	1	20.39
560677	LEANO LAKE AREA, TELESCOPE LAKE AREA	(100) Canadian Shield Developments Corp.	1	20.392
560678	LEANO LAKE AREA, TELESCOPE LAKE AREA	(100) Canadian Shield Developments Corp.	1	20.392
560679	LEANO LAKE AREA, TELESCOPE LAKE AREA	(100) Canadian Shield Developments Corp.	1	20.392
560680	LEANO LAKE AREA, TELESCOPE LAKE AREA	(100) Canadian Shield Developments Corp.	1	20.392
560681	LEANO LAKE AREA, TELESCOPE LAKE AREA	(100) Canadian Shield Developments Corp.	1	20.392
560682	LEANO LAKE AREA, TELESCOPE LAKE AREA	(100) Canadian Shield Developments Corp.	1	20.392
560683	LEANO LAKE AREA, TELESCOPE LAKE AREA	(100) Canadian Shield Developments Corp.	1	20.392
560684	LEANO LAKE AREA	(100) Canadian Shield Developments Corp.	1	20.394
560685	LEANO LAKE AREA	(100) Canadian Shield Developments Corp.	1	20.394
560686	LEANO LAKE AREA	(100) Canadian Shield Developments Corp.	1	20.394
560687	LEANO LAKE AREA	(100) Canadian Shield Developments Corp.	1	20.394
560688	LEANO LAKE AREA	(100) Canadian Shield Developments Corp.	1	20.394
560689	LEANO LAKE AREA	(100) Canadian Shield Developments Corp.	1	20.394
560690	LEANO LAKE AREA	(100) Canadian Shield Developments Corp.	1	20.394

560691	LEANO LAKE AREA	(100) Canadian Shield Developments Corp.	1	20.396
560692	LEANO LAKE AREA	(100) Canadian Shield Developments Corp.	1	20.396
560693	LEANO LAKE AREA	(100) Canadian Shield Developments Corp.	1	20.396
560694	LEANO LAKE AREA	(100) Canadian Shield Developments Corp.	1	20.396
560695	LEANO LAKE AREA	(100) Canadian Shield Developments Corp.	1	20.396
560696	LEANO LAKE AREA	(100) Canadian Shield Developments Corp.	1	20.396
560697	LEANO LAKE AREA	(100) Canadian Shield Developments Corp.	1	20.396
560698	LEANO LAKE AREA	(100) Canadian Shield Developments Corp.	1	20.397
560699	LEANO LAKE AREA	(100) Canadian Shield Developments Corp.	1	20.397
560700	LEANO LAKE AREA	(100) Canadian Shield Developments Corp.	1	20.397
560701	LEANO LAKE AREA	(100) Canadian Shield Developments Corp.	1	20.397
560702	LEANO LAKE AREA	(100) Canadian Shield Developments Corp.	1	20.397
560703	LEANO LAKE AREA	(100) Canadian Shield Developments Corp.	1	20.397
560704	LEANO LAKE AREA	(100) Canadian Shield Developments Corp.	1	20.397
560705	LEANO LAKE AREA	(100) Canadian Shield Developments Corp.	1	20.399
560706	LEANO LAKE AREA	(100) Canadian Shield Developments Corp.	1	20.399
560707	LEANO LAKE AREA	(100) Canadian Shield Developments Corp.	1	20.399
560708	LEANO LAKE AREA	(100) Canadian Shield Developments Corp.	1	20.399
560709	LEANO LAKE AREA	(100) Canadian Shield Developments Corp.	1	20.399
560710	LEANO LAKE AREA	(100) Canadian Shield Developments Corp.	1	20.399
560711	LEANO LAKE AREA	(100) Canadian Shield Developments Corp.	1	20.399
560712	LEANO LAKE AREA	(100) Canadian Shield Developments Corp.	1	20.401
560713	LEANO LAKE AREA	(100) Canadian Shield Developments Corp.	1	20.401
560714	LEANO LAKE AREA	(100) Canadian Shield Developments Corp.	1	20.401

560715	LEANO LAKE AREA	(100) Canadian Shield Developments Corp.	1	20.401
560716	LEANO LAKE AREA	(100) Canadian Shield Developments Corp.	1	20.401
560717	LEANO LAKE AREA	(100) Canadian Shield Developments Corp.	1	20.401
560718	LEANO LAKE AREA	(100) Canadian Shield Developments Corp.	1	20.401
560719	LEANO LAKE AREA	(100) Canadian Shield Developments Corp.	1	20.403
560720	LEANO LAKE AREA	(100) Canadian Shield Developments Corp.	1	20.403
560721	LEANO LAKE AREA	(100) Canadian Shield Developments Corp.	1	20.403
560722	LEANO LAKE AREA	(100) Canadian Shield Developments Corp.	1	20.403
560723	LEANO LAKE AREA	(100) Canadian Shield Developments Corp.	1	20.403
560724	LEANO LAKE AREA	(100) Canadian Shield Developments Corp.	1	20.403
560725	LEANO LAKE AREA	(100) Canadian Shield Developments Corp.	1	20.403
560726	LEANO LAKE AREA	(100) Canadian Shield Developments Corp.	1	20.405
560727	LEANO LAKE AREA	(100) Canadian Shield Developments Corp.	1	20.405
560728	LEANO LAKE AREA	(100) Canadian Shield Developments Corp.	1	20.405
560729	LEANO LAKE AREA	(100) Canadian Shield Developments Corp.	1	20.405
560730	LEANO LAKE AREA	(100) Canadian Shield Developments Corp.	1	20.405
560731	LEANO LAKE AREA	(100) Canadian Shield Developments Corp.	1	20.405
560732	LEANO LAKE AREA	(100) Canadian Shield Developments Corp.	1	20.405
			Total Area	2141.16

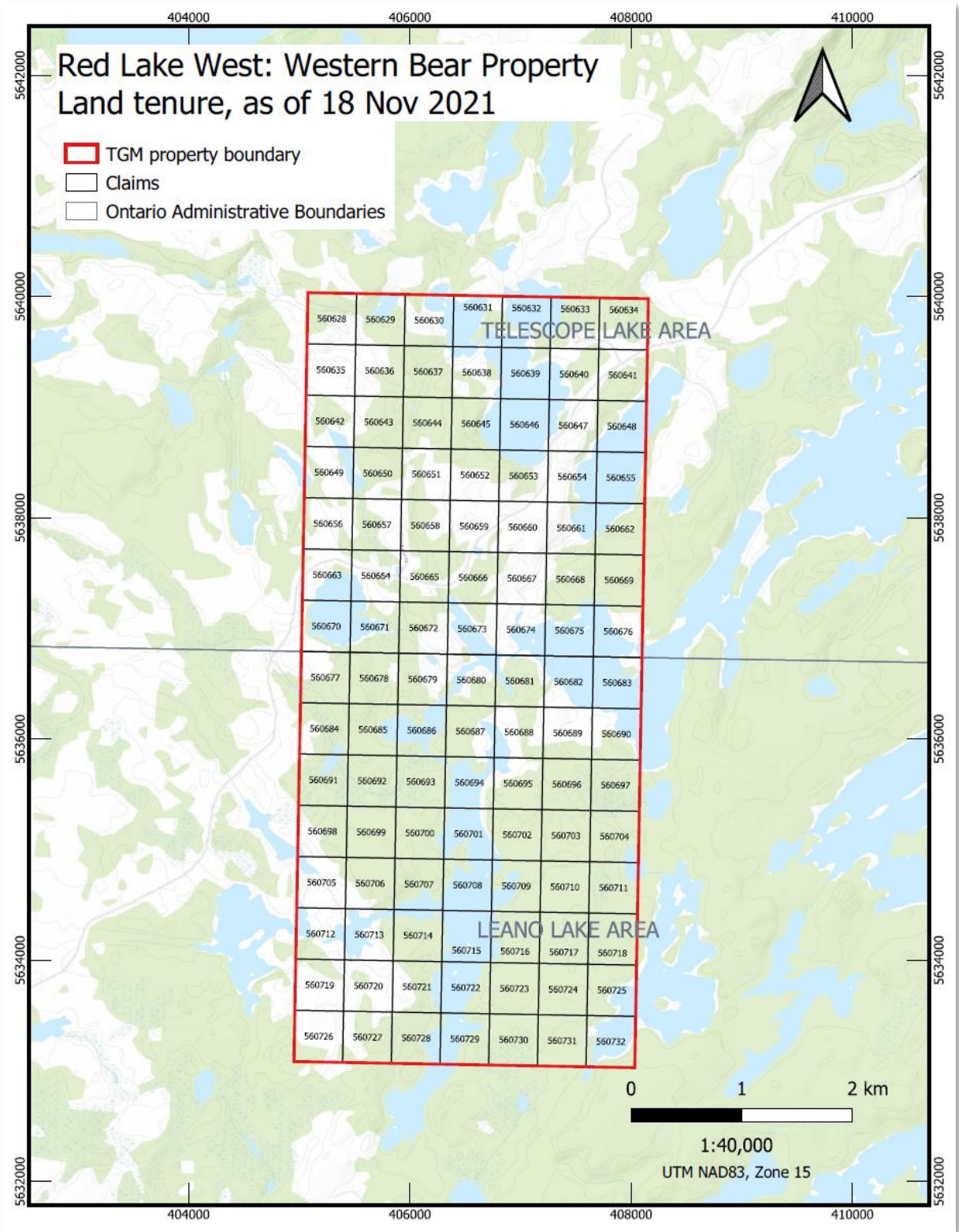


Figure 3 Land tenure

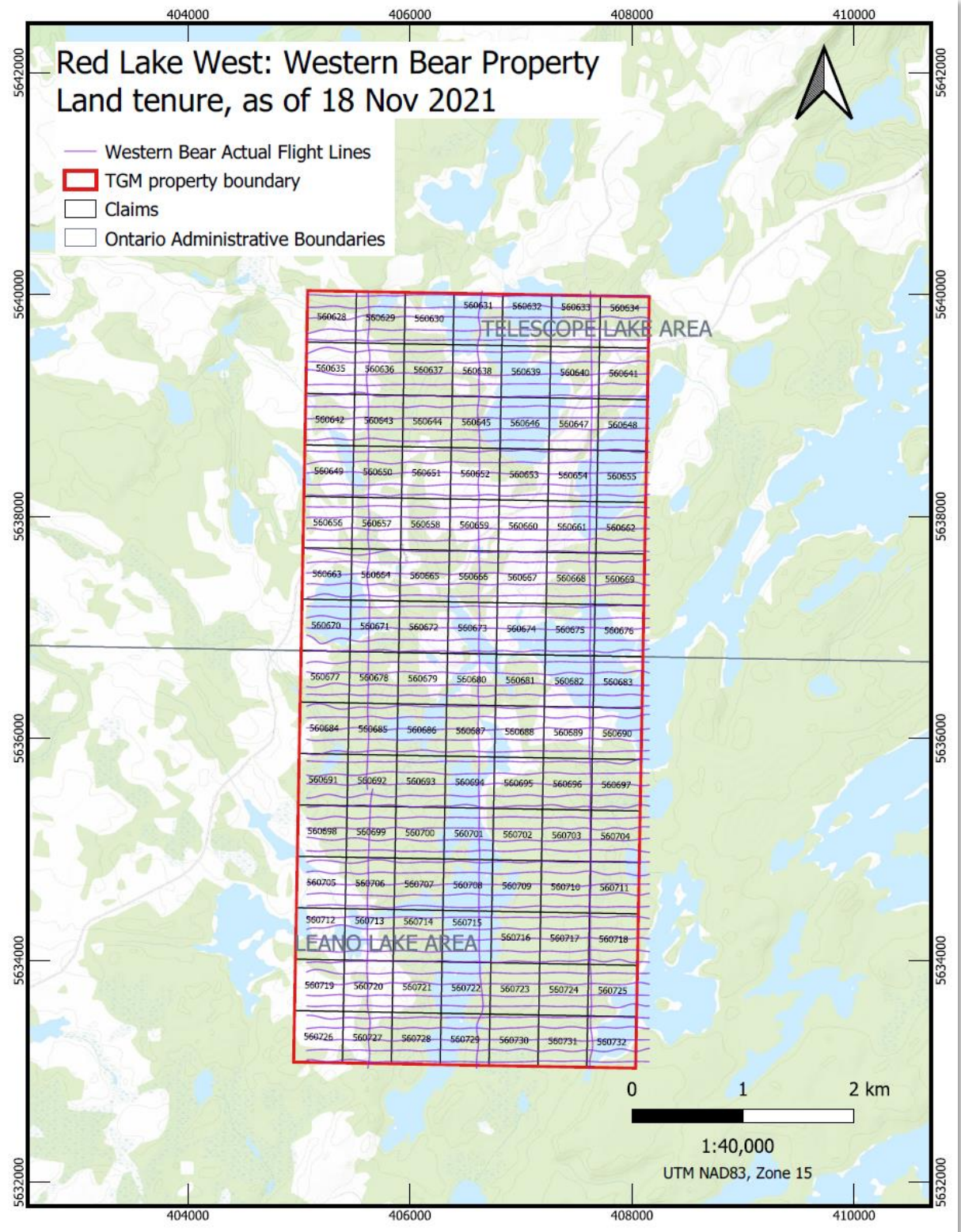


Figure 4 Claim map with flight lines

3.0 HISTORY

3.1 Government & Institutional

The earliest survey in the map area was performed by Robert Bell of the Geological Survey of Canada in his canoe journey on the English River and Albany River systems (Bell 1873). A second expedition by Bell (1886) traversed the English River Subprovince, between Lonely Lake (now Lac Seul) and Lake St. Joseph via the Root River. Fawcett (1885) conducted a line survey using transit and micrometre from Rat Portage (Kenora) to Osnaburgh House, returning via the Wenasaga River.

In 1921, G. Gilbert carried out shoreline and waterway mapping over a large areas south- west of Western Bear, over to the Manitoba boundary, including traverses in what is now the Bee Lake greenstone belt. Only Algoman?-type granite and granite gneiss was mapped in the Sydney Lake area. (Map 36f publication).

As part of the Operation Kenora-Sydney Lake project, Breaks et al. (1974) conducted region mapping that included the Sydney Lake area, recording unmetamorphosed late tectonic to post tectonic felsic to intermediate intrusive rocks, metamorphosed early tectonic to syntectonic plutonic felsic to intermediate intrusive rocks ranging from foliated biotite trondhjemite, foliated biotite granodiorite with gneissic equivalents; metatexite and amphibolite gneiss; unsubdivided and amphibolitised mafic metavolcanic rocks.

Their work divided the region into two halves separated by the Sydney Lake Cataclastic Zone, which defines the boundary between the English River subprovince and the Uchi subprovince.

Preliminary Map P.950, Bulging-Embryo Lakes area (Breaks et al., 1974), covers the property, though specific outcrops are few, with much of the terrane 'mapped' as areas of continuous outcrop.

In 1990, the Northern Ontario Engineering Geology Terrain Study published the Sydney Lake sheet. The work was largely a desk-top study augmented by, in some areas, actual groundwork.

1993 saw the publication of Map.3091, English River subprovince. The publication sourced work from various OGS preliminary and past compilation maps.

Seismic signatures have been studied by Hall and Hajnal (1969), Hall (1971) and Brown (1968).

Much of the body of earlier geological studies work was conducted by Breaks and Beakhouse as principal authors, with additional work by Harris, Corfu, Cruden, and Stott. See, Breaks et al., (1976, 1978), Breaks, (1991), Breaks and Bond, (1993).

In 1999, Map P.3397, Precambrian geology, Medicine Stone Lake area was published, (Atkinson, 1999). This was essentially a desk study and update of previous regional work, published as several ODM preliminary maps.

Percival, J.A. et al., 2000 published an extensive study of the western Superior province, covering NW Ontario and eastern Manitoba. See also, Sanborn-Barrie et al., 2000, and Sanborn-Barrie et al., 2001 for additional information.

The GSC OF4256-2004/P3469 publication is a compilation of regional mapping for Red Lake and the Confederation greenstone belts, and provides references for work therein. The western portion of the map covers the Western Bear property. (Sanborne-Barrie et al., 2004)

3.2 Industry Exploration

A check of the Ontario Assessment file database indicated no records of work that cover this property.

4.0 REGIONAL GEOLOGY

The property lies within the centre-west portion of the Uchi subprovince, north-western Ontario.

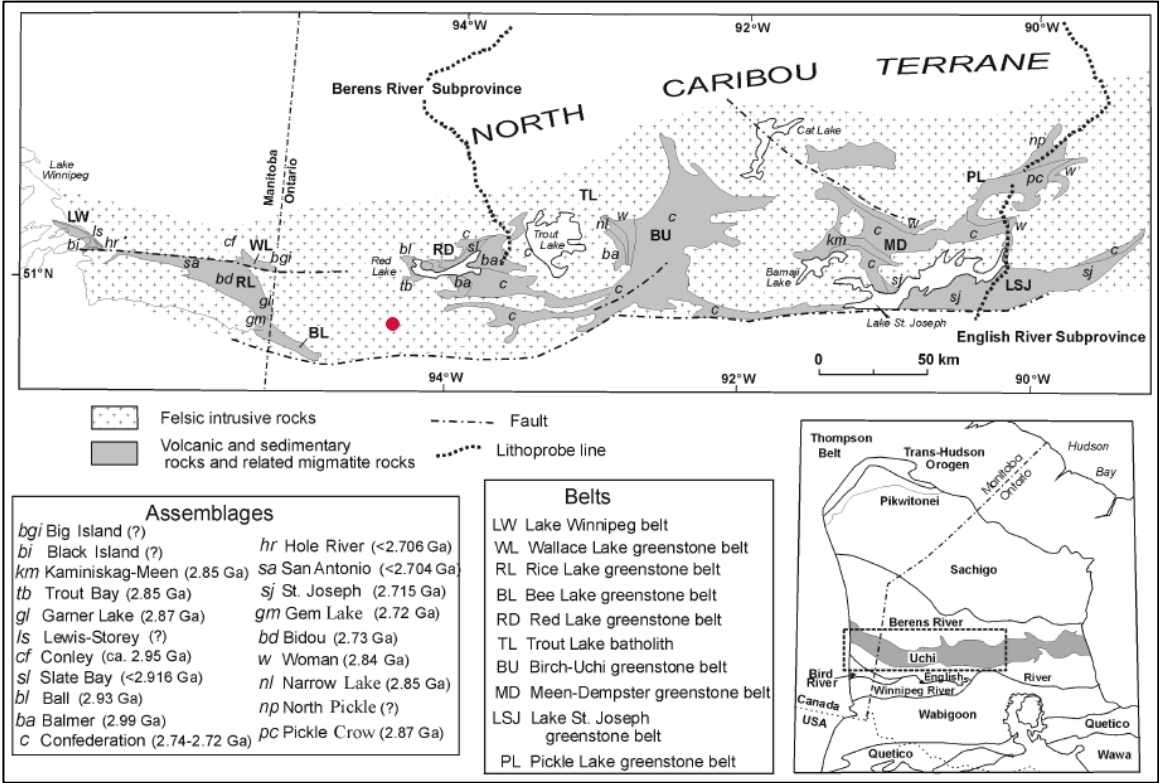


Figure 5 Generalized tectonic map of the western Uchi Subprovince

From Percival et al., 2000. The red dot covers approximate location of the property

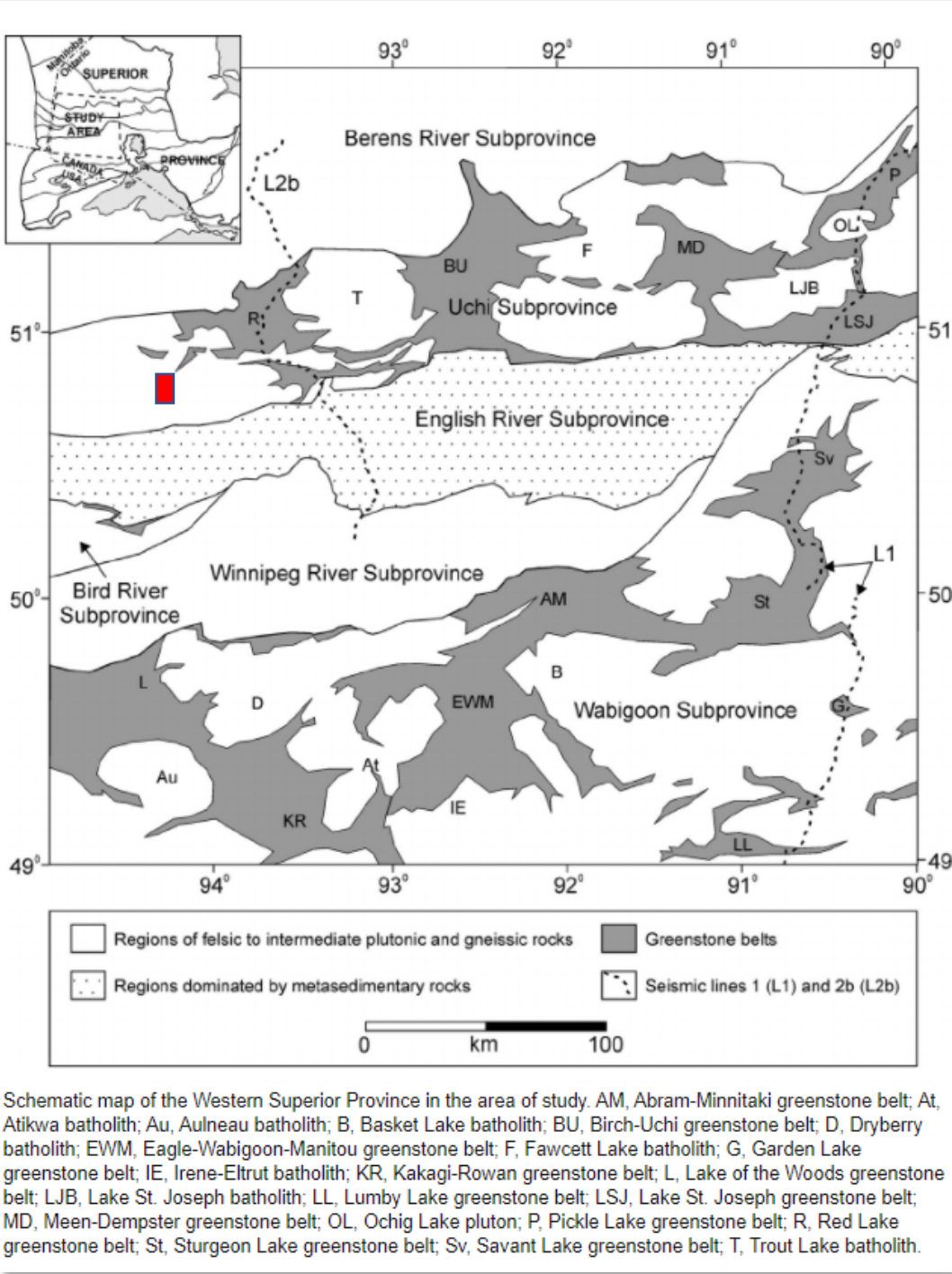


Figure 6 Schematic map, Western Superior Province

From Hradi & Cruden, 2006. The red rectangle covers the approximate location of the property.

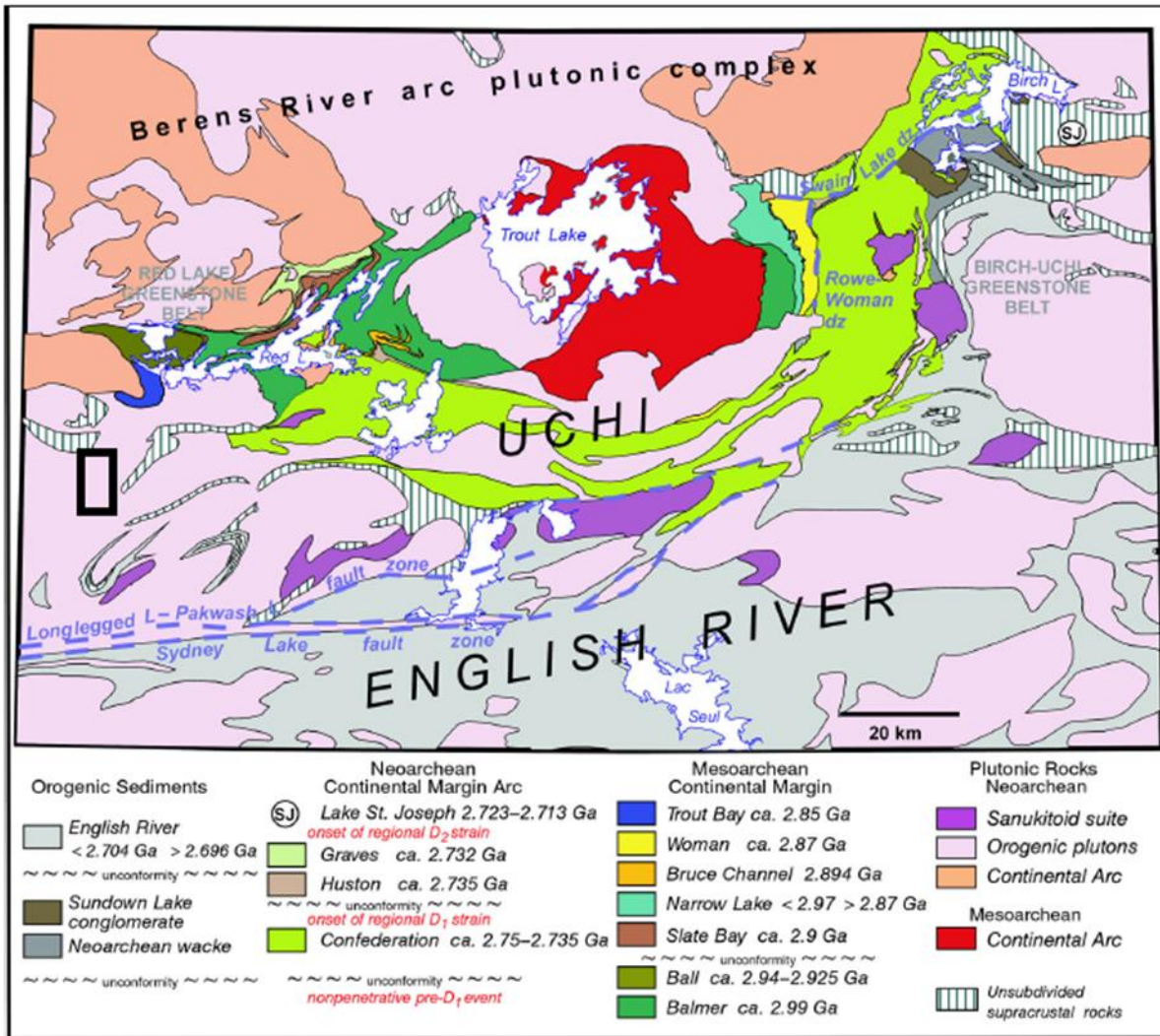


Figure 2. Major tectonostratigraphic assemblages and tectonic affinities assigned to volcanic, sedimentary and plutonic rocks of the eastern Uchi Subprovince and adjacent English River Subprovince (dz = deformation zone).

Figure 7 Major tectonic assemblages

From P3460, Sanborn-Barrie et al., 2004. Property area outlined in black

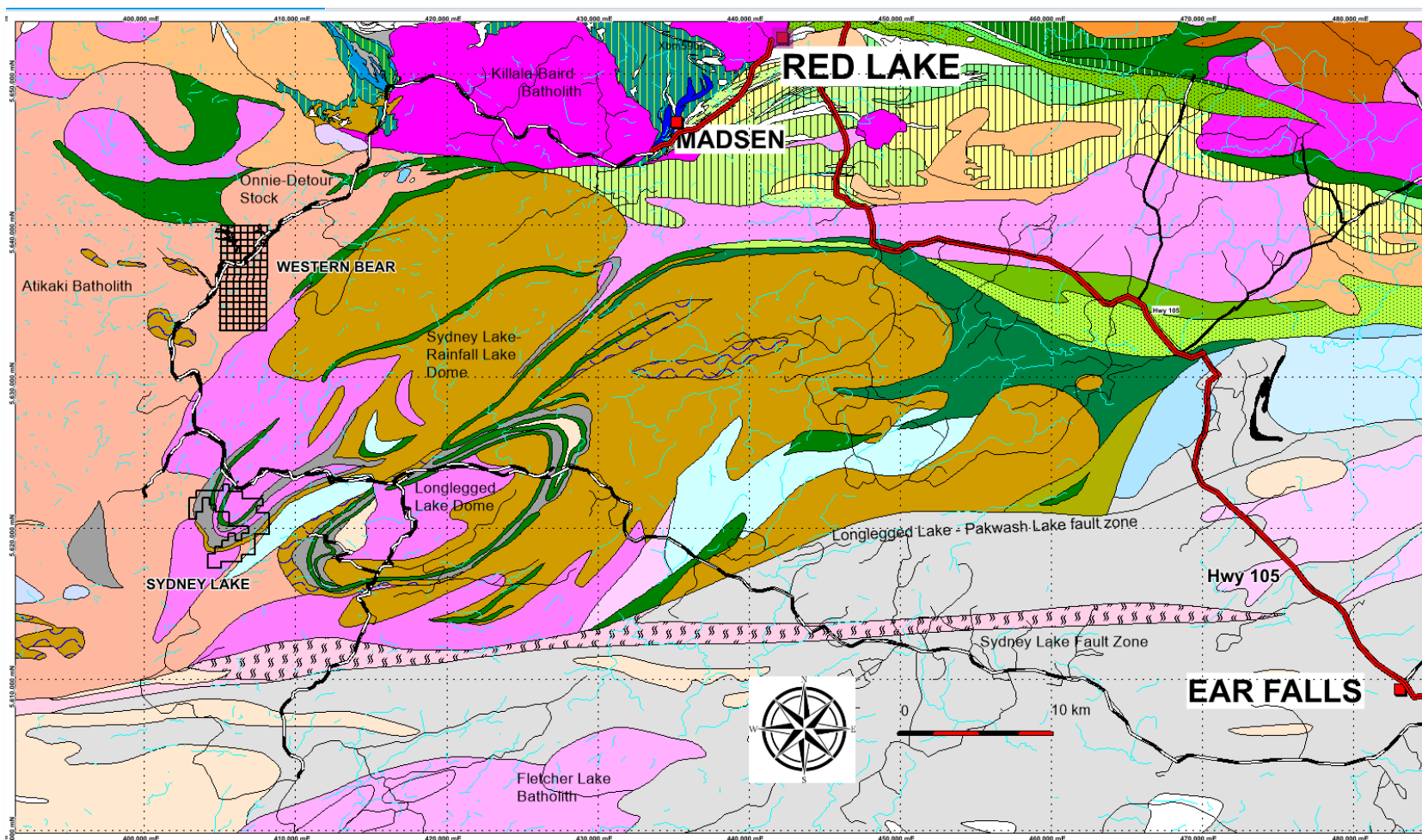


Figure 8 Geology of the centre-west Uchi Subprovince

Western Bear and Sydney Lake properties shown. Legend is provided below. For the complete regional legend, refer to GSC OF4256 2004

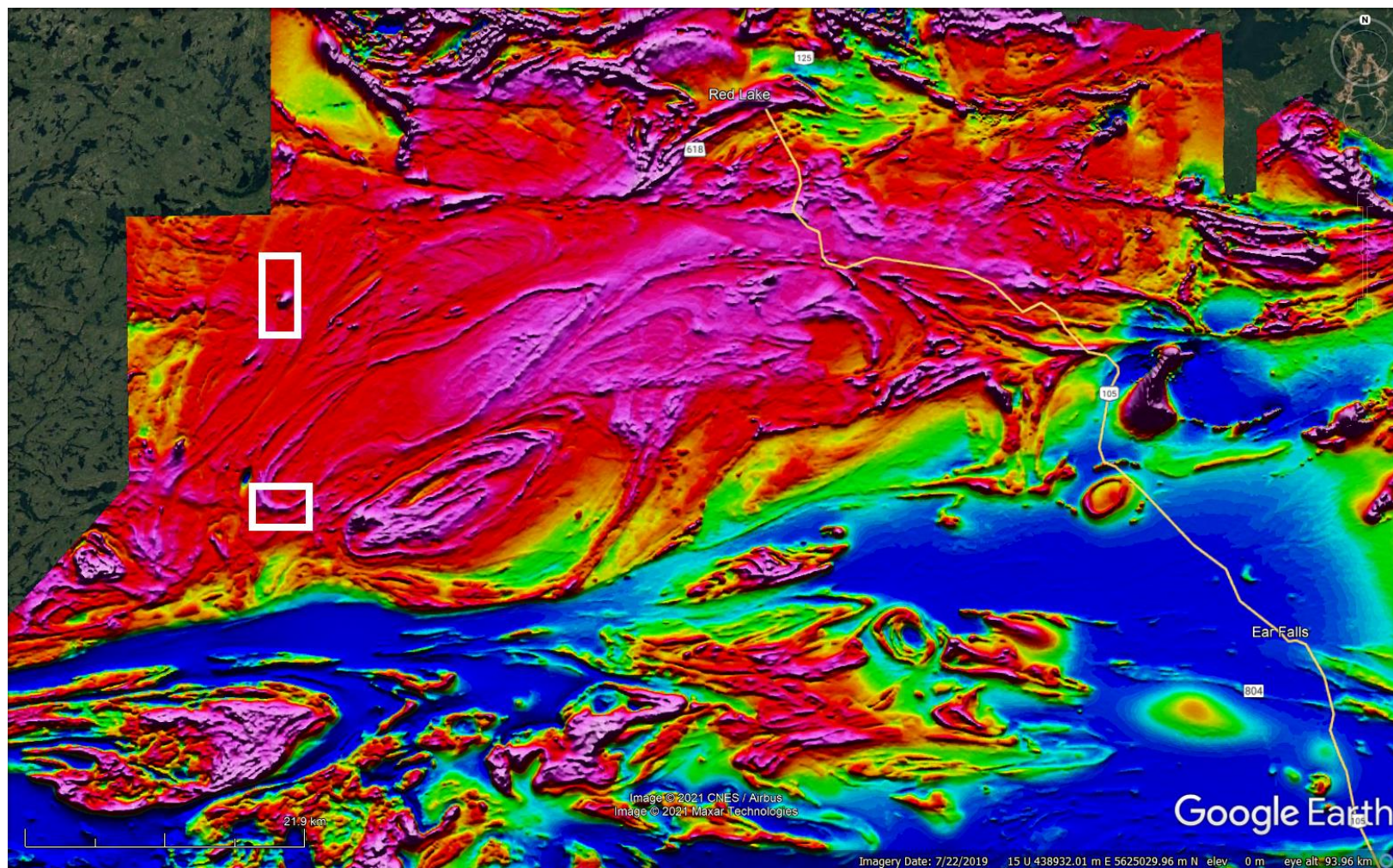


Figure 9 Regional residual magnetic intensity data

North rectangle, Western Bear property, south rectangle covers Sydney Lake property

The property area is dominated by the Mesoarchean to Neoproterozoic Atikaki Batholith, a biotite±hornblende bearing often massive tonalite to granodiorite intrusion which may contain mafic inclusions and xenoliths, and/or pegmatite. Supracrustal mafic gneiss and amphibolite is exposed as infolded, large-scale layering representing relict greenstone, in this instance, deformed extensions to supracrustal belts at Telescope, Embryo, Medicine Stone, Longlegged and Dedee lakes. The region is 'dotted' with relatively small mafic to ultramafic intrusive bodies that range from diorite and gabbro to amphibolite, hornblende and pyroxenite. Several are metamorphosed and/or differentiated phenomena.

Within are smaller, often elliptic in plan bodies of tonalite to granodiorite gneiss, containing anywhere from 5% to >15% mafic minerals, observed as inclusions, xenoliths, layering and/or folding. These may also contain mafic gneiss.

Intruded into these are Neoproterozoic biotite granodiorite and granite stocks and plugs

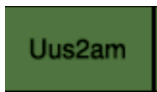
Legend and map from GSC of 4256 2004/P.3460

Only lithologies on or near the properties are displayed.

Supracrustal rocks of unknown affinity



Uus2wk **Wacke:** wacke, feldspathic wacke; near north-western Shabu Lake occurs with lesser quartzite and quartzose wacke; locally cut by gabbro; quartzose wacke may be interbedded with conglomerate, marble, calc-silicate rocks and chert-magnetite formation; occurs as narrow screens with migmatite texture locally, in structural domes at Longlegged and Sydney lakes.



Uus 2am **Amphibolite**



Uus2mv **Mafic –(UM) volcanic rocks:** foliated, massive to pillowed basalt, amphibolite, and associated gabbroic rocks, locally plagioclase-phyric near Springpole and Pakwash lakes; lesser associated intermediate to felsic flows, tuff and wacke near Dixie Lake.

Heyson Sequence, Red Lake c. 2739 Ma



Zcf74it **Intermediate Volcanic rocks:** massive and pyroclastic rocks of tholeiitic affinity, generally dacitic to andesitic flows, tuff, lapilli tuff and pyroclastic tuff; flows may be pillowed and plagioclase-phyric; commonly cut by quartz-porphyrus near Madsen

Neoarchæan (2800 – 2500 Ma)

- Gsk11dl** **Diorite, quartz diorite:** hornblende and biotite-hornblende diorite, syenodiorite+/-diorite with inclusions of English River metasedimentary rocks locally (i.e. Pakwash pluton) and mafic volcanic rocks (i.e. eastern Bruce Lake pluton)
- Gbe6gd** Gbe6gd **unsubdivided Quartz monzonite** to granodiorite; variably foliated biotite quartz monzonite, granodiorite and granite; locally leucocratic and quartz and/or K-feldspar porphyritic; xenolithic south of Gullrock Lake
- Gbe6gr** Gbr6gr **Neoarchæan (2800 – 2500 Ma) unsubdivided Granite, granodiorite:** massive to weakly foliated, lineated, fine- to coarse-grained, monzogranite±quartz monzodiorite±tonalite and associated pegmatitic rocks, locally K-feldspar porphyritic.
- Kbe6tn** Kbe6tn **Neoarchean Tonalite to granodiorite:** variably foliated biotite-tonalite to quartz diorite+/-granodiorite; coarse-grained, granular, white to grey with 10-30% hornblende+/-biotite
- Gbe11tn** Gbe11tn **Neoarchean Tonalite, granodiorite:** massive to variably foliated biotite+/-hornblende tonalite to granodiorite, commonly xenolithic or containing biotite schlieren; locally leucocratic (trondhjemite (CI<5); intrusive into English River metasedimentary assemblage (i.e. < 2.7 Ga); with associated diorite and quartz diorite phases (Bluffy Lake batholith); cataclastic within the Sydney Lake fault zone.
- Tbe12tn** Tbe12tn **Neoarchean Tonalite:** massive to weakly foliated biotite-tonalite to trondhjemite±diorite typically associated with, or intrusive into, <2,745 Ga Confederation assemblage
- Migmatite ca. 2690 Ma**
- Gms65gr** **Peraluminous granite to granodiorite:** homogeneous diatexite with >= 95% medium-grained to pegmatitic granitoid mobilizate, typically garnet and muscovite bearing; locally apatite and tourmaline bearing (i.e. south of Jubilee Lake); commonly contains inclusions and rafts of inhomogeneous diatexite; cataclastic within the Sydney Lake fault zone
- Gms65gg** **Inhomogeneous diatexite** with 70-95% medium-grained to pegmatitic granitoid mobilizate, typically garnet and muscovite bearing; commonly contains inclusions and rafts of metatexite; cataclastic within the Sydney Lake fault zone

English River assemblage >2696 Ma <2704 Ma

Feg6sm

Feg6sm Metasedimentary migmatite: garnet-biotite-feldspar-quartz gneiss, generally metatexite with 10-70% interbanded granitoid mobilizate.

Ube2tn

Ube2tn Archæan (4000-2500 Ma) Unsubdivided Tonalite to granodiorite: medium-grained, variably foliated biotite-hornblende-biotite tonalite and associated rocks; cataclastic adjacent to Longlegged Lake - Pakwash Lake fault Zone.

Ugc2tg

Ube2tg Tonalite gneiss of unknown age and affinity

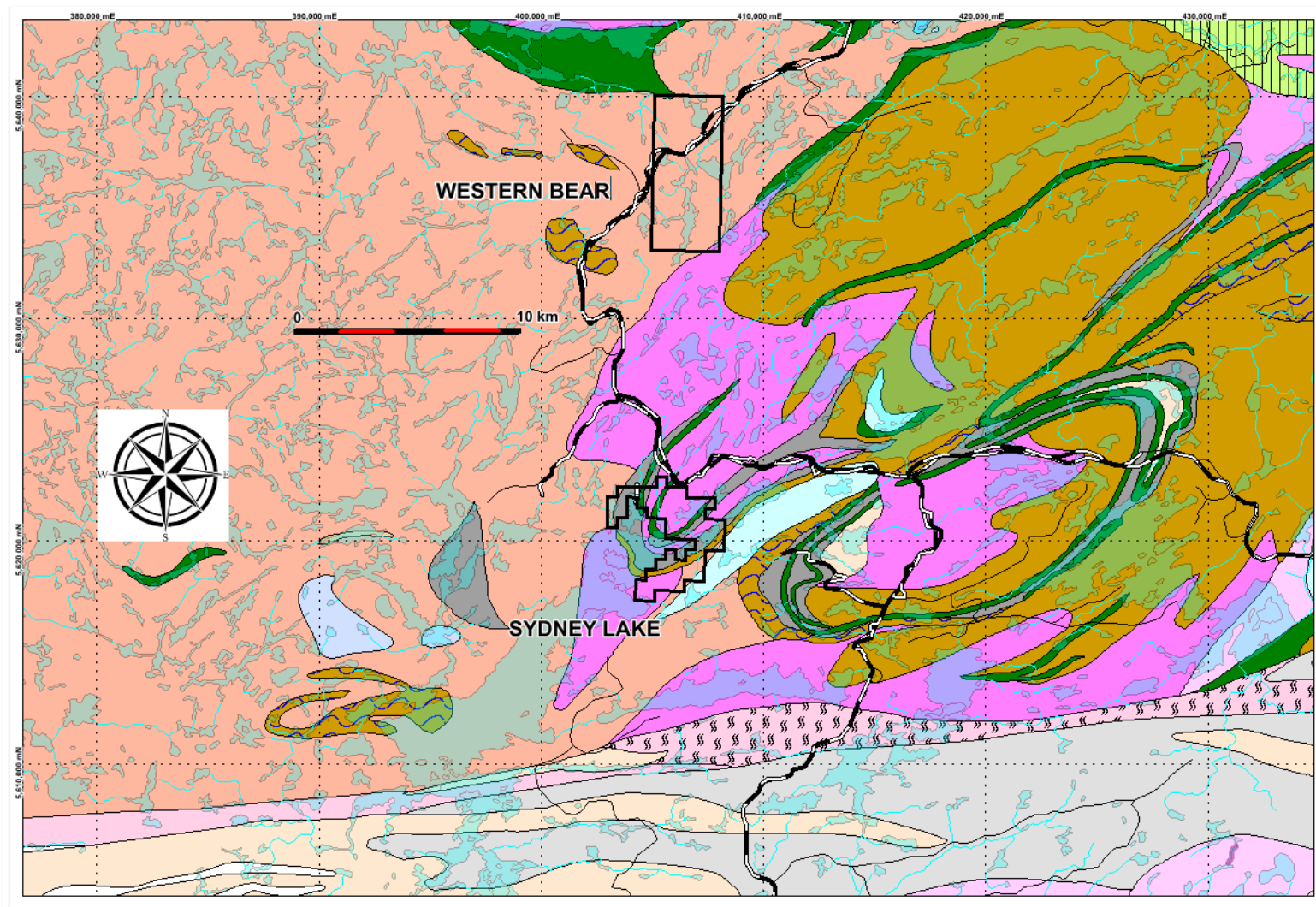


Figure 10 Regional Geology 2

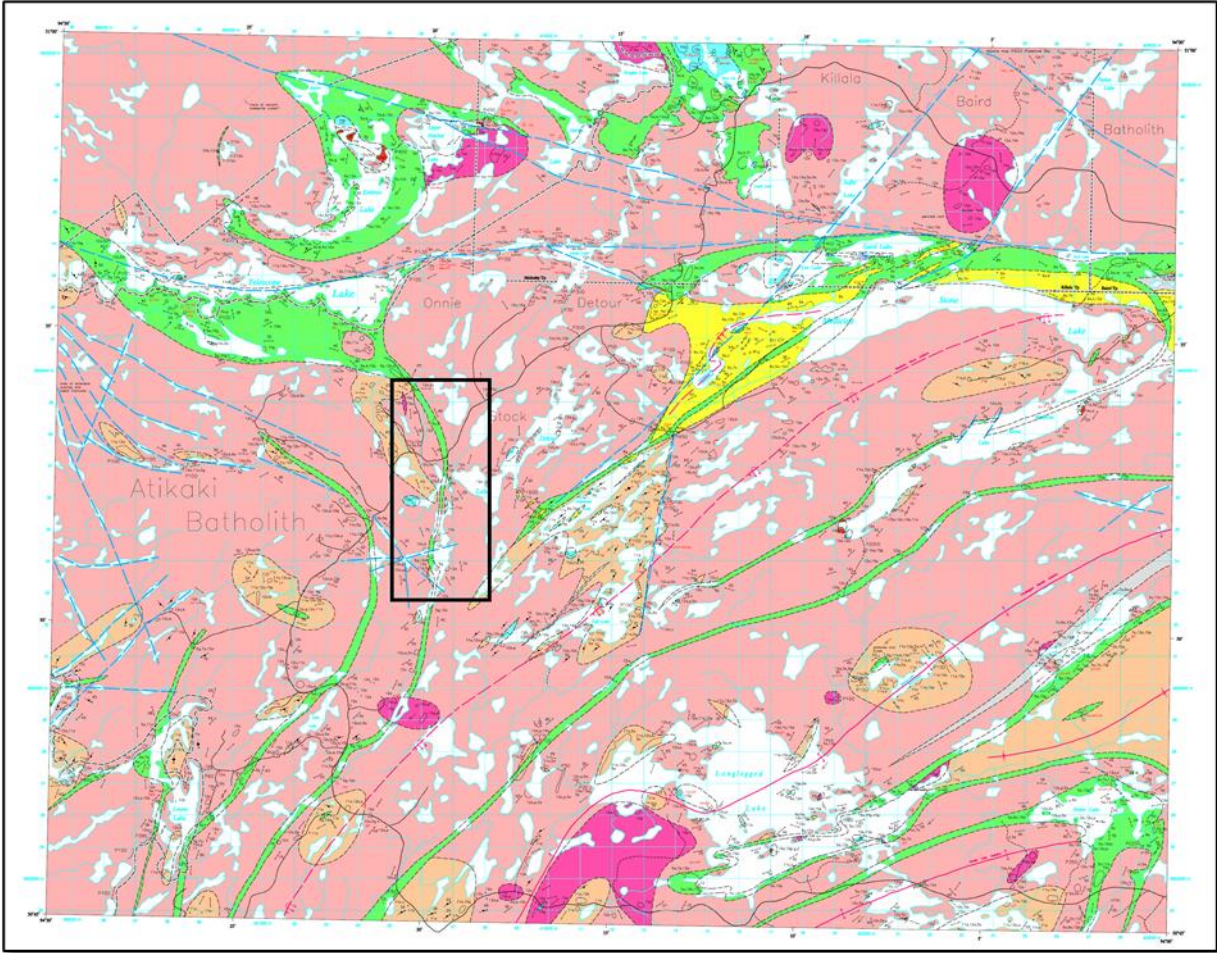


Figure 11 Regional Geology 3

Map P.3397, Medicine Stone area geology Legend overleaf

PRECAMBRIAN

NEOARCHEAN

INTRUSIVE CONTACT

Granitic Suite

- 15** **Biotite Granodiorite to Granite**
- 15a Unsubdivided; pink to grey, inequigranular, <15% biotite
- 15p Pegmatitic

INTRUSIVE CONTACT

Sanukitoid Suite

- 14** **Mafic to Intermediate Intrusive Rocks**
- 14a Diorite, quartz diorite, tonalite; dark grey, variable % pyroxene, hornblende and biotite
- 14b Lamprophyre dikes; dark grey to black
- 14f Amphibolite; black, coarse grained, feather texture biotite phenocrysts
- 14s Hornblende syenite; pink to black, coarse grained, variable % mafic minerals

INTRUSIVE CONTACT

MESOARCHEAN TO NEOARCHEAN

Tonalitic Suite

- 12** **Tonalite to Granodiorite**
- 12a Biotite-bearing; grey-white to pink, fine to coarse grained, 5 to 15% mafic minerals
- 12b Biotite ± hornblende-bearing; grey to white, medium to coarse grained, > 10% mafic minerals
- 12m Mafic Inclusions
- 12p Pegmatitic
- 12q Quartz phenocrysts
- 12z Xenolithic

INTRUSIVE CONTACT

Gneissic Suite[®]

11 Tonalite to Granodiorite Gneiss

- 11a Felsic to intermediate; grey to white, <15% mafic minerals, short discontinuous layers, folded
- 11b Mafic; grey to dark grey, >15% mafic minerals, typically has mafic inclusions and/or pronounced continuous layers, folded

Mafic Suite

10 Mafic to Ultramafic Intrusive Rocks

- 10a Amphibolite; black, fine to medium grained, foliated, occurs as inclusions or dikes
- 10d Leucogabbro
- 10g Gabbro, diorite
- 10h Hornblende; black, very coarse grained, massive
- 10p Metapyroxenite, metaperidotite; very coarse grained, massive

INTRUSIVE CONTACT

7 Metasedimentary Rocks

- 7a Unsubdivided (mainly wacke)
- 7c Calc-silicate skarn
- 7f Iron formation, ferruginous chert

6 Felsic to Intermediate Metavolcanic Rocks

- 6a Unsubdivided
- 6b Breccia, tuff breccia
- 6f Flow
- 6g Gneissic
- 6t Tuff, lapilli tuff, lapillistone

5 Mafic Metavolcanic Rocks

- 5a Unsubdivided
- 5b Pillowed flow
- 5g Gneissic
- 5m Migmatite

4 Ultramafic Metavolcanic Rocks

- 4a Unsubdivided
- 4k Komatiite

4.1 Regional Quaternary Geology

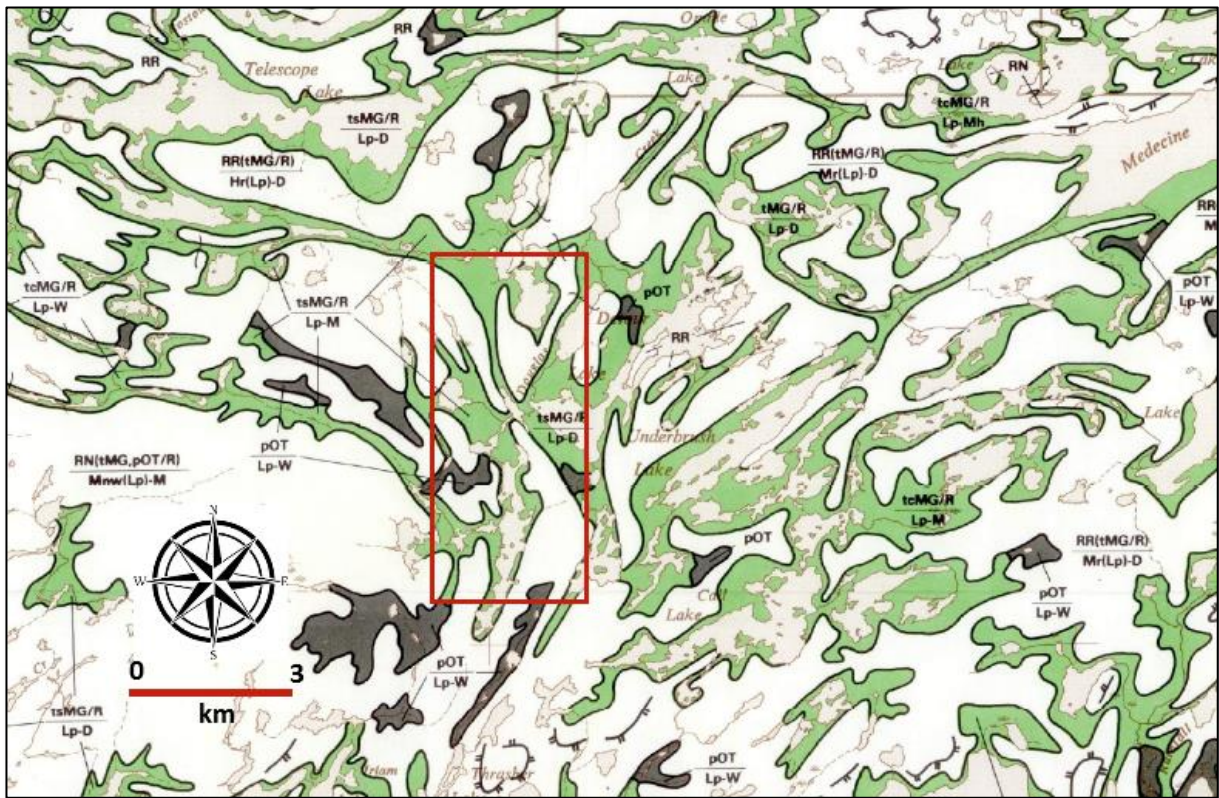


Figure 12 Quaternary Geology

From NOEGTS M5105, Sydney Lake sheet. Property boundary outlined

The property is covered with two landform-topographic types, ground moraine with moderate relief, knobby exposed ridges and minor lowland plain (green); and ground moraine and sand, with minor, moderate relief and moderate to wet drainage (white).

The main glacial direction appears to be south-west, though few maps or reports deal with this area.


LEGEND

LANDFORM


MORAINAL

	ME <i>End moraine</i>
	MG <i>Ground moraine</i>
	MH <i>Hummocky moraine</i>

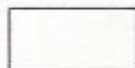
GLACIOFLUVIAL

	GD <i>Ice contact delta, esker delta, kame delta, delta moraine</i>
	GE <i>Esker, esker complex, crevasse filling</i>
	GK <i>Kame, kame field, kame terrace, kame moraine</i>
	GO <i>Outwash plain, valley train</i>

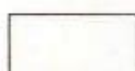
GLACIOLACUSTRINE

	LB <i>Raised (abandoned) beach form</i>
	LD <i>Glaciolacustrine delta</i>
	LP <i>Glaciolacustrine plain</i>

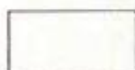
ALLUVIAL

	AP <i>Alluvial plain</i>
---	---------------------------------


COLLUVIAL

	CS <i>Slope failure</i>
	CT <i>Talus pile</i>
	CW <i>Slopewash and debris creep sheet; minor talus</i>

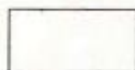
EOLIAN

	ED <i>Sand dunes</i>
---	-----------------------------

ORGANIC

	OT <i>Organic terrain</i>
---	----------------------------------

BEDROCK

	RL <i>Bedrock plateau</i>
	RN <i>Bedrock knob</i>
	RP <i>Bedrock plain</i>
	RR <i>Bedrock ridge</i>
	IR <i>Bedrock below a drift veneer</i>

MATERIAL

b	<i>boulders, bouldery</i>
c	<i>clay, clayey</i>
g	<i>gravel, gravelly</i>
p	<i>peat, muck</i>
r	<i>rubble</i>
s	<i>sand, sandy</i>
m	<i>silt, silty</i>
t	<i>till</i>

TOPOGRAPHY

LOCAL RELIEF

H	<i>Mainly high local relief</i>
M	<i>Mainly moderate local relief</i>
L	<i>Mainly low local relief</i>

VARIETY

c	<i>channelled</i>
d	<i>dissected, gullied</i>
j	<i>jagged, rugged, cliffed</i>
j*	<i>cliffed volcanic rock signature</i>
k	<i>kettled, pitted</i>
n	<i>knobby, hummocky</i>
p	<i>plain</i>
r	<i>ridged</i>
s	<i>sloping</i>
t	<i>terraced</i>
u	<i>undulating to rolling</i>
w	<i>washed, reworked</i>

DRAINAGE

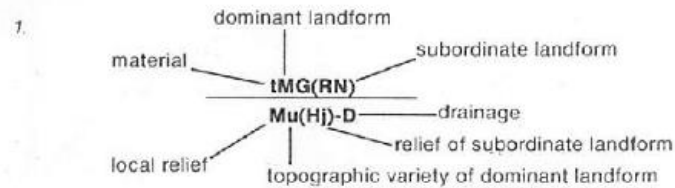
SURFACE CONDITION

W	<i>Wet</i>
D	<i>Dry</i>
M	<i>Mixed wet and dry</i>
h	<i>Suspected high water table</i>







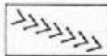
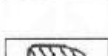
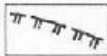
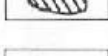



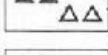

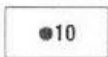
The letter codes describing the terrain units are made up of four components arranged as follows:—

MATERIAL	LANDFORM
TOPOGRAPHY	DRAINAGE

Examples:



SYMBOLS

	Significant end moraine or linear moraine-like feature		Small landslide scar
	Well expressed drumlins and drumlinoid ridges		Sand or gravel pit
	All other linear ice-flow features		Quarry or mine workings evident from airphotos or field observation (crossed picks are shown in the area of open excavation)
	Esker ridge (continuous, discontinuous; the symbol does not indicate direction of flow)		Other man-made features (rock dumps, tailings, lagoons, landfills, etc.: type of feature mentioned where identifiable)
	Abandoned shoreline (continuous, discontinuous)		Steep-walled valleys, often bed-rock-controlled features
	Local dune area (type and location of individual dunes not indicated)		Talus (defined, inferred; base of talus triangle indicates down-slope side of escarpment)
	Abandoned river channel, spillway, or ice marginal channels		Line joining the same terrain units
	Escarpment		
	Sample location		

5.0 PROPERTY GEOLOGY

There is no known industry reconnaissance or systematic mapping, sampling, ground geophysics or drilling on the property, and local geological information is almost wholly reliant on the regional data.

Government and academic work is preliminary or reconnaissance in nature, instance GSC OF4256 (above), indicating 90% plus of the property is underlain by the Neoproterozoic syntectonic granodioritic to tonalite Onnie-Detour Stock (east half) and the tonalitic to granodioritic Atikaki Batholith, (west half). The south-eastern corner may be underlain by a small portion of Neoproterozoic unfoliated massive to foliated, to porphyritic granite-granodiorite with minor pegmatite, and the north-west corner underlain by unfoliated mafic volcanic rocks that form part of the Telescope Lake greenstone terrane.

A little more data is provided overleaf, from Map P.3397, Medicine Stone Lake area geology. Based on data from the Precision airborne survey there is a considerable error in the grid displayed in the preliminary map. As such, the geology below has been distorted to match as close as possible the respective topographies with the geology tied to the Precision DTM map's UTM grid.

A thin band of north-south trending mafic volcanic rocks appears to demarcate the boundary between the Atikaki Batholith and a Onnie-Detour Stock complex in the east.

The primary target on the property is shown as '10p', coarse-grained metapyroxenite to metaperidotite. A single outcrop in the centre is probably located at its western margin (see 'Results').

Lithology legend provided with fig. 11, above.

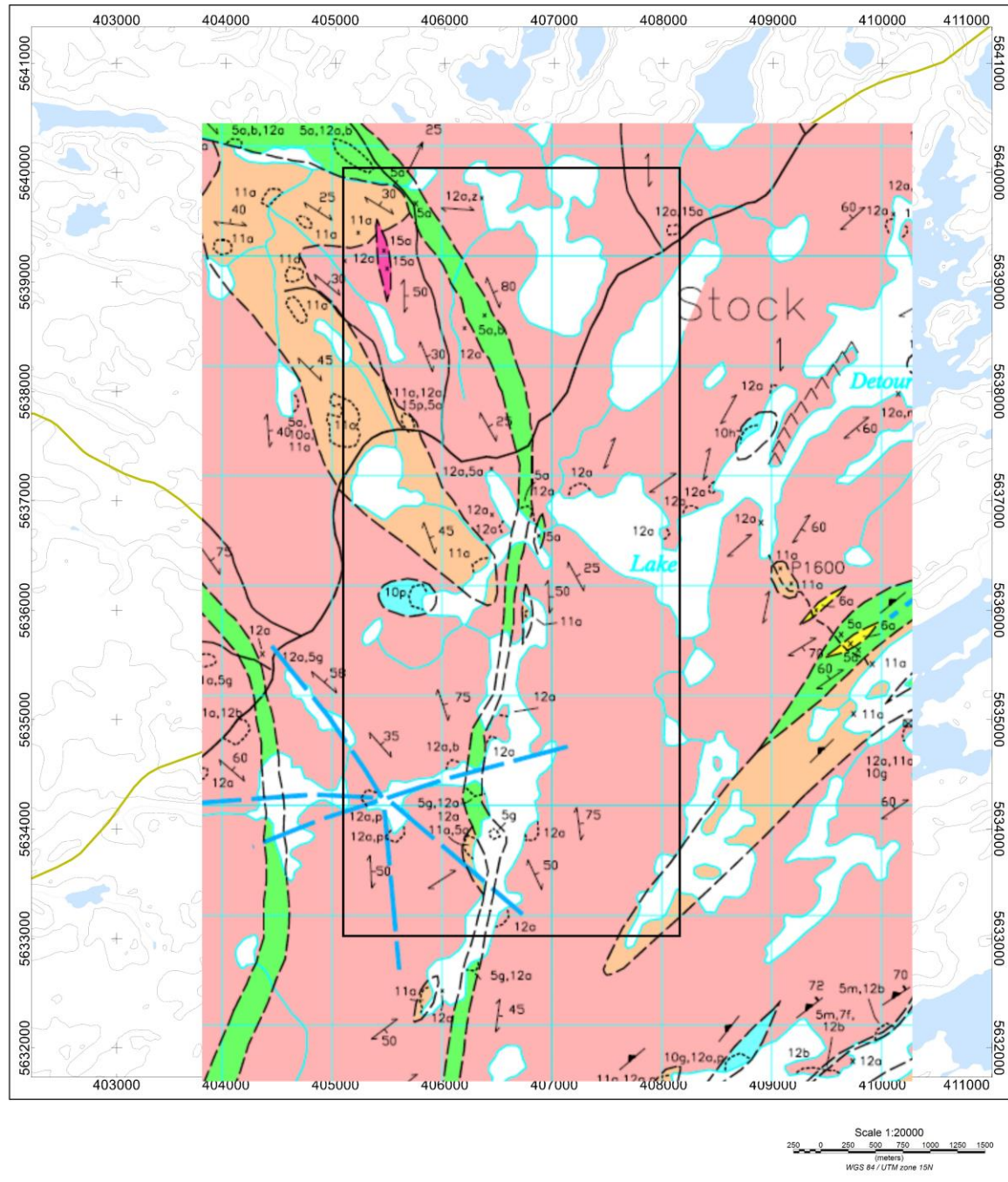


Figure 13 Western Bear Property Geology

From OGS Preliminary Map P.3397

The provincial lake sediment sampling database yielded several areas of interest on and adjacent to the property. A very brief assessment of what may be anomalous metals is shown below.

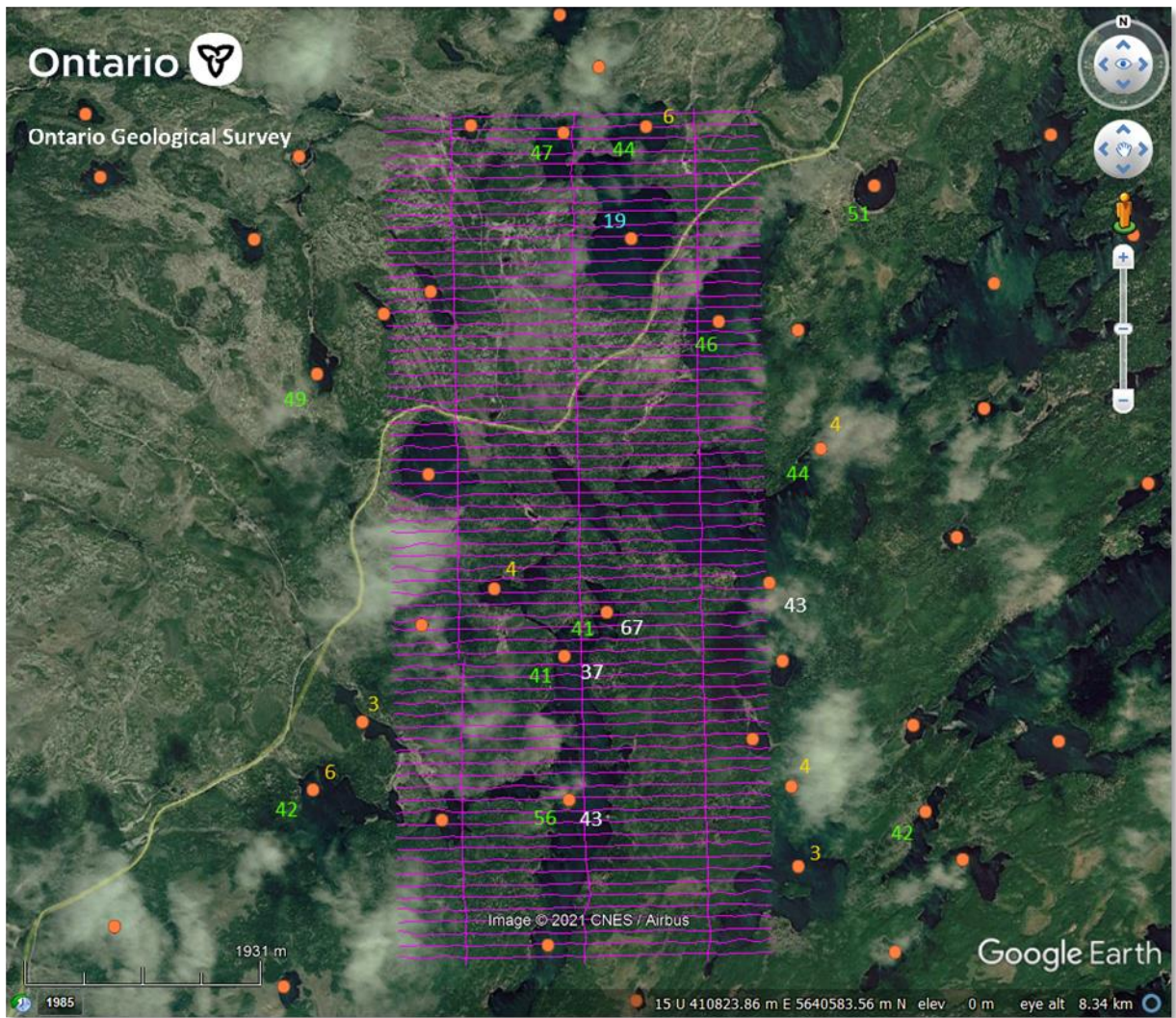
Au >2 yellow

Ni >40 white

Cr >40 green

Co >15 blue

Values are in ppm. These 'cut-offs' are based on a visual assessment of the area, so caution is advised,



The information is discussed later in the report.

6.0 DEPOSIT TYPES

There is minimal information on the geology of the main target which is recorded only as a single exposure on the regional geology map P.3397. As such, analogues are not necessarily reliable and caution is advised.

Mafic intrusion-hosted Ni-Cu magmatic sulphide deposits would represent a possible target. From Brozdowski et al., 2010:

“General characteristics of nickel-sulphide deposits associated with mafic magmatic systems MMG Canada Exploration Inc. Sumach Lake Property include: regional-scale association of districts and deposits with sub-vertical, trans-lithospheric structural zones; originally sulphur-undersaturated mafic magmas and mafic large igneous provinces. At the deposit scale, formation of Ni-sulphide deposits is favored in magma conduits that represent zones of high magma flux, resulting in a wide variety of intrusive features consistent with multiple intrusive events, formation of strongly differentiated intrusions, and active, pulsed magma flux. Local assimilation of country-rock sulphides or emplacement of late magmatic sulphide-laden melts from deeper staging chambers represent alternate methods of forming magmatic sulphides. In mafic systems, magmatic sulphides are commonly emplaced dynamically rather than settling as basal accumulations. Presence of primary biotite, amphibole, and varitextured rocks indicates the importance of volatiles. Presence of olivine, orthopyroxene and melanocratic rocks are considered favorable indicators of relatively high-MgO mafic magmas. Tectonic settings are interpreted to span a range of tectonic environments, from: the root zones of continental flood basalt provinces (Norilsk, Russia; Wellgreen, Yukon Territory, Canada); to settings associated with trans-tensional or incipient extensional regimes, including post-orogenic deposits (Hongqiling, Jilin, China; Aguablanca, Spain); to deposits in AMCG* settings [*Anorthosite-Mangerite-Charnockite-Granite] settings (Voisey’s Bay, Labrador, Canada); or more rarely, synorogenic settings (Giant Mascot, British Columbia, Canada).”

Archæan intrusion-related Ni-Cu-PGE and Ni-Cr deposits are, in comparison to the Proterozoic Large Igneous Province (‘LIP’), relatively small and much fewer globally.

“The tectonic setting of these magmatic sulfide deposits is principally flood basalt dominated LIPs, which are generally attributed to the upwelling and melting of buoyant mantle as a plume beneath crustal lithosphere (Condie, 2001). The sulfide deposits and their host intrusions range in age from Archean to Middle Jurassic. They are generally found close to deeply penetrating structures that allow for the efficient transport of sulfur-undersaturated mantle magma to relatively shallow crustal depths. Although sulfur-bearing crustal rocks such as black shales, evaporates, or paragneisses are proximal to many deposits, they may not be the primary source of sulfur (Hoatson and others, 2006). Deposits are hosted by a wide range of olivine-bearing mantle-derived rocks; these rocks and example locations include ferropicrite (Pechenga, Russia), tholeiitic picrite (Noril’sk-Talnakh, Russia), and high aluminum basalt (Voisey’s Bay, Canada). No

known economic deposits are associated with mid-ocean ridge basalts (MORB), ophiolites, or alkaline rocks.”

And:

“Magmatic sulfide-rich Ni-Cu±PGE deposits range in age from Archean to Mesozoic and have been emplaced into a broad spectrum of country rock and basement terranes (table 3). However, as noted by Hoatson and others (2006), the presence of Ni-Cu±PGE mineralization shows no obvious correlation with the composition or metamorphic grade of basement rock lithologies. Thus, the importance of the country rocks that host magmatic Ni-Cu±PGE deposits lies not in their chemical composition but in whether the rocks may contribute to sulfur saturation of magma and to the physical controls that country rocks may exert on intrusion dynamics.” Schultz et al., (2010)

Analogues could include the large Munni Munni intrusion, Pilbara Craton, Western Australia (Hoatson et al, 2006, Pirajno & Hoatson, 2012). Several are associated with Large Igneous Provinces – ‘LIP’s’.

“The 2925 Ma Munni Munni intrusion (Fig. 18) in the west Pilbara Craton contains the largest resource of PGEs and a small nickel resource (24 Mt @ 2.9 g/t Pt+ Pd+Au, 0.3% Cu, and 0.2% Ni: Helix Resources Ltd, 2004) associated with a layered intrusion in Australia. The large size of the intrusion, its Precambrian age, tholeiitic fractionation trends, and the presence of a distinctive porphyritic plagioclase websterite layer at the contact between the ultramafic and overlying gabbroic zones indicated there was considerable potential for stratabound PGE–Cu–Ni mineralization of Merensky Reef-type (Hoatson, 1984). The intrusion is a 5.5-km-thick elongated body interpreted to be a slightly asymmetric boat-like structure plunging moderately to the south – southwest (Fig. 18). The lower 1.85-km-thick ultramafic zone comprises macrorhythmic cycles of olivine and olivine–clinopyroxene mesocumulates and adcumulates, and the overlying 3.6-km-thick gabbroic zone consists largely of intergranular gabbro, magnetite gabbro, and granophyric gabbro. The upper part of the ultramafic zone contains a distinctive 30- to 80-m-thick orthocumulate layer referred to as the porphyritic websterite layer (PWL: Figs. 18 and 19). Persistent PGE mineralization associated with disseminated chalcopyrite, pentlandite, and pyrrhotite (up to 2 vol.%) occurs along the exposed 22 km strike extent of the PWL. Hoatson and Keays (1989) proposed that the PGE mineralization resulted from the combined processes of crystal fractionation, and mixing of sulfur-undersaturated, PGE-bearing magnesian magma with more evolved sulfur-saturated tholeiitic mafic magma.” (Hoatson et al., 2006).

The Radio Hill Cu-Ni sulphide deposit is one of several other layered Archæan mafic-ultramafic intrusions including Munni Munni, Andover, Mt. Sholl and Sherlock that were emplaced in a ca. 140 km long belt in the western Pilbara Craton. The 2.892 Ga deposit associated with metavolcanic rocks, gneisses and migmatites. “The Radio Hill intrusion is a small mafic-ultramafic body with an outcrop extent of 1.8 km x 2 km. It comprises an upper gabbroic zone(~870 m) and a lower ultramafic zone (~330 m) containing seven sub-zones of interlayered peridotite,

pyroxenite and minor gabbro. Lenses of massive sulphide occur in hosts of gabbro, gabbronorite and plagioclase websterite at the base of the ultramafic zone.”

See <https://dmgeode.com/DepositPortal.aspx?DepositID=2363> and also, Frick et al., 2001

A 2018 News Release from Artemis Resources: “Indicated JORC resource of 1.15 Mt @ 0.52% Ni, 0.73% Cu and 277ppm Co for 5,980 t contained Nickel, 8,395 t contained Copper and 318 t contained Cobalt.” Further:

“RADIO HILL DEPOSIT GEOLOGY AND MINERALISATION

Radio Hill is a small Archaean, 2892 ± 34 Ma, synorogenic-synvolcanic Ni-Cu bearing mafic intrusion containing a minor ultramafic component near its basal contact and is probably comagmatic with nearby Mount Sholl and Munni Munni intrusions. It is considered to be a Voisey's Bay analogue. The massive and disseminated Ni-Cu-Co sulphides are hosted by thin gabbroic units underlying layered ultramafic-mafic sequence. Sulphides are confined to feeder conduit or depressions of basal contact.

Mineralisation is patchy blebs of medium grained disseminated to matrix sulphides in the basal peridotite to olivine pyroxenite. Pyrrhotite, with sub-ordinate pentlandite, and chalcopyrite, forms lobate aggregates up to 12% volume of the Ultramafic host. Pyrrhotite forms layers up to 20 metres thick, 8 metres above the basal contact of an intrusion.

Post-intrusion deformation has tilted the deposit 25-40 degrees to the southeast. The geometry has been modified by northerly trending sinistral faults that, in the A and B massive zone, have created independent mining blocks. These faults have a displacement between one and ten metres and have been named, from east to west, Ebenezer, Newman, Toth, Forster, Irvin and 3-Names.

These faults are all displaced by Brutus fault, which is the most significant fault in the deposit. Brutus is a brittle-ductile deformation zone that has an approximate dip between 35-60 degrees and strikes approximately NNW (approx. 330 degrees mine grid). This fault has a sinistral normal movement with a horizontal translation of approximately 30 metres.

Dolerite dykes have intruded the orebody with relaxation, following deformation, into pre-existing weakness created by faulting. Two mine-site wide dolerite dykes, named Aminya and Zen, have truncated the orebody and act as pillars for the underground mining.

In the 1980's AGIP Australia Pty Ltd divided observed mineralisation, from south to north, into zones A to F although it is potentially misleading as different mineralisation types transverse zonal boundaries. Within these zones three types of mineralisation have been observed at the Radio Hill mine, which are summarised as follows:

“Massive medium to very coarse grained pyrrhotite-chalcopyrite-pentlandite ore that is often strongly brecciated and displays quartz-carbonate-chlorite veining,

Stringer/gash vein, disseminated and blebby pyrrhotite-chalcopyrite-pentlandite mineralisation associated with tremolite-actinolite-chlorite alteration and minor carbonate veining,

Disseminated fine grained pyrrhotite-chalcopyrite-pentlandite sulphides hosted by the gabbro, and pyrrhotite dominant sulphides within the ultramafic immediately overlying the gabbro.

A, B and H zones are characterised by massive and some minor disseminated mineralisation. Stringer type mineralisation is not observed in the A and B zones. The division between A and B zones is arbitrary. A zone occurs below the 875 mRL in the eastern domain of the mine overlying, and in parts incorporating, the underlying basement. B zone occurs above the 875 mRL in the western domain of the mine subparallel to Brutus, discordant to basement, but stratabound within the orebody gabbro. A and B zone's geometry is intimately associated with the Brutus Fault. H zone is a faulted offset (by Brutus) of A zone.

C and D zones are characterised by stringer mineralisation overlying a basal interval of massive sulphides. Mineralisation in the C and D zones is strata-form as it mainly occurs 10-20 metres above the basement contact, but is not strictly speaking primary mineralisation because it has been remobilised into veins/stringers and blebs. The C and D zones are also intimately associated with the Brutus Fault. D zone is a faulted offset (by Brutus) of C zone."

See also De Angelis et al., 1987

In north-west Ontario, Archæan orthomagmatic intrusions are less well documented. Breaks (1991), describes several in the south adjacent English River subprovince, including the Conifer Lake stock.

"Plutonic rocks forming gabbro-pyroxenite-peridotite intrusive complexes are rare in the English River Subprovince and are confined to 3 areas. These areas generally coincide with zones of granulite-grade metamorphism: areas adjacent to Conifer-Sumach lakes; areas adjacent to Reynar, Rex, Treelined and Gone lakes; and the eastern Lac Seul region (see Figure 7.2). Ultramafic inclusions, a metre or less in diameter, are widespread in the English River Subprovince.

"Ultramafic to gabbroic rocks consist of clinopyroxene-, orthopyroxene- and olivine-bearing pyroxenite and peridotite, and associated gabbroic rocks (Cadson 1957; Panagapko 1976; Breaks and Bond, in prep.).

"The largest single mass of ultramafic to gabbroic rocks is the Conifer stock (see Figure 7.2), a circular complex 1200 m across, (Panagapko 1976). This complex lies in the centre of the northeast arm of a large peraluminous mass composed of biotite + garnet ± sillimanite ±

cordierite bearing granite delineated by Breaks, Bond, McWilliams et al. (1975). This granite intrudes the core of the ultramafic-mafic pluton (Panagapko 1976).

“The Conifer stock consist of metamorphosed, massive, medium- to coarse-grained ultramafic rocks which are chemically similar m pyroxenite, and to a lesser extent to subordinate melagabbro and meladiorite. The ultramafic rocks form a 280m wide outer ring and are composed of hypersthene + biotite + hornblende + plagioclase t opaque iron-oxide. The associated meladiorite, composed of hornblende + augite + andesine ± biotite ± olivine ± hypersthene, has a lower colour index (75 to 85) than pyroxenite.

“Foliations developed along the inner and outer granite contacts have a cataclastic appearance (Panagapko 1976), with foliation consistently dipping inwards between 30 and 55, which suggests a funnel-like morphology for this body.”

Doug Panagapko’s mapped the complex as part of his M.Sc., which he described as olivine-bearing meladiorite, foliated diorite and granite.

In 1993, Teryl Resources drilled two holes into part of the stock on its Conifer Lake property though only one was reported. It intersected ‘mainly alternating bands of granite and pyroxenite or melagabbro and from 157.8 ft to 537 ft (EOH), alternating bands of melagabbro-pyroxenite and granite and granite gneiss. Bands are somewhat wide than in the first 157 ft.” The log indicates Noranda was directly involved in the programme. Mafic-ultramafic rocks were typically two to five metres wide and comprised approximately 25% of the section.

The same target was drilled by MMG Canada Exploration Inc. in 2010 (who noted Teryl drilled two holes). Newgenco (Oz Minerals) had previously sampled the stock with no anomalous Ni or Cu results were returned. Their thin section work noted 0.1% to 1% microscopic three phase po-cp-pentlandite immiscible sulphide blebs.

Mapping and sampling (soil, whole rock and stream sediment) led to the following conclusions:

Dimensions of the Complex are a maximum 1100 x 700 metres. It lacks mesoscopically visible sulphide minerals. The majority of the mafic-ultramafic complex comprises biotite/phlogopite – bearing gabbros, norites, olivine gabbros, websterites and olivine websterites with in and around the complex, a significant granite component.

Sampling was hampered by a lack of outcrop and in at least one large area, covered by a beaver pond. Newgenco rock sample results ranged from 47.4 ppm to 188.5 ppm Cu, 72.6 ppm to 430.5 ppm Ni, 1 ppm to 9.9 ppm Pd and 2 ppm to 11.1 ppm Pt. MMG rock sample results ranged from 61.7 ppm to 365 ppm Ni, and 71.1 ppm to 124.5 ppm Cu. Co ranged from 44.8 ppm to 68.2 ppm; and Cr from 297 ppm to 1260 ppm.

The Complex is located approximately 38 km south-east of Western Bear and 51 km west of Ear Falls. *No inference is made regarding the Cu and Ni analyses or potential between the two properties, only the possibility of a gross similar geology.*

7.0 RESULTS

On the 12th October, 2020, Precision GeoSurveys Inc. of Langley, B.C. flew a high resolution helicopter-borne aeromagnetic survey for Trillium Gold Mines Inc over the 105 claim Western Bear block which is located approximately 46 km south-west of Red Lake, Ontario.

The survey was flown at 100 metre line spacing at a heading of 090°/270°; tie lines were flown at 1000 metre spacing at a heading of 000°/180°. A total of 237.4 line km was flown, over an of 21.6 km².



Figure 14 Plan View – Western Bear survey block

Flight lines are shown in yellow. Summary is provided, below.

Survey Block	Area (km ²)	Line Type	No. of Lines Planned	No. of Lines Completed	Line Spacing (m)	Line Orientation (UTM grid)	Survey Height (m)	Total Planned Line km	Total Actual km Flown
Western Bear	21.6	Survey	70	70	100	090°/270°	40	216	216.4
		Tie	3	3	1000	000°/180°	40	21	21.0
		Total:	73	73			40	237	237.4

Specifics of the geophysical equipment and processing are provided in the accompanying report by Precision GeoSurveys Inc., author, S. Walker, M.Sc., P. Geo. This includes polygon co-ordinates for the survey block (in Appendix A, separate file

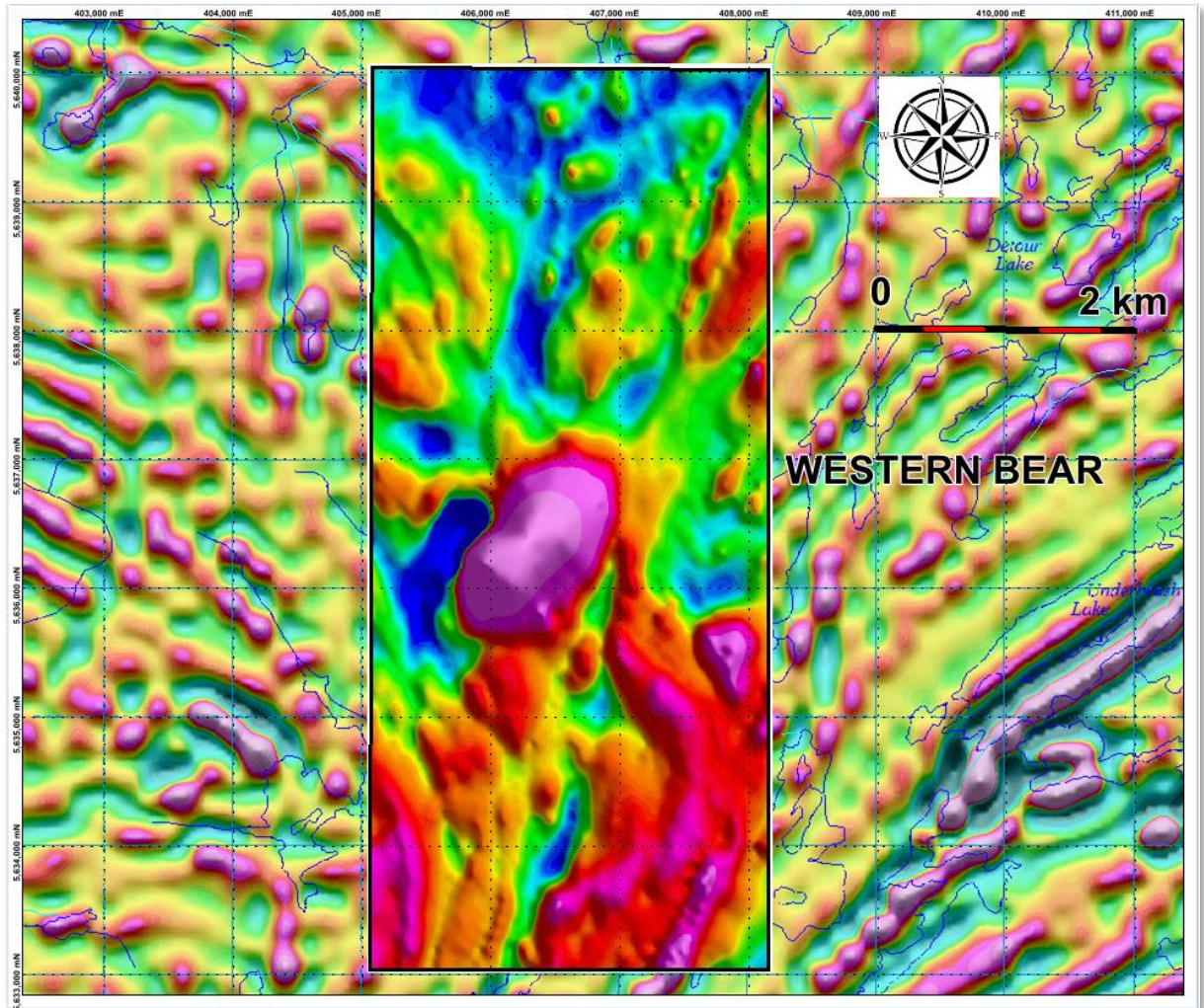


Figure 15 Regional and TGM residual magnetic data

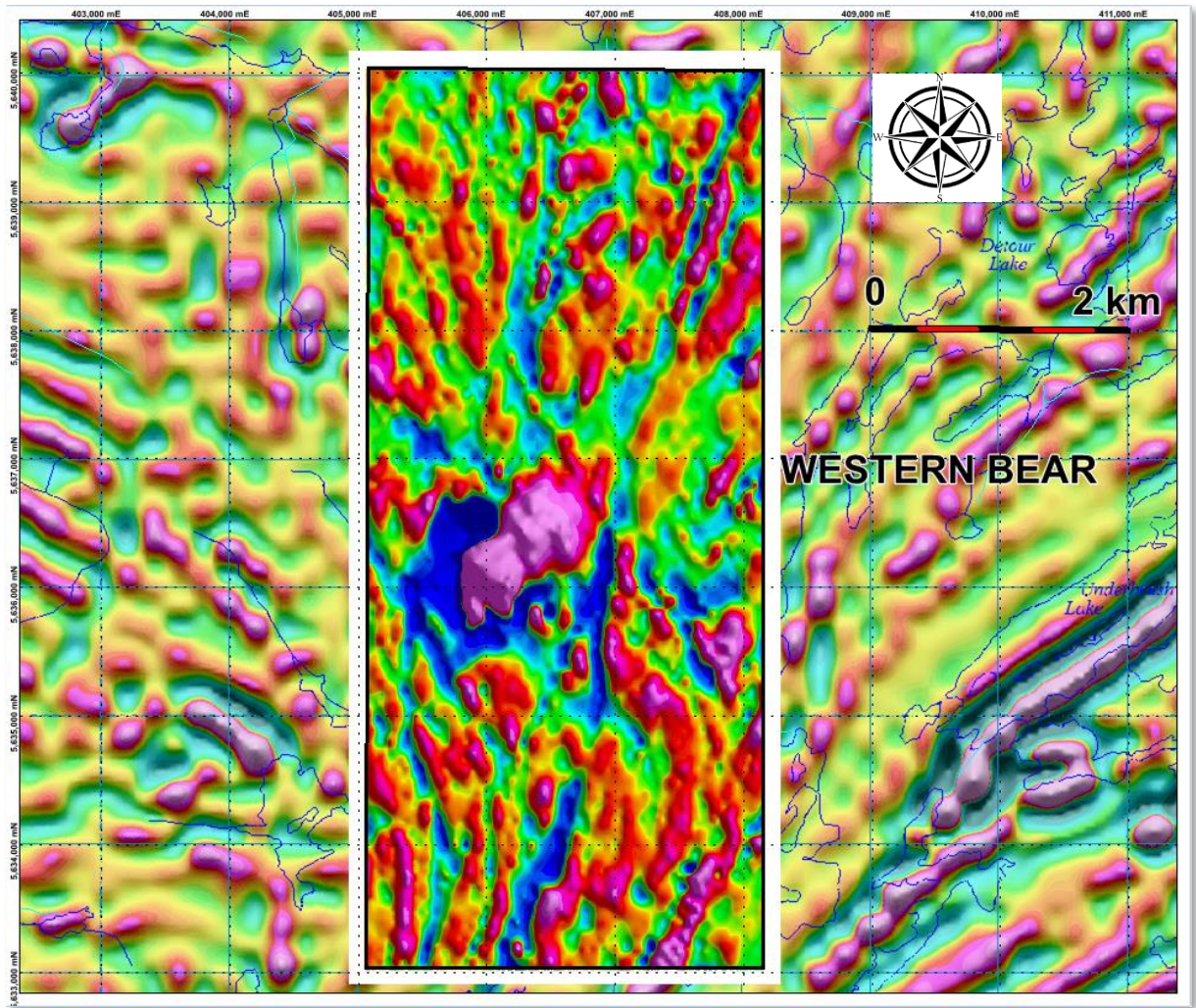


Figure 16 Regional residual magnetic data and TMI vertical gradient data

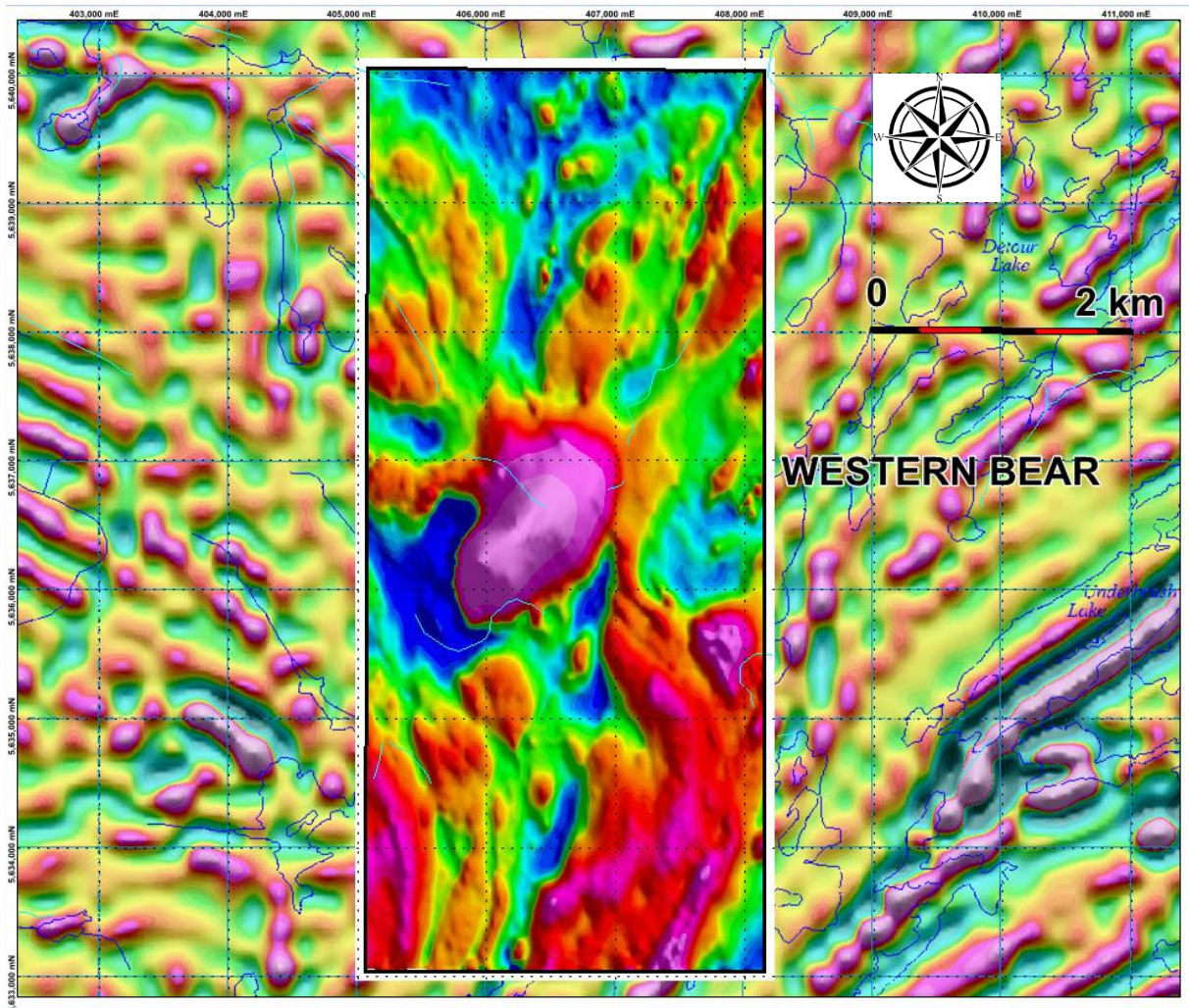


Figure 17 Regional residual magnetic data with TGM RTP data

Lakes and Woodland Caribou Provincial park boundary shown

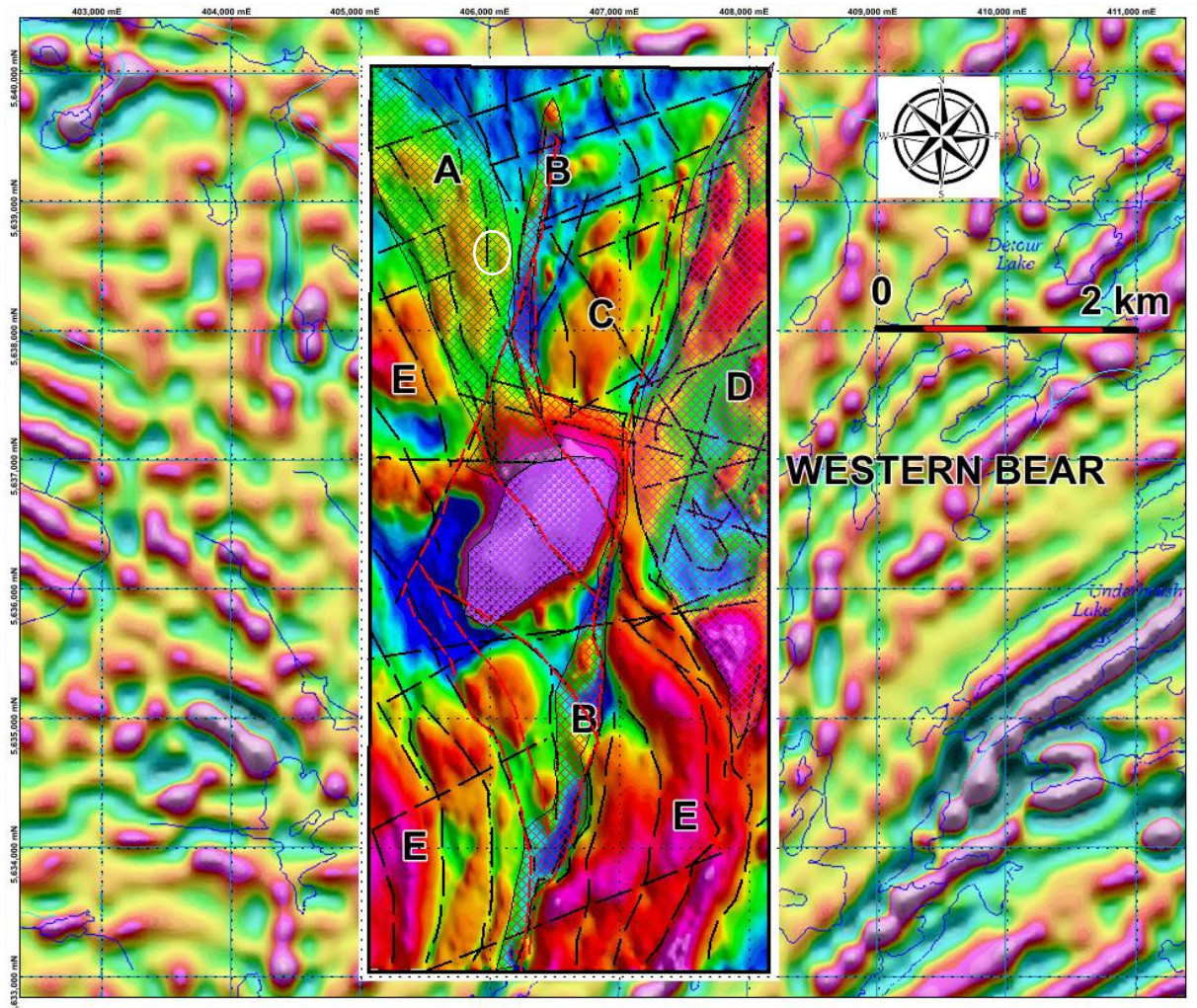


Figure 18 Interpretation I

White - Structural & lithological trends; black – faults/breaks; red – antiformal axis, Sydney Lake-Rainfall Lake dome

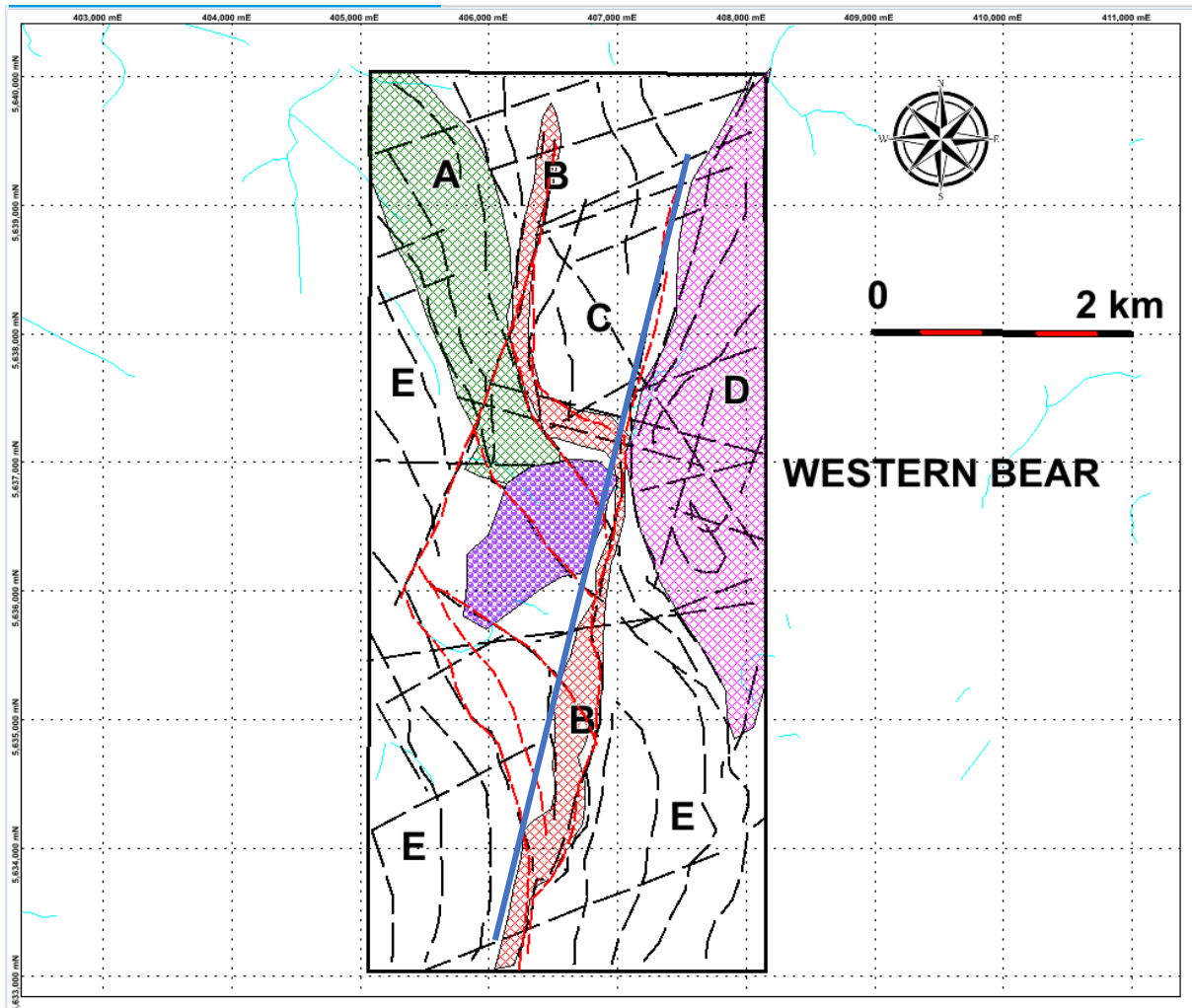
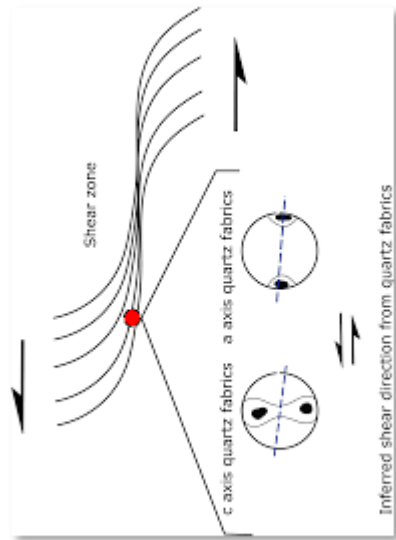


Figure 19 Interpretation II

The purple area covers the approximate extent of the north-east plunging mafic to ultramafic intrusion. It has been described in P.3397 as '10p', a metaperidotite to metapyroxenite.

A Green Possible extent of the mainly mafic volcanic greenstone belt extending south-east then south south-east from Telescope Lake. It is highly probable much of the sequence has been significantly modified by the Atikaki Batholith, with considerable assimilation of an amphibolite metamorphic facies gneissic suite. Compression and attenuation would also be prominent with pinching out of the sequence near or at the contact with the ultrabasic intrusion.

B Red A major, generally north-south deformation zone produced during a large-scale east-west to east south-east – west north-west shortening event. The zone could be ductile in nature with overall sinistral sense of shear.

Figure 20 Diagramme of a simple shear

C Extent of the Onnie-Detour stock with the western contact partially defined by the North-South trending deformation zone.

D **Pink** The Neoproterozoic tonalite-granodiorite, massive to foliated, locally gneissic to xenolithic intrusive complex forming part of the Sydney Lake – Rainfall Lake dome

E Atikaki batholith with extent and boundaries defined by slight differences in magnetic/lithostructural trends and magnetic intensity between it and the dome

complex. The TGM and regional magnetic clearly shows within several curvilinear magnetic high trends which are concluded to be relict supracrustal sequences, and in the region, typically amphibolite.

Black dashed lines trending approximately north-south to north north-west south-south-east define the overall lithostructural fabric of the area.

Linear black dashed lines cut the sequence and the intrusions and are likely related to a west-north-west to east-west crustal shortening.

Linear black dashed lines trending east north-east - west south-west are small scale, low intensity brittle ?-normal faults with a very small horizontal displacement.

The red dashed lines define a simple shear parallelogram-shaped sub-domain, possibly a rhomb graben formed during overall sinistral strike-slip. The enclosed strain ellipse would be low-strain, permitting ingress by the ultrabasic body. Superimposed on this is the dextral shearing, resulting in rotation north and east, with deformation of the host. It is conceivable that a later intrusive event may lie within along preferred structurally defined paths, in this instance, curvilinear, possibly extensional west north-west oriented features.

Possibly a cataclastic zone, the north north-east – south south-west trending blue line cuts the shear zone but is likely a late stage phenomenon of the shears development.

Targets are:

1. The ?-ultrabasic body, the contact zone between the shear zone and the Telescope Lake greenstone. Based on the magnetic 'signature', it is estimated the body is approximately 1.2 km long and 1 km wide, with a north-easterly elongation and similar plunge.
2. The ductile shear zone, with either mylonitic-cataclastic or semi-brittle environments as potential hosts for precious metal targets, with the Telescope Lake area a lower strain target (image, left.)

Note: Additional areas recommended for follow-up are provided by E. Mueller-Markham in her report (appendix, separate file). These areas are also shown below, fig. 21.

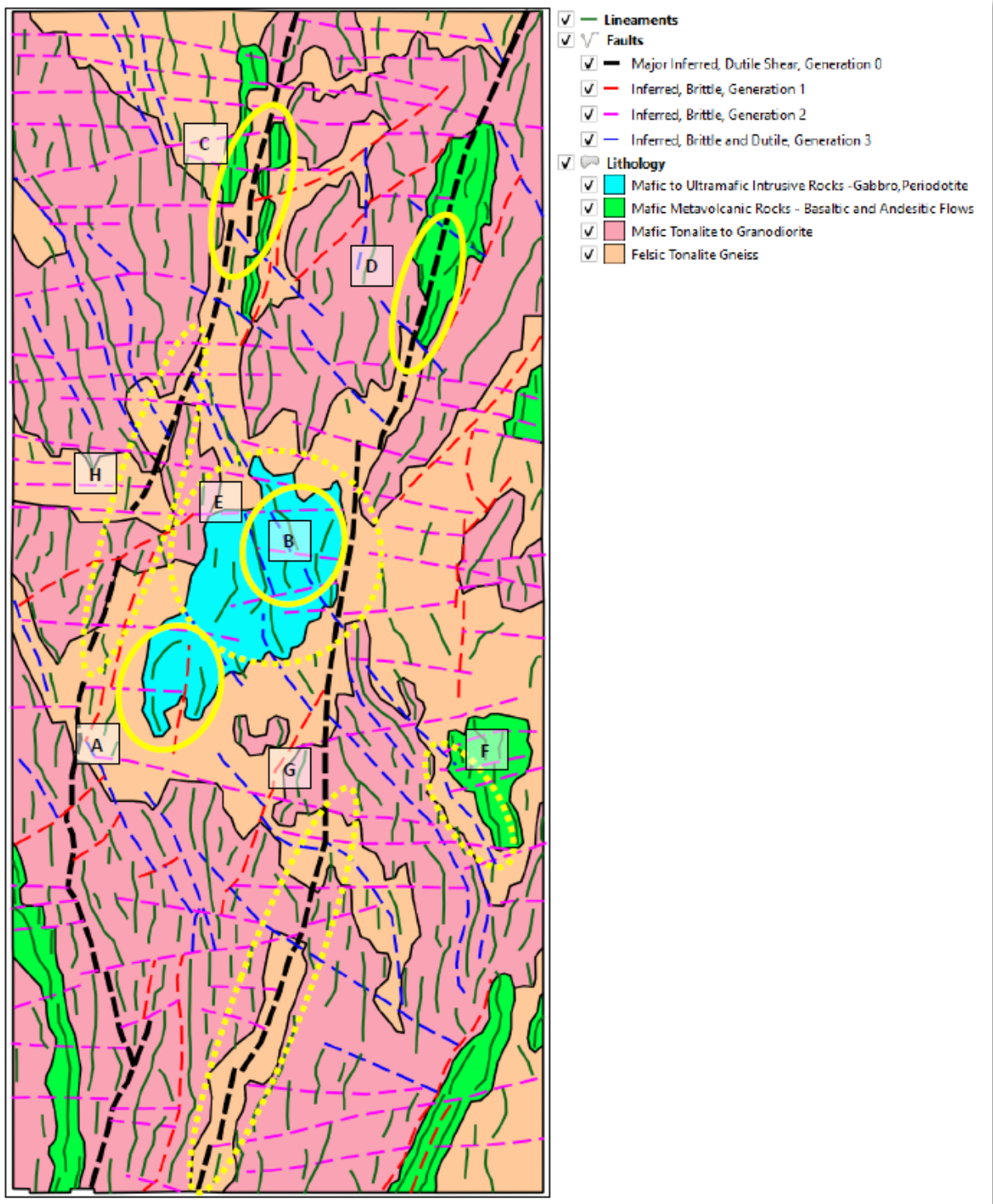


Figure 21 PGW recommended primary and secondary targets

8.0 CONCLUSIONS

The airborne survey outlined a mafic-ultramafic intrusion, some 1.2 by 1 km in aerial extent. The body has unknown composition, and it could represent an ultrabasic or differentiated mafic to ultramafic orthomagmatic target. It is important to obtain samples for lithochemical and trace element analysis prior to developing a full exploration strategy.

“Recognition of LIPs in the Archean is more uncertain because most volcanic rocks and associated intrusions occur in deformed and fault-segmented greenstone belts (de Wit and Ashwal, 1997) and generally cannot be traced over LIP-scale areas.” Shultz et al., (2010)

Partially preserved crustal sequences lie at the boundary between the Atikaki Batholith and the Onnie-Detour Stock, and the Batholith and a western portion of the Longlegged Lake – Rainfall Lake dome.

A possible ductile shear zone transects the property with a geometry that could be amenable to transport and deposition of mineralised fluids.

The ‘anomalous’ lake sediment sample results on and adjacent to the property suggest there is at least some potential for the discovery of Cu and Ni and Au mineralisation. There appears to be some spatial correlation between Ni, Cu and Cr with the mafic-ultramafic body.

9.0 RECOMMENDATIONS

Map and sample the mafic-ultramafic intrusion. Much of it appears under cover, so detail soil/humus or SGH sampling is recommended.

Map and prospect area B, the proposed ductile shear zone and include the rhomb graben area.

Recce the entire property with a clear focus on structural geology, metamorphic assemblages, differentiating these from alteration assemblages which is critical for both orogenic, high grade metamorphic VMS and hypozonal precious/base metal targets. Locate areas with retrograde metamorphic assemblages (for hypozonal targets).

Determine the overall ice direction which would aid in understanding lake sediment results and their provenance. Also recommended is prospecting and boulder tracing (covered by the PG and assistant).

Refer to the accompanying PGW report for specific targets by E. Mueller-Markham.

Respectfully Submitted,

T.N.J. Hughes, P. Geo.

Proposed Budget

Item	Days/Unit	Base Cost	Total
Mapping, Prospecting			
Project Geologist	21	700	14700
Junior geologist	21	350	7350
Room and board	21	300	6300
Sampling			
Rock Sampling	100	50	5000
Soil/SGH sampling/samplers	800	90	72000
Transportation			
Truck, gas	21	150	3150
Float Plane	8	2000	16000
Boat rental	8	300	2400
Reports and Maps			
	6	700	4200
Contingencies			
	15%		19665
Total Proposed Budget			<u>150765</u>

10.0 REFERENCES

Assessment files:

None

Other

ODM Maps

M-1942 Leano Lake area

M-2210 Sydney Lake both 1: to 2640 ft.

Map No. 36f Gammon River Area, District of Kenora, Patricia Portion. G. Gilbert in Vol. XXXVI, Part 3, ODM Ann. Rept., 192. Scale 4 miles=1 inch.

ODM, Toronto. MDMNR-ODM-GSC Aeromagnetic Map: 7124G, scale 1 inch to 4 miles or 1:253,440

Breaks, F.W. et al, (1975) Geology of Operation Kenora-Sydney Lake.

Breaks, F.W., et al., 1974 Operation Kenora-Sydney Lake, Eagle-Sydney Lakes, District of Kenora; ODM Prelim. Geol. Ser., scale 1" to 1 mile or 1:63630. 1974

Breaks, F.W. et al., 1993 Compilation Map, English River Subprovince, OGS Preliminary Map P.3091, Scale 1:253 440. 1993

Map 2175 Red Lake-Birch Lake geological Compilation Series, ODM 1968

Neilson, J.V., 1990 NOEGTS Sydney Lake Data Base Map OGS Map 5105 NTS 52L/NE , T, 1:100,000 Geology 1979

Asudeh, I; White, D; Roberts, R; Forsyth, D; Kay, I; Cartwright, T; Carroll, P; Hajnal, Z; Koperwhats, B; Musacchio, G; Farrell, D. (1996) LITHOPROBE Western Superior seismic refraction survey: field acquisition and processing report; Geological Survey of Canada, Open File 3583, 1999, 223 pages, doi:10.4095/210198

Atkinson, B.T., (1999) Precambrian geology, Medicine Stone Lake area: OGS, Prelim. Map).3397, scale 1:50,000

Beakhouse, G.P., (1977) A subdivision of the western English River subprovince. CJES, 14, pp; 1481-1489.

Bell, R. (1873) Report on the country between Lake Superior and Lake Winnipeg, Geological Survey of Canada, Report of Progress, 1872-1873, 87-111.

- Breaks, F.W., W.D. Bond, D.W. Desnoyers, D. Stone, and N. Harris, (1975) Operation Kenora - Ear Falls, Bruce-Bluffy Lakes Sheet, District of Kenora; Ontario Div. Mines, Prelim. Map P.1199, Geol. Scr., scale 1:63,360 or 1 inch to 1 mile. Geology 1975.
- Breaks, F.W. et al., (1974) Bulging Lake-Embryo Lake, District of Kenora, (Patricia Portion): ODM, Prelim. Map P.950. Geol. Ser., scale 1"=1 mile. Geology 1972.
- Breaks, F.W., et al., (1978) Preliminary geological synthesis of the English River subprovince, Northwestern Ontario and its bearing upon mineral exploration. OGS MP 72, 55 p.
- Breaks, F.W., (1991) English River subprovince. *In* Geology of Ontario. Spec. Vol. 4, Part 1. *Edited by* Thurstone, H.R. et al.. OGS pp. 239-277.
- Breaks, F.W., 1991. English River Subprovince in Geology of Ontario, Ontario Geological Survey, Special Volume 4, Part 1, pp. 239-277.
- Breaks, F.W. & Bond, W.D. (1993) The English River Subprovince – An Archæan Gneiss Belt: Geology. Geochemistry and Associated Mineralization. Vols 1 & 2, 1993. OGS OFR 5846 884 p.
- Brozdowski, R.A. et al., (2010) Sumach Lake area Ni-Cu exploration: Geological mapping and prospecting. MMH Canada Exploration Inc., Sumach Lake Property Ontario. MNDM Assess. report 20009048, 2010
- Burwash, E.M. (1920) A geological reconnaissance into Patricia; Ontario Department of Mines 29, part 1, 157-192.
- Dowling, D.B. (1894) Report on the country in the vicinity of Red Lake and part of the basin of Berens River, Keewatin; Geological Survey of Canada 7, part F, 5-54.
- De Angelis, M., Hoyle, M.W.H., Peters, W.S., and Wightman, D. 1987. The nickel– copper deposit at Radio Hill, Karratha, Western Australia. Australasian Institute Mining Metallurgy Bulletin and Proceedings, 292: 61–74.
- Fawcett, T. (1885) Annual Report; Department of the Interior, part 2, 30-38.
- Frick, L.R., Lambert, D.D., Hoatson, D.M., 2001. Re–Os dating of the Radio Hill Ni–Cu deposit, west Pilbara Craton, Western Australia. Australian Journal of Earth Sciences 48, 43–47.
- Friesen, R.G. et al., 1982 Geology of the Geco Base Metal Deposit. Precambrian Sulphide Deposits, H.S. Robinson Memorial Volume, ed. R.W. Hutchinson, C.D. Spence and J.M. Franklin, GAC Spec. Paper 25, 1982
- Gilbert, G. & Burwash, E.M., (1927) ARM36F, Gammon River area, District of Kenora, Ontario (Patricia Portion).
- Goldfarb, R.J. & Groves, D.I., (2015) Orogenic gold: Common or evolving fluid and metal sources through time. Lithos, 233 (2015) 2-16

- Groves, D., et al., (2003) Gold deposits in metamorphic belts: overview of current understanding, outstanding problems, future research, and exploration significance. *Econ. Geol.* Vol. 98, p. 1-29, 2003
- Hall, D.H. and Hajnal, Z. (1973) Deep seismic crustal studies in Manitoba; *Seismological Society of America Bulletin* 63, 885-910.
- Hoatson D.M., Jaireth, S., and Jaques, A.L., 2006. Nickel sulfide deposits in Australia: Characteristics, resources and potential. *Ore Geology Reviews*, 29, 177-241
- Hrabi, B. & Cruden, A.R. (2006) Structure of the Archæan English River subprovince: implications for the tectonic evolution of the western Superior Province, Canada. *CJES* 43, 2006
- Lafrance, B., 2018 Structural Settings of Gold Deposits in Low to High Metamorphic Grade Terranes. *MERC/PDAC Short Course*, March 2018
- Lodge, R.W.D., 2012 Winston Lake and Manitouwadge Revisited: Modern Views of Two Volcanogenic Massive Sulphide (VMS)-Endowed Greenstone Belts. *A Field Trip Guidebook*. OGS OFR 6282, 34 p.
- Mueller-Markham, E. (2021) Geophysical Interpretation of Western Bear, Sydney Lake and Leo Properties, March 23 2021. Paterson, Grant and Watson for Trillium Gold Mines Ltd.
- Panagapko, D. A., (1976) The Geology, Petrology and Chemistry of the Conifer Lake Igneous Complex, District of Kenora, Ontario. B.Sc. Honours Thesis, Carleton University, Ottawa, Ontario, April 1976, 40 pp.
- Percival, J.A. et al., (2000) Western Superior NATMAP: an integrated view of Archæan crustal evolution. *Report of Activities 2000*, Manitoba Industry, Trade and Mines, MGS GS-20 p. 108-116
- Percival, J.A., Sanborn-Barrie, M., Skulski, T., Stott, G.M., Helmstaedt, H. and White, D.J. 2006. Tectonic evolution of the western Superior Province from NATMAP and Lithoprobe studies; *Canadian Journal of Earth Sciences*, v.43, p.1085-1117
- Peterson, V.L. & Zaleski, E., 1999 Structural history of the Manitouwadge greenstone belt and its volcanogenic Cu-Zn massive sulphide deposits, Wawa subprovince, south-central Superior Province. *CJES* Vol. 36, No., 4, April, 1999
- Pirajno, F., and Hoatson, D.M., 2012. A review of Australia's Large Igneous Provinces and associated mineral systems: Implications for mantle dynamics through geological time. *Ore Geology Reviews*, 48, 2-54.
- Sanborn-Barrie, M., Skulski, T., Parker, J. and Dubé, B. 2000: Integrated regional analysis of the Red Lake greenstone belt and its mineral deposits, Ontario; *Geological Survey of Canada, Current Research 2000-C18*, 16 p

- Sanborn-Barrie, M. et al., (2001) Three hundred million years of tectonic history recorded by the Red Lake greenstone belt, Ontario. CSC Current Research 2001-C19, 32 p, 2001
- Sanborn-Barrie, M. et al., (2004) Geology and Tectonostratigraphic Assemblages, East Uchi Subprovince, Red Lake and Birch-Uchi belts, Ontario; GSC OF 4256; OGS Prelim. Map P. 3460, scale 1:250,000
- Schultz, K.J. et al., (2010) Magmatic Sulfide-Rich Nickel-Copper Deposits Related to Picrite and (or) Tholeiitic Basalt Dike-Sill Complexes: A Preliminary Deposit Model. USGS OFR 2010-1179
- Sharpe, D.R. & Russell, H.A.J., (1996) Quaternary Geology of the red Lake/Confederation Lake Area. GSC OF 2876, 1996
- Thurston, P.C., (1985) Physical Volcanology and Stratigraphy of the Confederation Lake Area. Ont. Geol. Surv. Rpt. 236, with Map M2498
- Wallis, C.S., (2004) Technical Report on the Gold Centre Property Red Lake, Northern Ontario prepared for Rupert Resources Ltd. Pub. Roscoe Postle Assoc. Ltd., 2004
- Wilson, A.W.G. and Johnston, J.F.E. (1904) Report on a traverse through the Severn River; Geological Survey of Canada 16, Part A, 143-152.
- Zaleski, E. and Peterson, V.L. 1995. Depositional setting and deformation of massive sulfide deposits, iron formation, and associated alteration in the Manitouwadge greenstone belt, Superior Province, Ontario; Economic Geology and the Bulletin of the Society of Economic Geologists v.90, 2244-2261.
- 2001. Geology of the Manitouwadge greenstone belt and the Wawa–Quetico subprovince boundary, Ontario. Geological Survey of Canada, Map 1917A.
- Zaleski, E., Peterson, V.L., Lockwood, H.C., and van Breemen, O. 1995. Geology, structure and age relationships of the Manitouwadge greenstone belt and the Wawa subprovince boundary, northwestern Ontario, Field Trip Guidebook; Institute on Lake Superior Geology, 41st annual meeting, Proceedings v.41, Part 2B, p.77.
- Zaleski, E., van Breemen, O., and Peterson, V.L. 1999. Geological evolution of the Manitouwadge greenstone belt and Wawa–Quetico subprovince boundary, Superior Province, Ontario, constrained by U-Pb zircon dates of supracrustal and plutonic rocks; Canadian Journal of Earth Science v.36, p.945-966.

11.0 STATEMENT OF QUALIFICATIONS

I, Toby Hughes of Vancouver, B.C. declare that:

- I graduated with an Hons. B.Sc. Geology, from Dundee University, Scotland in 1980
- I have worked as an exploration geologist for 40 years since graduation.
- I am a Practicing Geologist in good standing with Professional Geoscientists Ontario, No. 1318

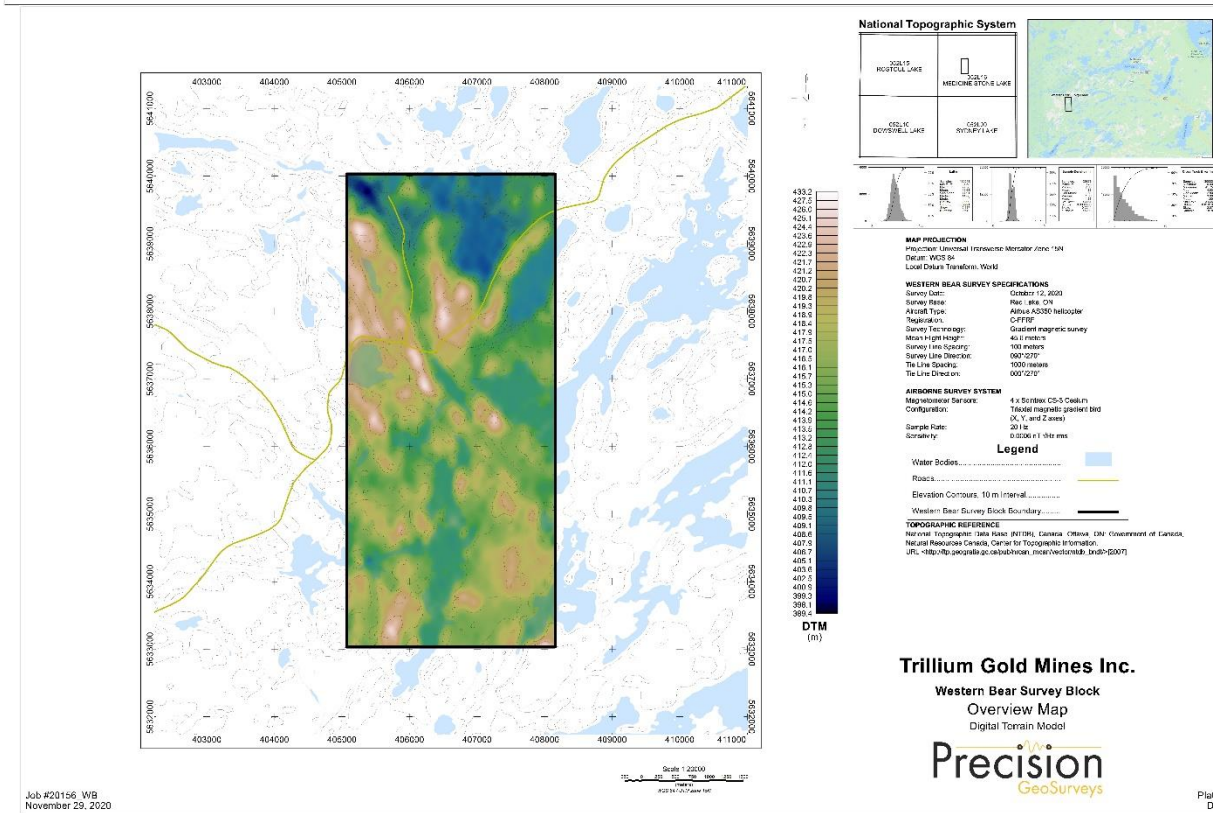
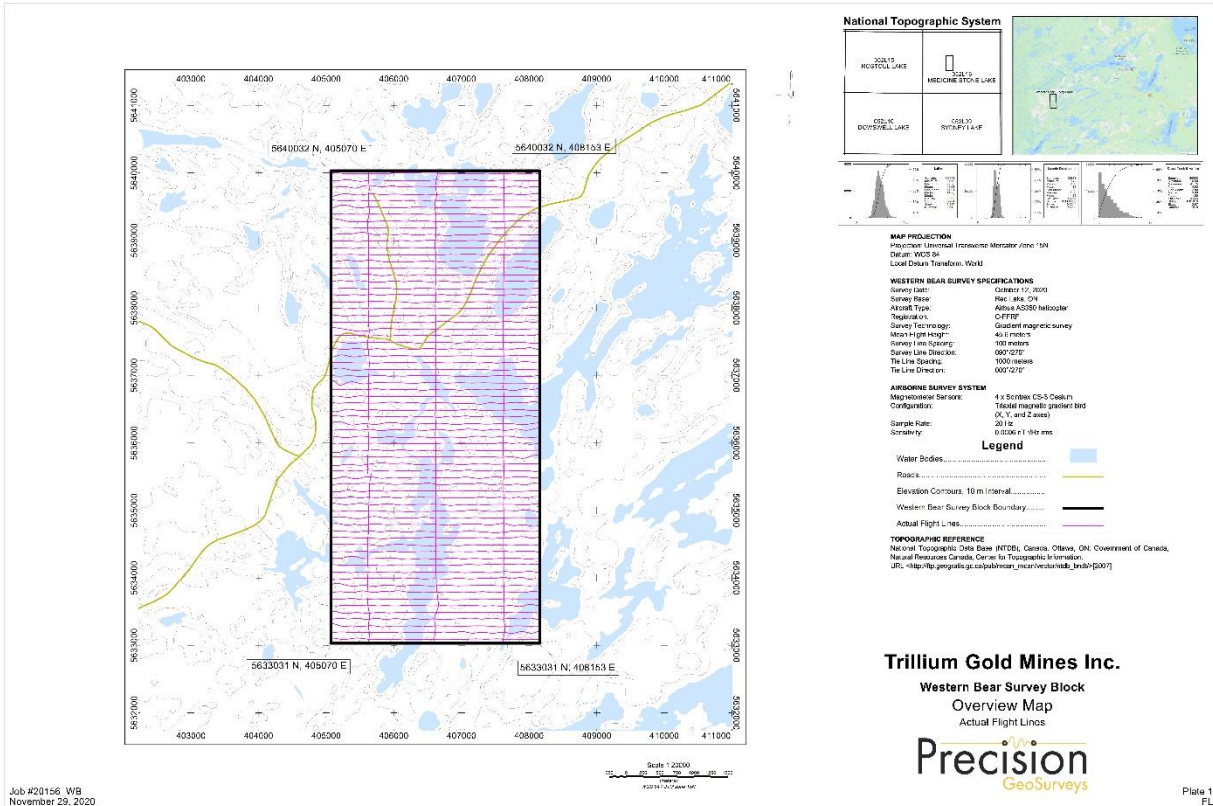
T. Hughes, P. Geo.

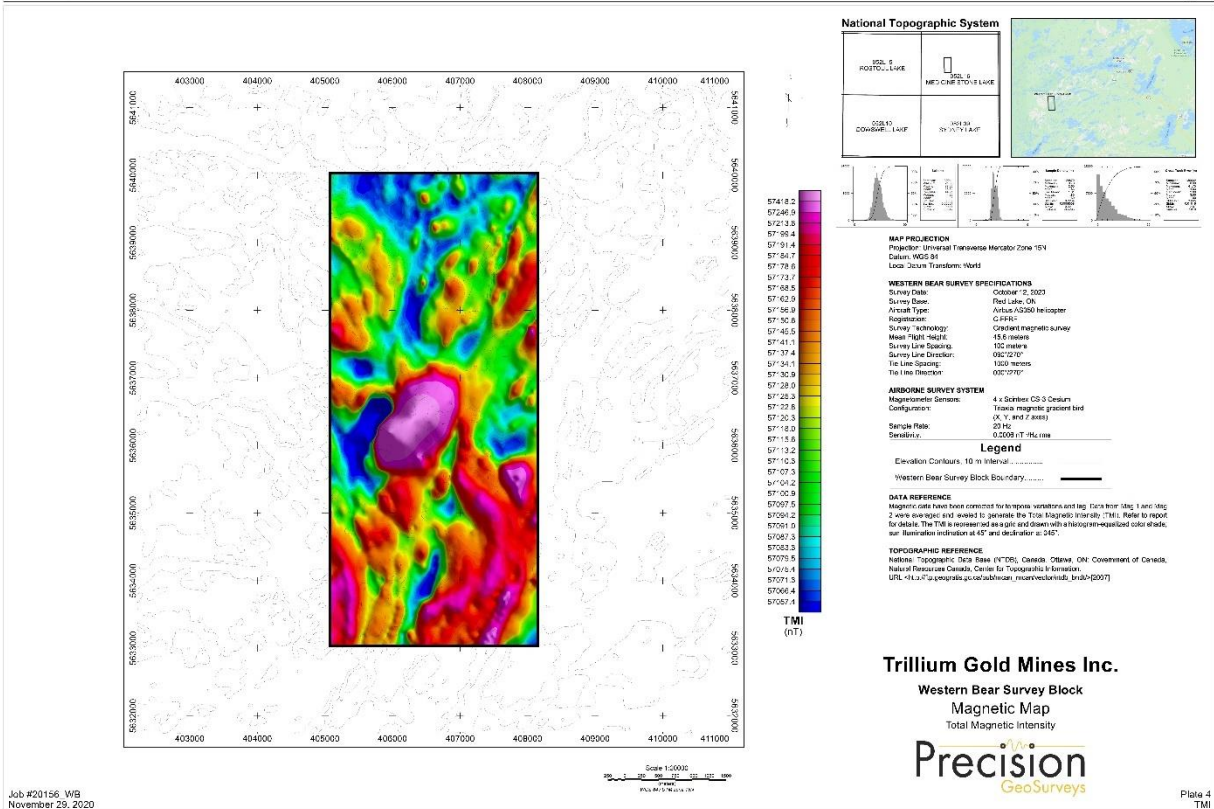
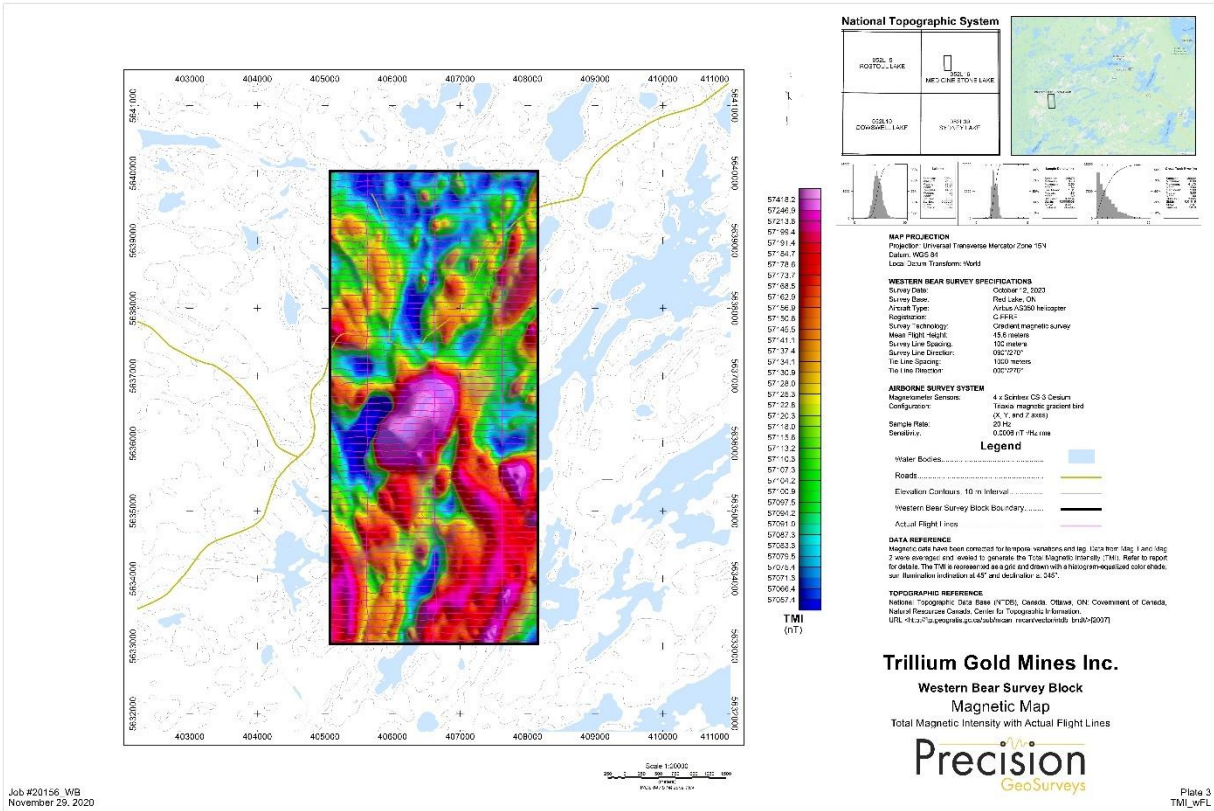


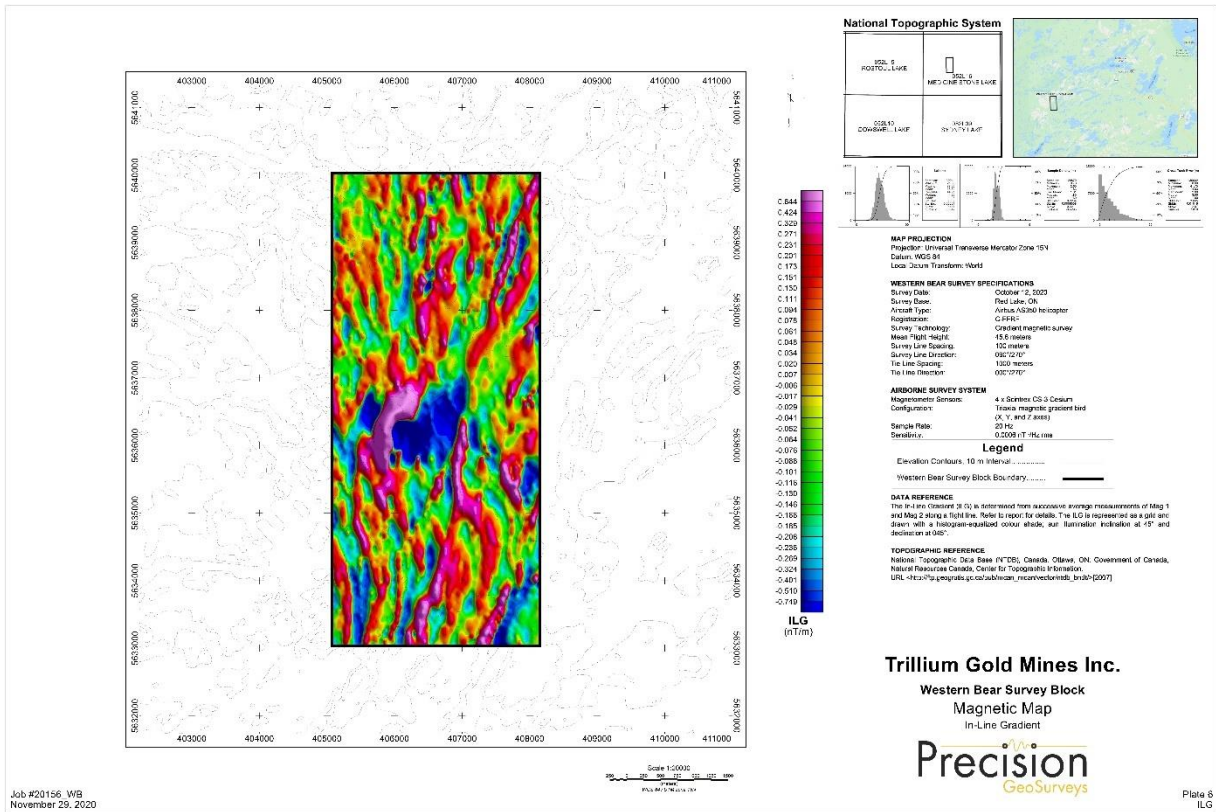
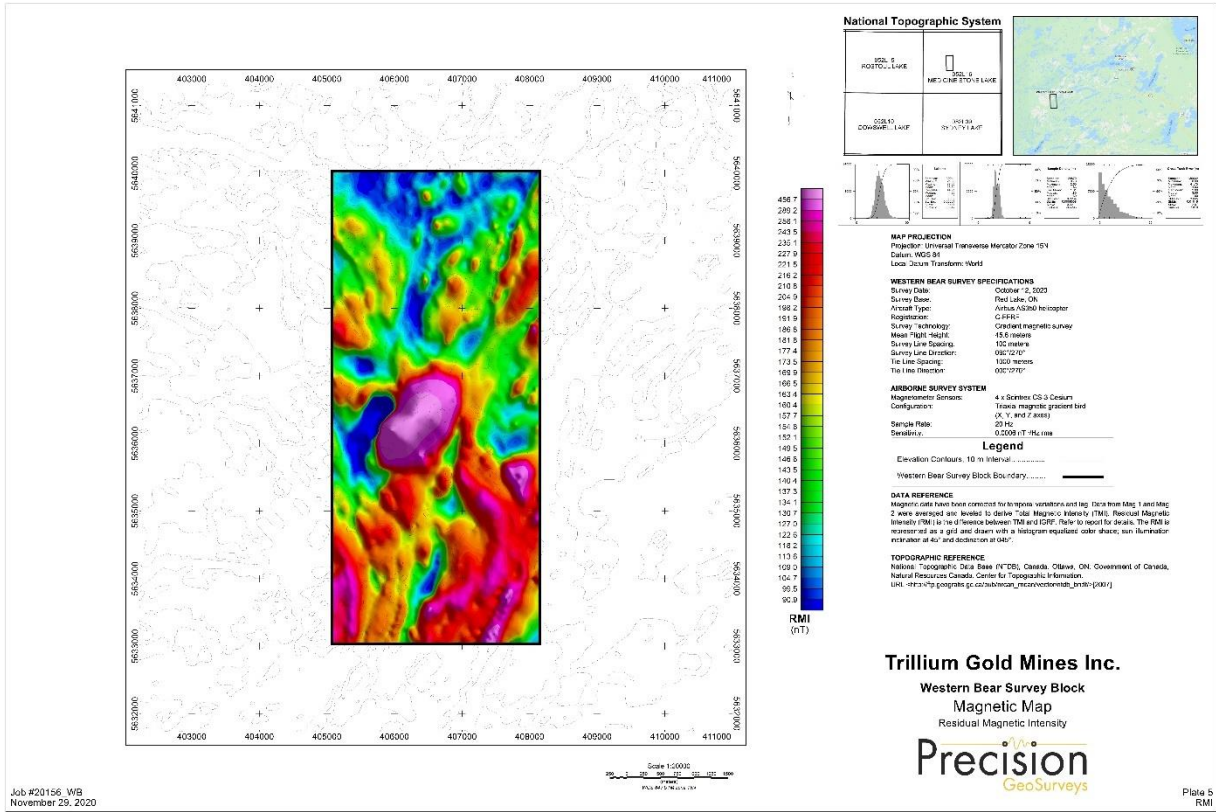
A handwritten signature in black ink, appearing to read "T. Hughes".

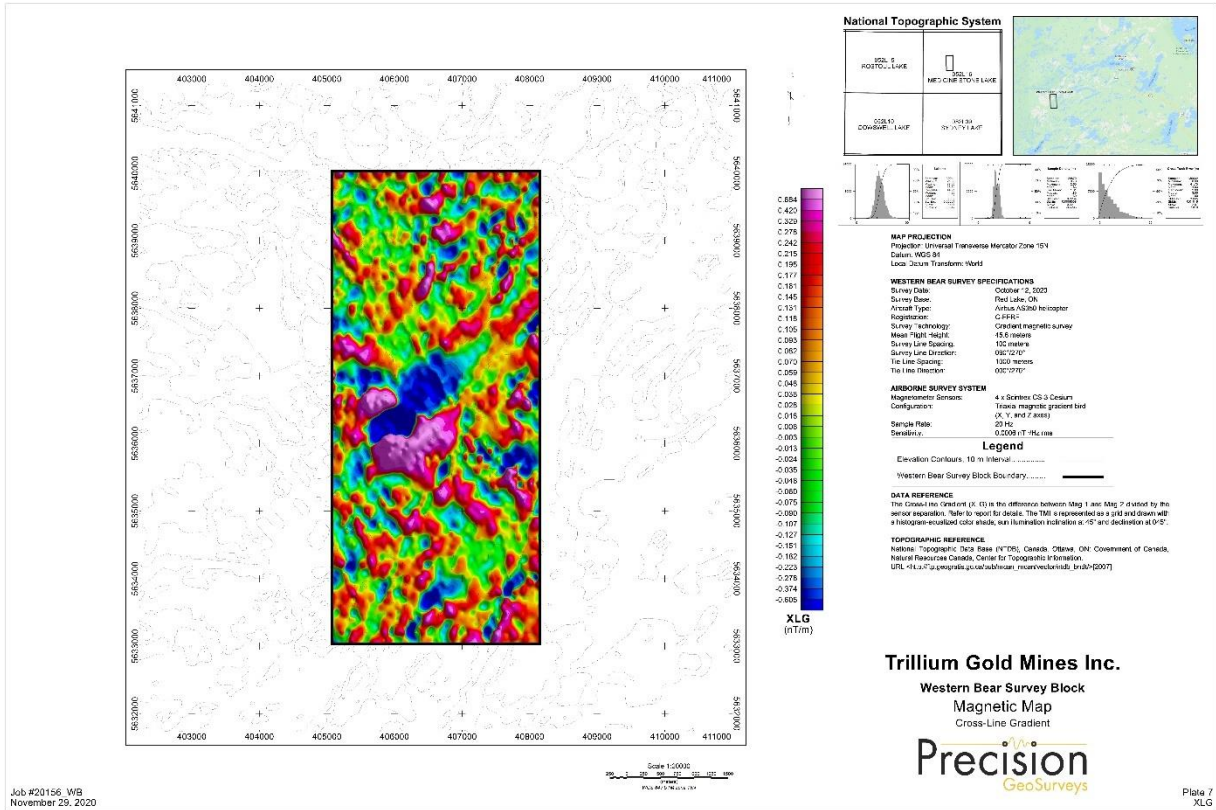
Dated this day, 2.12.21

APPENDIX I - Airborne Survey jpegs

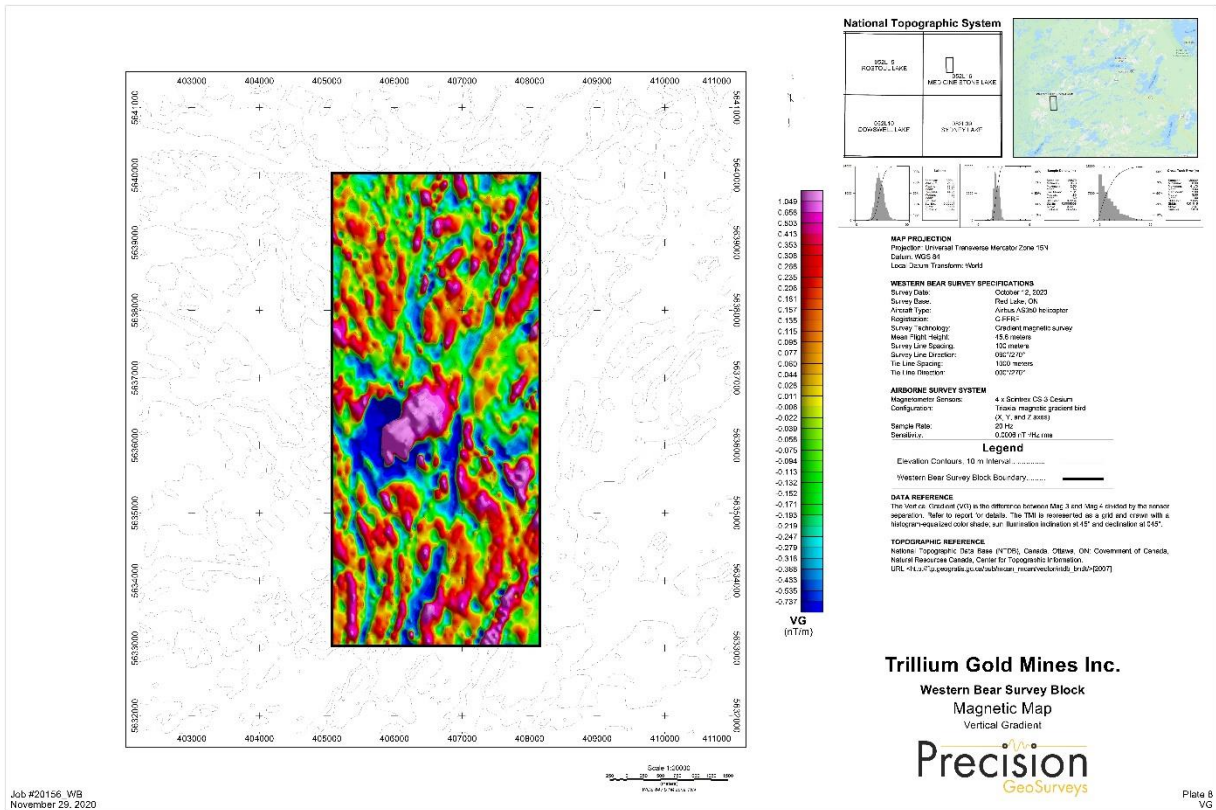




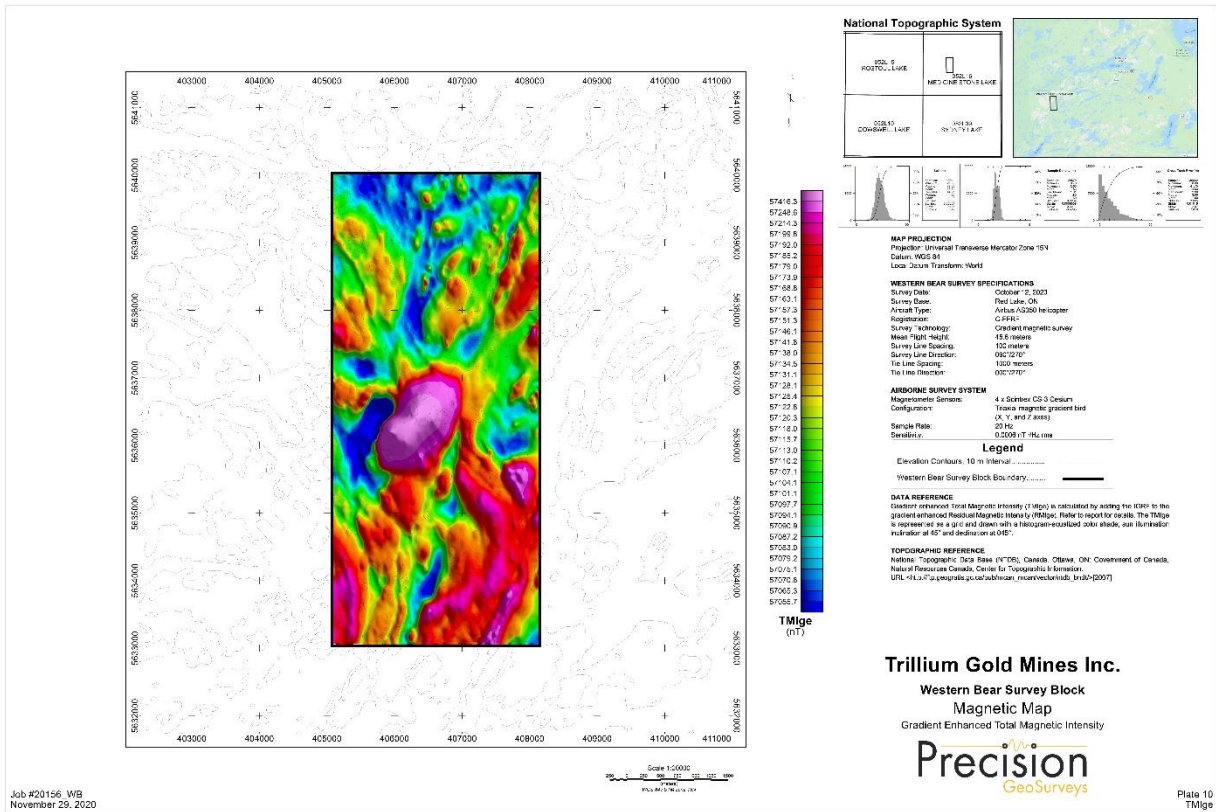
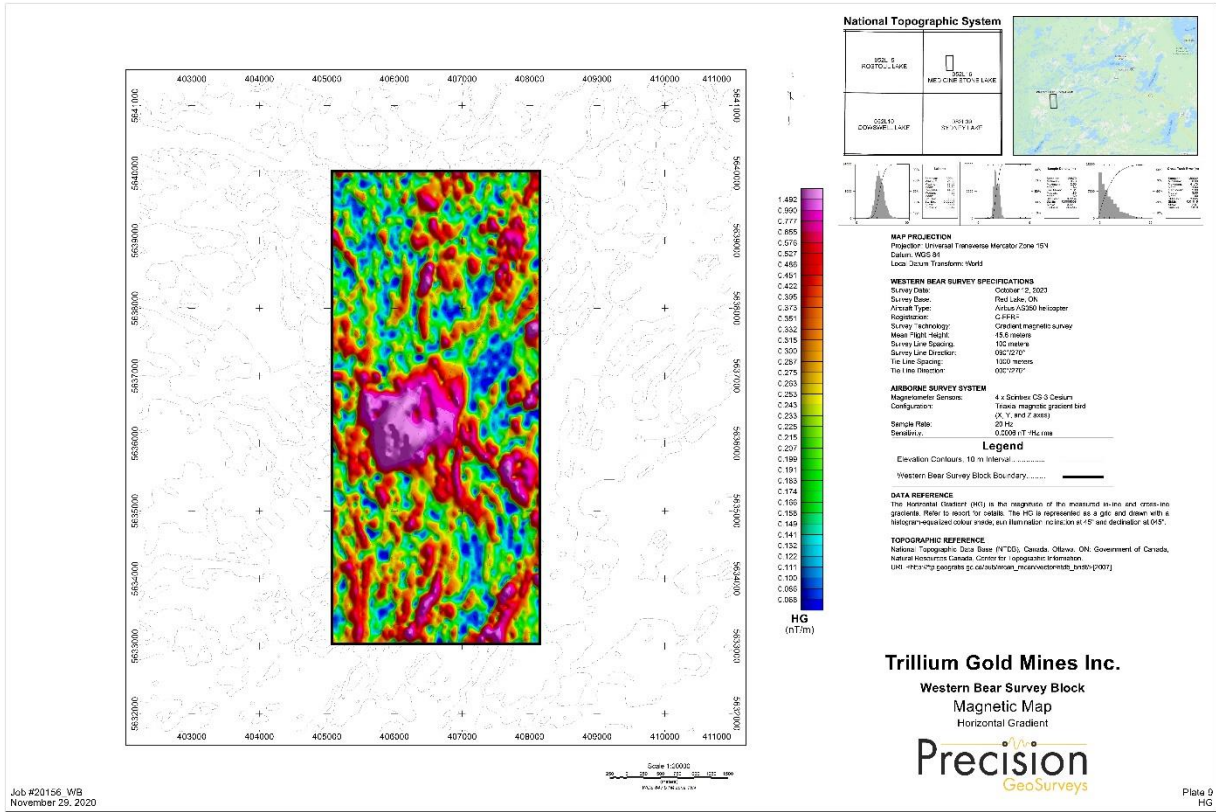


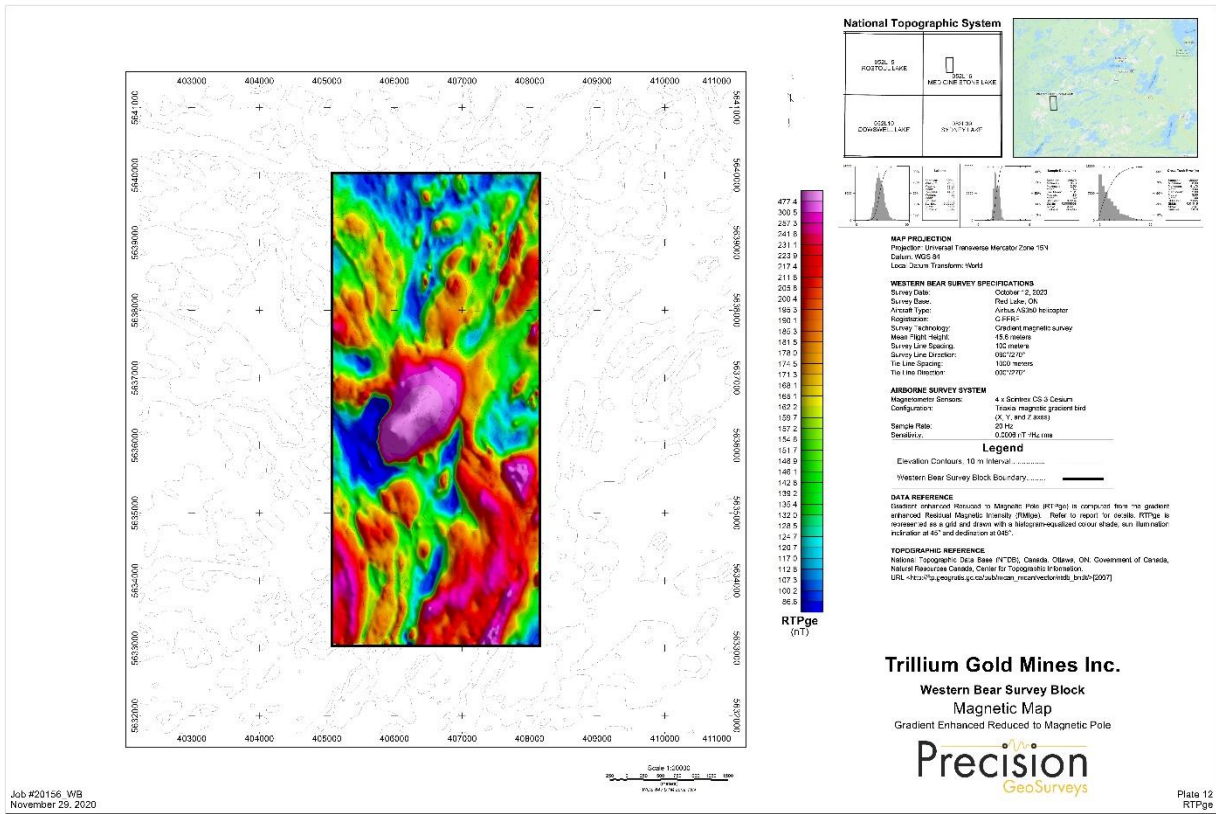
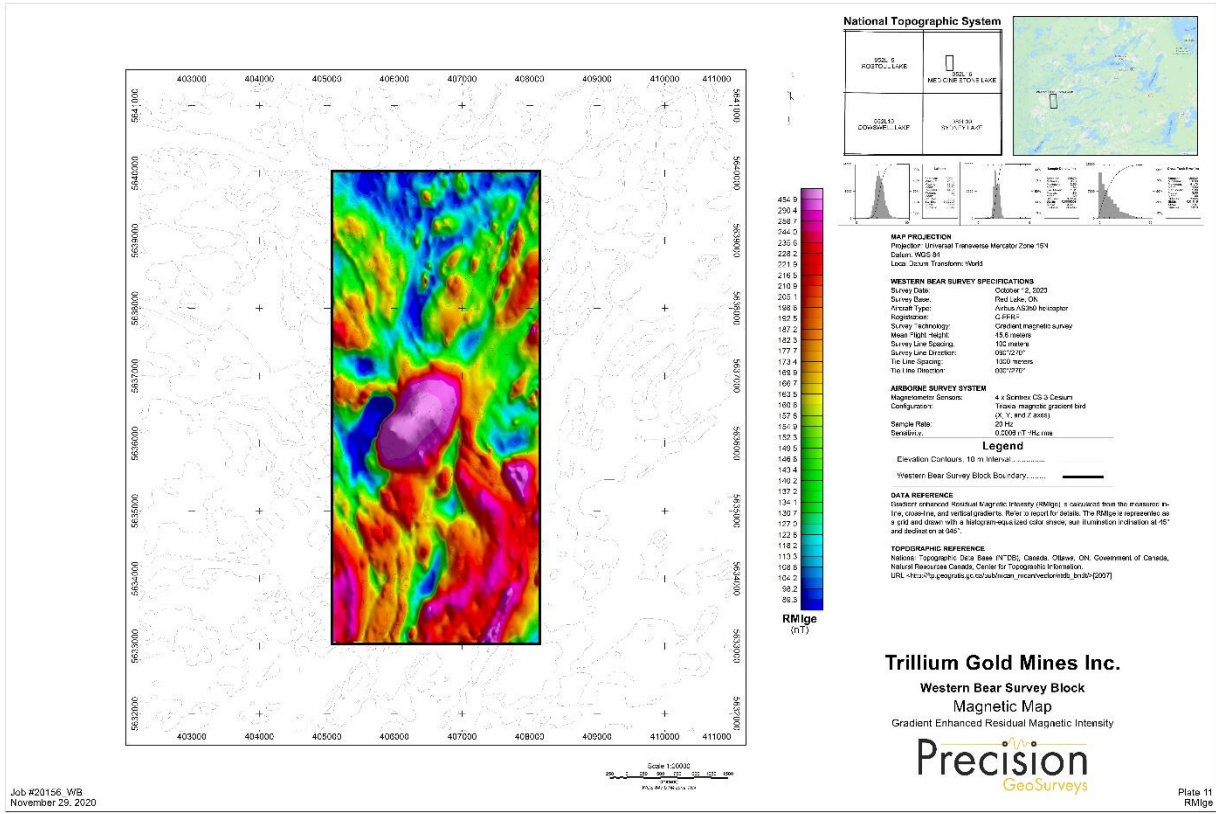


Job #20156_WB
 November 29, 2020



Job #20156_WB
 November 29, 2020





APPENDIX 2

Separate files:

Western Bear Airborne Geophysical Survey Logistics Report

PGW Geophysical report, Western Bear property

AIRBORNE GEOPHYSICAL SURVEY REPORT



Western Bear Survey Block
Red Lake, Ontario
Trillium Gold Mines Inc.

Precision GeoSurveys Inc.

www.precisiongeosurveys.com

Hangar 42 Langley Airport

21330 - 56th Ave., Langley, BC

Canada V2Y 0E5

604-484-9402

Shawn Walker, M.Sc., P.Geo.

December 2020

Job# 20157_WB

Table of Contents

Table of Contents	i
1.0 Introduction	1
1.1 Survey Area	1
1.2 Survey Specifications	3
2.0 Geophysical Data	3
2.1 Magnetic Data	4
3.0 Aircraft and Equipment	4
3.1 Aircraft	4
3.2 Geophysical Equipment.....	4
3.2.1 Triaxial Gradiometer.....	5
3.2.2 IMPAC.....	6
3.2.3 Magnetometer	8
3.2.4 Fluxgate Magnetometer.....	8
3.2.5 Magnetic Base Station.....	8
3.2.6 Laser Altimeter	9
3.2.7 Pilot Guidance Unit.....	10
3.2.8 GPS Navigation System	10
4.0 Survey Operations	11
4.1 Operations Base and Crew.....	11
4.2 Magnetic Base Station Specifications.....	11
4.3 Field Processing and Quality Control	13
5.0 Data Acquisition Equipment Checks	14
5.1 Lag Test	14
5.2 Heading Correction Test	15
6.0 Data Processing	15
6.1 Position Corrections	17
6.1.1 Lag Correction.....	17
6.2 Flight Height and Digital Terrain Model.....	17
6.3 Magnetic Processing	17
6.3.1 Temporal Variation Correction	18
6.3.2 IGRF Removal	18
6.3.3 Leveling and Micro-leveling	18
6.4 Magnetic Gradient.....	19
6.4.1 Horizontal Gradients	19
6.4.1.1 Gain Correction	20
6.4.1.2 Offset Correction	20
6.4.1.3 Total Horizontal Gradient.....	20
6.4.2 Vertical Gradient.....	21
6.4.3 Gradient Enhanced Magnetic Intensity.....	21
6.4.4 Gradient Enhanced Reduction to Magnetic Pole	21
7.0 Deliverables	22

7.1 Digital Data22
 7.1.1 Grids22
7.2 KMZ.....23
7.3 Maps23
7.4 Report24
8.0 Conclusions and Recommendations24

List of Figures

Figure 1: Western Bear survey area located in western Ontario.	1
Figure 2: Western Bear survey block (black) southwest of Red Lake, Ontario.	2
Figure 3: Plan View – Western Bear survey block.	2
Figure 4: Terrain View – Western Bear survey block.	3
Figure 5: Survey helicopter equipped with geophysical equipment.	5
Figure 6: Schematic diagram of magnetic gradiometer system.	6
Figure 7: IMPAC data acquisition system.	7
Figure 8: AGIS operator display.	7
Figure 9: View of CS-3 cesium vapor magnetometers.	8
Figure 10: Billingsley TFM100G2 triaxial fluxgate magnetometer.	8
Figure 11: GEM GSM-19T proton precession magnetometer.	9
Figure 12: Opti-Logic RS800 Rangefinder laser altimeter.	9
Figure 13: PGU screen displaying navigation information.	10
Figure 14: Hemisphere R330 GPS receiver.	11
Figure 15: GEM 5 and GEM 6 magnetic base stations.	12
Figure 16: GEM 5 (left) and GEM 6 (right) magnetic base stations at Poplar Point Resort.	12
Figure 17: Histogram showing survey bird elevation vertically above ground.	13
Figure 18: Histogram showing magnetic sample density.	14
Figure 19: Histogram showing cross track error of survey bird.	14
Figure 20: Magnetic data processing flow.	16

List of Tables

Table 1: Survey flight line specifications.	3
Table 2: Magnetometer details.	6
Table 3: List of survey crew members.	11
Table 4: Magnetic base station locations.	12
Table 5: Contract survey specifications.	13
Table 6: Survey lag correction values.	15
Table 7: Heading error test data.	15
Table 8: Geometric sensor relationship used to calculate magnetic gradients.	19

List of Appendices

- Appendix A: Polygon Coordinates
- Appendix B: Equipment Specifications
- Appendix C: Digital File Descriptions

List of Western Bear Survey Block Plates (Scale 1:20,000)

- Plate 1: Western Bear – Actual Flight Lines (FL)
- Plate 2: Western Bear – Digital Terrain Model (DTM)
- Plate 3: Western Bear – Total Magnetic Intensity with Actual Flight Lines (TMI_wFL)
- Plate 4: Western Bear – Total Magnetic Intensity (TMI)
- Plate 5: Western Bear – Residual Magnetic Intensity (RMI)
- Plate 6: Western Bear – In-Line Gradient (ILG)
- Plate 7: Western Bear – Cross-Line Gradient (XLG)
- Plate 8: Western Bear – Vertical Gradient (VG)
- Plate 9: Western Bear – Horizontal Gradient (HG)
- Plate 10: Western Bear – Gradient Enhanced Total Magnetic Intensity (TMIge)
- Plate 11: Western Bear – Gradient Enhanced Residual Magnetic Intensity (RMIge)
- Plate 12: Western Bear – Gradient Enhanced Reduced to Magnetic Pole (RTPge) of RMIge

1.0 Introduction

This report outlines the geophysical survey operations and data processing procedures taken during the high resolution helicopter-borne magnetic gradiometer survey flown over the Western Bear survey block for Trillium Gold Mines Inc. The survey block is located in western Ontario (Figure 1) and it was flown on October 12, 2020.



Figure 1: Western Bear survey area located in western Ontario.

1.1 Survey Area

The Western Bear survey block is centered approximately 38 km southwest of Red Lake, Ontario (Figure 2).



Figure 2: Western Bear survey block (black) southwest of Red Lake, Ontario.

The survey was flown at 100 m line spacing at a heading of 090°/270° normal to dominant geological structures; tie lines were flown at 1000 m spacing at a heading of 000°/180° (Figures 3 and 4).



Figure 3: Plan View – Western Bear survey block with actual flight lines in yellow and survey block boundary in red.

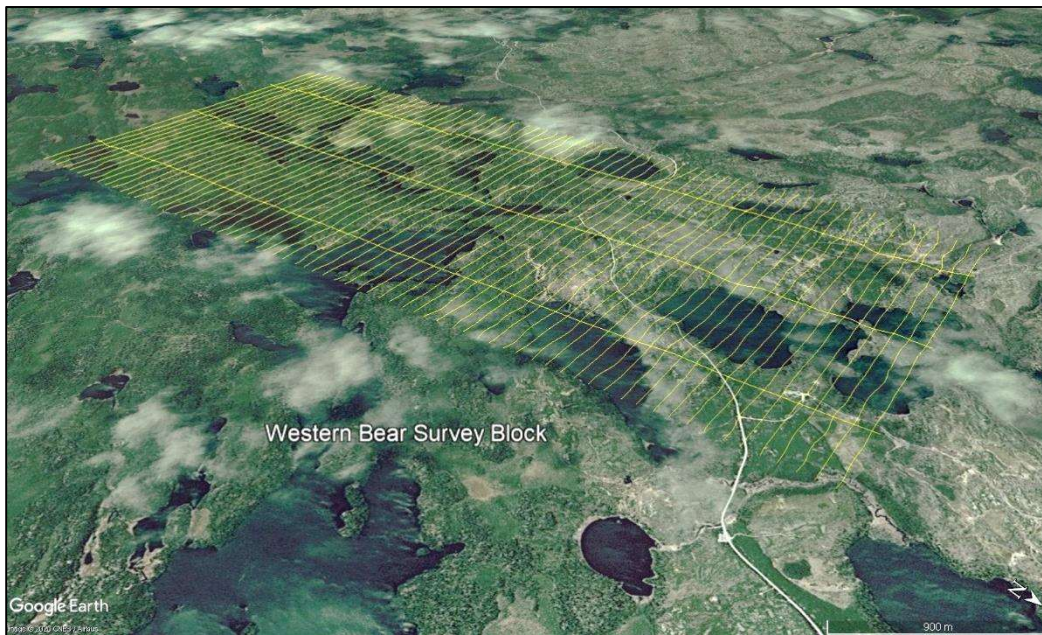


Figure 4: Terrain View – Western Bear survey block with actual flight lines displayed in yellow.

1.2 Survey Specifications

The geodetic system used for the geophysical survey was WGS 84 in UTM Zone 15N. A total of 237.4 line km was flown over an area of 21.6 km² (Table 1). Polygon coordinates for the Western Bear survey block are specified in Appendix A.

Survey Block	Area (km ²)	Line Type	No. of Lines Planned	No. of Lines Completed	Line Spacing (m)	Line Orientation (UTM grid)	Survey Height (m)	Total Planned Line km	Total Actual km Flown
Western Bear	21.6	Survey	70	70	100	090°/270°	40	216	216.4
		Tie	3	3	1000	000°/180°	40	21	21.0
		Total:	73	73			40	237	237.4

Table 1: Survey flight line specifications.

2.0 Geophysical Data

Geophysical data are collected in a variety of ways and are used for many purposes including aiding in the determination of geology, mineral deposits, oil and gas deposits, geotechnical investigations, contaminated land sites, and UXO (unexploded ordnance) detection.

For the purposes of this survey, airborne gradient magnetic data were collected to serve in geological mapping and exploration for mineral deposits.

2.1 Magnetic Data

Magnetic surveying is the most common airborne geophysical technology used for both mineral and hydrocarbon exploration. Aeromagnetic surveys measure and record the total intensity of the magnetic field at the magnetometer sensor, which is a combination of the desired magnetic field generated in the Earth as well as small variations due to temporal effects of the constantly varying solar wind and the magnetic field of the survey aircraft. By subtracting the temporal, regional, and aircraft effects, the resulting aeromagnetic maps show the spatial distribution and relative abundance of magnetic minerals - most commonly the iron oxide mineral magnetite - in the upper levels of Earth's crust, which in turn are related to lithology, structure, and alteration of bedrock. Survey specifications, instrumentation, and interpretation procedures depend on the objectives of the survey. Magnetic surveys are typically performed for:

- Geological Mapping - to aid in mapping lithology, structure, and alteration.
- Depth to Basement Mapping - for exploration in sedimentary basins or mineralization associated with the basement surface.

3.0 Aircraft and Equipment

All geophysical and subsidiary equipment were carefully installed on an aircraft by Precision GeoSurveys to collect gradient magnetic data.

3.1 Aircraft

Precision GeoSurveys flew the survey using an Airbus AS350 helicopter, registration C-FFRF, at a nominal height of 40 m AGL.

3.2 Geophysical Equipment

The survey aircraft (Figure 5) was equipped with a slung bird-type triaxial magnetic gradient system, data acquisition system, laser altimeter, barometer, pilot guidance unit (PGU), and GPS navigation systems. In addition, two magnetic base stations were used to record temporal magnetic variations.

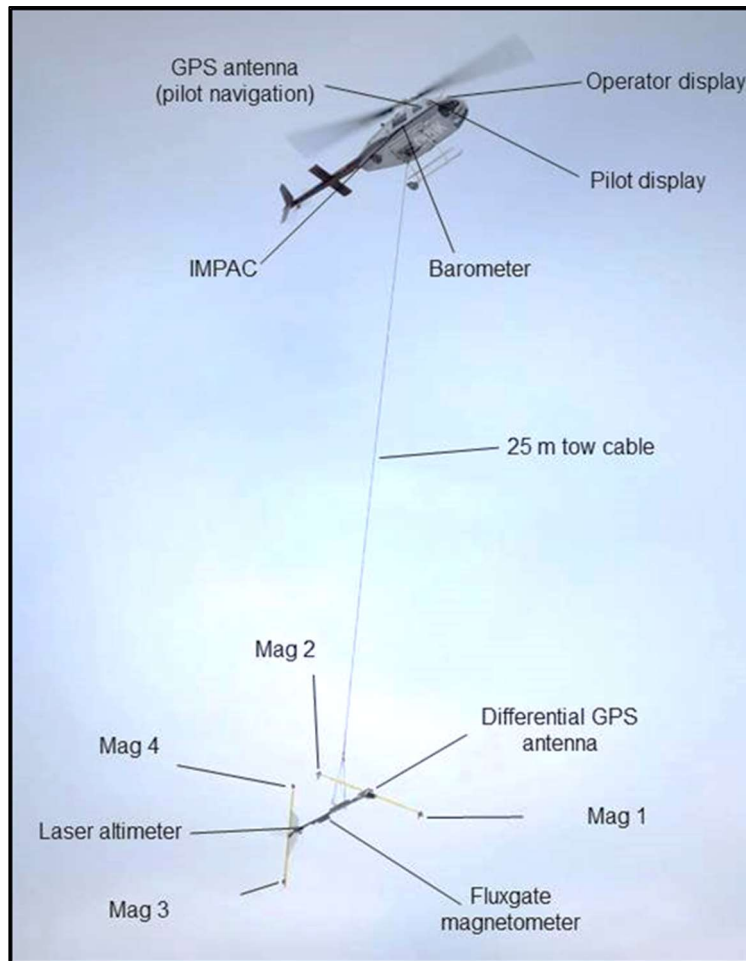


Figure 5: Survey helicopter equipped with geophysical equipment and the triaxial magnetic gradient bird-type configuration slung 25 m below the helicopter.

3.2.1 Triaxial Gradiometer

The primary geophysical technology used on this survey was a slung magnetic gradiometer, custom designed and manufactured by Precision GeoSurveys. The gradiometer bird is constructed completely from non-magnetic and non-conductive materials and provides the required sensor separation for triaxial gradient measurements in stable flight, while incorporating a laser altimeter, fluxgate magnetometer, and a GPS antenna. It is attached to the helicopter by a 25 m long tow cable that eliminates magnetic interference from the aircraft and holds the weight of the system. A shear pin is used as a safety weak link. Magnetic, laser altimeter, attitude, and GPS data are transmitted to the helicopter by wires routed along the tow cable. By design, this gradiometer separates the electronic equipment from the magnetic sensors to allow for cleaner data collection unaffected by electronic noise and the aircraft's magnetic fields. The bird weighs approximately 80 kg and can be disassembled into multiple components for ease of transport.

In total, the gradiometer (Figure 6) contains four Scintrex CS-3 cesium vapor magnetic sensors (Table 2) individually measuring the total magnetic intensity at their respective positions. The unique arrangement of the sensors allows direct measurement of the geomagnetic field gradient in the X (cross-line) axis with the two forward sensors (Mag 1 and Mag 2) and the Z (vertical) axis with the two aft sensors (Mag 3 and Mag 4).

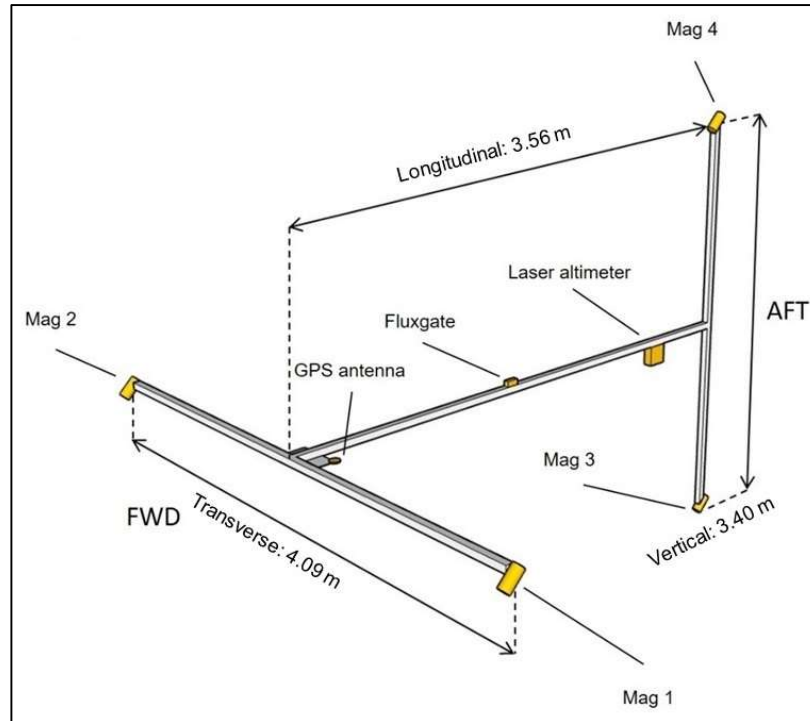


Figure 6: Schematic diagram of magnetic gradiometer system showing triaxial sensor separations. Not to scale.

Position	Location	Model	Serial Number
Mag 1	Forward left	Scintrex CS-3	0706248
Mag 2	Forward right	Scintrex CS-3	0612211
Mag 3	Aft lower	Scintrex CS-3	2008597
Mag 4	Aft upper	Scintrex CS-3	0712302

Table 2: Magnetometer details.

3.2.2 IMPAC

The Integrated Multi-Parameter Acquisition Console (IMPAC) (Figure 7), manufactured by Nuvia Dynamics Inc. (previously Pico Envirotec Inc.), is the main computer used in integrated data recording, data synchronizing, providing real-time quality control data for the geophysical operator display, and the generation of navigation information for the pilot and operator display systems.



Figure 7: IMPAC data acquisition system.

IMPAC uses the Microsoft Windows operating system and geophysical parameters are based on Nuvia's Airborne Geophysical Information System (AGIS) software. Depending on survey specifications, information such as magnetic field, electromagnetic response, total gamma count, counts of various radioelements (K, U, Th, etc.), cosmic radiation, barometric pressure, atmospheric humidity, temperature, aircraft attitude, navigation parameters, and GPS status can all be monitored on the AGIS on-board display (Figure 8).

While in flight, raw magnetic response, magnetic fourth difference, compensated and uncompensated data, radiometric spectra, aircraft position, survey altitude, cross track error, and other parameters are recorded and can be viewed by the geophysical operator for immediate QC (quality control). Additional software allows for post or real time magnetic compensation and radiometric calibration.

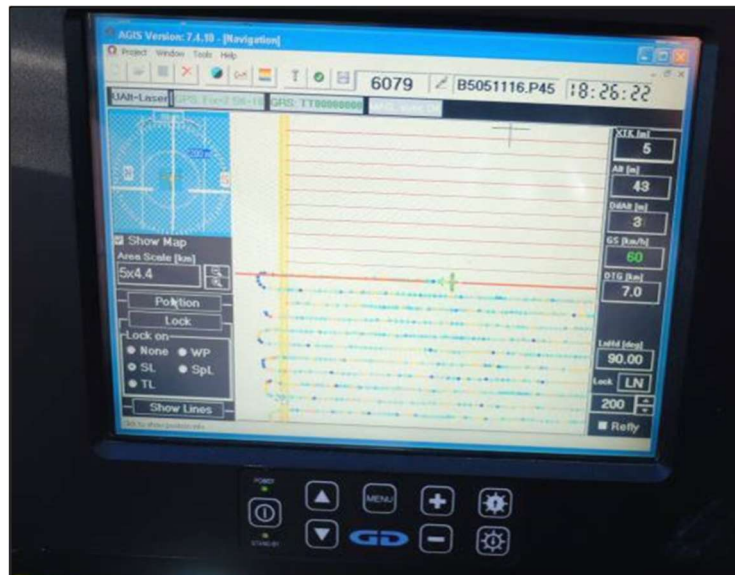


Figure 8: AGIS operator display showing real time flight line recording and navigation parameters. Additional windows display real-time geophysical data to operator.

3.2.3 Magnetometer

The survey was flown with four Scintrex CS-3 split-beam cesium vapor magnetometers (Figure 9) mounted in a non-magnetic and non-conductive slung bird-type configuration. The magnetometers were orientated at 45 degrees with respect to the horizontal to couple with local magnetic field at the Western Bear survey block.



Figure 9: View of CS-3 cesium vapor magnetometers.

3.2.4 Fluxgate Magnetometer

As the gradient bird flies along a survey line, small attitude changes (pitch, roll, and yaw) are recorded by a triaxial fluxgate magnetometer (Figure 10). The fluxgate consists of three magnetic sensors, X, Y, and Z, operating independently and simultaneously. Each sensor has an analog output corresponding to the declination and inclination component of the ambient magnetic field along its axis. Response of the sensors is proportional to the cosine of the angle between the applied field and the sensor's sensitive axis.



Figure 10: Billingsley TFM100G2 triaxial fluxgate magnetometer.

3.2.5 Magnetic Base Station

Temporal variations of Earth's magnetic field, particularly diurnal, were monitored and recorded by two GEM GSM-19T base station magnetometers. They were operated at all times while

airborne data were being collected. The base stations were located in an area with low magnetic gradient, away from electric power transmission lines and moving ferrous objects, such as motor vehicles, that could affect the survey data integrity.

The GEM GSM-19T magnetometer (Figure 11) with integrated GPS time synchronization uses proton precession technology with absolute accuracy of ± 0.20 nT and sensitivity of 0.15 nT at 1 Hz. Base station magnetic data were recorded on internal solid-state memory and downloaded onto a field laptop computer using a serial cable and GEMLink 5.4 software. Profile plots of the base station readings were generated, updated, and reviewed at the end of each survey day.



Figure 11: GEM GSM-19T proton precession magnetometer.

3.2.6 Laser Altimeter

Terrain clearance is measured by an Opti-Logic RS800 Rangefinder laser altimeter (Figure 12) attached to the aft end of the gradient bird. The RS800 laser is a time-of-flight sensor that measures distance by a rapidly modulated and collimated laser beam that creates a dot on the target surface. The maximum range of the laser altimeter is 700 m off natural surfaces with accuracy of ± 1 m on 1 x 1 m diffuse target with 50% ($\pm 20\%$) reflectivity. Within the sensor unit, reflected signal light is collected by the lens and focused onto a photodiode. Through serial communications and digital outputs, ground clearance data are transmitted to an RS-232 compatible port and recorded and displayed by the AGIS and PGU at 10 Hz in meters.

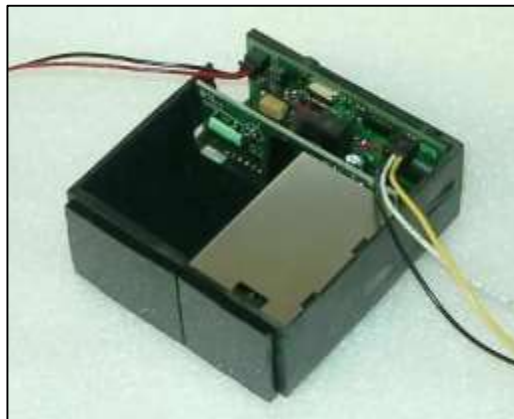


Figure 12: Opti-Logic RS800 Rangefinder laser altimeter.

3.2.7 Pilot Guidance Unit

Steering and elevation (ground clearance) information is continuously provided to the pilot by the Pilot Guidance Unit (PGU). The graphical display is mounted on top of the aircraft's instrument panel, remotely from the data acquisition system. The PGU is the primary navigation aid (Figure 13) to assist the pilot in keeping the aircraft on the planned flight path, heading, speed, and at the desired ground clearance.

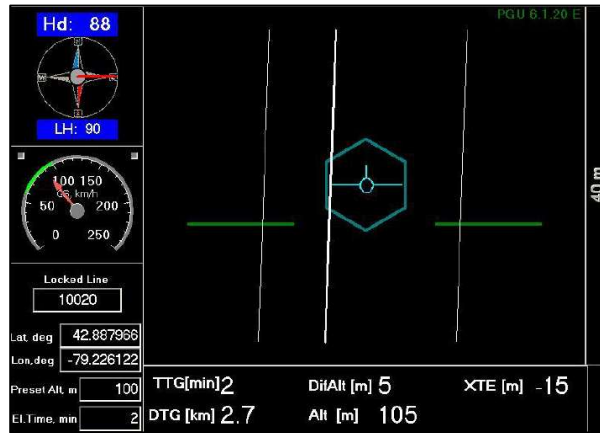


Figure 13: PGU screen displaying navigation information.

PGU information is displayed on a full VGA 600 x 800 pixel 7 inch (17.8 cm) LCD display. The CPU for the PGU is contained in a PC-104 console and uses Microsoft Windows operating system control, with input from the GPS antenna on the aircraft, laser altimeter, and AGIS.

3.2.8 GPS Navigation System

A Hemisphere R120 GPS receiver and a Novatel GPS antenna on the aircraft integrated with the AGIS navigation system and pilot display (PGU) provide accurate navigational information and control. A Hemisphere R330 GPS receiver (Figure 14) located in the helicopter connected to a Novatel GPS antenna located on the triaxial magnetic gradient bird airframe provide accurate position data for the bird independent of pilot navigation. The R120 and R330 GPS receivers support fast updates and outputs messages at a rate of up to 20 Hz (20 times per second); delivering sub-meter positioning accuracy in three dimensions. They support GNSS (GPS/GLONASS) L1 and L2 signals.

The Hemisphere receivers support differential correction methods including L-Band, RTK, SBAS, and Beacon. They employ innovative Hemisphere GPS Eclipse SureTrack technology, which allows modeling the phase on satellites that the airborne unit is currently tracking. With SureTrack technology, dropouts are reduced and speed of the signal reacquisitions is increased; enhancing accurate positioning when base corrections are not available.



Figure 14: Hemisphere R330 GPS receiver.

4.0 Survey Operations

The survey was flown on October 12, 2020 in late fall conditions; cool, low overcast, and light precipitation. The experience of the pilot ensured that the data quality objectives were met, and that safety of the flight crew was never compromised given the potential risks involved in airborne geophysical surveying. Field processing and quality control checks were performed daily.

4.1 Operations Base and Crew

The base of operation for the Western Bear survey was at Poplar Point Resort, east of the survey block.

Precision's geophysical crew consisted of three members (Table 3):

Crew Member	Position
Jordan Hatch	Helicopter survey pilot
Jonathan Passiniemi	Geophysical operator and electronics technician
Shawn Walker, M.Sc., P.Geol.	Geophysicist – data processor, mapping, and reporting

Table 3: List of survey crew members.

4.2 Magnetic Base Station Specifications

Changes in the Earth's magnetic field over time, such as diurnal variations, magnetic pulsations, and geomagnetic storms, were measured and recorded by two stationary GEM GSM-19T proton precession magnetometers. The magnetic base stations were installed at Poplar Point Resort in an area (Table 4; Figures 15 and 16) of low magnetic noise away from metallic items such as ferromagnetic objects, vehicles, and power lines that could affect the base stations and ultimately the survey data.

Station Name	Easting/Northing	Latitude/Longitude	Datum/Projection
GEM 5 S/N 1094678	446257 m E 5641970 m N	51° 55' 36.70" N 93° 45' 52.94" W	WGS 84, Zone 15N
GEM 6 S/N 5087249	446251 m E 5641970 m N	51° 55' 36.70" N 93° 45' 53.24" W	WGS 84, Zone 15N

Table 4: Magnetic base station locations.

Magnetic readings were reviewed at regular intervals to ensure that no airborne data were collected during periods of high magnetic activity (greater than 10 nT change per 5 minute period).



Figure 15: GEM 5 and GEM 6 magnetic base stations located east of the Western Bear survey block.



Figure 16: GEM 5 (left) and GEM 6 (right) magnetic base stations at Poplar Point Resort.

4.3 Field Processing and Quality Control

Survey data were transferred from the aircraft’s data acquisition system onto a USB memory stick and copied onto a field data processing laptop on a flight by flight basis. The raw data files in PEI binary data format were converted into Geosoft GDB database format. Using Geosoft Oasis Montaj 9.8, the data were inspected to ensure compliance with contract specifications (Table 5; Figures 17 to 19).

Parameter	Specification	Tolerance
Position	Line Spacing	Flight line deviation within 8 m L/R from ideal flight path. No exceedance for more than 1 km.
	Height	Nominal flight height of 40 m above ground level (AGL) with tolerance of ± 10 m. No exceedance for more than 1 km, provided deviation is not due to tall trees, topography, mitigation of wildlife/livestock harassment, cultural features, or other obstacles beyond the pilot’s control.
	GPS	GPS signals from four or more satellites must be received at all times, except where signal loss is due to topography. No exceedance for more than 1 km.
Magnetics	Temporal/Diurnal Variations	Non-linear temporal magnetic variations within 10 nT of a linear chord of length 5 minutes.
	Normalized 4 th Difference	Magnetic data within 0.05 nT peak to peak. No exceedance for distances greater than 1 km or more, provided noise is not due to geological or cultural features.

Table 5: Contract survey specifications.

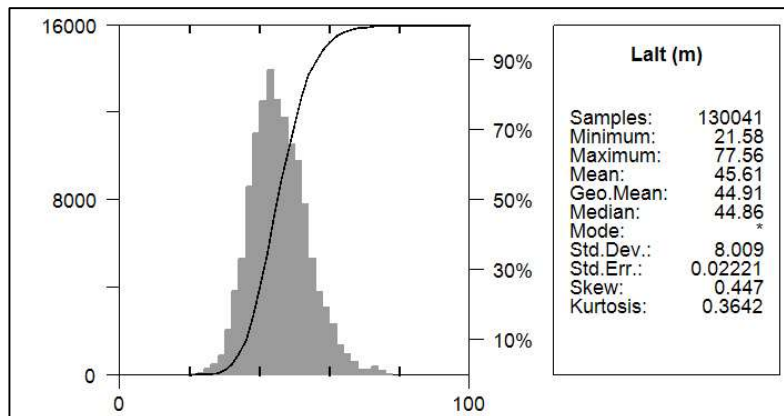


Figure 17: Histogram showing survey bird elevation vertically above ground.

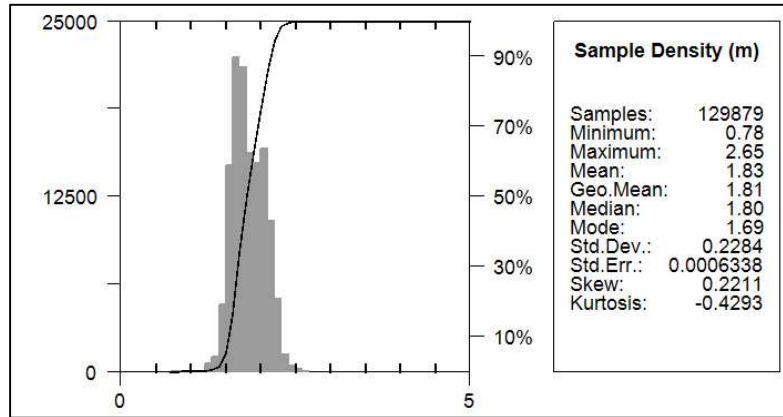


Figure 18: Histogram showing magnetic sample density. Horizontal distance in meters between adjacent measurement locations; magnetic sample frequency 20 Hz.

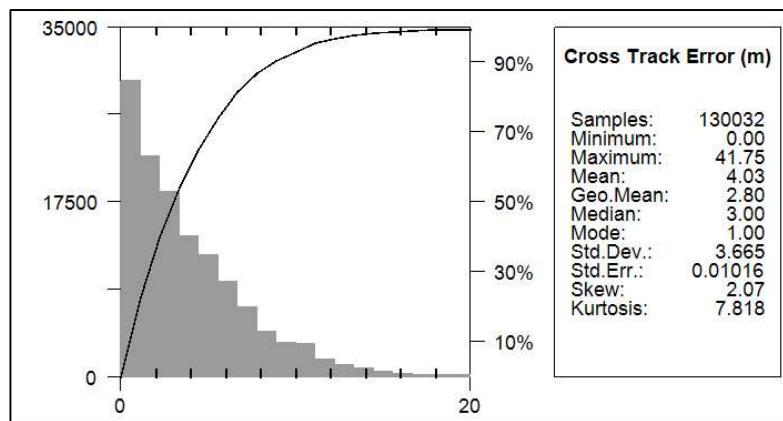


Figure 19: Histogram showing cross track error of survey bird.

5.0 Data Acquisition Equipment Checks

Equipment tests were conducted at the start of the survey to ensure compliance with contract specifications and to deliver high quality airborne geophysical data. A lag test was conducted for both the laser altimeter and magnetometers. For the airborne magnetometers, a heading error test was flown.

5.1 Lag Test

A lag test was performed to determine the difference in time the digital reading was recorded for the magnetometer and laser altimeter with the position fix time that the fiducial of the reading was obtained by the GPS system resulting from a combination of system lag and different locations of the various sensors and the GPS antenna. The test was flown in the four orthogonal survey headings over an identifiable magnetic anomaly at survey speed and height. The resulting data (Table 6) were used to correct for time and position.

Instrument	Source	Lag Fiducial	Correction (sec)
Mag 1	Logging equipment	42	2.1
Mag 2	Logging equipment	42	2.1
Mag 3	Logging equipment	42	2.1
Mag 4	Logging equipment	42	2.1
Laser	Sharp gully	6	0.6

Table 6: Survey lag correction values. Magnetic data at 20 Hz; laser altimeter at 10 Hz.

5.2 Heading Correction Test

To determine heading errors and other offsets, a cloverleaf pattern flight test was conducted at high altitude. The cloverleaf test was flown in the same orthogonal headings as the survey and tie lines (000°/090°/180°/270° in the case of this survey) at >2500 m AGL in an area with low magnetic gradient. For all four directions the gradient bird must pass over the same mid-point, at the same elevation, with the bird flown straight and level. The difference in magnetic values obtained in reciprocal headings is the heading error. Results of the test flight are summarized in Table 7.

Heading	Mag 1 Correction (nT)	Mag 2 Correction (nT)	Mag 3 Correction (nT)	Mag 4 Correction (nT)
000°	-2.27	-2.86	-2.90	-3.09
090°	1.21	1.50	1.39	1.53
180°	2.19	1.90	1.84	1.98
270°	-1.13	-0.54	-0.33	-0.42
Total:	0.00	0.00	0.00	0.00

Table 7: Heading error test data.

6.0 Data Processing

After all data were collected, several procedures were undertaken to ensure that the data met a high standard of quality. All magnetic data recorded by the AGIS were converted into Geosoft or ASCII file formats using Nuvia Dynamics software. Further processing (Figure 20) was carried out using Geosoft Oasis Montaj 9.8 geophysical processing software along with proprietary processing algorithms.

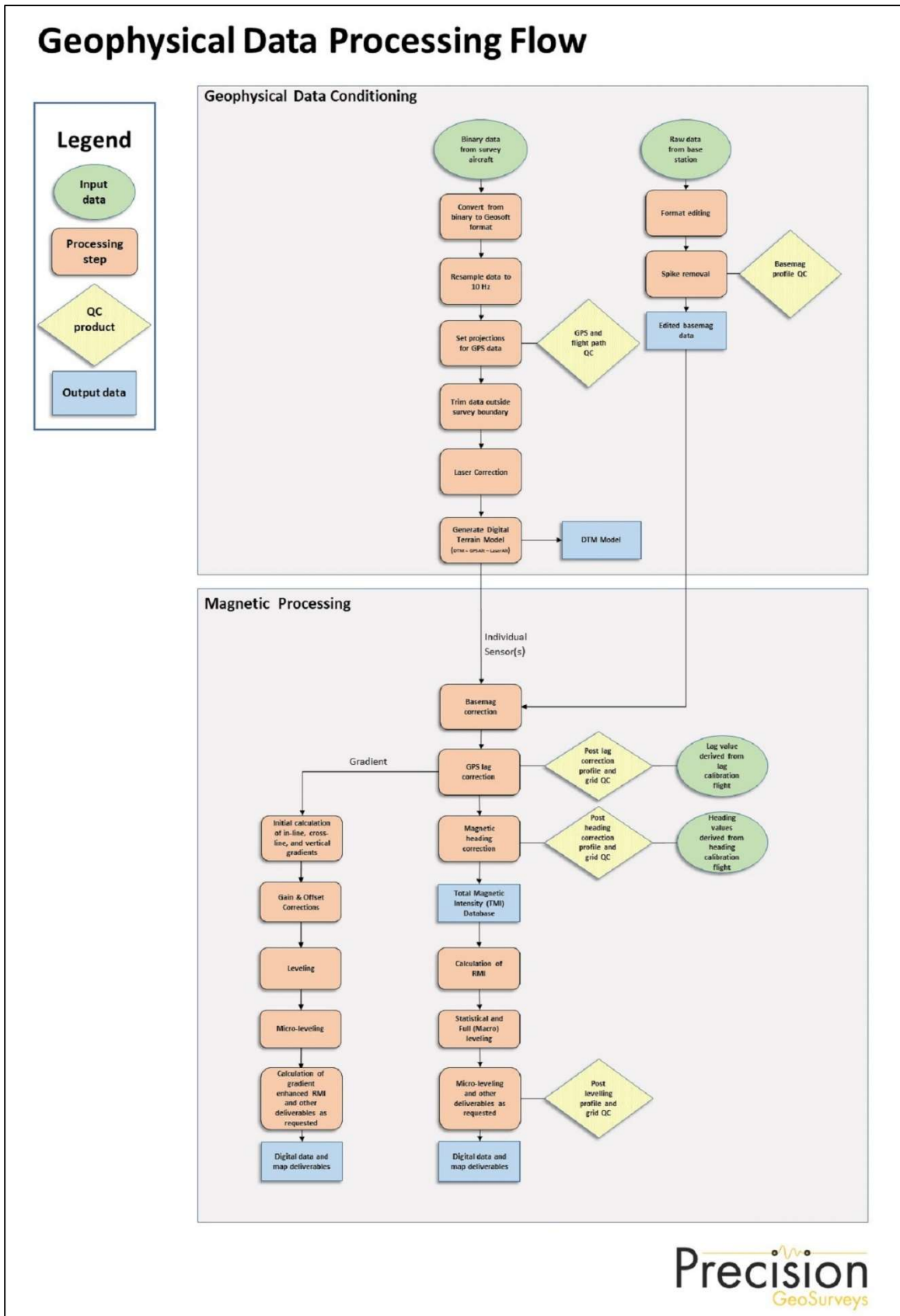


Figure 20: Magnetic data processing flow.

6.1 Position Corrections

In order to collect high resolution geophysical data, the location at which the data were collected and recorded must be accurate.

6.1.1 Lag Correction

A correction for lag error was applied to the geophysical data recorded at each individual sensor to compensate for the combination of lag in the recording system and the sensing instrument flying in a different location from the GPS antenna, as determined during the lag test. Validity of the lag corrections was confirmed by the absence of grid corrugations in adjoining reciprocal lines.

6.2 Flight Height and Digital Terrain Model

Laser altimeters are unable to provide valid data over glassy water or fog which dissipate the laser so that a “zero” reading is obtained. In these cases, estimates of correct height are inserted manually. Dense vegetation generates high frequency variations from leaf and branch reflections. A Rolling Statistics filter is applied to the lag corrected (0.6 seconds lag) laser altimeter data to remove vegetation clutter followed by a Low Pass filter to smooth out the laser altimeter profile to eliminate isolated high frequency noise and generate a surface closely corresponding to the actual ground profile.

A Digital Terrain Model (DTM) channel was calculated by subtracting the processed laser altimeter data from the filtered GPS altimeter data defined by the WGS 84 ellipsoidal height. DTM accuracy is affected by the geometric relationship between the GPS antenna and the laser altimeter as well as flight attitude of the aircraft, slope of the ground, sample density, and satellite geometry.

6.3 Magnetic Processing

Magnetic data from each individual sensor were corrected for temporal variations (including diurnal) and lag. The data were examined for magnetic noise and spikes, which were removed as required. The background magnetic field, International Geomagnetic Reference Field (IGRF) of the Earth was removed. Survey and tie line data of the resulting residual magnetic field were leveled. Magnetic gradients in the X, Y, and Z axes were determined to provide in-line, cross-line, and vertical gradients, respectively

6.3.1 Temporal Variation Correction

The intensity of Earth's magnetic field varies with location and time. The time variable, known as diurnal or more correctly temporal variation, is removed from the recorded airborne data to provide the desired magnetic field at a specified location. Magnetic data from base station GEM 6 were used for correcting the airborne magnetic survey data, and GEM 5 data were retained for backup. The data were edited, plotted, and merged into a Geosoft database (.GDB) on a daily basis.

Base station measurements were averaged to establish a magnetic reference datum of 57535.44 nT. Magnetic deviations relative to the reference datum were used to calculate the observed variations of the Earth's magnetic field over time. The airborne magnetic data were then corrected for temporal variations by subtracting the base station deviations from the data collected on the aircraft, effectively removing the effects of diurnal and other temporal variations.

6.3.2 IGRF Removal

The International Geomagnetic Reference Field (IGRF) model is the empirical representation of Earth's dynamic magnetic field (main core field without external sources) collected and disseminated from satellite data and from magnetic observatories around the world. The IGRF has historically been revised and updated every five years by a group of modellers associated with the International Association of Geomagnetism and Aeronomy (IAGA).

The initial unlevelled Residual Magnetic Intensity (RMI) was calculated by taking the difference between the 13th generation IGRF (IGRF-13, released in December 2019) and the non-levelled Total Magnetic Intensity (TMI) to create a more valid model of individual near-surface magnetic anomalies. This model is independent of time to allow for other magnetic data (previous or future) to be more easily incorporated into each survey database.

6.3.3 Leveling and Micro-leveling

Small inconsistencies in flight height and line orientation result in small spatial variabilities in magnetic intensity measured at the intersection points of survey lines and tie lines. Using the initial Residual Magnetic Intensity (RMI) data from the average of Mag 1 and Mag 2 (TMI with the IGRF removed), RMI data from survey and tie lines were leveled to each other. Two types of leveling were applied to the corrected data: conventional leveling and micro-leveling. There were two components to conventional leveling: statistical leveling to level tie lines and full leveling to level survey lines. The statistical leveling method corrected the SL/TL intersection errors that follow a specific pattern or trend. Through the error channel, an algorithm calculated a least-squares trend line and derived a trend error curve, which was then added to the channel to

be leveled. The second component was full leveling. This adjusted the magnetic value of the survey lines so that all lines matched the trended tie lines at each intersection point.

Following statistical leveling, micro-leveling was applied to the corrected conventional leveled data. This iterative grid-based process removed low amplitude components of flight line noise that still remained in the data after tie line and survey line leveling and resulted in fully leveled RMI data.

6.4 Magnetic Gradient

When magnetic values are obtained simultaneously from two or more sensors at a fixed separation, gradient of the magnetic field can be measured. Dividing the difference in magnetic values between the sensors by the distance between the sensors yields the magnetic gradient. The units are commonly reported as nT/m and, by convention, positive magnetic polarity is defined as to the north and east, and negative to the south and west. For vertical gradient, positive is defined as downwards. The sensors and the separations that were used to determine the various gradients are listed in Table 8.

Direction	Sensors	Separation (m)
Lateral (X)	Mag 1 and Mag 2	4.09
Longitudinal (Y)	Sequential TMI values	1.92*
Vertical (Z)	Mag 3 and Mag 4	3.40

Table 8: Geometric sensor relationship used to calculate magnetic gradients. Total magnetic intensity (TMI) was determined as the average of Mag 1 and Mag 2, and successive values of the TMI were used to determine the longitudinal (Y axis) gradient.

*average separation between sequential TMI values.

Because the magnetic field gradient varies more rapidly than total field strength, magnetic gradient provides higher spatial resolution, especially for shallow sources that are smaller than the survey line spacing or linear sources that are parallel to flight lines. Magnetic gradients, as compared to total magnetic intensities, have the additional benefits of being less sensitive to temporal variations and aircraft/sensor movement errors.

6.4.1 Horizontal Gradients

Horizontal magnetic gradients were determined in the in-line (Y axis) and cross-line (X axis) directions. Mag 1 (left) and Mag 2 (right) were used for both directions so that elevations were consistent in both axes. Gradients were calculated with respect to the magnetometer array with units provided as nT/m.

In-line gradient (ILG) at position i is determined from successive magnetic values of the average of Mag 1 and Mag 2 referenced to the distance between data points in accordance with the following formula:

$$ILG = \frac{a(i + 1) - a(i - 1)}{d(i + 1) + d(i - 1)}$$

where: a is the average total magnetic intensity of Mag 1 and Mag 2
 d is the distance between measurements
 i is the record number for the location

Cross-line gradient (XLG) was measured directly by dividing the difference between Mag 2 and Mag 1 by the sensor separation in accordance with the following formula:

$$XLG = \frac{\text{Mag 2} - \text{Mag 1}}{d_x}$$

where: d_x is the transverse sensor separation, 4.09 m

6.4.1.1 Gain Correction

Gain corrections were applied to the initial cross-line gradient. Overall, Mag 1 and Mag 2 should produce the same total magnetic field. If the ratio of the TMI between the sensors does not equal one, a gain correction needs to be applied to account for instrument error and asymmetric magnetic fields. The mean of the ratio between the TMI values for Mag 1 and Mag 2 for each line was calculated and applied to each Mag 2 value along the line. The cross line gradient was then re-calculated from the gain-corrected Mag 2 values.

6.4.1.2 Offset Correction

After correcting for gain in the cross-line gradient, offset corrections were applied. Offsets were determined by subtracting the first difference of the gain-corrected cross-line gradient from the gain-corrected gradient to reduce line-to-line errors (striping) in the gradient grid. The resulting data were then micro-leveled to remove any remaining striping.

6.4.1.3 Total Horizontal Gradient

Total Horizontal Gradient (HG) is the magnitude of the combined in-line and cross-line gradients. It is used to estimate contact locations of magnetic bodies at shallow depths, reveal anomaly textures, and highlight anomaly-pattern discontinuities.

Total Horizontal Gradient (HG) is calculated as:

$$HG(x, y) = \sqrt{ILG^2 + XLG^2}$$

where: *ILG* is the in-line gradient
XLG is the cross-line gradient

6.4.2 Vertical Gradient

Vertical gradient (Z axis) is useful for enhancing shorter wavelength signals; therefore, edges of magnetic anomalies are highlighted, and deep geologic sources in the data are suppressed.

Vertical gradient is determined directly with respect to the magnetometer array of Mag 3 (lower) and Mag 4 (upper) with units provided as nT/m as follows:

$$\text{Vertical Gradient} = \frac{\text{Mag 3} - \text{Mag 4}}{d_x}$$

where: d_x is the vertical sensor separation, 3.40 m

6.4.3 Gradient Enhanced Magnetic Intensity

Gradient data are insensitive to the long wavelength signals that are retained with the total magnetic intensity reported by a single sensor or, in this case, the average of the residual magnetic intensity data from Mag 1 and Mag 2. Therefore, the missing long wavelengths can be recovered by combining in-line, cross-line, and vertical gradients with the RMI to create a gradient-enhanced Residual Magnetic Intensity (RMIge) grid. A trend can be determined from the difference between the two versions of the RMI. The isolated long wavelengths are added back to the gradient-enhanced Residual Magnetic Intensity and the resulting grid is micro-leveled.

The gradient-enhanced Total Magnetic Intensity (TMIge) was then calculated by adding the IGRF to the gradient-enhanced Residual Magnetic Intensity.

6.4.4 Gradient Enhanced Reduction to Magnetic Pole

Gradient enhanced Reduced to Magnetic Pole (RTPge) data were computed from the gradient enhanced Residual Magnetic Intensity (RMIge) grid. The RTP filter was applied in the Fourier domain which migrates the observed magnetic inclination and declination field to what the field would look like at the north magnetic pole.

Inclination and declination were calculated by using the “Date” channel. The derived values were used in the following formula:

$$RTP(\theta) = \frac{[\sin(I) - I \cdot \cos(I) \cdot \cos(D - \theta)]^2}{[\sin^2(I_a) + \cos^2(I_a) \cdot \cos^2(D - \theta)] \cdot [\sin^2(I) + \cos^2(I) \cdot \cos^2(D - \theta)]}$$

where: I is geomagnetic inclination in ° from horizontal

D is geomagnetic declination in ° azimuth from magnetic north

I_a is the inclination for amplitude correction (never less than I). Default is +/- 20°. If $|I_a|$ is specified to be less than $|I|$, it is set to I

7.0 Deliverables

Western Bear survey block data are presented as digital databases, maps, and a logistics report.

7.1 Digital Data

Digital files have been provided in two formats, the first is a .GDB file for use in Geosoft Oasis Montaj and the second format is a text (.XYZ) file. Full descriptions of the digital data and contents are included in the report (Appendix B).

The digital data were represented as grids as listed below:

- Digital Terrain Model (DTM)
- Total Magnetic Intensity (TMI)
- Residual Magnetic Intensity (RMI) – removal of IGRF from TMI
- In-Line Gradient (ILG)
- Cross-Line Gradient (XLG)
- Vertical Gradient (VG)
- Horizontal Gradient (HG) – total magnitude of the horizontal gradients (in-line and cross-line)
- Gradient enhanced Total Magnetic Intensity (TMIge) – addition of IGRF to RMIge
- Gradient enhanced Residual Magnetic Intensity (RMIge)
- Gradient enhanced Reduced to Magnetic Pole (RTPge) – reduced to magnetic pole of RMIge

7.1.1 Grids

Non-gradient enhanced digital data were gridded and displayed using the following Geosoft parameters:

- Gridding method: minimum curvature
- Grid cell size: 25 m
- Low-pass desampling factor: 2

- Tolerance: 0.001
- % pass tolerance: 99.99
- Maximum iterations: 100

The gradient enhanced grids were generated using the following Geosoft parameters:

- Gridding method: gradient enhanced bi-directional
- Grid cell size: 25 m
- Gradient noise level: 0.75

All magnetic grids were drawn with a histogram-equalized colour shade; sun illumination inclination at 45° and declination at 045°. DTM grid was drawn with a linear topographic colour.

7.2 KMZ

Gridded digital data were exported into .KMZ files which can be displayed using Google Earth. The grids can be draped onto topography and rendered to give a 3D view.

7.3 Maps

Digital maps were created for the Western Bear survey block. The following map products were prepared:

Overview Maps (colour images with elevation contour lines and topographic features):

- Actual flight lines, with survey block boundary
- DTM

Magnetic Maps (colour images with elevation contour lines):

- TMI, with actual flight lines and topographic features
- TMI
- RMI
- ILG
- XLG
- VG
- HG

Gradient Enhanced Magnetic Maps (colour images with elevation contour lines):

- TMIge
- RMIge

- RTPge

All survey maps were prepared in WGS 84 and UTM Zone 15N.

7.4 Report

A .PDF copy of the logistics report is included along with digital data and maps. The report provides information on the data acquisition procedures, data processing, and presentation of the Western Bear survey block data.

8.0 Conclusions and Recommendations

The Western Bear survey resulted in the collection of 237.4 line km of high resolution gradient magnetic data over one survey block. The data have been processed and plotted on maps as a representation of the magnetic features of the survey area.

Processing of geophysical data, including the calculation of derivatives, can generate false features as the signal-to-noise ratio decreases. In addition, false features can appear near the edges of a survey block where gridding algorithms are unable to properly calculate grids, such as in “edge effects,” or where flight height between adjacent flight lines varied due to cultural obstacles or steep terrain. Therefore, subtle geophysical features in derivative-enhanced map products or near the survey margins must be evaluated with discretion.

The airborne geophysical data were acquired to map the geophysical characteristics of the survey area, which are in turn related to the distribution and concentration of magnetic minerals and radioactive elements in the Earth. Geophysical data are rarely a direct indication of mineral deposits and therefore interpretation and careful integration with existing and new geological, geochemical, and other geophysical data are recommended to maximize value from the survey investment.

Respectfully submitted,
Precision GeoSurveys Inc.

Shawn Walker, P.Geo.
December 2020

Appendix A
Polygon Coordinates

Western Bear – WGS 84 Zone 15N

Latitude (deg N)	Longitude (deg W)	Easting (m)	Northing (m)
50.90413	94.35011	405070	5640032
50.90463	94.30628	408153	5640032
50.84169	94.30452	408153	5633031
50.84119	94.34829	405070	5633031

Appendix B

Equipment Specifications

- GEM GSM-19T Proton Precession Magnetometer (Magnetic Base Station)
- Hemisphere R120 GPS Receiver
- Hemisphere R330 GPS Receiver
- Opti-Logic RS800 Rangefinder Laser Altimeter
- Setra Model 276 Barometric Pressure Sensor
- Scintrex CS-3 Survey Magnetometer
- Billingsley TFM100G2 Ultra Miniature Triaxial Fluxgate Magnetometer
- Nuvia Dynamics IMPAC data recorder system (for navigation and geophysical data acquisition)

GEM GSM-19T Proton Precession Magnetometer (Magnetic Base Station)

Sensitivity	0.15 nT @ 1 Hz
Resolution	0.01 nT (gamma), magnetic field and gradient
Absolute Accuracy	±0.2 nT @ 1 Hz
Operating Range	20,000 nT to 120,000 nT
Gradient Tolerance	Over 7,000 nT/m
Operating Ranges	Temperature: -40°C to +50°C Battery Voltage: 10.0 V minimum to 15 V maximum Humidity: up to 90% relative, non-condensing
Storage Temperature	-50°C to +50°C
Dimensions	Console: 223 x 69 x 40 mm Sensor Staff: 4 x 450 mm sections Sensor: 170 x 71 mm dia. Weight: console 2.1 kg, sensor and staff assembly 2.2 kg
Integrated GPS	Yes

Hemisphere R120 GPS Receiver Specifications

GPS Sensor	Receiver Type	L1, C/A code, with carrier phase smoothing (Patented COAST technology during differential signal outage)
	Channels	12-channel, parallel tracking (10-channel when tracking SBAS)
	Update Rate	Up to 20 Hz position
	Cold Start Time	<60 s
	SBAS Tracking	2-channel, parallel tracking
	Horizontal Accuracy	<0.02 m 95% confidence (RTK ¹ , 2) <0.28 m 95% confidence (L-Dif 1, 2) <0.6 m 95% confidence (DGPS 1,3) <2.5 m 95% confidence (autonomous, no SA1)
	Differential Options	SBAS, Autonomous, External RTCM, RTK, OmniSTAR (HP/XP)
Beacon Sensor Specifications	Channels	2-channel, parallel tracking
	Frequency Range	283.5 to 325 kHz
	MSK Bit Rates	50, 100, and 200 bps
L-Band Sensor	Channels	Single channel
	Frequency Range	1530 MHz to 1560 MHz
	Satellite Selection	Manual or Automatic (based on location)
	Startup and Satellite Reacquisition Time	15 seconds typical
Communications	Serial Ports	2 full duplex RS232C
	Baud Rates	4800 – 115200
	USB Ports	1 Communications
	Correction I/O Protocol	RTCM SC-104
	Data I/O Protocol	NMEA 0183
	Timing Output	1 PPS (HCMOS, active high, rising edge sync, 10 k Ω , 10 pF load)
	Raw Data	Proprietary binary (RINEX utility available)
Environmental	Operating Temperature	-30°C to +70°C
	Storage Temperature	-40°C to +85°C
	Humidity	95% non-condensing
Power GPS Sensor	Input Voltage Range	8 to 36 VDC
	Power Consumption	3 Watts
	Current Consumption	< 250 mA @ 12 VDC
	Antenna Voltage Output	5.0 VDC

¹ Depends on multipath environment, number of satellites in view, satellite geometry and ionospheric activity.² Up to 5 km baseline length.³ Depends also on baseline length.

Hemisphere R330 GPS Receiver

GPS Sensor	Receiver Type	L1 and L2 RTK with carrier phase	
	Channels	12 L1CA GPS 12 L1P GPS 12 L2P GPS 12 L2C GPS 12 L1 GLONASS (with subscription code) 12 L2 GLONASS (with subscription code) 3 SBAS or 3 additional L1CA GPS	
	Update Rate	10 Hz standard, 20 Hz available	
	Cold Start Time	<60 s	
	Warm Start Time 1	30 s (valid ephemeris)	
	Warm Start Time 2	30 s (almanac and RTC)	
	Hot Start Time	10 s typical (valid ephemeris and RTC)	
	Reacquisition	<1 s	
	Differential Options	SBAS, Autonomous, External RTCM, RTK, OmniSTAR (HP/XP)	
	Horizontal Accuracy		RMS (67%)
RTK ^{1,2}		10 mm + 1 ppm	20 mm + 2 ppm
OmniSTAR HP ^{1,3}		0.1 m	0.2 m
SBAS (WAAS) ¹		0.3 m	0.6 m
Autonomous, no SA ¹		1.2 m	2.5 m
L-Band Sensor	Channel	Single channel	
	Frequency Range	1530 MHz to 1560 MHz	
	Satellite Selection	Manual or Automatic (based on location)	
	Startup and Satellite Reacquisition Time	15 seconds typical	
Communications	Serial Ports	2 full duplex RS232	
	Baud Rates	4800 – 115200	
	USB Ports	1 Communications, 1 Flash Drive data storage	
	Correction I/O Protocol	Hemisphere GPS proprietary, RTCM v2.3 (DGPS), RTCM v3 (RTK), CMR, CMR+NMEA 0183, Hemisphere GPS binary	
	Timing Output	1 PPS (HCMOS, active high, rising edge sync, 10 kΩ, 10 pF load)	
	Event Marker Input	HCMOS, active low, falling edge sync, 10 kΩ	
Environmental	Operating Temperature	-40°C to +70°C	
	Storage Temperature	-40°C to +85°C	
	Humidity	95% non-condensing	
Power GPS Sensor	Input Voltage Range	8 to 36 VDC	
	Consumption, RTK	<3.5 W (0.30 A @ 12 VDC typical)	
	Consumption, OmniSTAR	<4.3 W (0.36 A @ 12 VDC typical)	

¹Depends on multipath environment, number of satellites in view, satellite geometry and ionospheric activity.² Depends also on baseline length.³ Requires a subscription from OmniSTAR.

Opti-Logic RS800 Rangefinder Laser Altimeter

Accuracy	±1 m on 1x1 m ² diffuse target with 50% reflectivity, up to 700 m
Resolution	0.2 m
Communication Protocol	RS232-8, N, 1 ASCII characters
Baud Rate	19200
Data Raw Counts	~200 Hz
Data Calibrated Range	~10 Hz
Data Rate	~200 Hz raw counts for un-calibrated operation; ~10 Hz for calibrated operation (averaging algorithm seeks 8 good readings)
Calibrated Range Units	Feet, Meters, Yards
Laser	Class I (eye-safe), 905 nm ± 10 nm
Power	7 - 9 VDC conditioned required, current draw at full power (~ 1.8 W)
Laser Wavelength	RS100 905 nm ± 10 nm
Laser Divergence	Vertical axis – 3.5 mrad half-angle divergence; Horizontal axis – 1 mrad half-angle divergence; (approximate beam “footprint” at 100 m is 35 cm x 5 cm)
Dimensions	32 x 78 x 84 mm (lens face cross section is 32 x 78 mm)
Weight	<227 g (8 oz)
Casing	RS100/RS400/RS800 units are supplied as OEM modules consisting of an open chassis containing optics and circuit boards. Custom housings can be designed and built on request.

Setra Model 276 Barometric Pressure Sensor

Performance	Accuracy RSS ¹ (at constant temp)	±0.25% FS ²
	Non-Linearity (BSFL)	±0.22% FS
	Hysteresis	0.05% FS
	Non-Repeatability	0.05% FS
	Thermal Effects ³	Compensated range: 0°C to +55°C (+30°F to +130°F) Zero shift (over compensated range): 1% FS Span shift (over compensated range): 1% FS
	Resolution	Infinite, limited only by output noise level (0.0005% FS)
	Time Constant	10 msec to reach 90% final output with step function pressure input
	Long Term Stability	0.25% FS / 6 months
Environmental	Temperature	Operating ⁴ : -18°C to +79°C (0°F to +175°F) Storage: -55°C to +121°C (-65°F to +250°F)
	Vibration	2 g from 5 Hz to 500 Hz
	Shock	50 g (Operating, 1/2 sine 10 ms)
	Acceleration	10 g
Electrical	Circuit	3-Wire ⁵ (Exc, Out, Com)
	Power Consumption	0.20 W (24 VDC)
	Output Impedance	5 Ω
	Output Noise	<200 μV RMS (0 to 100 Hz)

¹ RSS of non-linearity, hysteresis, and non-repeatability.

² FS = 300 mb for 800 – 1100 mb range; 500 for 600 – 1100 mb range; and 20 PSI for 0 to 20 PSIA.

³ Units calibrated at nominal 70°F. Maximum thermal error computed from this datum.

⁴ Operating temperature limits of the electronics only. Pressure media temperatures may be considerable higher or lower.

⁵ The separate leads for +EXC, -EXC, +Out, -Out are commoned internally. The shield is connected to the case. For best performance, either the -Exc or -Out should be connected to the case. Unit is calibrated at the factory with -Exc connected to the case. The insulation resistance between all signal leads are tied together and case ground is 10

Scintrex CS-3 Magnetometer

Operating Principal	Self-oscillating split-beam Cesium Vapor (non-radioactive ^{133}Cs)
Operating Range	15,000 nT to 105,000 nT
Gradient Tolerance	40,000 nT/m
Operating Zones	15° to 75° and 105° to 165°
Hemisphere Switching	a) Automatic b) Electronic control actuated by the control voltage levels (TTL/CMOS) c) Manual
Sensitivity	0.0006 nT $\sqrt{\text{Hz}}$ rms
Noise Envelope	Typically 0.002 nT peak to peak, 0.1 to 1 Hz bandwidth
Heading Error	± 0.20 nT (inside the optical axis to the field direction angle range 15° to 75° and 105° to 165°)
Absolute Accuracy	<2.5 nT throughout range
Output	a) Continuous signal at the Larmor frequency which is proportional to the magnetic field (proportionality constant 3.49857 Hz/nT) sine wave signal amplitude modulated on the power supply voltage b) Square wave signal at the I/O connector, TTL/CMOS compatible
Information Bandwidth	Only limited by the magnetometer processor used
Sensor Head	Diameter: 63 mm (2.5") Length: 160 mm (6.3") Weight: 1.15 kg (2.6 lb)
Sensor Electronics	Diameter: 63 mm (2.5") Length: 350 mm (13.8") Weight: 1.5 kg (3.3 lb)
Cable, Sensor to Sensor Electronics	3 m (9' 8"), lengths up to 5 m (16' 4") available
Operating Temperature	-40°C to +50°C
Humidity	Up to 100%, splash proof
Supply Power	24 to 35 VDC
Supply Current	Approx. 1.5 A at start up, decreasing to 0.5 A at 20°C
Power Up Time	Less than 15 minutes at -30°C

Billingsley TFM100G2 Ultra Miniature Triaxial Fluxgate Magnetometer

Axial Alignment	Orthogonality better than $\pm 1^\circ$
Input Voltage Options	15 to 34 VDC @ 30 mA
Field Measurement Range Options	$\pm 100 \mu\text{T} = \pm 10 \text{ V}$
Accuracy	$\pm 0.75\%$ of full scale (0.5% typical)
Linearity	$\pm 0.015\%$ of full scale
Sensitivity	100 $\mu\text{V/nT}$
Scale Factor Temperature Shift	0.007% full scale/ $^\circ\text{C}$
Noise	$\leq 12 \text{ pT rms}/\sqrt{\text{Hz}}$ @ 1 Hz
Output Ripple	3 mV peak to peak @ 2 nd harmonic
Analog Output at Zero Field	$\pm 0.025 \text{ V}$
Zero Shift with Temperature	$\pm 0.6 \text{ nT}/^\circ\text{C}$
Susceptibility to Perming	$\pm 8 \text{ nT}$ shift with $\pm 5 \text{ Gs}$ applied
Output Impedance	$332 \Omega \pm 5\%$
Frequency Response	3 dB @ $> 500 \text{ Hz}$ (to $> 4 \text{ kHz}$ wide band)
Over Load Recovery	$\pm 5 \text{ Gs}$ slew $< 2 \text{ ms}$
Random Vibration	$> 20 \text{ G rms}$ 20 Hz to 2 kHz
Temperature Range	-55°C to $+85^\circ\text{C}$
Acceleration	$> 60 \text{ G}$
Weight	100 g
Size	3.51 cm x 3.23 cm x 8.26 cm
Connector	Chassis mounted 9 pin male "D" type

Nuvia Dynamics IMPAC data recorder system

(for navigation and geophysical data acquisition)

Functions	Integrated Multi-Parameter Airborne Console (IMPAC) with integrated dual Global Positioning System Receiver (GPS) and all necessary navigation guidance software. Inputs for geophysical sensors - portable gamma ray spectrometer GRS-10/AGRS, MMS4/MMS8 Magnetometer, Totem 2A EM, A/D converter, temperature/humidity probe, barometric pressure probe, and laser/radar altimeter. Output for the multi-parameter PGU (Pilot Guidance Unit)
Display	Monitor display 600 x 800 pixels; customized keypad and operator keyboard. Multi-screen options for real-time viewing of all data inputs, fiducial points, flight line tracking, and GPS channels by operator
Navigation	Pilot/operator navigation guidance. Software supports preplanned survey flight plan, along survey lines, way-points, preplanned drape profile surfaces
Data Sampling	Sensor dependent
Data Synchronization	Synchronized to GPS position. Supports dual GPS
Data File	PEI Binary data format
Storage	80 GB
Software	PEIView: Allows fast data verification and conversion of PEI binary data to Geosoft GBN or ASCII formats PEIConv: For survey preparation, calibration and conversion of maps, and survey plot after data acquisition PEIComp: For calculation of magnetic compensation coefficients AGRS/GRS10 Calibration: High voltage adjustment, linearity correction coefficients calculation, and communication test support AGIS: Real time data acquisition and navigation system. Displays chart/spectrum view in real-time for fast data Quality Control (QC)
Electrical	Multiple ethernet connections, RS232 serial ports, USB ports, and 16-bit differential analog input channels. It can support up to 4 magnetometer sensors
Power Requirement	24 VDC

Appendix C

Digital File Descriptions

- Magnetic Database Descriptions
- Geosoft Grid Descriptions
- Map Descriptions

Magnetic Database:

Abbreviations used in the GDB/XYZ files listed below:

CHANNEL	UNITS	DESCRIPTION
X_WGS84	m	UTM Easting – WGS84 Zone 15N
Y_WGS84	m	UTM Northing – WGS84 Zone 15N
Lat_deg	Decimal degree	Latitude – WGS84
Lon_deg	Decimal degree	Longitude – WGS84
Date	yyyy/mm/dd	Dates of the survey flight(s) – Local
FLT		Flight Line numbers
LineNo		Line numbers
STL		Number of satellite(s)
GPSfix		1 = non-differential 2 = WAAS/SBAS differential
Heading	degree	Heading of the aircraft
GPStime	HH:MM:SS	GPS time (UTC)
Geos_m	m	Geoidal separation
XTE_m	m	Cross track error
Galt	m	GPS height – WGS84 Zone 15N (ASL)
Lalt	m	Laser altimeter readings (AGL)
DTM	m	Digital Terrain Model
Sample_Density	m	Horizontal distance in meters between adjacent measurement locations; sample frequency is 20 Hz
Speed_km_hr	km/hr	Ground speed of aircraft in km/hr
basemag	nT	Base station temporal variation data
IGRF	nT	International Geomagnetic Reference Field, IGRF-13
Declin	Decimal degree	Calculated declination of magnetic field
Inclin	Decimal degree	Calculated inclination of magnetic field
Mag1_Head	nT	Mag 1 – Diurnal, lag, and heading corrected
Mag2_Head	nT	Mag 2 – Diurnal, lag, and heading corrected
Mag3_Head	nT	Mag 3 – Diurnal, lag, and heading corrected
Mag4_Head	nT	Mag 4 - Diurnal, lag, and heading corrected
TMI	nT	Total Magnetic Intensity (average of Mag 1 and Mag 2)
RMI	nT	Residual Magnetic Intensity (average of Mag 1 and Mag 2)
ILG	nT/m	In-Line Gradient (Mag 1 and Mag 2)
XLG	nT/m	Cross-Line Gradient (Mag 1 and Mag 2)
VG	nT/m	Vertical Gradient (Mag 3 and Mag 4)
HG	nT/m	Total horizontal gradient (in-line and cross-line)
TMIge	nT	Gradient enhanced Total Magnetic Intensity
RMIge	nT	Gradient enhanced Residual Magnetic Intensity

Grids:

Western Bear Survey Block, WGS 84 Datum, Zone 15N, cell size at 25 m

FILE NAME	DESCRIPTION
20157_WesternBear_DTM_25m.grd	Digital Terrain Model gridded at 25 m cell size
20157_WesternBear_TMI_25m.grd	Total Magnetic Intensity gridded at 25 m cell size
20157_WesternBear_RMI_25m.grd	Residual Magnetic Intensity gridded at 25 m cell size
20157_WesternBear_ILG_25m.grd	Measured In-Line Gradient (Mag 1 and Mag 2) gridded at 25 m cell size
20157_WesternBear_XLG_25m.grd	Measured Cross-Line Gradient (Mag 1 and Mag 2) gridded at 25 m cell size
20157_WesternBear_VG_25m.grd	Measured Vertical Gradient (Mag 3 and Mag 4) gridded at 25 m cell size
20157_WesternBear_HG_25m.grd	Total Horizontal Gradient (in-line and cross-line) gridded at 25 m cell size
20157_WesternBear_TMIge_25m.grd	Gradient enhanced Total Magnetic Intensity (in-line, cross-line, and vertical gradients) gridded at 25 m cell size
20157_WesternBear_RMIge_25m.grd	Gradient enhanced Residual Magnetic Intensity (in-line, cross-line, and vertical gradients) gridded at 25 m cell size
20157_WesternBear_RTPge_25m.grd	Gradient enhanced Reduced to Magnetic Pole of RMIge gridded at 25 m cell size

Maps:

Western Bear Survey Block, WGS 84 Datum, Zone 15N (jpegs, pdfs, and georeferenced pdf)

Plate Number	Plate Name	FILE NAME	DESCRIPTION
1	FL	20157_WesternBear_ActualFlightLines	Plotted actual flown flight lines
2	DTM	20157_WesternBear_DTM_25m	Digital Terrain Model gridded at 25 m cell size
3	TMI_wFL	20157_WesternBear_TMI_wFL_25m	Total Magnetic Intensity gridded at 25 m cell size with actual flown flight lines
4	TMI	20157_WesternBear_TMI_25m	Total Magnetic Intensity gridded at 25 m cell size
5	RMI	20157_WesternBear_RMI_25m	Residual Magnetic Intensity gridded at 25 m cell size
6	ILG	20157_WesternBear_ILG_25m	In-Line Gradient gridded at 25 m cell size
7	XLG	20157_WesternBear_XLG_25m	Cross-Line Gradient gridded at 25 m cell size
8	VG	20157_WesternBear_VG_25m	Vertical Gradient gridded at 25 m cell size
9	HG	20157_WesternBear_HG_25m	Horizontal Gradient gridded at 25 m cell size
10	TMIge	20157_WesternBear_TMIge_25m	Gradient enhanced Total Magnetic Intensity gridded at 25 m cell size
11	RMIge	20157_WesternBear_RMIge_25m	Gradient enhanced Residual Magnetic Intensity gridded at 25 m cell size
12	RTPge	20157_WesternBear_RTPge_25m	Gradient enhanced Reduced to Magnetic Pole of RMIge gridded at 25 m cell size

Plates

Western Bear Survey Block Scale 1:20,000

- Plate 1: Western Bear – Actual Flight Lines (FL)
- Plate 2: Western Bear – Digital Terrain Model (DTM)
- Plate 3: Western Bear – Total Magnetic Intensity with Actual Flight Lines (TMI_wFL)
- Plate 4: Western Bear – Total Magnetic Intensity (TMI)
- Plate 5: Western Bear – Residual Magnetic Intensity (RMI)
- Plate 6: Western Bear – In-Line Gradient (ILG)
- Plate 7: Western Bear – Cross-Line Gradient (XLG)
- Plate 8: Western Bear – Vertical Gradient (VG)
- Plate 9: Western Bear – Horizontal Gradient (HG)
- Plate 10: Western Bear – Gradient Enhanced Total Magnetic Intensity (TMlge)
- Plate 11: Western Bear – Gradient Enhanced Residual Magnetic Intensity (RMlge)
- Plate 12: Western Bear – Gradient Enhanced Reduced to Magnetic Pole (RTPge) of RMlge



GEOPHYSICAL INTERPRETATION OF WESTERN BEAR, SYDNEY LAKE AND LEO PROPERTIES

Red Lake, Ontario

March 23, 2021

Authored by: Edna Mueller-Markham, M.Sc., P.Geo.
Vice-President and Senior Consulting Geophysicist
Paterson, Grant and Watson Limited
1510 – 155 University Ave.
Toronto, ON M5H 3B7
edna.mueller@pgw.ca



Contents

Executive Summary.....	1
Introduction	1
Survey Areas	1
Geological Setting	3
Background Material.....	4
Magnetic Methods.....	4
Data Processing.....	6
Data Deliverables	7
Maps	7
Grids.....	7
Databases.....	8
VOXI Modelling	8
QuickMag Modelling.....	10
Interpretation	10
Landform Analysis.....	12
Analytic Hill Shade.....	12
Slope	13
Aspect	13
Landform Classification.....	13
Magnetic Interpretation	13
Leo.....	14
Lithological Interpretation	14
Lineaments.....	22
Faults.....	23
Folds.....	25
VOXI Modelling Interpretation	26
Landform Analysis.....	34
SRTM and Analytic Hill Shade	34
Slope Analysis.....	35
Aspect Analysis.....	35
Landform Classification.....	36
Sydney Lake.....	37
Lithological Interpretation	37
Lineaments.....	39
Faults.....	41
Folds.....	43
VOXI Modelling Interpretation	44



Landform Analysis.....	52
SRTM and Analytic Hill Shade	52
Slope Analysis.....	53
Aspect Analysis.....	54
Landform Classification.....	54
Western Bear	55
Lithological Interpretation	55
Lineaments.....	58
Faults.....	60
VOXI Modelling Interpretation	62
Landform Analysis.....	69
SRTM and Analytic Hill Shade	70
Slope Analysis.....	71
Aspect Analysis.....	72
Landform Classification.....	73
Recommended Target Areas	74
Leo.....	75
Sydney Lake.....	79
Western Bear	81
Recommendations Summary.....	85
Primary Targets	85
Leo.....	85
Sydney Lake.....	85
Western Bear	85
Secondary Targets.....	86
Leo.....	86
Sydney Lake.....	86
Western Bear	86
Certificate of Qualification and Declaration	87
Appendix A - Processing Details.....	88
Enhanced Derivative Grids.....	88
Reduction to the Magnetic Pole (RTP).....	88
First Vertical Derivative of the Pole Reduced Field (1VD).....	89
Second Vertical Derivative of the Pole Reduced Field (2VD).....	89
Tilt Angle of the Pole Reduced Field	89
Horizontal Gradient Magnitude.....	90
Analytic Signal Amplitude	90
Source Parameter Imaging (SPI)	91
Source Edge Detection.....	91
Encom Special Filters – Area and Edge	91
Digital Elevation Model.....	92
VOXI Modelling	92
Appendix B – Selected Papers.....	93



Figures

Figure 1. Location and flight line path of the Western Bear survey area.	2
Figure 2. Location and flight line path of the Sydney Lake survey area.	2
Figure 3. Location and flight line path of the Leo survey area.	3
Figure 4. 1:250 000 scale bedrock geology of Ontario; Ontario Geological Survey.	4
Figure 5. Example of enhanced images of (1) reduction to the pole, (2) analytic signal, (3) second vertical derivative and (4) interpretation of the same original image of the magnetic field.	6
Figure 6. Interpretation layer of the Leo property and legend.	11
Figure 7. Interpretation layer of the Sydney Lake property and legend.	11
Figure 8. Interpretation layer of the Western Bear property and legend.	12
Figure 9. Pakwash-Longlegged Lake geological map and the current lithological interpretation.	15
Figure 10. Ontario Geological Survey 1:250 000 scale geological map and the current lithological interpretation.	15
Figure 11. Lithological interpretation and location of three area subsets.	16
Figure 12. West Subset: Residual magnetic intensity reduced to the pole (left) and the current geophysical interpretation (right).	16
Figure 13. South Central Subset: Residual magnetic intensity reduced to the pole (above), the second vertical derivative of the pole reduced magnetic field (centre) and the current geophysical interpretation (below).	18
Figure 14. North Central Subset: Residual magnetic intensity reduced to the pole (above) and the current geophysical interpretation (below).	20
Figure 15. Reduced to the pole images with interpreted lithology (top) and with hydrology (bottom). ..	21
Figure 16. 3D view of the residual magnetic intensity reduced to the pole.	21
Figure 17. 3D view of the residual magnetic intensity reduced to the pole looking east.	22
Figure 18. Lineaments or trends overlain upon the tilt derivative (50% transparency applied).	22
Figure 19. Rose diagram of orientations of lineaments.	23
Figure 20. Interpreted faults overlain upon the second vertical derivative of the pole reduced field (50% transparency).	23
Figure 21. Rose diagram of fault orientations.	24
Figure 22. Fold axes (green) with the reduced to the pole (above) and 2nd vertical derivative of the pole reduced field (below).	25
Figure 23. Rose diagram of fold orientations.	25
Figure 24. Magnetic susceptibility model of the survey area. The top of the model is at surface at 443 m above sea level.	26
Figure 25. Magnetic susceptibility model with the top of the model is at 200 m above sea level.	27
Figure 26. Magnetic susceptibility model with the top of the model is at 400 m below sea level.	27
Figure 27. Magnetic susceptibility model with the top of the model is at 1600 m below sea level.	28
Figure 28. Northern granodiorite model depth slices.	29
Figure 29. Southern undeformed granodiorite model depth slices.	29
Figure 30. Eastern granodiorite model depth slices.	29



Figure 31. Multiple isosurfaces of susceptibility.....	30
Figure 32. Multiple isosurfaces with only the three highest susceptibility surfaces and clipped to remove the isosurfaces at depths below 3,400 sea level.	30
Figure 33. with three highest susceptibility surfaces and clipped to depths below 1,400 sea level.....	31
Figure 34. VOXI and QuickMag models of the entire survey area.....	31
Figure 35. Location of the close-up views of the VOXI and QuickMag models.	32
Figure 36. VOXI and QuickMag models of the northern granodiorite looking west.	32
Figure 37. VOXI and QuickMag models of the central undeformed granodiorite intrusion	33
Figure 38. VOXI and QuickMag models of the eastern granodiorite.....	34
Figure 39. SRTM combined with analytic hill shade (top) and with interpreted faults (bottom).	35
Figure 40. Slope derived from the SRTM (top) and with interpreted faults (bottom).	35
Figure 41. Aspect derived from the SRTM (top) and with interpreted faults (bottom).	36
Figure 42. Landform Classification derived from the SRTM (top) and with interpreted faults (bottom). .	36
Figure 43. Residual magnetic intensity reduced to the pole (left) and the current geophysical interpretation (right).....	38
Figure 44. 3D view of the residual magnetic intensity reduced to the pole.....	38
Figure 45. Published geology (left) and the reduced to the pole magnetics of the same area (right).....	39
Figure 46. Lineaments or trends overlain upon the tilt derivative (50% transparency applied).....	40
Figure 47. Rose diagram of orientations of lineaments.....	41
Figure 48. Interpreted faults overlain upon the second vertical derivative of the pole reduced field (50% transparency).....	42
Figure 49. Rose diagram of fault orientations.	43
Figure 50. Fold axes (green) with the reduced to the pole (left) and 2nd vertical derivative of the pole reduced field (right).	43
Figure 51. Rose diagram of fold orientations.	44
Figure 52. Magnetic susceptibility model of the survey area. The top of the model is at surface at 411 m above sea level.....	45
Figure 53. Magnetic susceptibility model with the top of the model is at 200 m above sea level.	46
Figure 54. Magnetic susceptibility model with the top of the model is at 400 m below sea level.	47
Figure 55. Magnetic susceptibility model with the top of the model is at 1000 m below sea level.	48
Figure 56. Multiple isosurfaces of susceptibility.....	49
Figure 57. Multiple isosurfaces of susceptibility viewed from above with a transparency of the geophysical interpretation.....	50
Figure 58. A cross section through multiple isosurfaces of susceptibility viewed from above towards the northwest without some of the lower isosurfaces.....	51
Figure 59. Higher susceptibility isosurfaces and the calculated QuickMag model with a view towards the northeast.....	51
Figure 60. Higher susceptibility isosurfaces and the calculated QuickMag model with a view from overhead.	52
Figure 61. DEM combined with analytic hill shade (left) and with interpreted faults (right).....	53
Figure 62. Slope derived from the DEM (left) and with interpreted faults (right).	53



Figure 63. Aspect derived from the DEM (left) and with interpreted faults (right). 54

Figure 64. Landform Classification derived from the DEM (left) and with interpreted faults (right)..... 55

Figure 65. Residual magnetic intensity reduced to the pole (left) and the current geophysical interpretation (right)..... 56

Figure 66. 3D view of the residual magnetic intensity reduced to the pole..... 57

Figure 67. Published geology (left) and the current lithological interpretation (right). 58

Figure 68. Lineaments or trends overlain upon the tilt derivative (50% transparency applied)..... 59

Figure 69. Rose diagram of orientations of lineaments..... 60

Figure 70. Interpreted faults overlain upon the second vertical derivative of the pole reduced field (50% transparency). 61

Figure 71. Rose diagram of fault orientations. 62

Figure 72. Magnetic susceptibility model of the survey area. The top of the model is at surface at 432 m above sea level..... 63

Figure 73. Magnetic susceptibility model with the top of the model is at 200 m above sea level. 64

Figure 74. Magnetic susceptibility model with the top of the model is at 400 m below sea level. 65

Figure 75. Magnetic susceptibility model at a depth of 1300 m below sea level..... 66

Figure 76. Multiple isosurfaces of susceptibility..... 67

Figure 77. Multiple isosurfaces of susceptibility viewed from above with a transparency of the geophysical interpretation..... 68

Figure 78. A cross section through multiple isosurfaces of susceptibility viewed from above towards the northwest without some of the lower isosurfaces. 69

Figure 79. Higher susceptibility isosurfaces and the calculated QuickMag model with a view from the top (left) and a site view looking towards the northwest (right). 69

Figure 80. DEM combined with analytic hill shade (left) and with interpreted faults (right)..... 71

Figure 81. Slope derived from the DEM (left) and with interpreted faults (right). 72

Figure 82. Aspect derived from the DEM (left) and with interpreted faults (right). 73

Figure 83. Landform Classification derived from the DEM (left) and with interpreted faults (right)..... 74

Figure 84. Local mapped geology of the Leo property. 75

Figure 85. Recommended primary and secondary targets for follow-up for the Leo property..... 76

Figure 86. Subset areas of recommended targets..... 76

Figure 87. Recommended primary and secondary targets for follow-up for the Western Leo property. . 77

Figure 88. Recommended primary and secondary targets for follow-up for the Central Leo property. ... 78

Figure 89. Recommended primary and secondary targets for follow-up for the Eastern Leo property.... 79

Figure 90. Local mapped geology of the Sydney Lake-Rainfall Lake Dome. 80

Figure 91. Recommended primary and secondary targets for follow-up for the Sydney Lake property... 81

Figure 92. Recommended primary and secondary targets for follow-up for the Western Bear property. 83

Figure 93. Recommended primary and secondary targets for follow-up for the Western Bear property with the VOXI modelling results. 84

Executive Summary

In December 2020, Trillium Gold engaged Paterson, Grant & Watson Limited for a geophysical interpretation of an airborne magnetic survey over the Western Bear, Sydney Lake and Leo Properties located near Red Lake, Ontario. The main goal of the geophysical interpretation program is to better define the structural and lithological controls of mineralization in the area, and to define follow-up targets for ground geophysical and/or geochemical work. This includes identification of major regional structures and extension of intrusives underneath the surficial cover.

A high-resolution magnetic survey was flown for Trillium Gold Inc. by Precision Geophysics. It is a heliborne magnetics only survey with a 100 m line spacing in 2020. The data was processed and enhanced into numerous derivative grids. The magnetic data was modelled using Geosoft's magnetic vector inversion software known as VOXI and Encom's QuickMag software. A survey wide model of the subsurface magnetic susceptibility was produced for each survey area and some specific magnetic anomalies were modelled.

An interpretation of the lineaments, faults and lithology was prepared as a QGIS project workspace. The survey areas contain a series of ultramafics, mafic, intermediate and felsic metavolcanics intruded by some local ultramafics/pyroxenites and metasedimentary units. The areas are cut by multiple generations of faults.

A number of ground follow-up targets were suggested for geological mapping, drilling and gold assaying. They are classified as primary and secondary targets.

Introduction

In December 2020, Trillium Gold engaged Paterson, Grant & Watson Limited for a geophysical interpretation of an airborne magnetic survey over the Western Bear, Sydney Lake and Leo properties located near Red Lake, Ontario.

The main goal of the geophysical interpretation program is to better define the structural and lithological controls of mineralization in the area, and to define follow-up targets for ground geophysical and/or geochemical work. This includes identification of major regional structures and extension of intrusives underneath the surficial cover.

Survey Areas

Magnetic data were acquired in 2020 at a 100 m line spacing over the Western Bear, Sydney Lake and Leo properties.

The Western Bear survey had an average sensor altitude of 45 m above terrain and at a traverse line direction of 90°. The control lines were flown at a spacing of 1,000 m at an orientation of 0°. The total line kilometers of the survey are 237 km (**Figure 1**). The terrain is relatively smooth with an average elevation

of 414 m above sea level with a range from 389 to 432 m above sea level. The survey area has a size of approximately 6.9 km by 3.2 km. Multiple small lakes are located in the survey area.

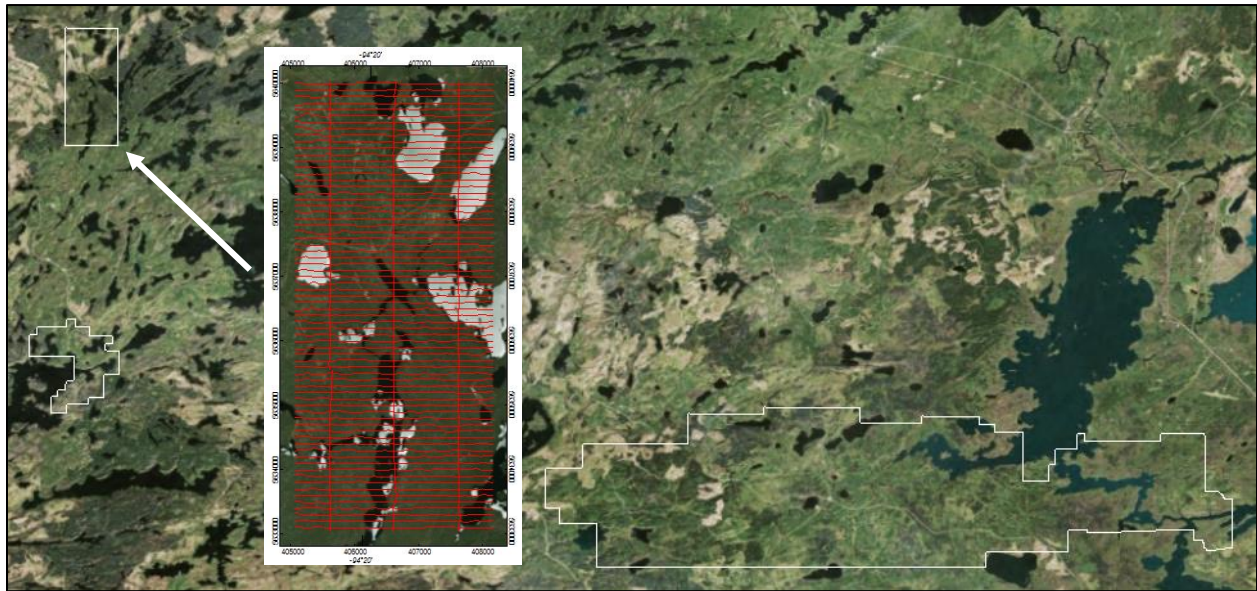


Figure 1. Location and flight line path of the Western Bear survey area.

The Sydney Lake survey had an average sensor altitude of 41 m above terrain and at a traverse line direction of 90°. The control lines were flown at a spacing of 1,000 m at an orientation of 0°. The total line kilometers of the survey are 170 km (Figure 2). The terrain is relatively smooth with an average elevation of 369 m above sea level with a range from 337 to 410 m above sea level. The survey area has a size of approximately 5.3 km by 5.5 km. Multiple small lakes are located in the survey area and it borders a larger lake.

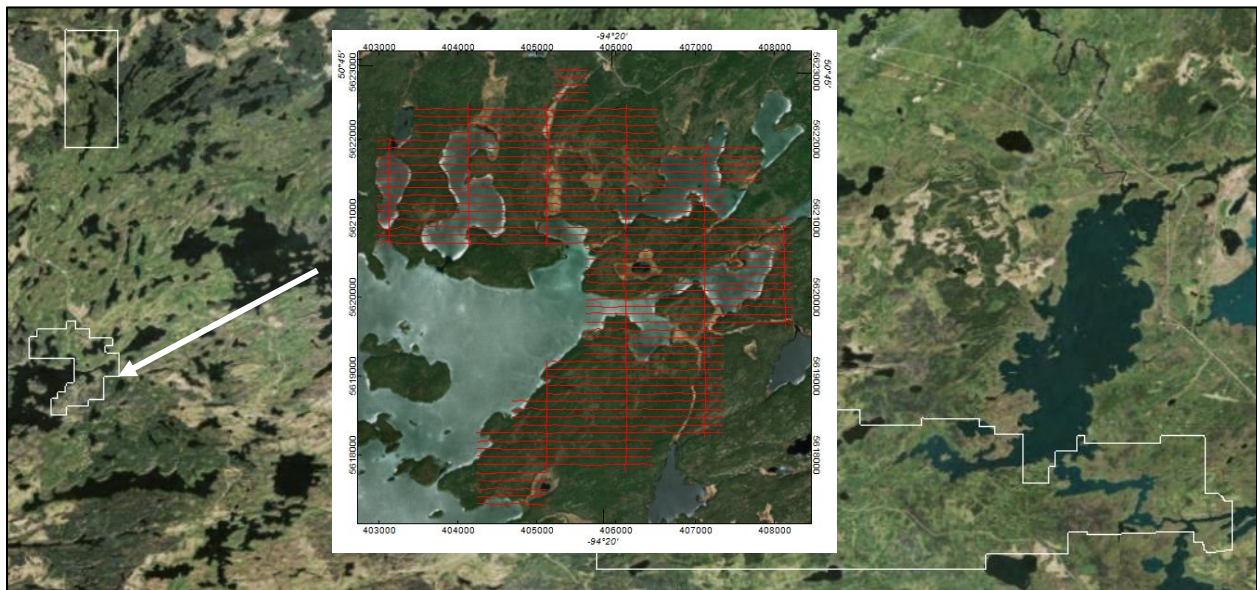


Figure 2. Location and flight line path of the Sydney Lake survey area.

The Leo survey had an average sensor altitude of 34 m above terrain and at a traverse line direction of 0°. The control lines were flown at a spacing of 1,000 m at an orientation of 90°. The total line kilometers of the survey are 3,133 km (**Figure 3**). The terrain is relatively smooth with an average elevation of 377 m above sea level with a range from 329 to 443 m above sea level. The survey area has a size of approximately 40.5 km by 9.5 km. There are few small lakes located in the survey area and it is crossed by a few roads.

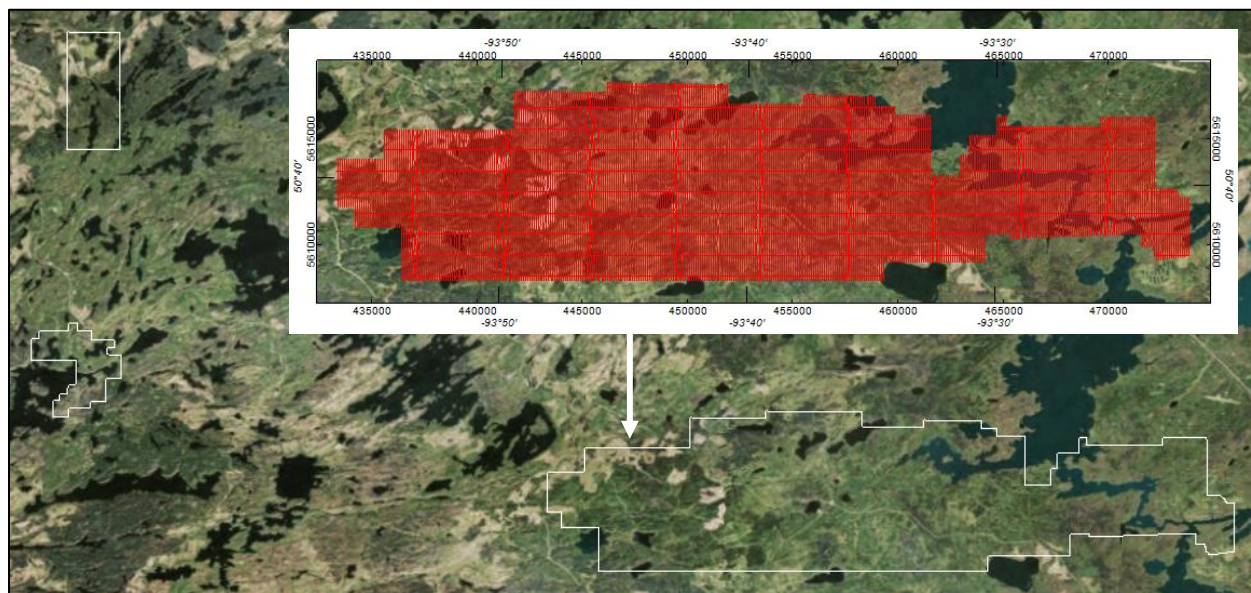


Figure 3. Location and flight line path of the Leo survey area.

Geological Setting

Both the Western Bear and Sydney Lake properties are north and west of the Leo property and occur within the Uchi subprovince. This volcanic-rich subprovince is separated from the more metasediment-rich English River subprovince by the Sydney Lake and the Longlegged Lake - Pakwash Lake fault zones.

Western Bear property is located within a mapped biotite tonalite to granodiorite terrain known as the Atikaki batholith and intruded by a more felsic tonalite to granodiorite series of gneisses and mafic to intermediate metavolcanics. Small outcroppings of peridotite, metagabbros and metasedimentary iron formations have been noted in the surrounding area. A north to south narrow band of mafic to intermediate metavolcanics bisects the Western Bear property.

The Sydney Lake property is located within the Sydney Lake-Rainfall Lake Dome, a deformed sequence of massive granite to granodiorite, metasedimentary rocks of paragneiss origin and migmatites, mafic to

intermediate metavolcanic rocks within a tonalite to granodiorite suite. The anticlinal fold axis of the dome is orientated southwest to northeast. It is located west of the much larger Longlegged Lake Dome.

The regional geology of the Leo property is well summarized in Toby Hughes' targeting report². The property lies within the mostly metasedimentary English River subprovince. The Ontario Geological Survey³ shown in the map below (**Figure 4**) confirms this with a mapped dominant metasedimentary migmatite lithology within the Leo property. An east to west band of cataclastic migmatite is associated with the Sydney Lake fault zone. The map shows minor intrusions of tonalite to granodiorite and diorite bodies, much less than is illustrated by the following geophysical interpretation.

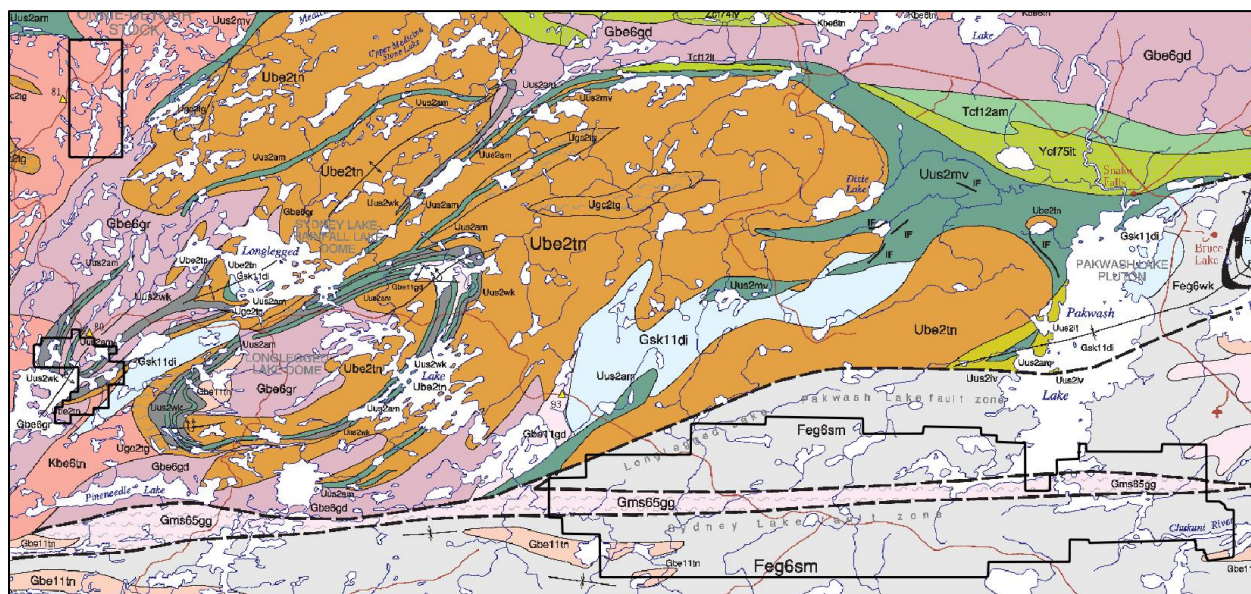


Figure 4. 1:250 000 scale bedrock geology of Ontario; Ontario Geological Survey.

Background Material

Magnetic Methods

Magnetic methods measure the magnetic response of rocks and minerals that is induced by the magnetic field of the earth. The size of the induced field is dependent upon iron bearing minerals such as magnetic iron and iron-titanium oxide minerals, including magnetite, titanomagnetite, titanomaghemite and titanohematite, and some iron sulphide minerals, including pyrrhotite and greigite. These mineral are most commonly found in high concentrations in volcanic rocks such as basalts or sedimentary banded iron formations (BIFs), but also to a lesser extent in plutonic rocks such as granites. Measurements of the magnetic field display the distribution of magnetic rocks in the earths crust and reflect the geological history of the area. So long as there is a sufficient physical property contrast (i.e., sufficient change in magnetic mineral content between adjacent rock packages), the magnetic method will show structural

² Hughes, T.N.J., P.Geol., 2020, Targeting in the Leo Property, English River Subprovince, Red Lake Mining Division, Ear Falls, Ontario for Trillium Gold Mines Inc.

³ Ontario Geological Survey 2011. 1:250 000 scale bedrock geology of Ontario; Ontario Geological Survey, Miscellaneous Release–Data 126 - Revision 1.



features including faults, folds, shear zones, intrusions, and/or alteration from ground surface to the Curie point (depth at which magnetic properties are destroyed due to heat). Surficial sediments such as soils and overburden, and most sedimentary rock types (e.g., limestones and sandstones) contain very little magnetic mineral content, thus they appear almost invisible to the magnetic sensors and we are able to resolve the underlying magnetic basement or intra-sedimentary magnetic features (i.e., intrusions).

Enhanced images of the magnetic field can be easily produced with computer software packages and displayed in a variety of ways. These enhanced images are created to bring out subtle features and trends, to find edges of geological bodies and to make the image more easily interpretable. Examples of such enhanced images are the Magnetic Field Reduced to the Pole, its First and Second Vertical derivatives, Tilt derivative and Analytic Signal to list a few (**Figure 5**).

Modelling and inversion of the magnetic data can resolve the approximate depth to the magnetic source as well as its dip, strike, size and shape. In this project we utilized Geosoft's magnetic inversion software known as VOXI and Encom's QuickMag Pro.

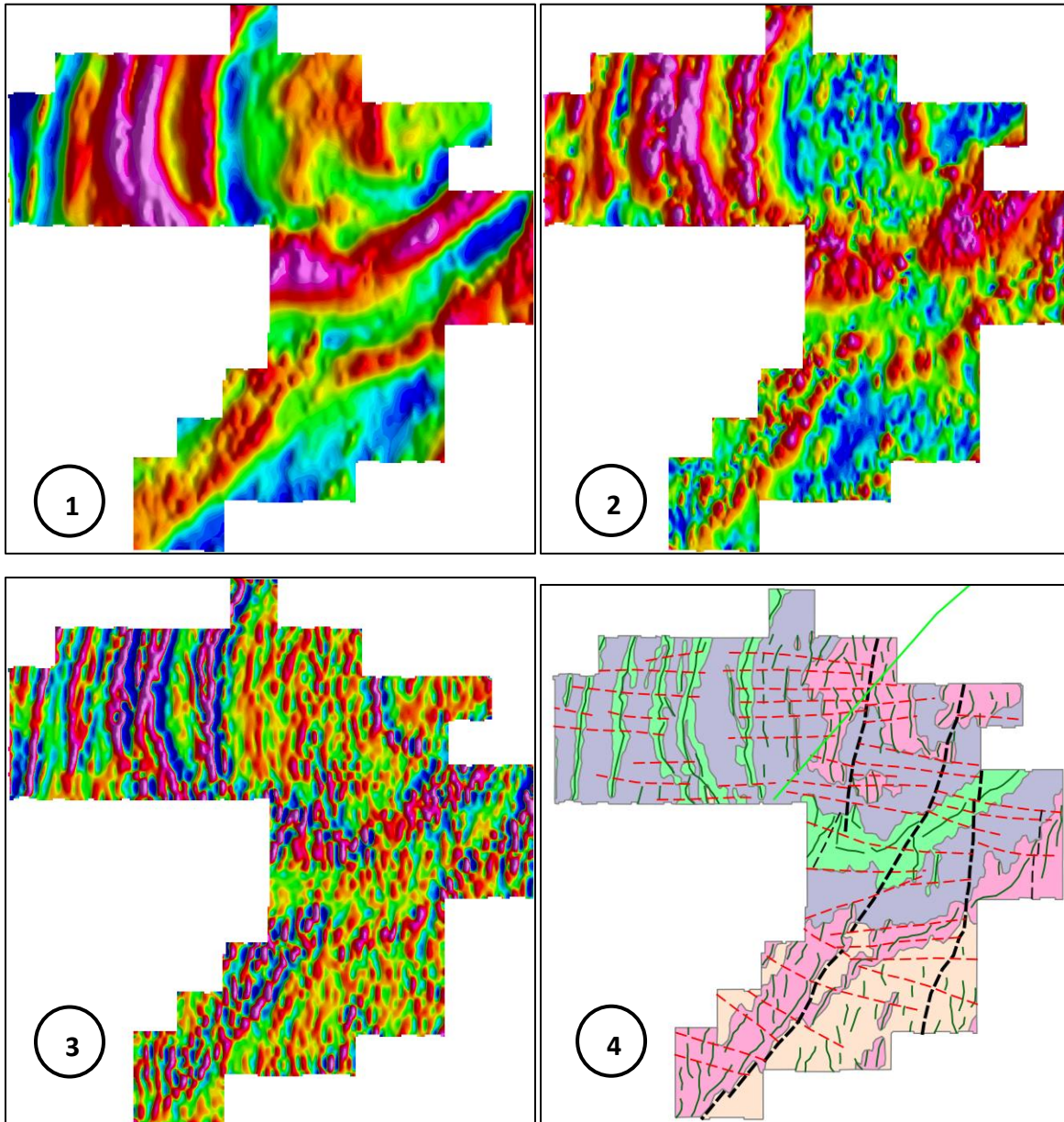


Figure 5. Example of enhanced images of (1) reduction to the pole, (2) analytic signal, (3) second vertical derivative and (4) interpretation of the same original image of the magnetic field.

Data Processing

A complete discussion of the processing of the magnetic data, landform classification and VOXI modelling is provided in [Appendix A](#) and some selected papers in [Appendix B](#).

The magnetic data did not require any microlevelling to remove linear anomalies visible along the flight path. The contractor's gradient enhanced residual magnetic intensity grid was of very high quality. This grid was the basis for all of the subsequent enhanced and derivative grids.

Finally, the residual magnetic intensity and topographic data were used to create a 3D model of the subsurface magnetic susceptibility using the magnetic vector intensity (MVI).

Data Deliverables

Maps

For each property, the following maps were produced with a datum/projection of WGS84/UTM15N. The scale was chosen for the data to fit on one E-sized (36"x48") map sheet. The scales of the maps were:

Leo at 1:50,000
Sydney Lake at 1:10,000
Western Bear at 1:10,000

- *scale_RMI.map* – IGRF corrected residual magnetic intensity
- *scale_RTP.map* – Residual total magnetic intensity reduced to the pole
- *scale_RTP1VD.map* – First vertical derivative of the pole reduced field
- *scale_RTP2VD.map* – Second vertical derivative of the pole reduced field
- *scale_TILT.map* – Tilt derivative of the pole reduced field
- *scale_ASIG.map* – Analytic Signal of the residual magnetic intensity
- *scale_HGRTP.map* – Horizontal gradient of the pole reduced field
- *scale_TDX.map* – Total horizontal gradient of the pole reduced field.
- *scale_SED.map* – Source edge detection symbols with the second vertical derivative of the pole reduced field
- *scale_SPI.map* – Depth to magnetic sources using Source Parameter Imaging (SPI)
- *scale_Edge.map* – Edge detection filter using Encom's special filters
- *scale_Area.map* – Area detection filter using Encom's special filters
- *scale_DEM.map* – Radar derived digital elevation model (DEM)
- *scale_Interpretation* – Geophysical interpretation results

All maps are "packed", meaning that all data layers including grids are contained within the map so that only the map file needs to be transferred between computers. Adobe pdfs of the above maps were also created at the same map scale.

Grids

The following Geosoft grids were produced with a datum/projection of WGS84/UTM15N:

- *RMI.grd* – IGRF corrected total magnetic intensity
- *RTP.grd* – Total magnetic intensity reduced to the pole
- *RTP1VD.grd* – First vertical derivative reduced to the pole
- *RTP2VD.grd* – Second vertical derivative reduced to the pole
- *TILT.grd* – Tilt derivative of the pole reduced field
- *ASIG.grd* – Analytic signal of the total magnetic intensity
- *RTP_HG.grd* – Horizontal gradient of the pole reduced field
- *TDX.grd* – Total horizontal gradient of the pole reduced field
- *SPI_depth.grd* – Depth to magnetic sources using source parameter imaging (SPI)



- RTP_ZS_Area.grd – Encom special filter Area
- RTP_ZS_Block.grd – Encom special filter Block
- RTP_ZS_Edge.grd – Encom special filter Edge
- RTP_ZS_EdgeZone.grd – Encom special filter Edge Zone
- RTP_ZS_Plateau.grd – Encom special filter Plateau
- SRTM_DEM.grd – Digital elevation model derived from the 30 m SRTM grid
- DTM.grd – Digital elevation model derived from the survey data

Databases

The following Geosoft databases were modified or produced with a datum/projection of WGS84/UTM15N:

Leo Property

- 20156_Leo_Final_Magnetic_Data.gdb – Magnetic airborne survey data
- Leo_SED.gdb – Source edge detection database with locations of 1, 2, 3, or 4 gradient directions
- Leo_SPI.gdb - Depth to magnetic sources with respect to survey height and ground surface

Sydney Lake Property

- 20157_SydneyLake_Final_Magnetic_Data.gdb
- SL_SED.gdb – Source edge detection database with locations of 1, 2, 3, or 4 gradient directions
- SL_SPI.gdb - Depth to magnetic sources with respect to survey height and ground surface

Western Bear Property

- 20157_WesternBear_Final_Magnetic_Data.gdb
- WB_SED.gdb – Source edge detection database with locations of 1, 2, 3, or 4 gradient directions
- WB_SPI.gdb - Depth to magnetic sources with respect to survey height and ground surface

VOXI Modelling

An unconstrained magnetic inversion model using the Magnetization Vector Inversion (MVI) technique was created using the Geosoft application known as VOXI. “MVI allows the magnetization direction to vary within the model and thus take into account the combined effects of remanence, demagnetization, anisotropy and induced magnetization. The result is a more realistic representation of rock magnetization, which is the fundamental rock property measured with the magnetic method.”⁴ Thus, in areas of remanence or low magnetic latitude, the inversion based upon the MVI method is more reliable than other magnetic susceptibility inversion algorithms.

⁴ Introduction of VOXI Earth Modelling technology: Accessible 3D modelling technology advances exploration geophysics for improved drill targeting. Earth Explorer, March 9, 2012.
http://www.earthexplorer.com/2012/introduction_of_voxi_earth_modelling_technology.asp

The VOXI modelling was further refined by using an “iterative weighting” that uses the initially derived VOXI model as the input for two further iterations of the inversion. This improved the model by focusing the boundaries of the high susceptibility sources at depth.

Each survey area was inverted as one complete block with a model resolution as listed below. The inversion locates areas of high magnetic susceptibility and its depth and possible shape.

Leo VOXI Modelling

- Extents: Easting – 433390 to 473850 m Northing – 5608270 to 5617750 m
- Horizontal Cell size: 100 m
- Vertical cell size: 50 m at surface and increasing with depth
- Vertical Extents: 442.8 m to -3,803.6 m above see level (asl)
- 3D View: Leo.geosoft_3dv
- MVI Voxel model: VOX_Leo_Ampl
- MVI Isosurfaces: SURF_Leo_Ampl

Further details are available in the file Leo inversion_parameters.html

Sydney Lake VOXI Modelling

- Extents: Easting – 402930 to 408270 m Northing – 5617350 to 5622910 m
- Horizontal Cell size: 25 m
- Vertical cell size: 12.5 m at surface and increasing with depth
- Vertical Extents: 411.0 m to -1,226.9 m above see level (asl)
- 3D View: SL.geosoft_3dv
- MVI Voxel model: VOX_SL_Ampl
- MVI Isosurfaces: SURF_SL_Ampl

Further details are available in the file Sydney Lake inversion_parameters.html

Western Bear VOXI Modelling

- Extents: Easting – 405050 to 408170 m Northing – 5633070 to 5640030 m
- Horizontal Cell size: 25 m
- Vertical cell size: 12.5 m at surface and increasing with depth
- Vertical Extents: 432.1 m to -1,589.4 m above see level (asl)
- 3D View: WB.geosoft_3dv
- MVI Voxel model: VOX_WB_Ampl
- MVI Isosurfaces: SURF_WB_Ampl

Further details are available in the file Western Bear inversion_parameters.html

The VOXI model is best viewed in Geosoft’s Oasis Montaj viewer so that the voxel, isosurfaces and various data layers can interacted with. Also included is a 3D pdf of the isosurfaces of the model that can be rotated, panned and zoomed.

The project workspace is **VOXI.gpf** contains the three separate 3D views, one for each survey area. The various surface layers, QuickMag models, voxels (3D block models) and isosurfaces of magnetic susceptibility can be viewed, made transparent and clipped in X, Y, Z and susceptibility extents. The susceptibility values are in SI units.

QuickMag Modelling

Encom's QuickMag magnetic modelling software was utilized to the model shape of various oblate and linear magnetic anomalies. By setting constraints to the model and allowing the other parameters to vary, the software can attempt to fit the data with a model with parameters of depth to top, depth extent, susceptibility, thickness and dip.

The aim of the QuickMag models were to determine the depth to top and dip of various limbs of the folded structures to determine whether they were basins or domes in the Leo and Sydney lake properties. The central highly magnetic intrusion in the Western Bear property was modelled as an oblate pipe-like intrusion.

The derived models were exported as 3D AutoCAD DXF files and included as a layer in the corresponding 3D view, i.e., Leo.geosoft_3dv.

Interpretation

The geophysical interpretations (**Figure 6**, **Figure 7** and **Figure 8**) is presented as a QGIS (version 3.14.1-Pi) project which consists of a number of grouped data layers:

- Base – survey flight path and survey outline presented as ESRI shapefiles
- Interpretation – containing targets, source edge detection results, lineaments, faults and lithology presented as ESRI shapefiles
- Planimetry –CANVEC (ESRI shapefile) sources of rivers and lakes presented as ESRI shapefiles
- Geophysical images – presented as geotiffs
- Landform images – presented as geotiffs
- Georeferenced geological maps – presented as geotiffs

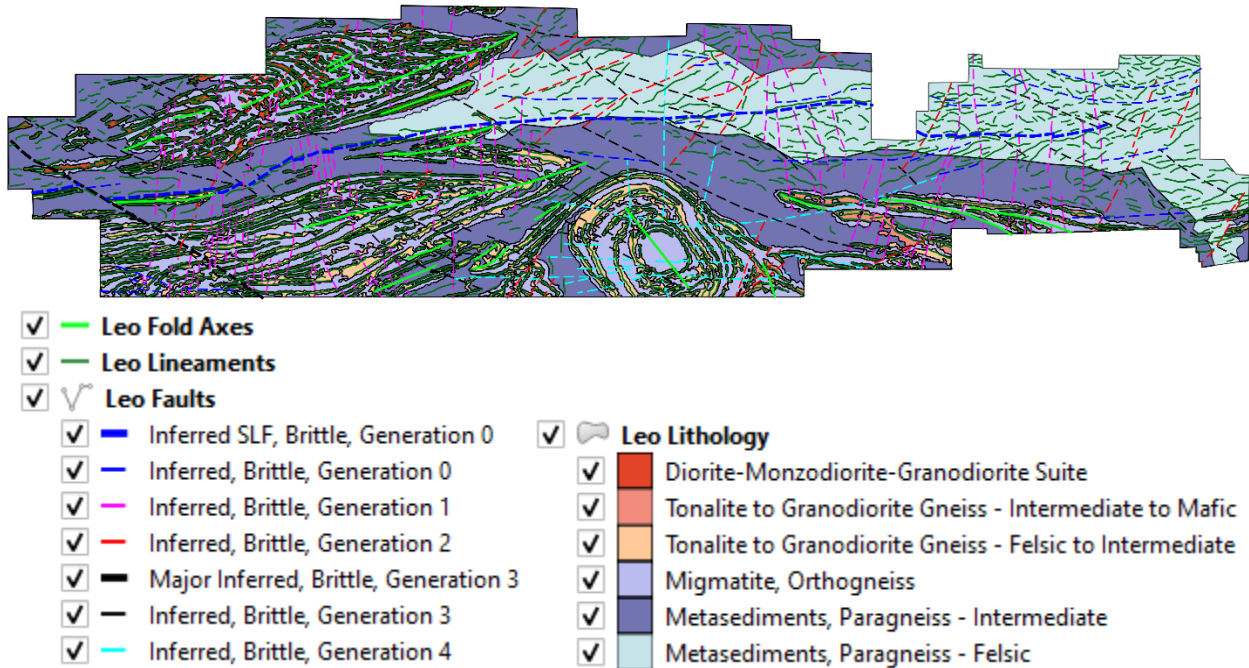


Figure 6. Interpretation layer of the Leo property and legend.

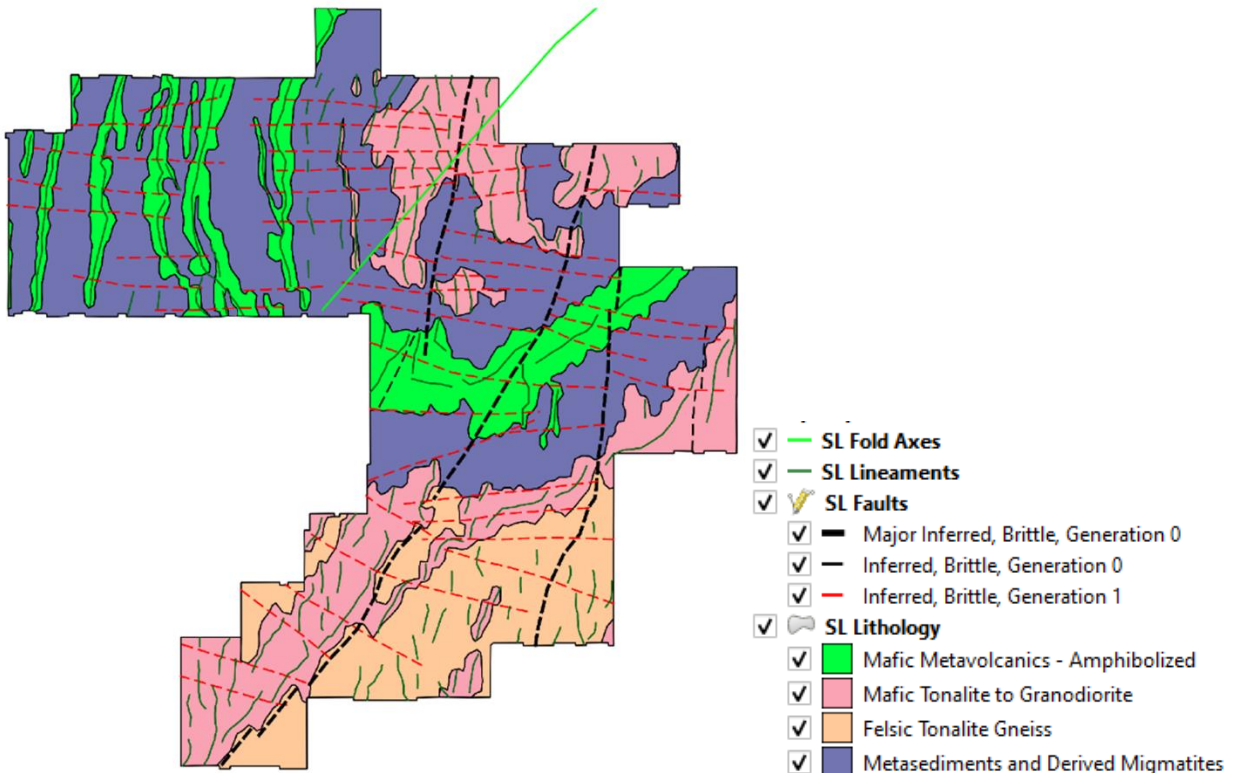


Figure 7. Interpretation layer of the Sydney Lake property and legend.

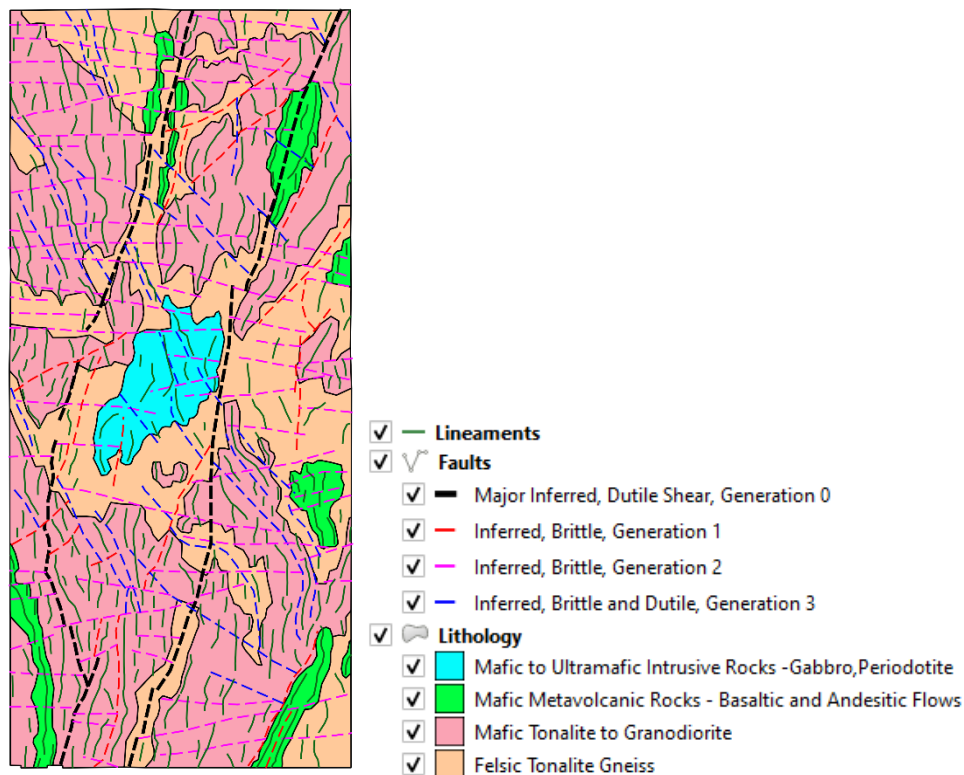


Figure 8. Interpretation layer of the Western Bear property and legend.

Landform Analysis

SRTM30 digital elevation data is provided through Geosoft’s Data Access Protocol (DAP) server with a grid cell size of 1 arc second (30.7 m) reprojected from a geographic WGS84 to a WGS 84/UTM 15N projection. If the Digital Elevation Model data from the survey GPS and altimeter difference was of higher quality, that DEM was used instead of the SRTM30 grid. The SRTM grid was windowed to the airborne survey extents. Topographic derivatives were then calculated from the SRTM terrain data for use in the interpretation of lithologies and faults expressed in the topography. The following terrain products were calculated for each survey block:

- Analytic hill shade
- Aspect
- Slope
- Landform classification

Analytic Hill Shade

The analytic hill shade grid shows the hypothetical illumination of a grid surface at a user-defined inclination (altitude angle) and declination (azimuth angle). It can greatly enhance the visualization and interpretability of surfaces (such as topography) by providing a third dimension to the two-dimensional map. Features perpendicular to the sun declination are emphasized by this imaging method so multiple illumination directions should be used for interpretation.

The delivered analytic hill shade grids use an inclination of 45°, a declination of 0°, and vertical exaggeration dependent upon the topographic range within the property.

Slope

Slope is the angle, in radians, of the topographic surface from 0 (flat) to $\pi/2$ (vertical). It can be thought of as the first derivative of the topographic surface. Slope has many important applications in remote sensing including delineating tectonic structures (folds, faults, fractures), identifying areas of potential instability, determining hydrological flow rates and sedimentation.

Aspect

Aspect is the facing direction of a slope calculated from the digital elevation model. It is measured clockwise from 0° (due north) to 360° (due north) degrees. It defines the direction of flow and is important for studies where the slope facing direction can be a control. Aspect can also be useful to quantify topographic trends and recognize geological structures.

Landform Classification

The landform classification divides an area of continuous topography into categories of surface form from three morphometric variables: slope gradient, local convexity and surface texture (Iwahashi and Pike, 2007)⁵. The taxonomic criteria are calculated from the DEM within a given window size and classified using an unsupervised nested-means algorithm. The classification can be set from a minimum of 8 to 12 or 16 classes to allow for increasingly subtle topographic forms to be subdivided. As the process is unsupervised, the output classes are not assigned to specific geomorphic features, but certain values tend to cluster that correspond to topographic regions or other spatial assemblages of landform (Iwahashi and Pike, 2007).

For this study 9 classes were used with for all survey blocks. A window size of 3x3 was used for slope, convexity and texture from 9x9 mean filtered grid.

Magnetic Interpretation

The magnetic lithology is interpreted from the analytic signal, first and second vertical derivatives and supplemented by other magnetic images. Distinct units are characterized based on the signal amplitude, frequency content (wavelength), texture and overall geometry. The grids that were the most useful were the residual magnetic intensity reduced to the pole (RTP.grd shown in **Figure 5**Figure 65) for the absolute amplitude of the magnetic anomalies. The second vertical derivative of the pole reduced field (RTP2VD.grd), Tilt derivative (TILT.grd), the total horizontal derivative of the pole reduced field (TDX.grd), and the Encom special filtered grids of Edge and Area (RTP_ZS_Edge.grd and RTP_ZS_Area.grd) for the location of contacts, faults and possible fold axes.

⁵ Iwahashi, J. and Pike, R.J., 2007. Automated classifications of topography from DEMs by an unsupervised nested-means algorithm and a three-part geometric signature. *Geomorphology*, 86(3-4), pp.409-440.



Leo

Lithological Interpretation

The following **Table 1** briefly describes the magnetic amplitude and textures that were used to assign the various interpreted lithologies.

	Lithology	Amplitude	Comments
1	Diorite-Monzodiorite-Granodiorite Suite	Mid 100's to 2,000 nT	Curvilinear, continuous, narrow bands, mapped as a Diorite-Monzodiorite - Granodiorite Suite, north of the Sydney Lake fault zone.
2	Tonalite to Granodiorite Gneiss – Intermediate to Mafic	High 100's to 2,000 nT	Curvilinear, continuous, narrow bands, tightly folded, mapped as a Tonalite to Granodiorite Gneiss, south of the Sydney Lake fault zone. Overall, higher magnetic values than the felsic to intermediate phase (3).
3	Tonalite to Granodiorite Gneiss – Felsic to Intermediate	Mid 100's to 1,200 nT	Curvilinear, continuous, narrow bands, mapped as a Tonalite to Granodiorite Gneiss, south of the Sydney Lake fault zone. Overall, lower magnetic values than the intermediate to mafic phase (2).
4	Migmatites, Orthogneiss	Mid 100's nT	Low magnetic signal between the layers of Diorite-Monzodiorite - Granodiorite Suite (1), Tonalite to Granodiorite Gneiss – Intermediate to Mafic (2) or Tonalite to Granodiorite Gneiss – Felsic to Intermediate (3). Derived from their igneous counterparts.
5	Metasediments, paragneiss - Intermediate	Low to Mid 100's nT	Low magnetic signal, background metasediments, derived from their sedimentary or metamorphic counterparts. Short wavelength, small amplitude features.
6	Metasediments, paragneiss - Felsic	Low to Mid 100's nT	Lower magnetic signal than Metasediments, paragneiss – Intermediate (5), background metasediments, derived from their sedimentary or metamorphic counterparts. Longer wavelength, small amplitude features.

Table 1. Geophysical criteria for various lithological units.

The Pakwash-Longlegged Lake geological map (P.1027, **Figure 9**)⁶ and the digital bedrock geology from Ontario Geological Survey⁷ (**Figure 10**) were used as guides to assign the likely lithological units. There was fair agreement with the geological maps though there was more detail to be seen in the geophysical images. For example, the location of the Sydney Lake fault zone in both geological maps is shown as an approximately 1 km wide zone of migmatites mapped as cataclastic diatexite or metatexite extending from east to west. This would have the fault zone pass through the southern portion of the granodiorite (Diorite-Monzodiorite -Granodiorite Suite, (1)) and the northern portion of the granodiorite (Tonalite to Granodiorite Gneiss – Felsic to Intermediate, (3)). Is it more likely, as in this interpretation, that the fault zone passes between the two granodiorites in an S-type fold or shape.

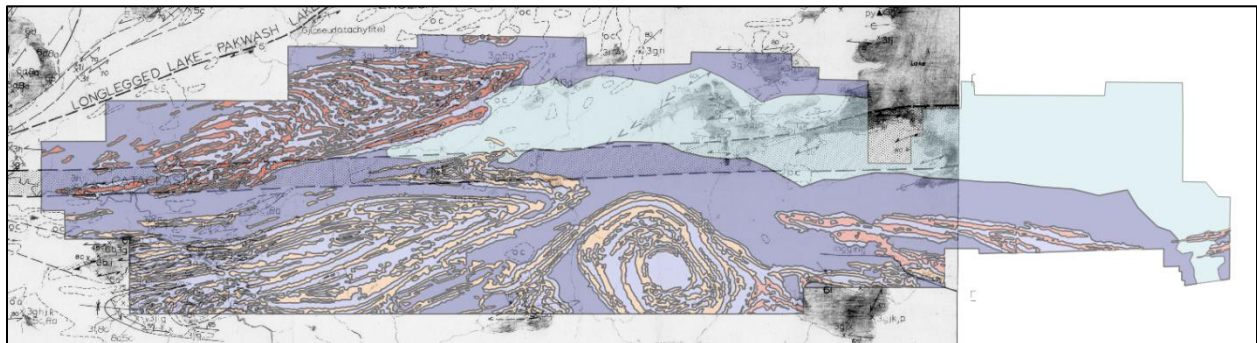


Figure 9. Pakwash-Longlegged Lake geological map and the current lithological interpretation.

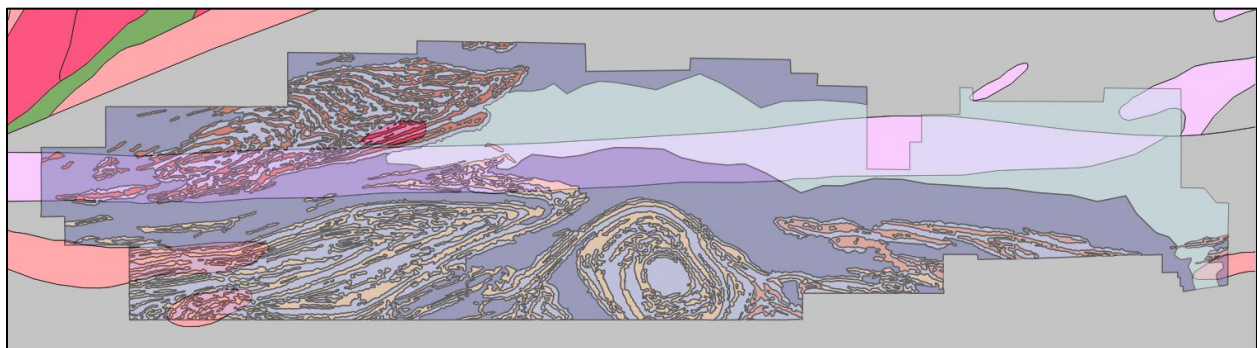


Figure 10. Ontario Geological Survey 1:250 000 scale geological map and the current lithological interpretation.

Examples of these units can be seen in the following subsets (**Figure 11**) of the lithological interpretation: West (red), South-Central (cyan) and North-Central (green).

<input checked="" type="checkbox"/>		Leo Lithology
<input checked="" type="checkbox"/>		Diorite-Monzodiorite-Granodiorite Suite
<input checked="" type="checkbox"/>		Tonalite to Granodiorite Gneiss - Intermediate to Mafic
<input checked="" type="checkbox"/>		Tonalite to Granodiorite Gneiss - Felsic to Intermediate
<input checked="" type="checkbox"/>		Migmatite, Orthogneiss
<input checked="" type="checkbox"/>		Metasediments, Paragneiss - Intermediate
<input checked="" type="checkbox"/>		Metasediments, Paragneiss - Felsic

⁶ Breaks, F. W., Bond, W. D., McWilliams, G. H., Gower, C. F., and Stone, Denver 1975 Operation Kenora-Sydney Lake, Pakwash-Longlegged Lakes Sheet, District of Kenora; Ontario Div. Mines, Prelim. Map P.1027 Geol. Ser., scale 1 inch to 1 mile or 1:63,360. Geology 1974.

⁷ Ontario Geological Survey 2011. 1:250 000 scale bedrock geology of Ontario; Ontario Geological Survey, Miscellaneous Release–Data 126 - Revision 1.

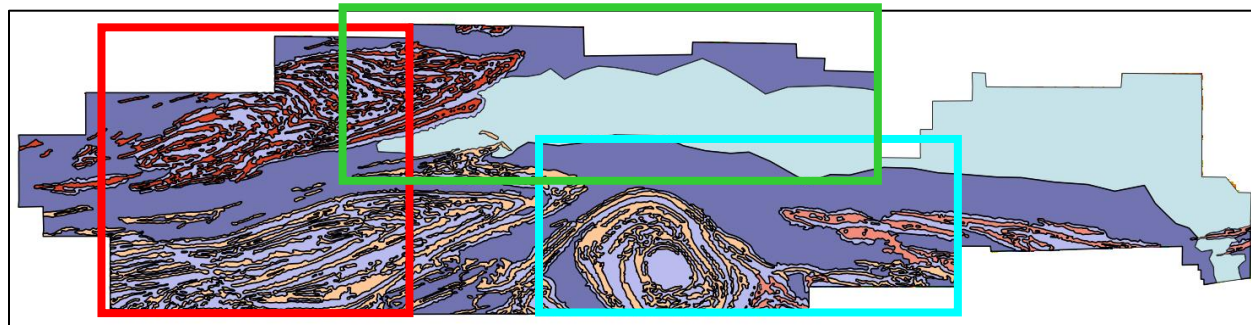


Figure 11. Lithological interpretation and location of three area subsets.

West Subset

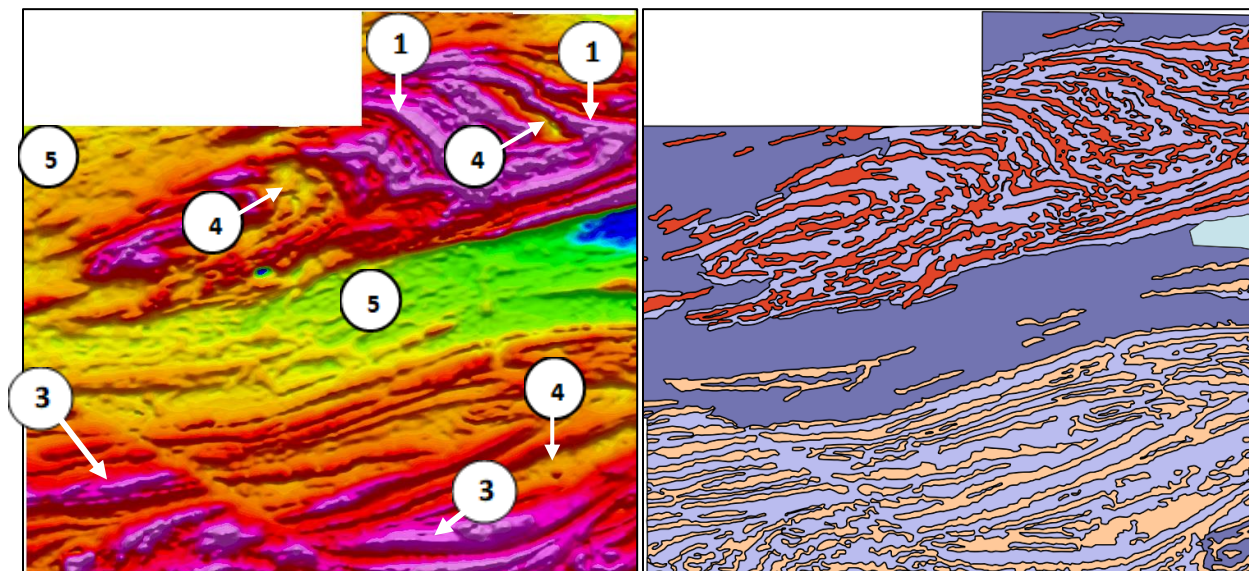


Figure 12. West Subset: Residual magnetic intensity reduced to the pole (left) and the current geophysical interpretation (right).

The west subset of the lithological interpretation contrasts the difference between the northern and southern folded and deformed granodiorite suites. The northern granodiorite intrusion (Diorite-Monzodiorite -Granodiorite Suite) has a much higher mafic content as reflected by its overall higher magnetic signal. The southern granodiorite (Tonalite to Granodiorite Gneiss – Felsic to Intermediate) has a moderate magnetic signal, thus the designation that it is of felsic to intermediate composition. The image above (**Figure 12**) does not highlight the difference in magnetic signal between they two granodiorite types since the colour transform is an equal area histogram which emphasizes variations in the mid values (yellow and green colours). The 3D surface of the magnetic field reduced to the pole is shown in **Figure 16**. 3D view of the residual magnetic intensity reduced to the pole. and **Figure 17**. In these images it can be seen that the northern granodiorite has about twice the magnetic signal as the southern granodiorite. Thus, it is implied that the are of different compositions.

The northern and southern granodiorites are separated by the Sydney Lake fault zone that was mapped through the metasediments between them.



Within each granodiorite there are alternating bands of magnetically high and low continuous units. The magnetically high bands are the corresponding granodiorite. The magnetic lows in between are interpreted to be migmatized granodiorite. It is defined as an orthogneiss since the migmatite is derived from the partial melt of the host granodiorite. In both cases, the migmatization destroys the magnetic mineral such as magnetite. The migmatite units were interpreted to be within and directly surrounding the granodiorite units.

South-Central Subset

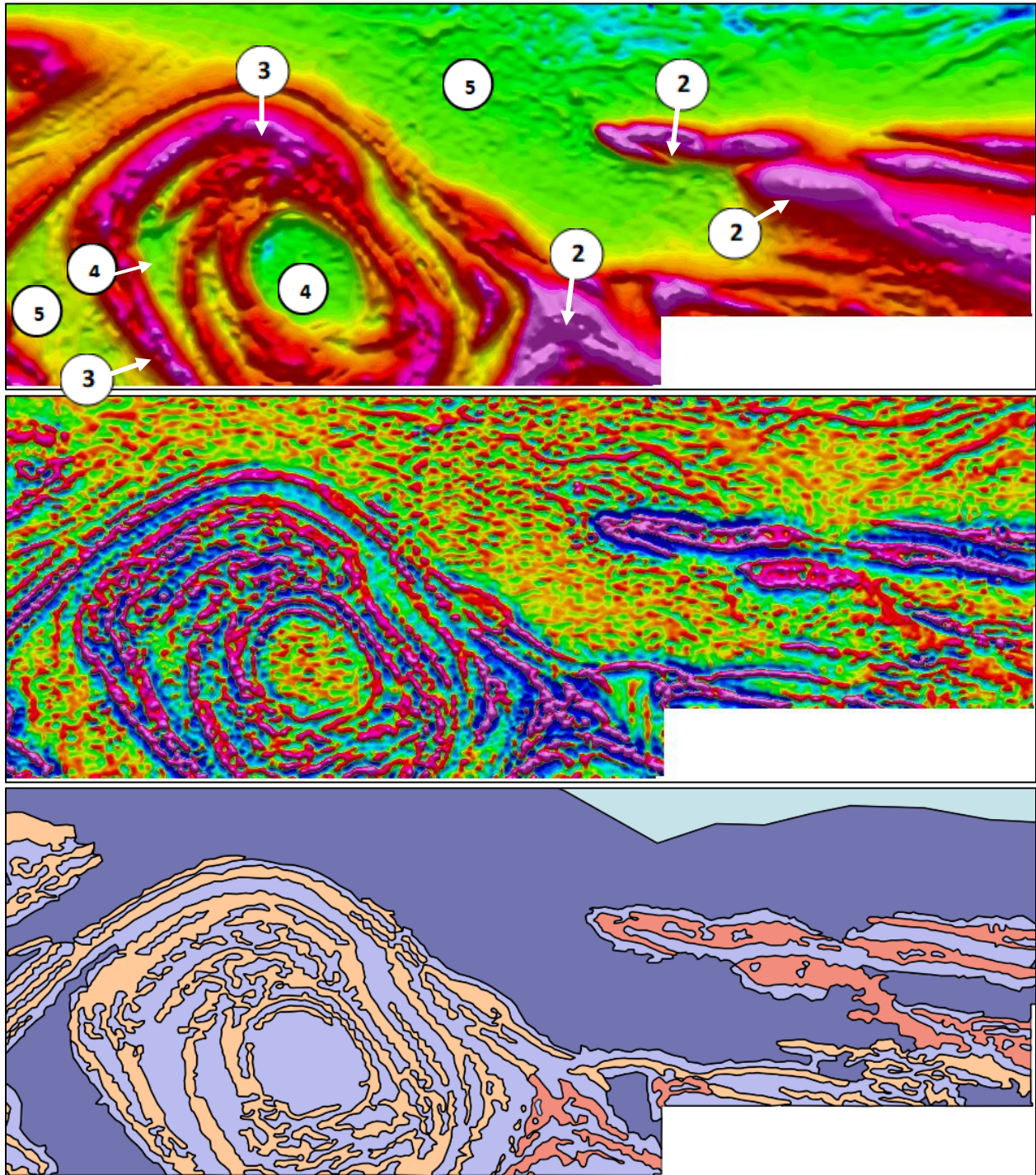


Figure 13. South Central Subset: Residual magnetic intensity reduced to the pole (above), the second vertical derivative of the pole reduced magnetic field (centre) and the current geophysical interpretation (below).

A prominent feature of this South-Central subset (**Figure 13**) is the undeformed granodiorite intrusion (Tonalite to Granodiorite Gneiss – Felsic to Intermediate) in the centre of this area. Its magnetic intensity is similar to the granodiorite intrusion to the west, but it appears undeformed. Thus, it is implied that this is a later intrusion but similar in composition.

To the east of this intrusion there are some units that are much higher in magnetic susceptibility. This is best seen in the 3D view of the reduced to the pole image (**Figure 16** and **Figure 17**). Thus, this was interpreted still to be a Tonalite to Granodiorite Gneiss with an intermediate to mafic composition. There are two localities of this intermediate to mafic unit. Further to the east is a tightly folded gneissic intrusion and there is a smaller component to the southeast of the undeformed granodiorite intrusion.

The South-Central subset illustrates the difficulty between distinguishing between the migmatite (4) and the metasediments (5). Both are magnetically low in value and have a relatively smooth texture with a slightly dimpled appearance (short wavelength, very low amplitude). Likely the magnetic susceptibility of the migmatite and metasediments are similar so that little or no magnetic contrast is seen. However, they were differentiated by their character in the second vertical derivative of the pole reduced field. Within the granodiorite bands, the migmatite is shown as deep lows (blues) in the second vertical derivative. The surrounding metasediments have values in the second vertical derivative of the pole reduced field that were approximately zero, i.e., yellows and greens in the image above. However, this criteria does not always hold. In the areas designated as migmatite (4) in that centre of the undeformed granodiorite intrusion and the metasediment (5) outside of that intrusion look the same in the reduced to the pole image and its second vertical derivative (**Figure 13**). The areas within the limbs and bands of this granodiorite as designated as migmatite and areas mainly outside of the intrusions are designated as metasediments.

North-Central Subset

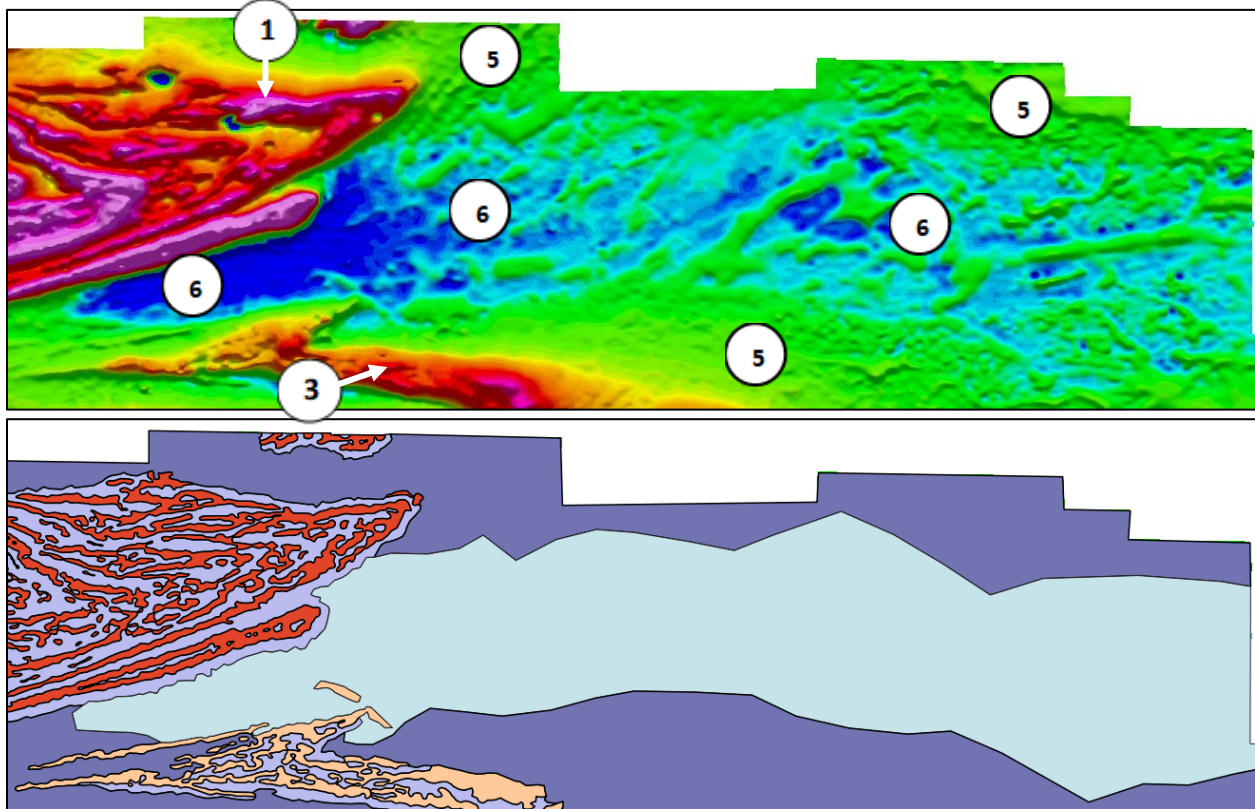


Figure 14. North Central Subset: Residual magnetic intensity reduced to the pole (above) and the current geophysical interpretation (below).

The North-Central subset (**Figure 14**) highlights the difference between two metasedimentary units with a tendency to an intermediate or felsic composition. Both are paragneisses, i.e., derived from their sedimentary or metamorphic counterparts. The intermediate version (5) is more common throughout the survey area. This unit divides the northern and southern granodiorites and extends to the west. The boundaries of this felsic unit are rough or blocky since the contacts are difficult to define.

The felsic version (6) is lower in magnetic value than the intermediate version (5). There is also a textural difference. The intermediate version (5) has a slightly dimpled appearance (short wavelength, very low amplitude) as noted previously. The felsic version (6) also seems to have some linear and longer wavelength features and loss of the dimpled appearance. Some of the linear features can be attributed to the presence of lakes in the area. The lake depths add distance between the bedrock and the magnetometer sensor as if the aircraft was flying at a greater height. Increased distance to bedrock diminishes the short wavelength features. When the outlines of the local waterbodies are overlain on the reduced to the pole image, there is correlation between the lakes and the linear longer wavelength in some places, but not in others (see **Figure 15** below).

At the western extent of the felsic metasediments (6), its presence becomes indistinct between the northern and southern granodiorites. At the western end of the felsic metasediments (6), the Sydney Lake fault zone is interpreted to pass near and along the southern contact between the felsic and intermediate

units. Further to the east, the Sydney Lake fault zone is interpreted to pass near the middle of this felsic metasedimentary unit.

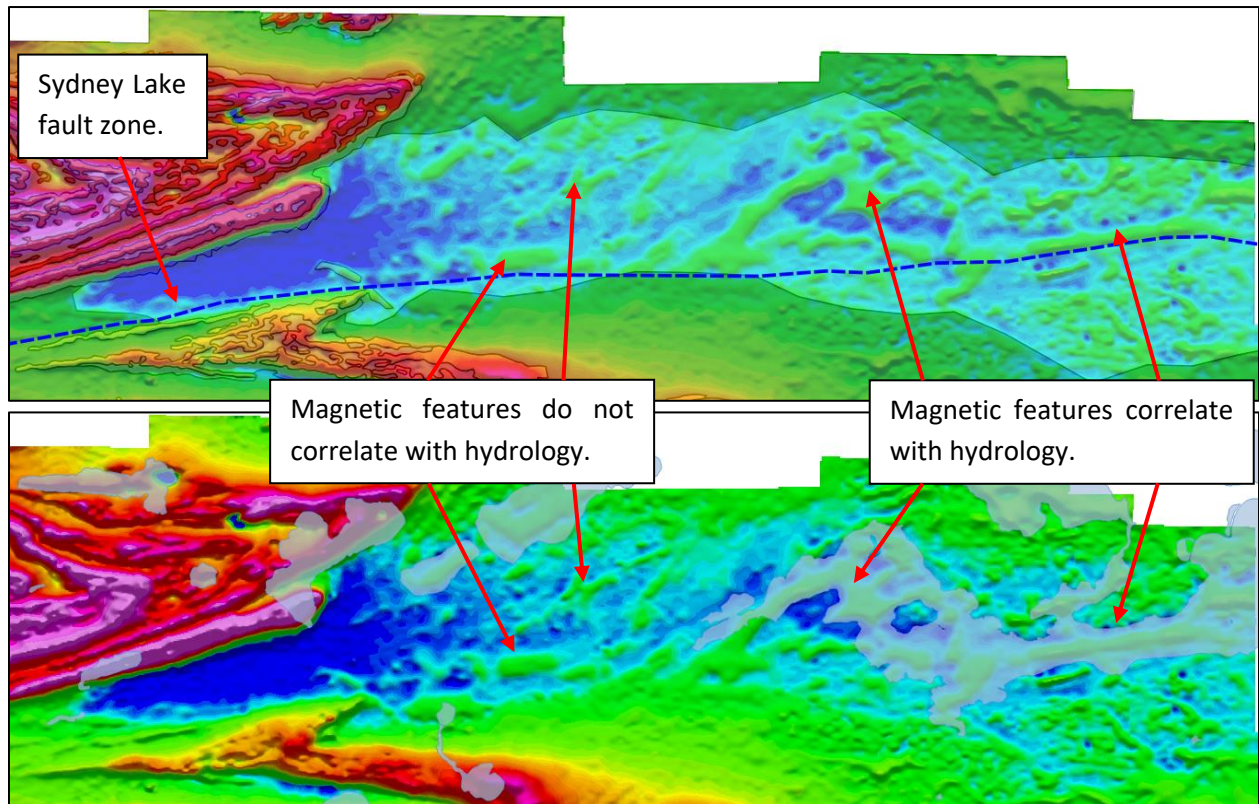


Figure 15. Reduced to the pole images with interpreted lithology (top) and with hydrology (bottom).

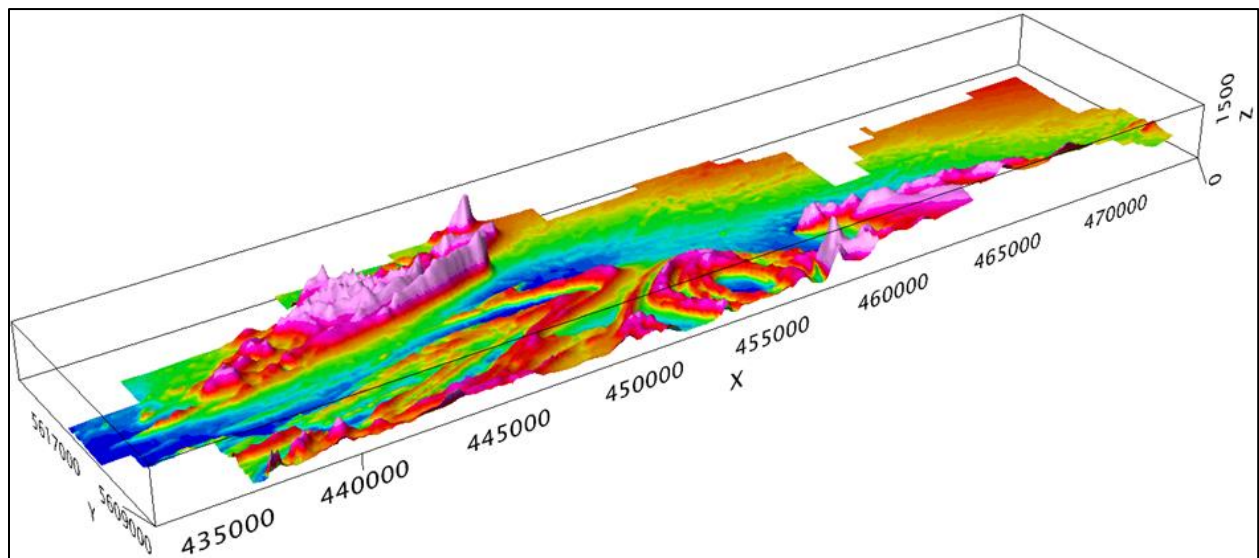


Figure 16. 3D view of the residual magnetic intensity reduced to the pole.

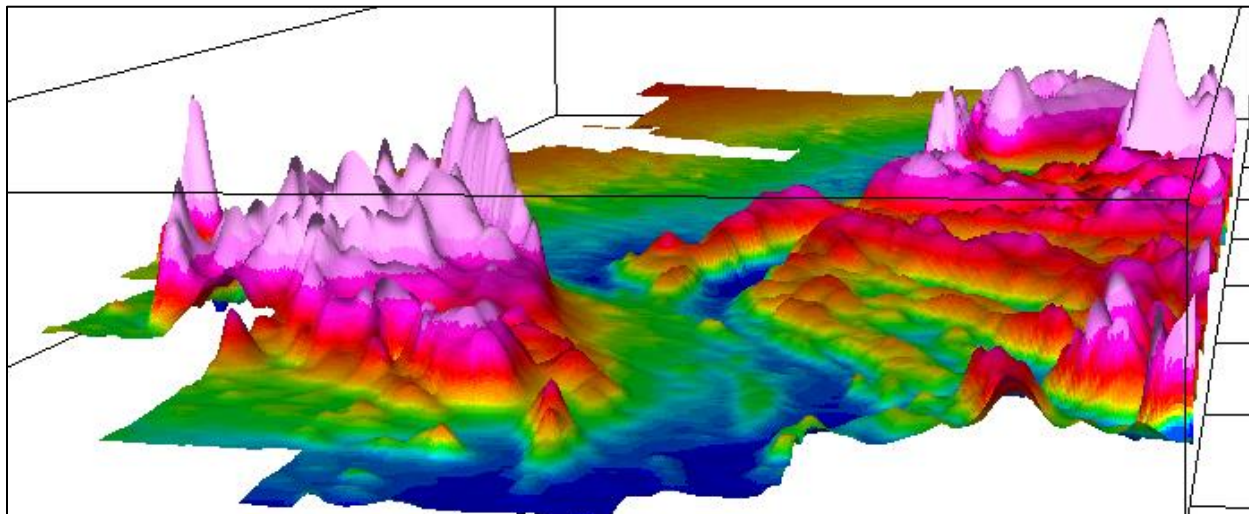


Figure 17. 3D view of the residual magnetic intensity reduced to the pole looking east.

Lineaments

Lineaments were traced along highs in the second vertical derivative of the pole reduced field (RTP2VD.grd), tilt derivative (TILT.grd) and total horizontal gradient (TDX.grd). The tilt derivative with lineaments is shown in the image below (**Figure 18**).

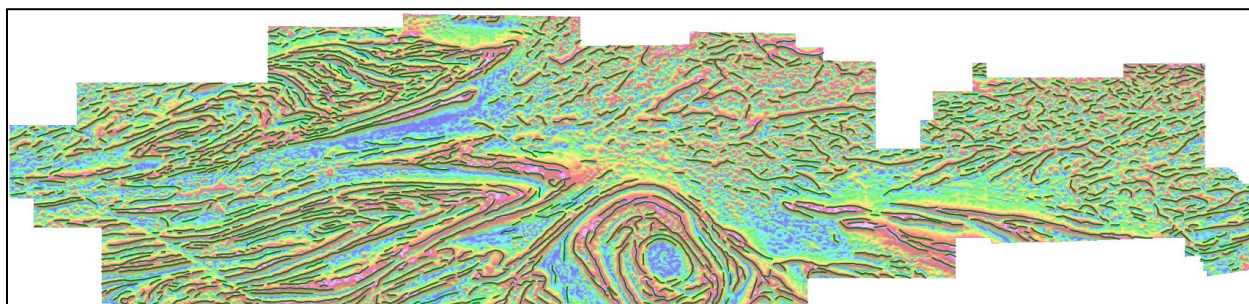


Figure 18. Lineaments or trends overlain upon the tilt derivative (50% transparency applied).

A rose diagram of the orientations of the lineaments (**Figure 19**) show a vast majority of the orientations lie within the ENE and E directions. Minor amounts of lineaments occur in the quarters on either side of the majority direction in the NE to ENE and E to ESE directions. Very few lineaments are in the remaining orientations. The lineaments within the compressed granodiorites are very continuous. Within the metasediments, the lineaments tend to be less continuous, shorter and more randomly orientated.

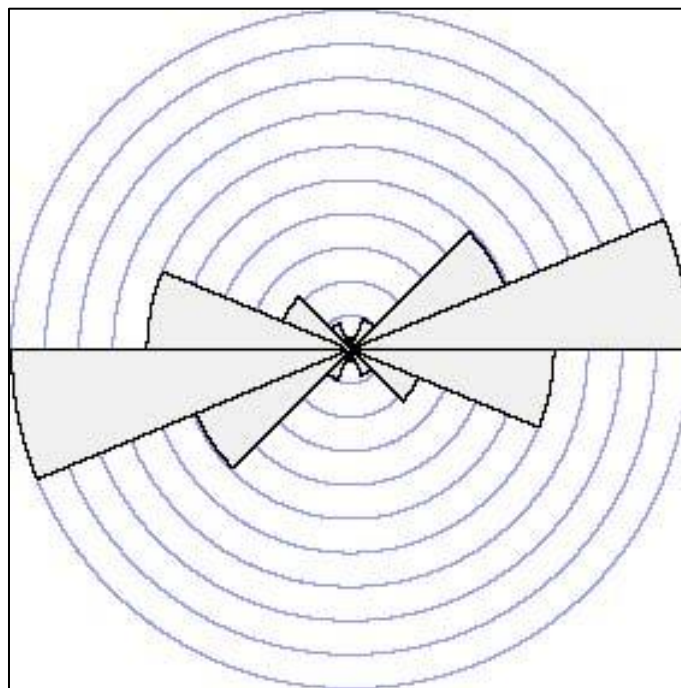


Figure 19. Rose diagram of orientations of lineaments.

Faults

The location and length of inferred faults were determined from various derivative grids such as the second vertical derivative of the pole reduced field (Figure 20). They were determined by an offset or disruption in character of the linear magnetic anomalies.

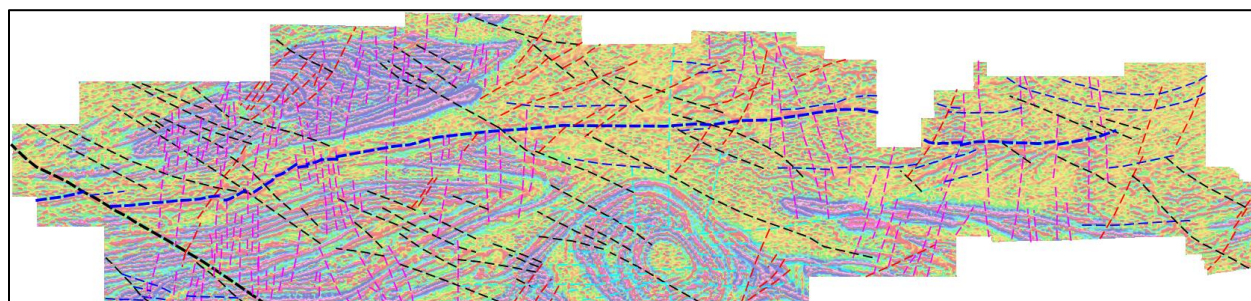


Figure 20. Interpreted faults overlain upon the second vertical derivative of the pole reduced field (50% transparency).

A Rose diagram of the fault orientations (Figure 21) shows multiple orientations of the interpreted faults. A majority of faults are between 0° (N) to 22.5° (NNE) followed by orientations of 90° (E) to 135° (SE). The faults have been divided into 5 generations generally defined by their orientations, as follows:

- Leo Faults
- Inferred SLF, Brittle, Generation 0
- Inferred, Brittle, Generation 0
- Inferred, Brittle, Generation 1
- Inferred, Brittle, Generation 2
- Major Inferred, Brittle, Generation 3
- Inferred, Brittle, Generation 3
- Inferred, Brittle, Generation 4

- Generation 0: 67.5° (ENE) to 90° (E) are interpreted to the oldest and are associated with the Sydney lake fault zone and related parallel faults. Generation 0 faults are offset by faults of the other fault generations.

- Generation 1: -22.5° (NNW) to 22.5° (NNE) and are generally N in orientation. They are interpreted to be younger than Generation 0. Where offsets are seen, Generation 1 faults are mostly dextral and occur throughout the study area.
- Generation 2: 45° (NE) to 67.5° (ENE) are interpreted to be younger than Generation 1. Very few offsets are seen. They occur throughout the study area.
- Generation 3: Generally 135° (SE) in orientation. A major fault in this direction is seen in the western portion of the property with a dextral offset of approximately 1.2 to 1.5 km. Other faults in this orientation are seen throughout the study area.
- Generation 4: The faults of this generation are associated with the undeformed granodiorite intrusion in the south. The faults are radial to this intrusion and are confined to this general location.

Due to the lack of clear and consistent offsets of the different fault generations, I can not be confident in the absolute order of the different generations, especially that of Generations 1, 2 and 3.

The number of faults and generations in such a small study area indicates a complex structural history. The structural interpretation of the magnetic data adds substantial information regarding possible fault location to the geology of the Leo area. For a better understanding of the fault character (e.g., associated alteration, slip direction) ground truthing of the interpreted structures is necessary.

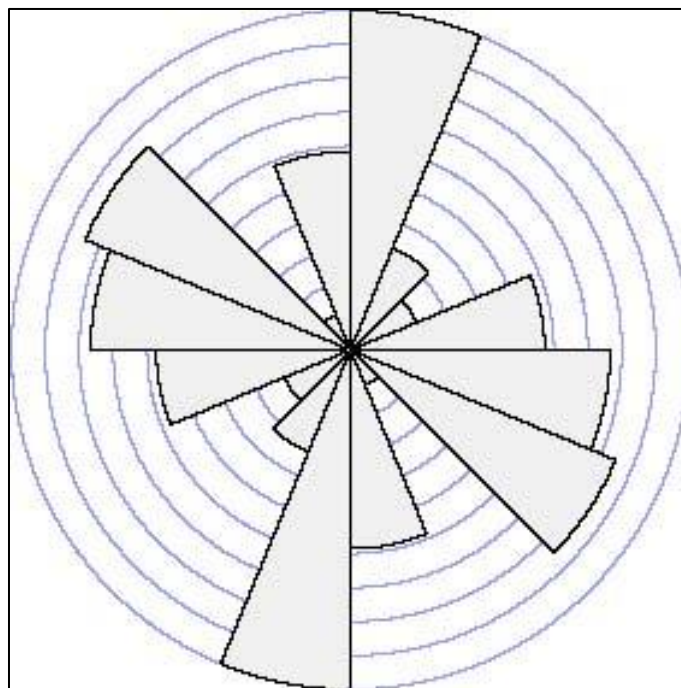


Figure 21. Rose diagram of fault orientations.

Folds

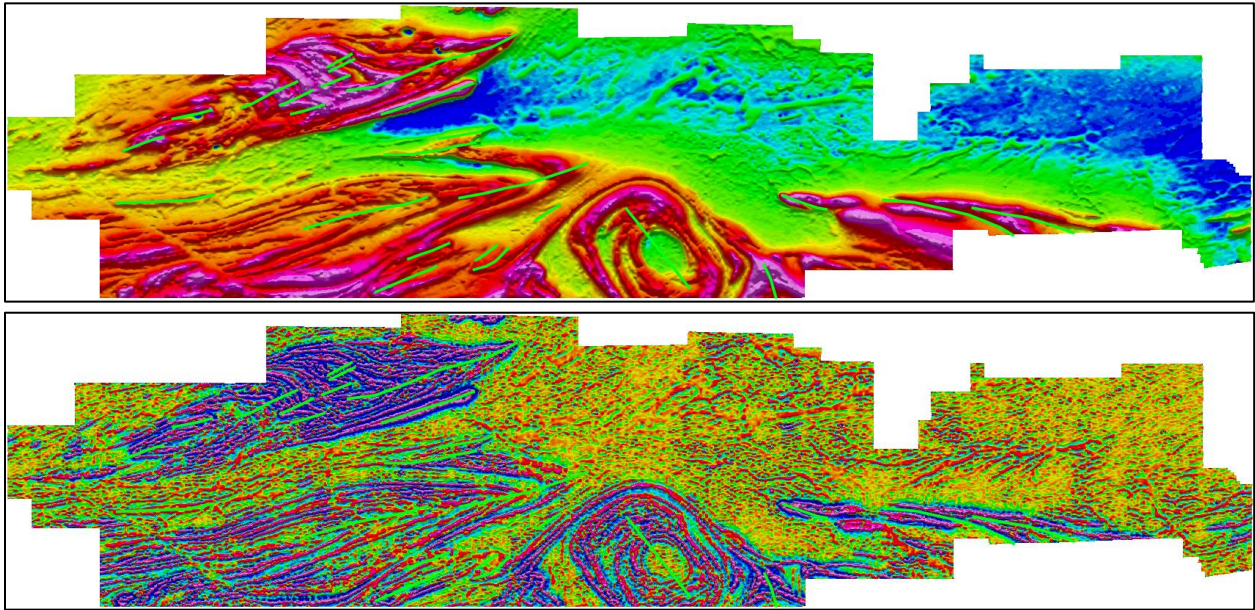


Figure 22. Fold axes (green) with the reduced to the pole (above) and 2nd vertical derivative of the pole reduced field (below).

There are generally three fold directions with a majority in the 90° (E) to 67.5° (ENE) orientations found in the two western granodiorites north and south of the Sydney Lake fault zone (**Figure 22** and **Figure 23**). The south-central granodiorite intrusion is generally circular with a slight oblateness in the 135° (SE) direction. The tightly folded intermediate to mafic granodiorite in the east has folds with an orientation of 90° (E) to 112.5° (ESE).

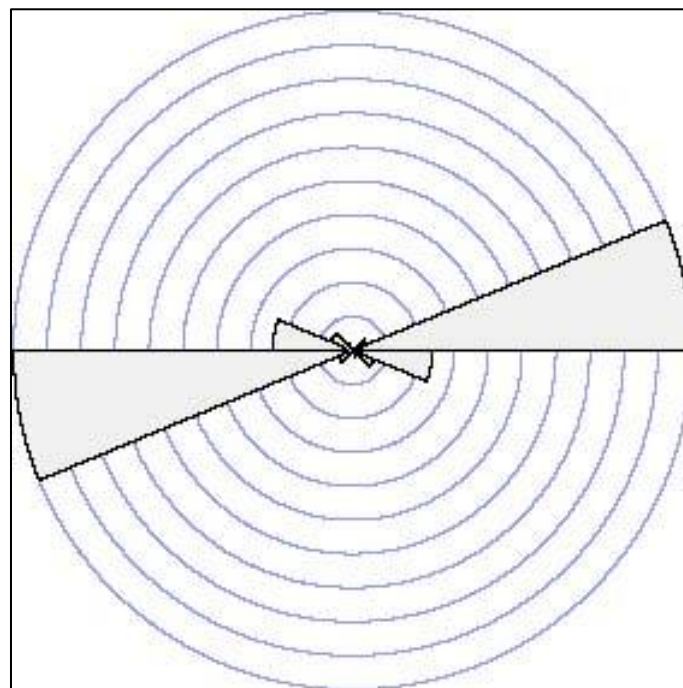


Figure 23. Rose diagram of fold orientations.

VOXI Modelling Interpretation

The VOXI 3D model of the magnetic susceptibility of the survey area is shown below in **Figure 24**. At surface, the susceptibility distribution appears similar to the image of the residual magnetic intensity such as the magnetic highs from the various granodiorite units. This implies that the modelling has forced many of the magnetic sources to be near the surface. The top of the model surfaces is at 443 m above sea level. The data has been clipped to different depth slices such as 200 m, -400 m and -1,600 m above sea level (asl) or 243 m, 843 m and 2,043 m below surface, respectively (**Figure 25**, **Figure 26** and **Figure 27**).

The VOXI model and its derived isosurfaces of the Leo property are very complex. The models are much easier to visualize the 3D view in the Geosoft oasis montaj viewer where one can zoom, pan and rotate the view and clip the models to their X, Y, Z and susceptibility extents. The following 2D representations are a poor representation of the detail that can be seen in the 3D models.

At a depth slice at 200 m below sea level (243 m below surface) show that the granodiorite layers maintain their continuity as seen from the lithological interpretation (**Figure 25**). In these views it is difficult to see in which direction the various limbs dip. The **Figure 28**, **Figure 29** and **Figure 30** are close-up views from overhead to aid in the determination of the dip directions.

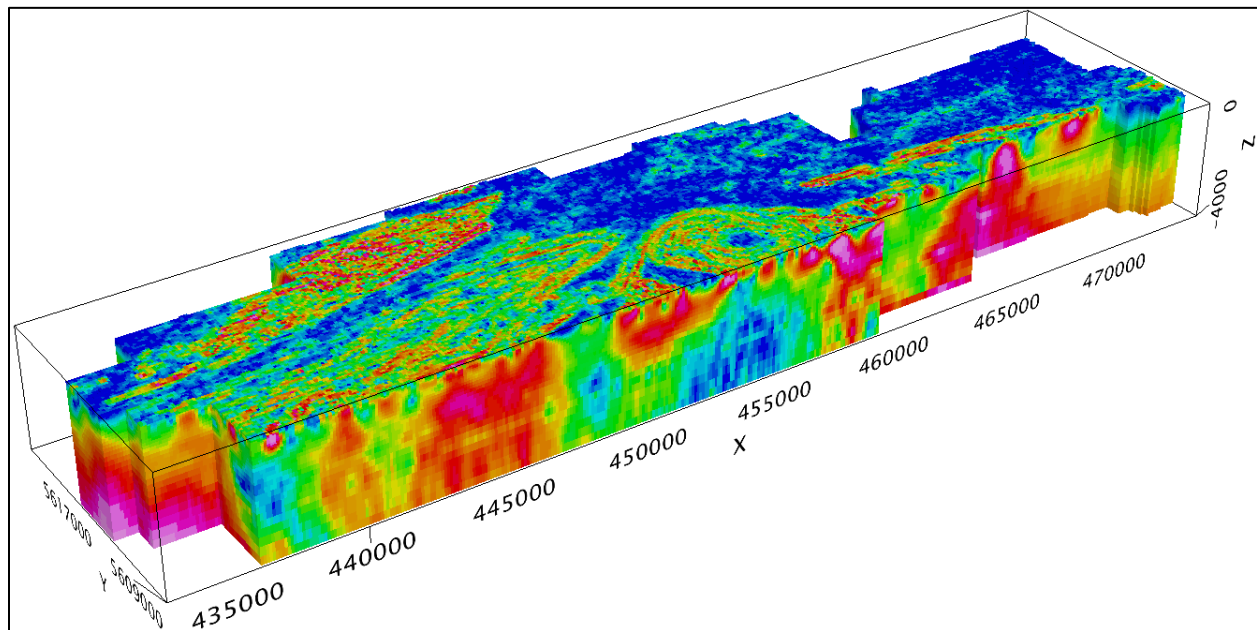


Figure 24. Magnetic susceptibility model of the survey area. The top of the model is at surface at 443 m above sea level.

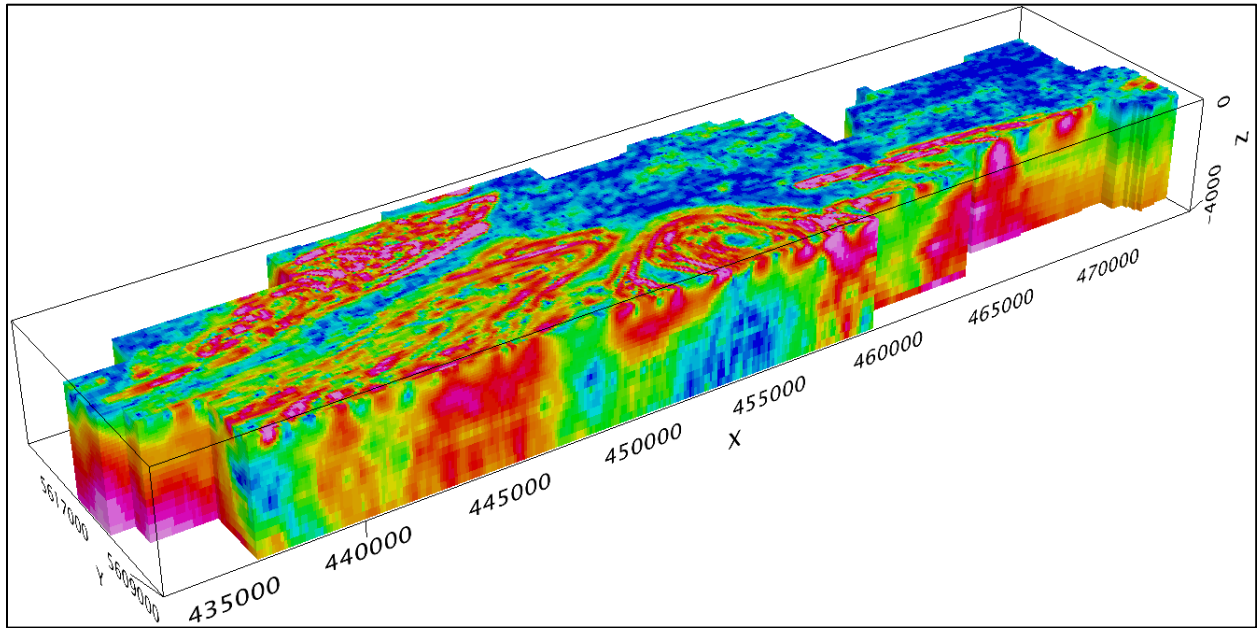


Figure 25. Magnetic susceptibility model with the top of the model is at 200 m above sea level.

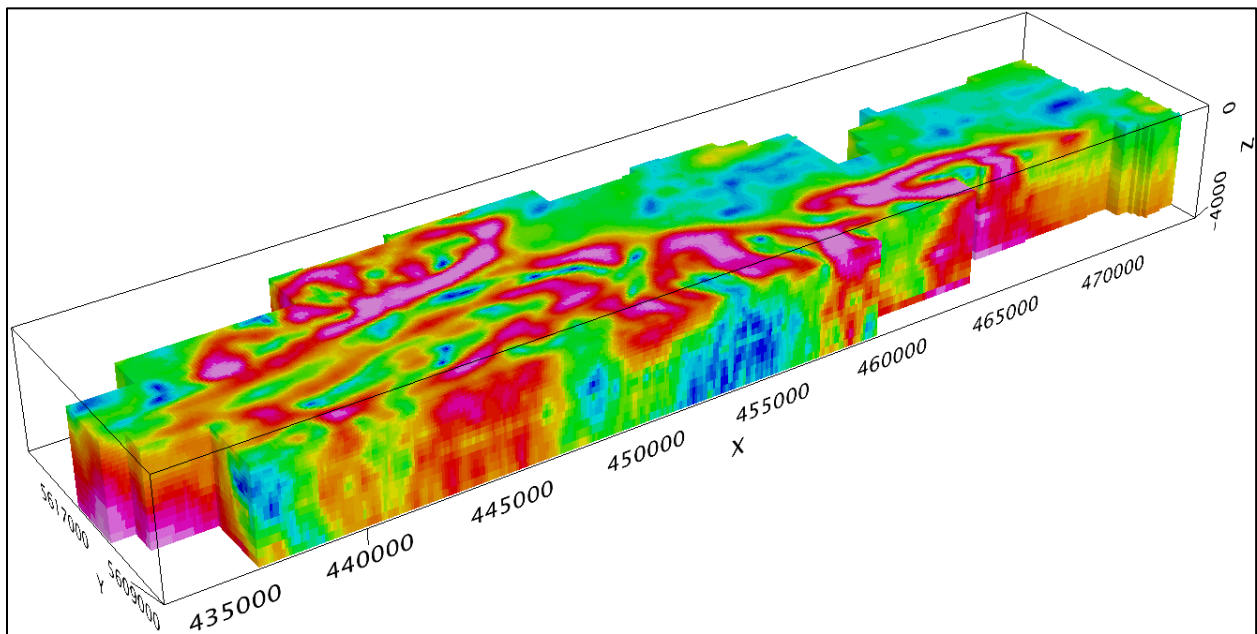


Figure 26. Magnetic susceptibility model with the top of the model is at 400 m below sea level.

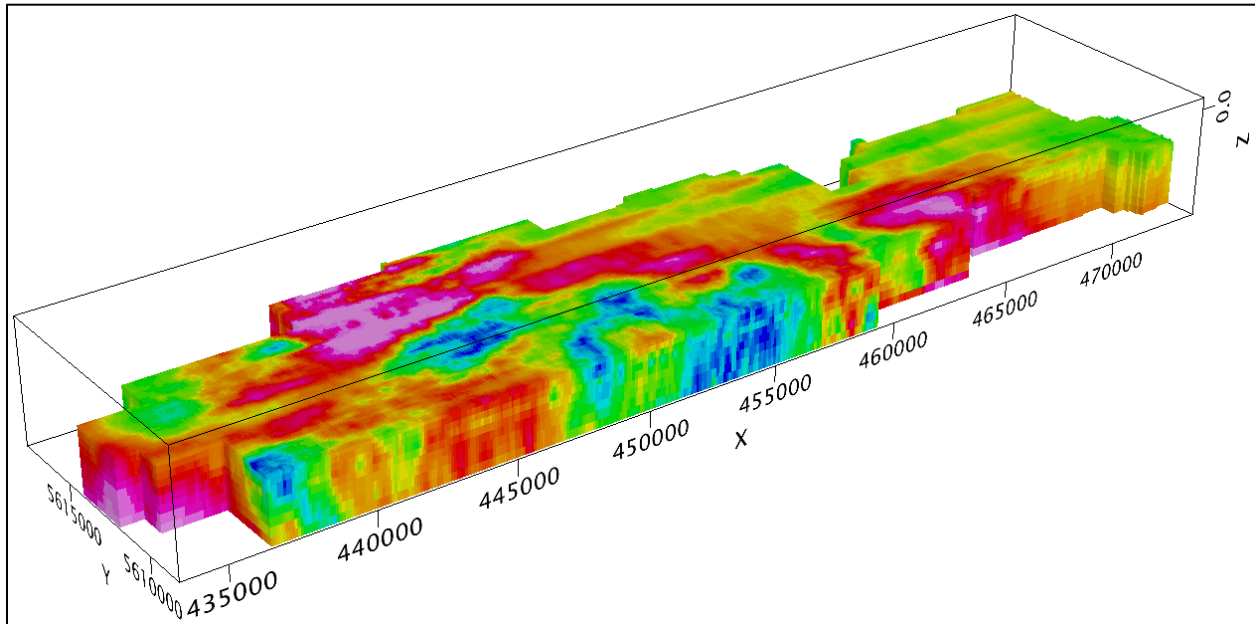
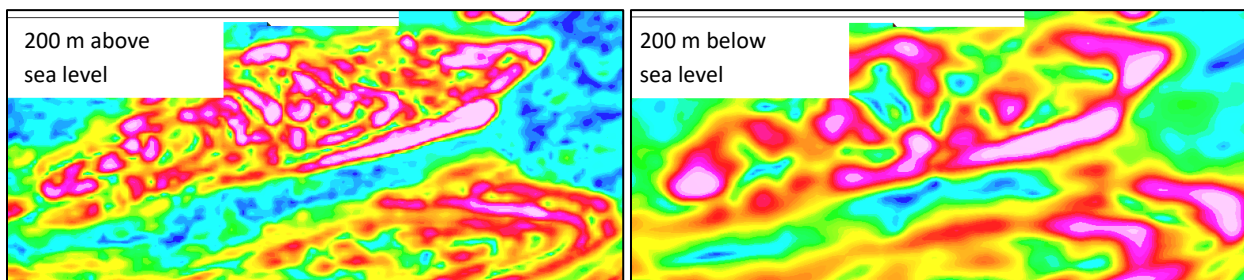


Figure 27. Magnetic susceptibility model with the top of the model is at 1600 m below sea level.

The depth slice view of the northern granodiorite (**Figure 28**) show that the limbs or bands of magnetic susceptible material remains continuous at 200 m above and below sea level. At further depths the highly susceptible material along the southern limb remains high throughout the model.

The depth slice view of the central undeformed granodiorite (**Figure 29**) also show that the limbs or bands of magnetic susceptible material remains continuous at 200 m above and below sea level. At further depths the magnetic susceptible material coalesces into one body dipping to the north.

The depth slice view of the eastern deformed granodiorite (**Figure 30**) shows a tightly folded intrusion. With just the view of the surface magnetic image it could be interpreted to be a highly faulted vertical dyke-like intrusion. At depths such as 200 m below sea level, the model reveals the two limbs of the tight fold. At depth the fractured limb becomes continuous in shape.



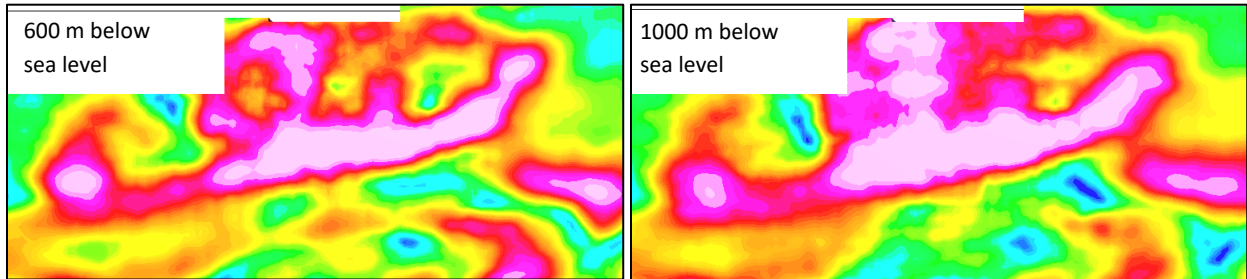


Figure 28. Northern granodiorite model depth slices.

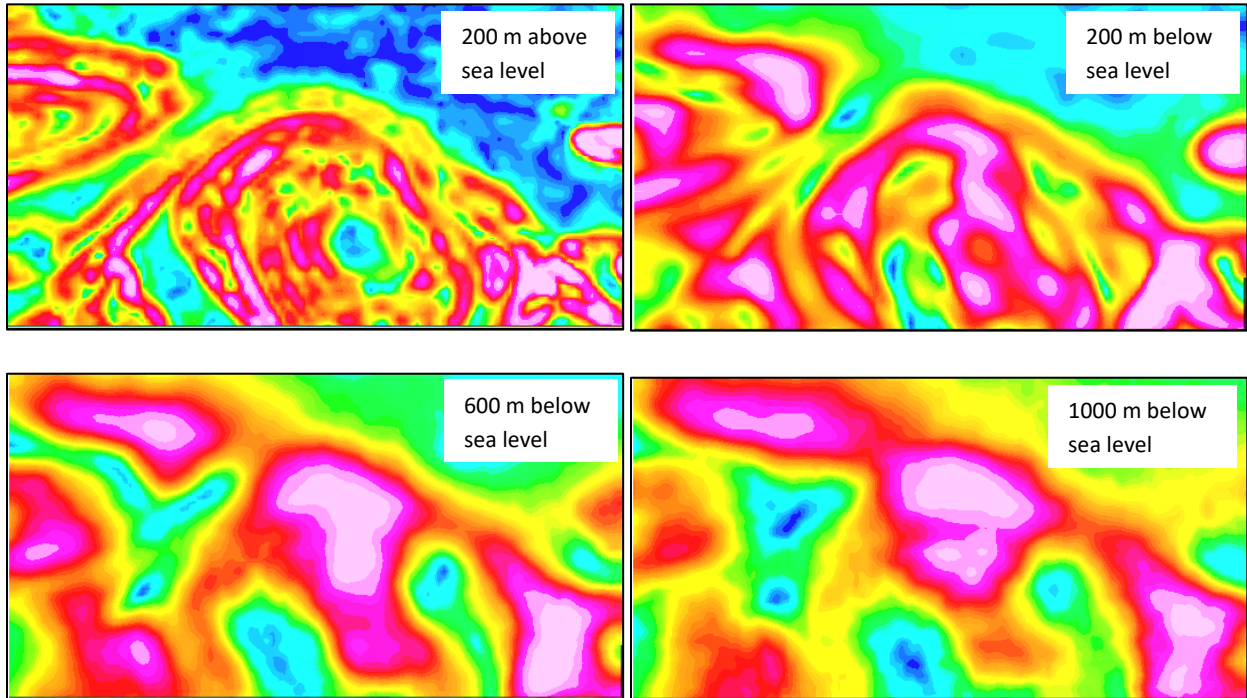


Figure 29. Southern undeformed granodiorite model depth slices.

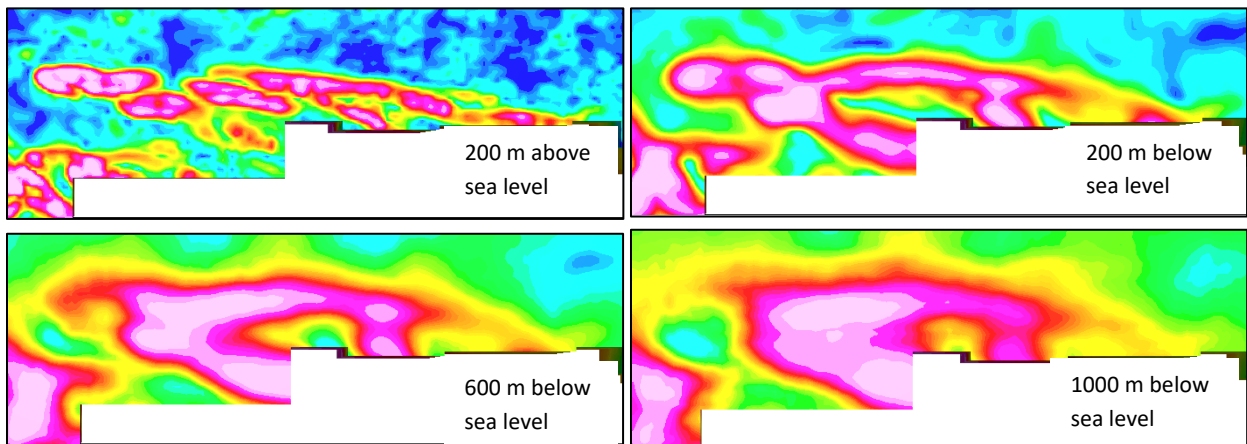


Figure 30. Eastern granodiorite model depth slices.

Another way to view the susceptibility models is as a series of isosurfaces or shells of constant susceptibility. The following susceptibility surfaces (legend to the right, units in SI) were imaged in **Figure 31** and the subsequent isosurfaces images. Rather than viewing slices or sections of the magnetic susceptibility model, an isosurface emphasises the 3-dimensional shape of the model. The isosurface of 0.001 SI was calculated but was not used in the following images since it obscures some of the finer detail. Some of the isosurface images had further lower values isosurfaces removed so that only the three highest susceptibility values are shown. At depths at and below 3,200 m below sea level some east-west banding in the models were seen that appeared to be artificial and not geological (**Figure 32**). Thus, some of those models were limited to depths above that depth value as shown in **Figures 33 to 38**.

- SURF_Leo_Ampl
- Isosurface 0.001
- Isosurface 0.0025
- Isosurface 0.005
- Isosurface 0.0075
- Isosurface 0.01
- Isosurface 0.025
- Isosurface 0.05

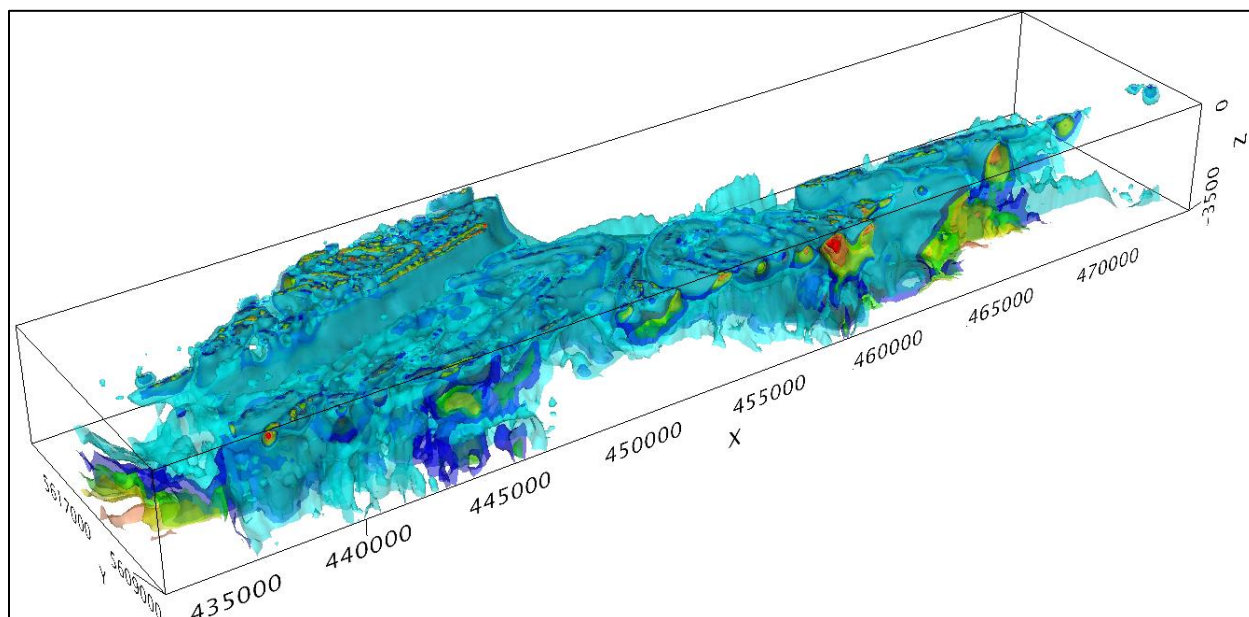


Figure 31. Multiple isosurfaces of susceptibility.

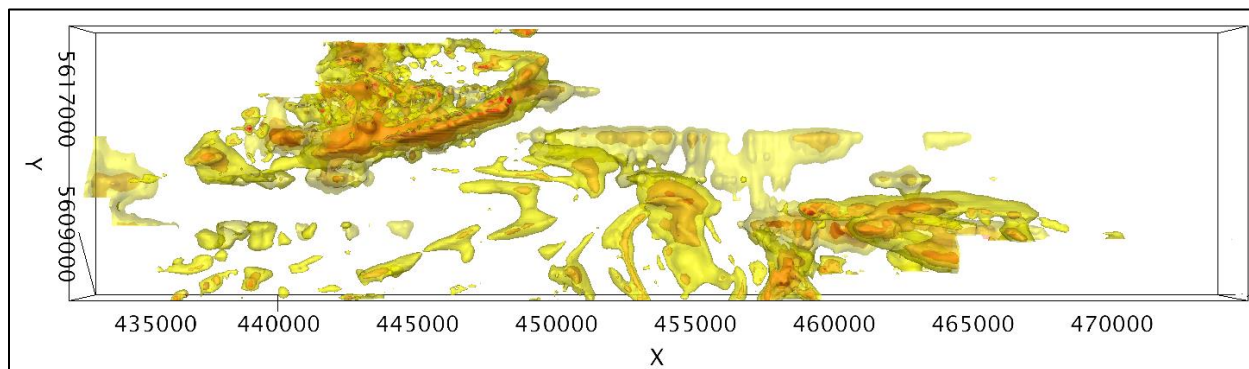


Figure 32. Multiple isosurfaces with only the three highest susceptibility surfaces and clipped to remove the isosurfaces at depths below 3,400 sea level.

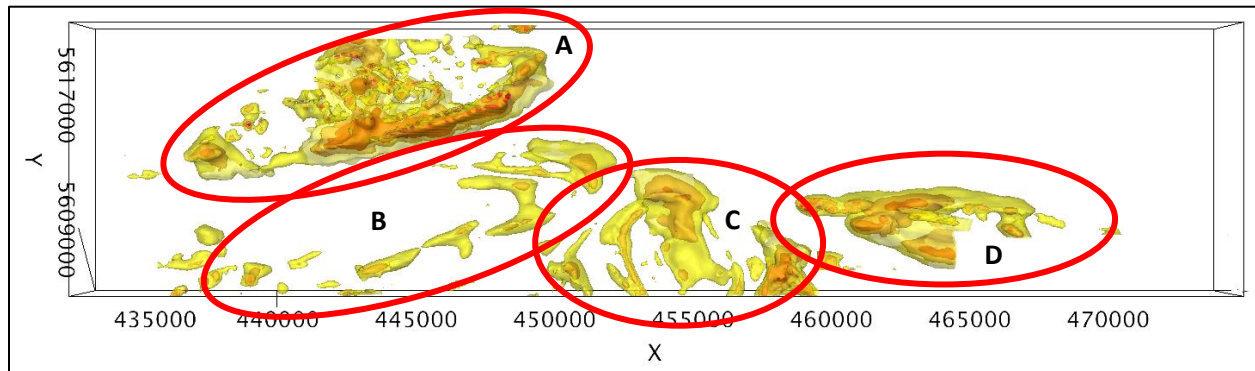


Figure 33. with three highest susceptibility surfaces and clipped to depths below 1,400 sea level

What can be seen in the VOXI models above is the higher overall susceptibility of the northern granodiorite (A) with respect to the granodiorite directly to the south (B) across the Sydney Lake fault zone. This is followed by the eastern granodiorite (D), the central undeformed granodiorite (C). The southern granodiorite (B) appears to have the least susceptibility.

Quickmag models were calculated for various linear magnetic anomalies as shown as the grey tabular bodies in **Figure 34** and the close-ups in **Figure 36**, **Figure 37** and **Figure 38**. The location of the close-up areas is outlined in **Figure 35**. Generally, all of the granodiorite intrusions are domal in structure with varying degrees of tilt. The QuickMag software models a specific magnetic anomaly while the VOXI modelling models the entire magnetic image. Thus, there is not always exact agreement with the two modelling methods. The QuickMag models are also geared towards the depth, dip and susceptibility of the near surface magnetic anomalies.

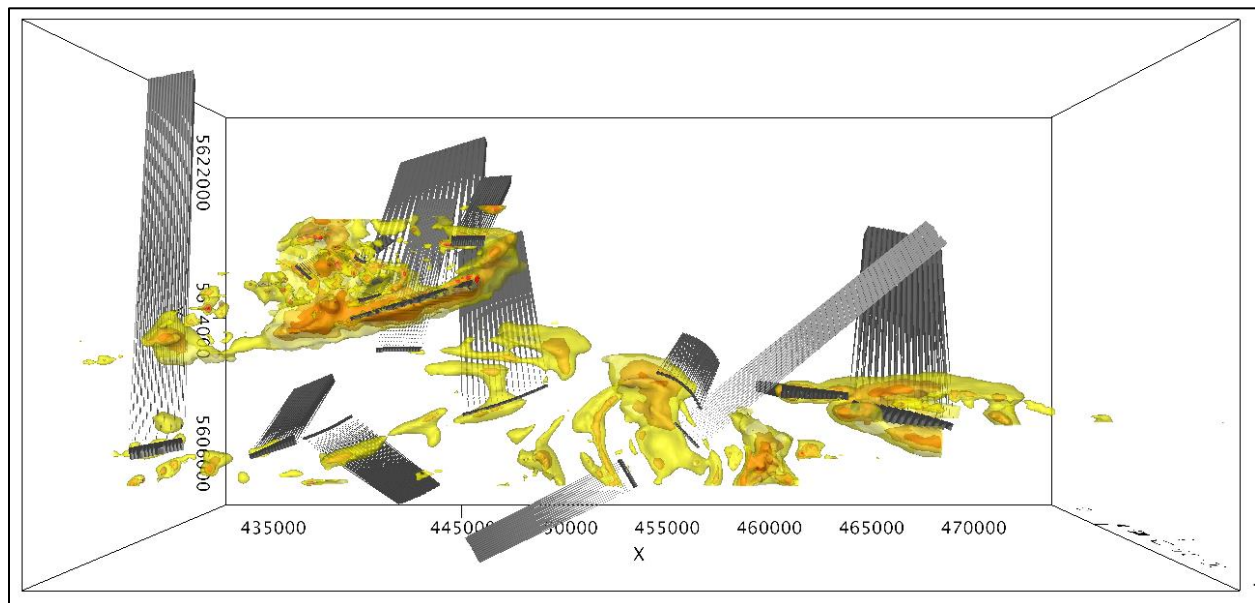


Figure 34. VOXI and QuickMag models of the entire survey area.

The northern granodiorite (Diorite-Monzodiorite-Granodiorite Suite) has a highly susceptible southern limb (**Figure 36**). The QuickMag model suggests that it is dipping to the north, while the VOXI model

indicates a vertical to slightly southerly dipping structure. The latter orientation is more likely. Other areas of the intrusion have north dipping limbs indicating a domal structure or a dome that has been deformed and is dipping to the north.

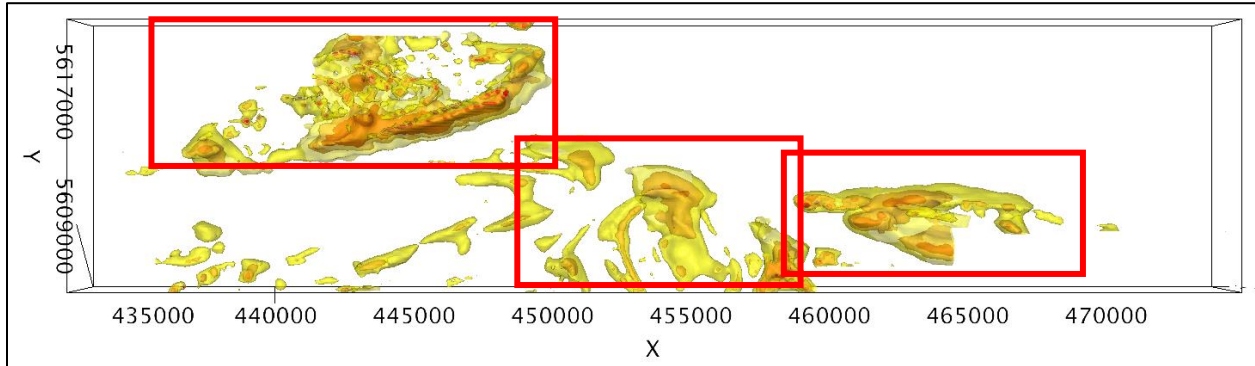


Figure 35. Location of the close-up views of the VOXI and QuickMag models.

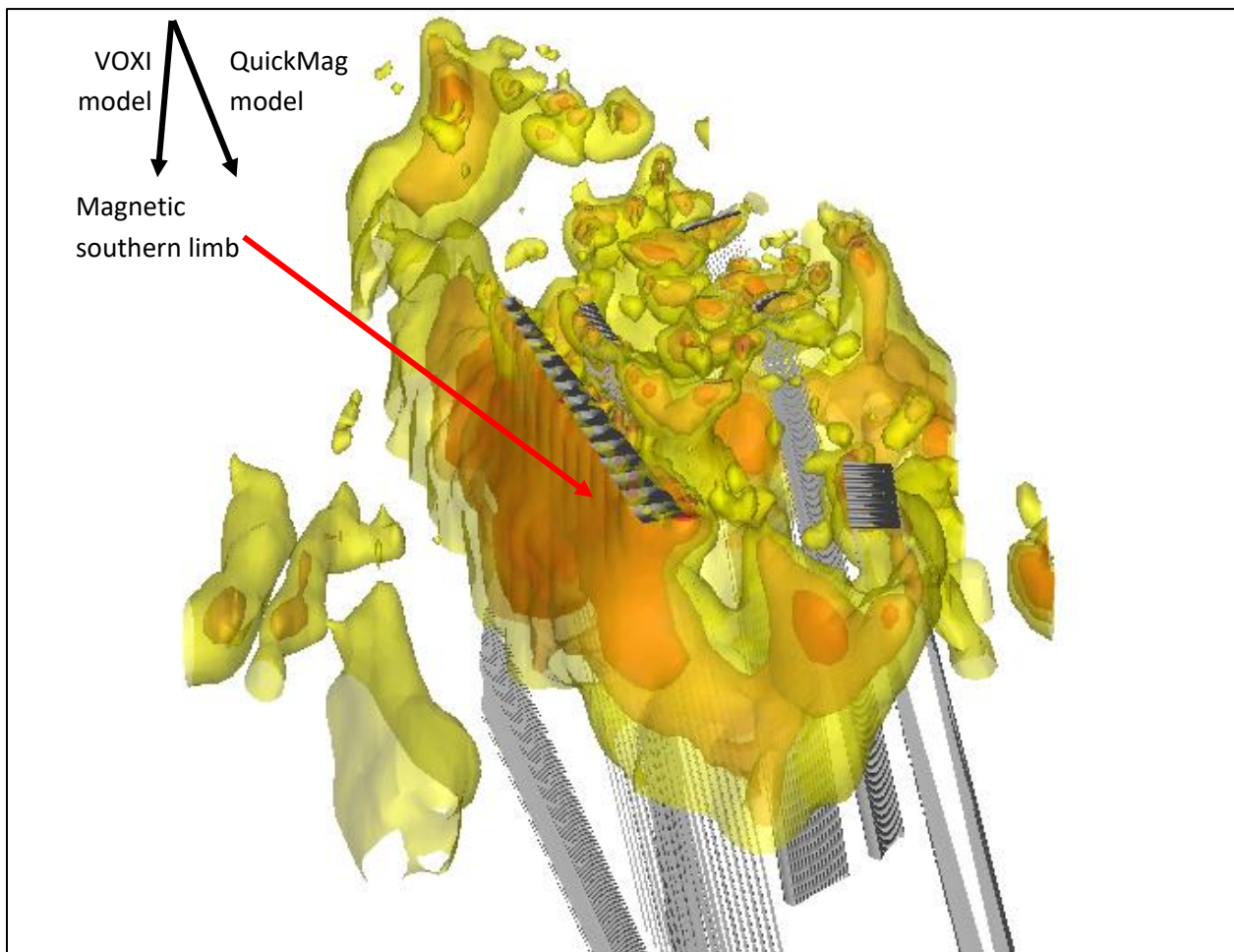


Figure 36. VOXI and QuickMag models of the northern granodiorite looking west.

The southern deformed granodiorite (Tonalite to Granodiorite Gneiss) is similar in dip to its northern neighbour. The southern limbs tend to be vertical to slightly north dipping and the eastern and northern limbs definitely dip to the north. It is interpreted to be a domal structure deformed to dip to the north.

The southern undeformed intrusion (Tonalite to Granodiorite Gneiss) has the expected dips from an undeformed domal structure (**Figure 37**). Three QuickMag models were calculated with a western limb dipped to the west, an eastern limb dipped to the east and another eastern-northern limb dipped slightly eastwards from vertical.

The eastern deformed intrusion (Tonalite to Granodiorite Gneiss, but more mafic) shows the tightly folded limbs (**Figure 38**). Both northern and southern limbs dip to the north and the nose of the fold dips vertical.

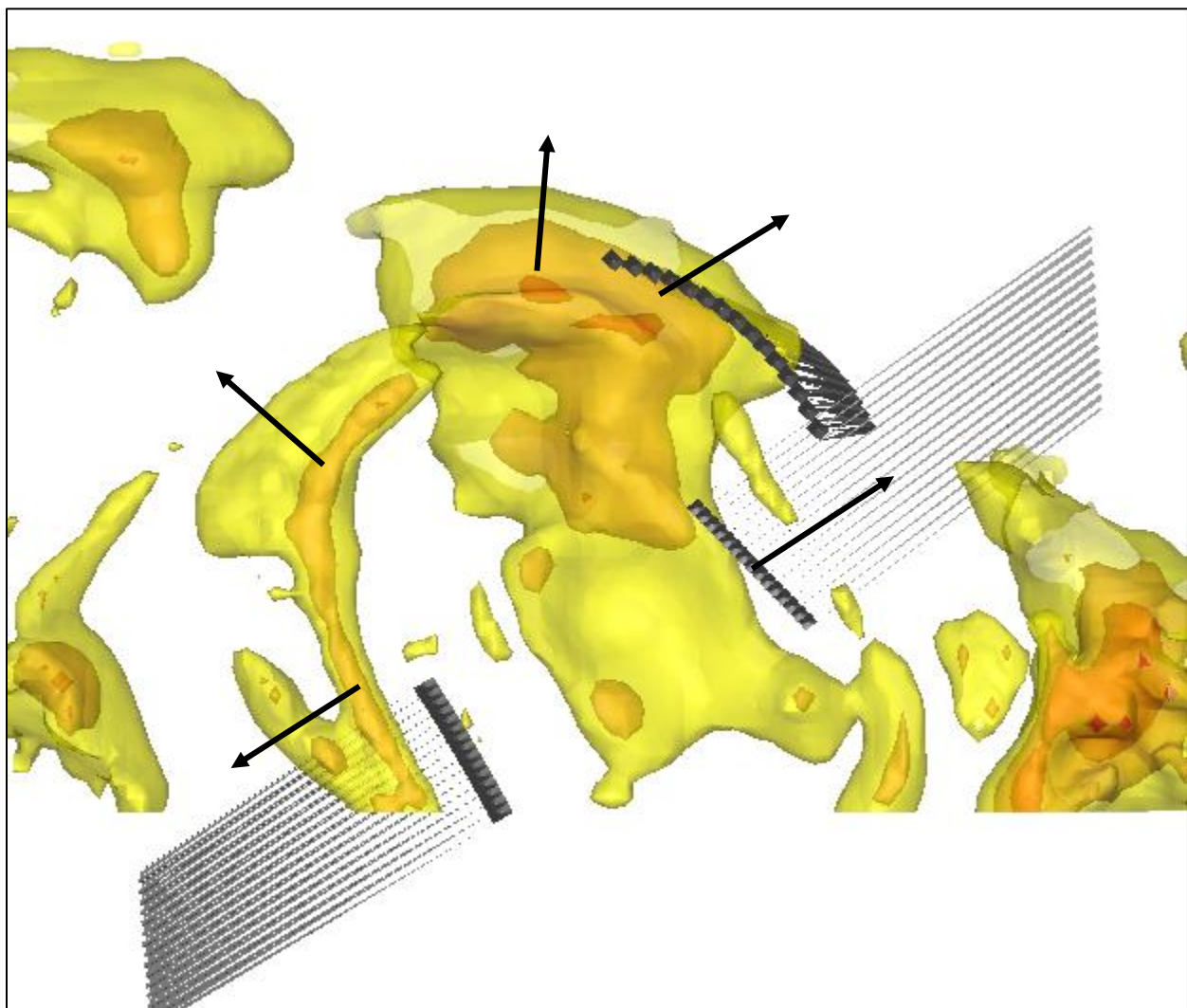


Figure 37. VOXI and QuickMag models of the central undeformed granodiorite intrusion

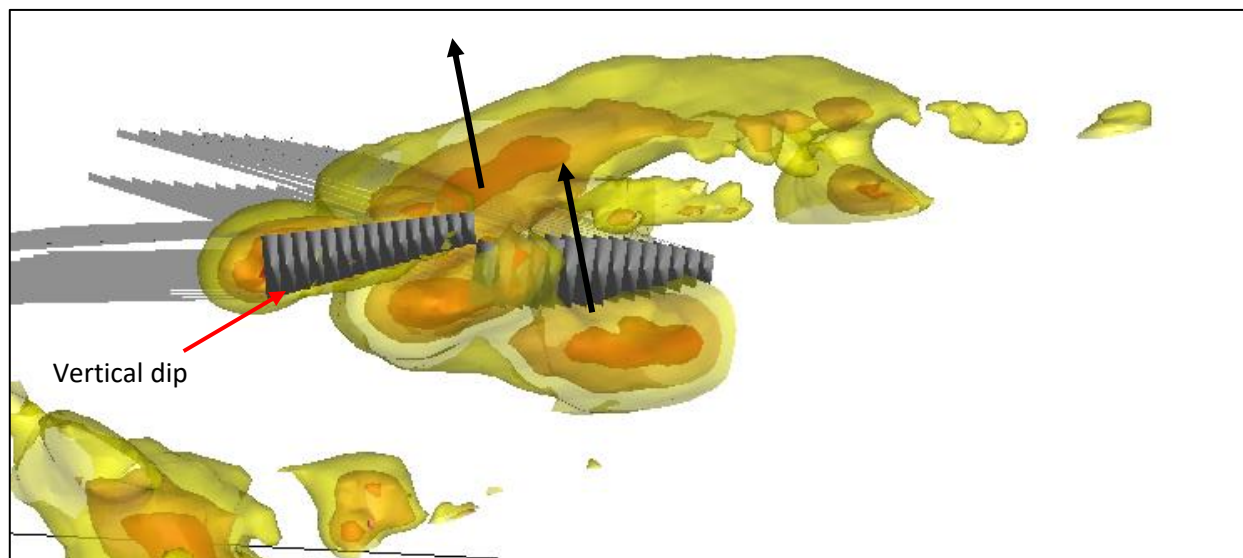


Figure 38. VOXI and QuickMag models of the eastern granodiorite.

Landform Analysis

Landform analysis of the topography to delineate structures such as faults, lineaments and folds had some limited usefulness. Some faults seen in the magnetic could also be confirmed in the landform analysis and occasionally a fault would be included based on topography alone. The following landform analysis was included for completeness sakes.

SRTM and Analytic Hill Shade

The SRTM derived elevation model with a grid cell size of 30.7 m was incorporated with the analytic hill shade image with an inclination of 45°, a declination of 0°, and vertical exaggeration of 49.7. The elevation varied from 329 to 443 m above sea level with a mean of 377 m.

The Sydney Lake fault and its fault zone and its encompassing fault zone can be seen as a general band of topographic lows. Many of the other fault generations can also be seen to be reflected in the topography. With some imagination the ring shape of the south central undeformed granodiorite intrusion can be seen in the topography.

It is difficult to correlate the lithology with the topography other than the fault zone and metasediments. The more felsic metasediments tend to be lower in topography as shown by the abundant lakes that overlie them.

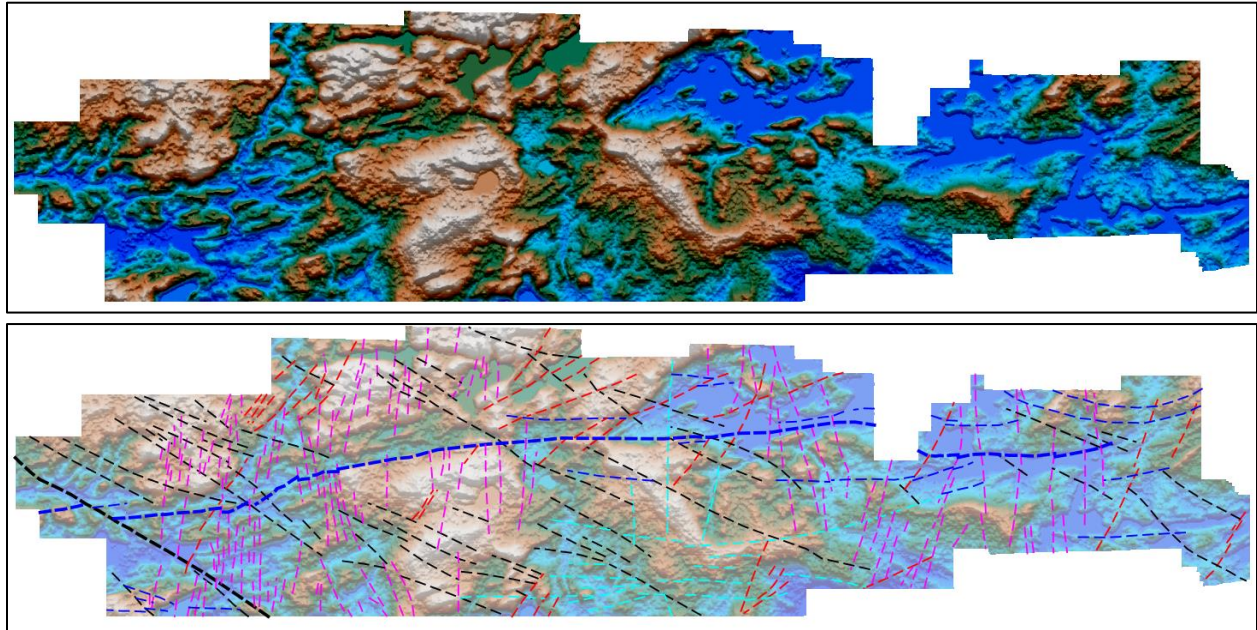


Figure 39. SRTM combined with analytic hill shade (top) and with interpreted faults (bottom).

Slope Analysis

There is not much to be gleaned from the slope analysis. As with the SRTM and Analytic Hill Shade, some fault generations can be correlated with low values of slope indicating topographic valleys.

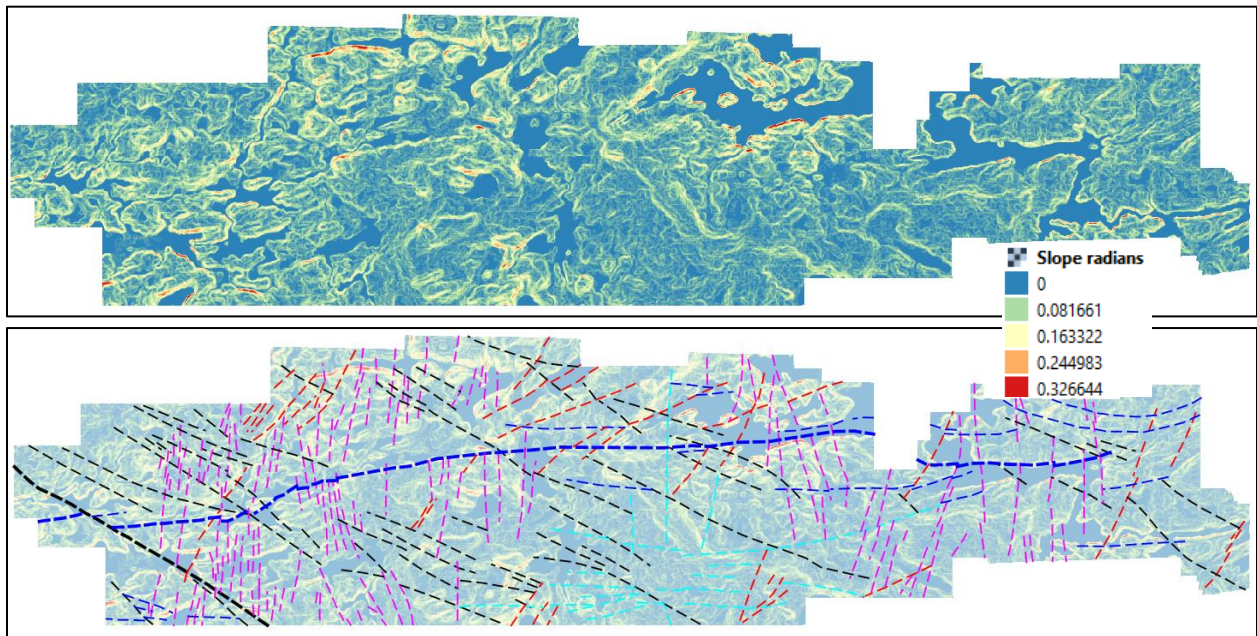


Figure 40. Slope derived from the SRTM (top) and with interpreted faults (bottom).

Aspect Analysis

Some faults correlate with changes in slope aspect, i.e., a change in slope direction, from all of the different generations of faults.

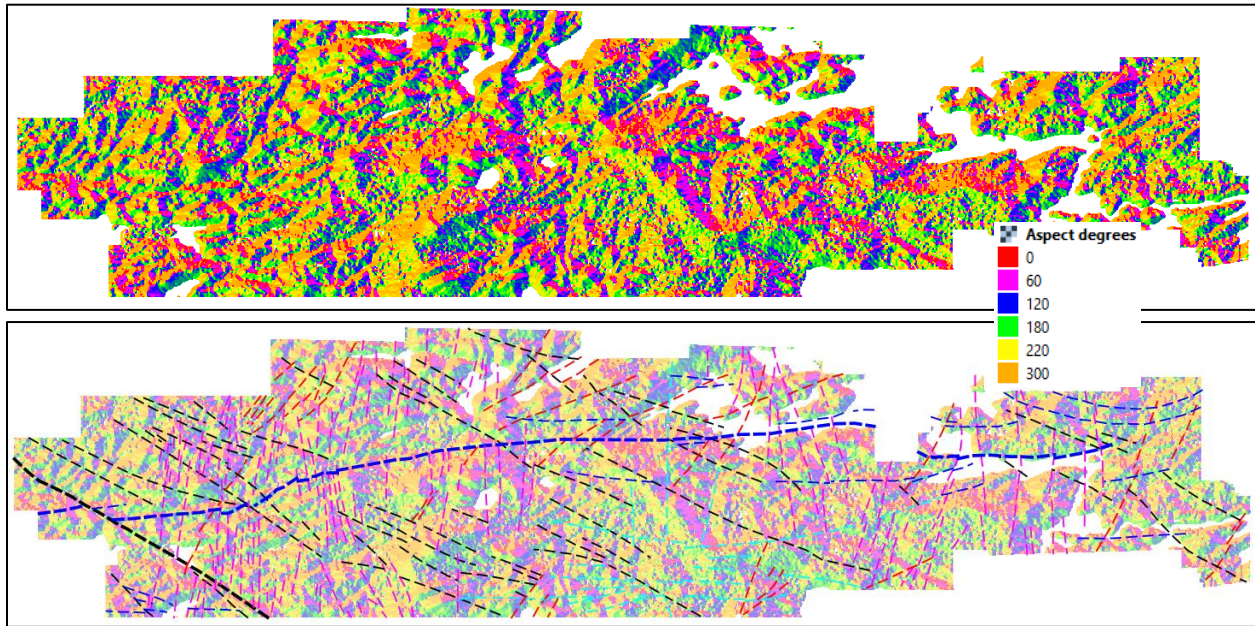


Figure 41. Aspect derived from the SRTM (top) and with interpreted faults (bottom).

Landform Classification

Structure or lithology is very difficult to correlate with the landform classification. Most of the area is classified as “Plains” as most of the area has low topographic relief which generally correlates with the metasedimentary units. Largely, the faults correlate with the various degrees of incised valleys (1 – Canyons, deeply incised streams, 2 – Midslope drainages, shallow valleys, 3 – Upland drainages, headwaters, deeply incised streams, 4 – U-shaped valleys).

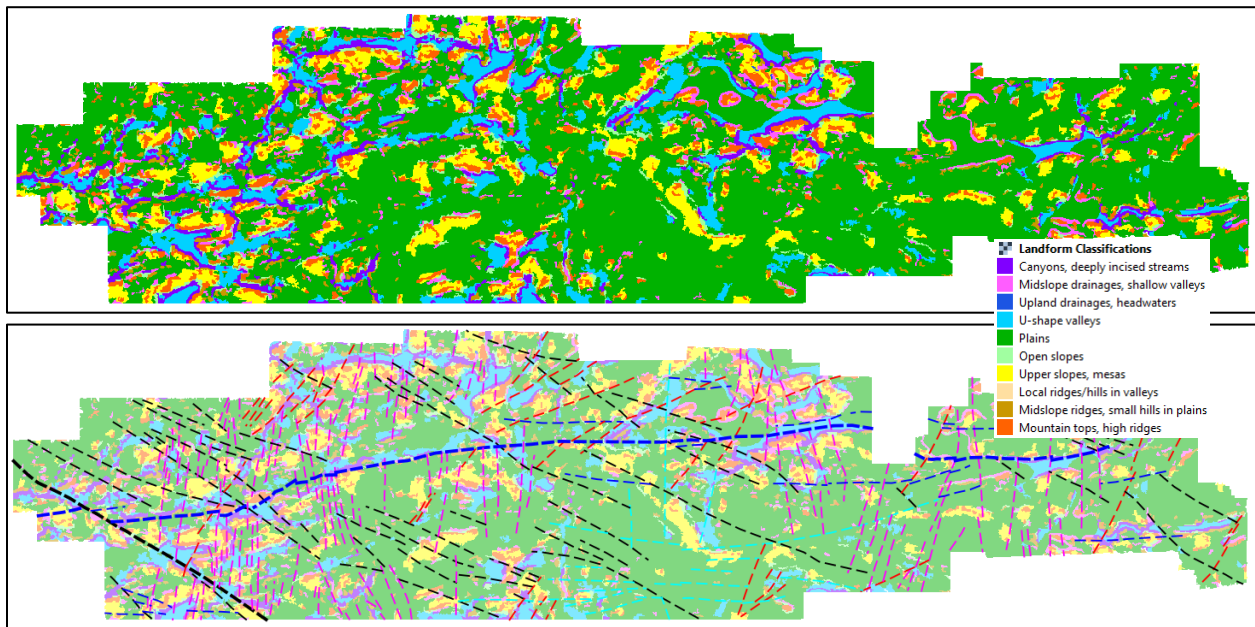


Figure 42. Landform Classification derived from the SRTM (top) and with interpreted faults (bottom).

Sydney Lake

Lithological Interpretation

The following **Table 2** briefly describes the magnetic amplitude and textures that were used to assign the various interpreted lithologies.

	Lithology	Amplitude	Comments
1	Mafic Metavolcanic Rocks	Low to mid 100's nT	Curvilinear, continuous, mapped as amphibolized metavolcanics
2	Mafic Tonalite to Granodiorite	200-300 nT	Massive to fractured texture
3	Felsic Tonalite Gneiss	100-200 nT	Massive to fractured texture, similar
4	Metasediments and Derived Migmatites	<100 nT	Narrow, curvilinear, continuous

Table 2. Geophysical criteria for various lithological units.

The Eagle-Sydney Lake geological map (P.1026, **Figure 45**)⁸ and the digital bedrock geology from the Ontario Geological Survey⁹ were used as guides to assign the likely lithological units. There was good agreement with the geological map though there was more detail to be seen in the geophysical images.

A plan (**Figure 43**) and 3D view (**Figure 44**) of the reduced to the pole image illustrates these four units well.

⁸ Breaks, F. W., Bond, W. D., McWilliams, G. H., Gower, C. F., and Stone, Denver 1975 Operation Kenora-Sydney Lake, Eagle-Sydney Lakes Sheet, District of Kenora; Ontario Div. Mines, Prelim. Map P.1026 Geol. Ser., scale 1 inch to 1 mile or 1:63,360. Geology 1974.

⁹ Ontario Geological Survey 2011. 1:250 000 scale bedrock geology of Ontario; Ontario Geological Survey, Miscellaneous Release–Data 126 - Revision 1.

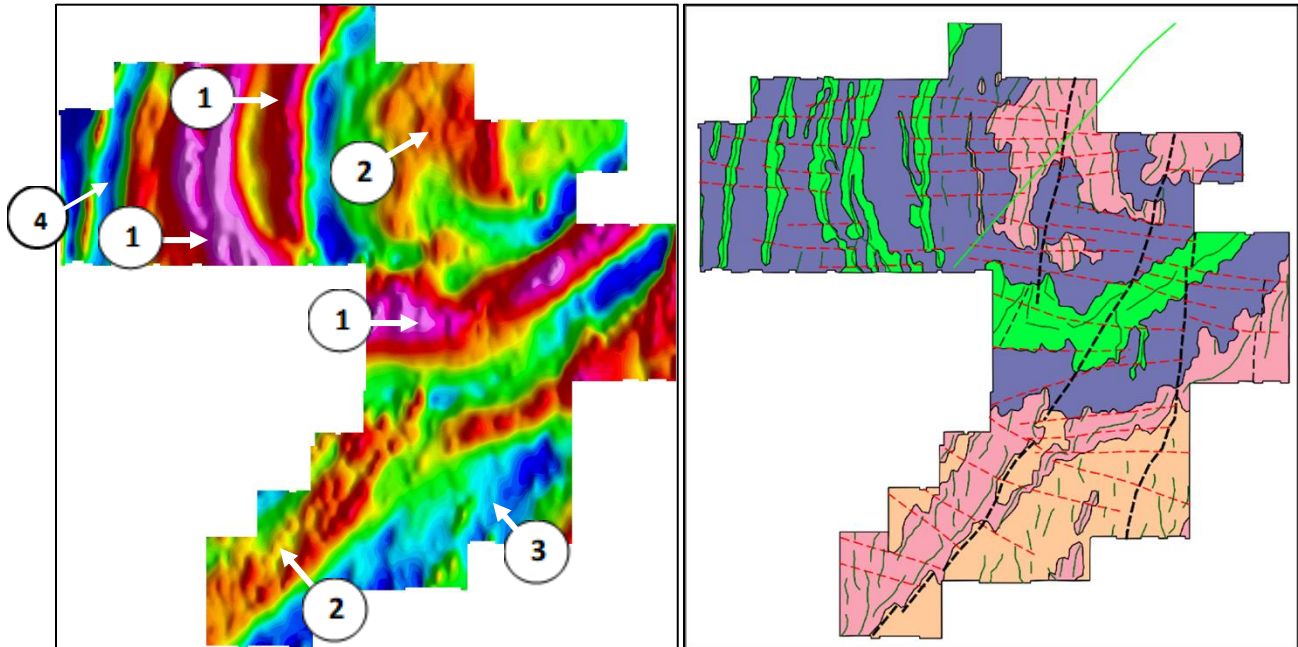


Figure 43. Residual magnetic intensity reduced to the pole (left) and the current geophysical interpretation (right).

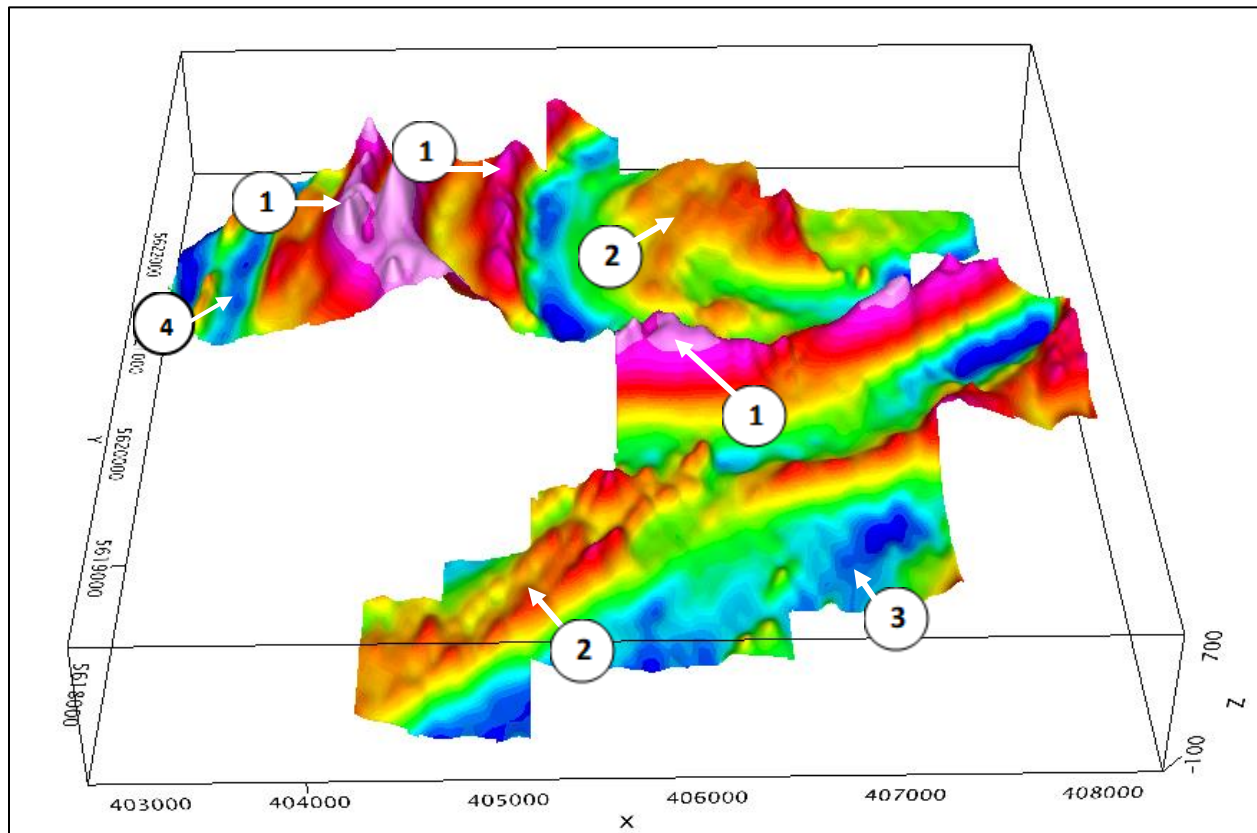


Figure 44. 3D view of the residual magnetic intensity reduced to the pole.

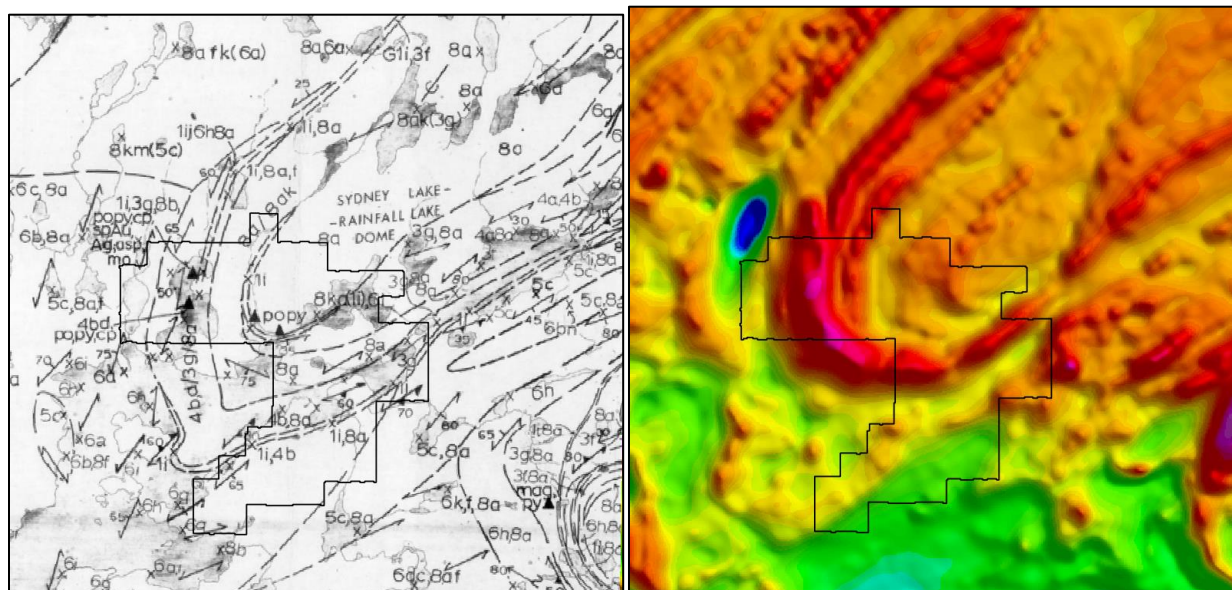


Figure 45. Published geology (left) and the reduced to the pole magnetics of the same area (right).

If only this survey data were available, the features would have been interpreted as a circular dome. However, the availability of the geological map and a regional magnetic survey flown in 2016 show that this area is at the southwestern limb of the Sydney Lake-Rainfall Lake Dome. The regional magnetic survey (Separation Lake, Data Set 1083b) was flown for the Ontario Ministry of Northern Development and Mines¹⁰. It was a magnetic gradiometry and radiometric survey with a flight line separation of 200 m. I did the quality control of the field data and final deliverables on behalf of the ministry.

At least six separate bands of mafic metavolcanics are seen in the western portion of the survey area. These bands are narrow, well defined and interlaced with very low magnetic units ascribed to be metasediments and their derived migmatites such as metatextite, i.e., a migmatite produced by metatexis or by a “process of segregation (usually of quartz and feldspar) by metamorphic differentiation and partial fusion”¹¹. In the central area and to the east, the mafic metavolcanic bands coalesce into one broad band. The mafic tonalite to granodiorite is exposed in the central area of the dome and to the south. A less mafic phase of felsic tonalite gneiss is interpreted in the southern portion of the survey area.

Lineaments

Lineaments were traced along highs in the second vertical derivative of the pole reduced field (RTP2VD.grd), tilt derivative (TILT.grd) and total horizontal gradient (TDX.grd). The tilt derivative with lineaments is shown in the image below (**Figure 46**).

¹⁰ Ontario Geological Survey 2017. Survey report on Separation Lake area, 88p. [PDF document]; in Ontario airborne geophysical surveys, magnetic gradiometer and gamma-ray spectrometric data, grid and profile data (Geosoft® formats) and vector data, Separation Lake area, Ontario Geological Survey, Geophysical Data Set 1083b.

¹¹ Brown, M. The definition of metatexis, diatexis and migmatite. 1973 Proceedings of the Geologist’s Association, 84, 371-497.

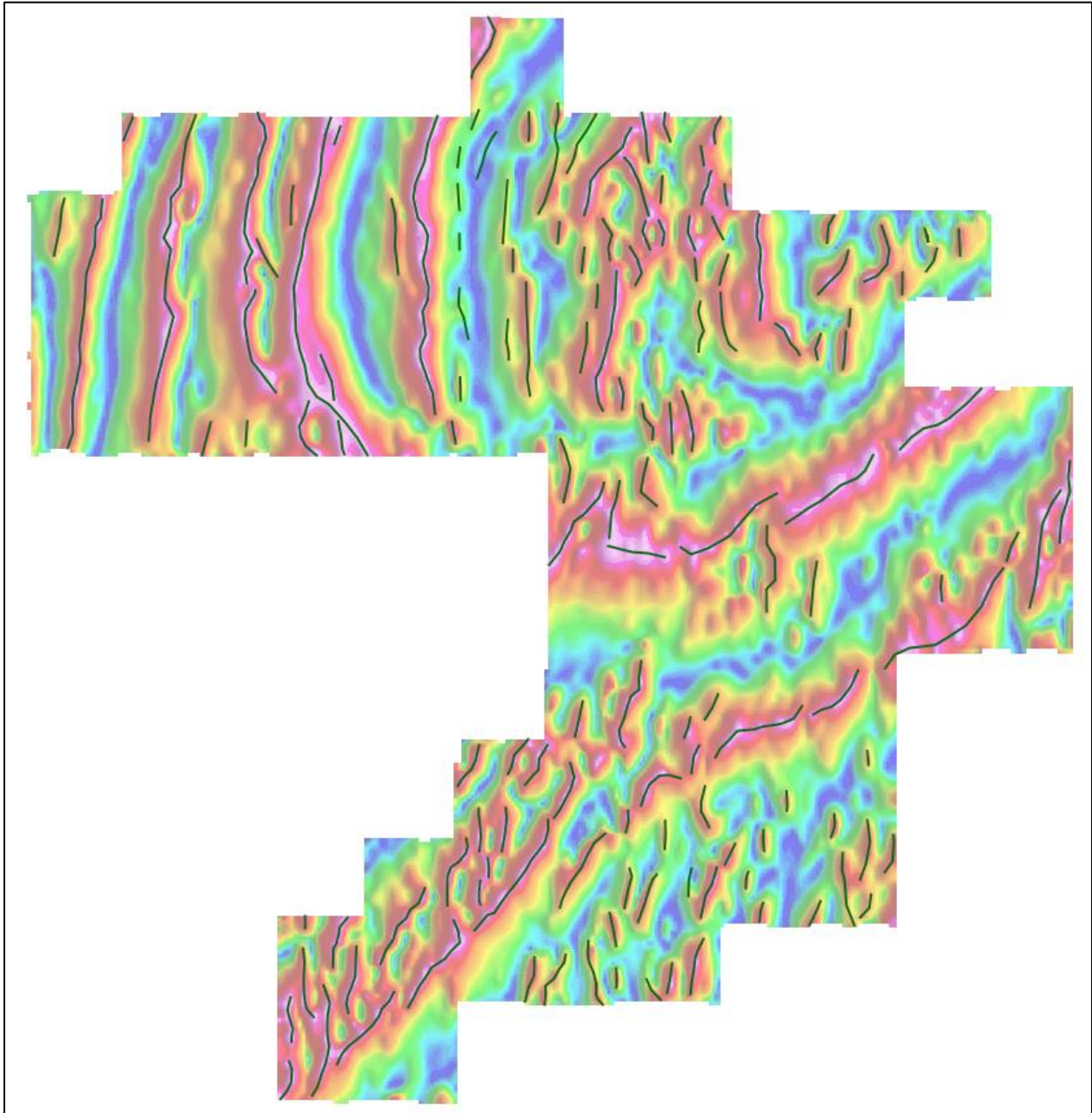


Figure 46. Lineaments or trends overlain upon the tilt derivative (50% transparency applied).

A rose diagram of the orientations of the lineaments (**Figure 47**) show a vast majority of the orientations lie within the N and NNE directions. Minor amounts of lineaments occur in the N to NNW and NNE to NE directions. These orientations are very similar to the Western Bear property to the north.

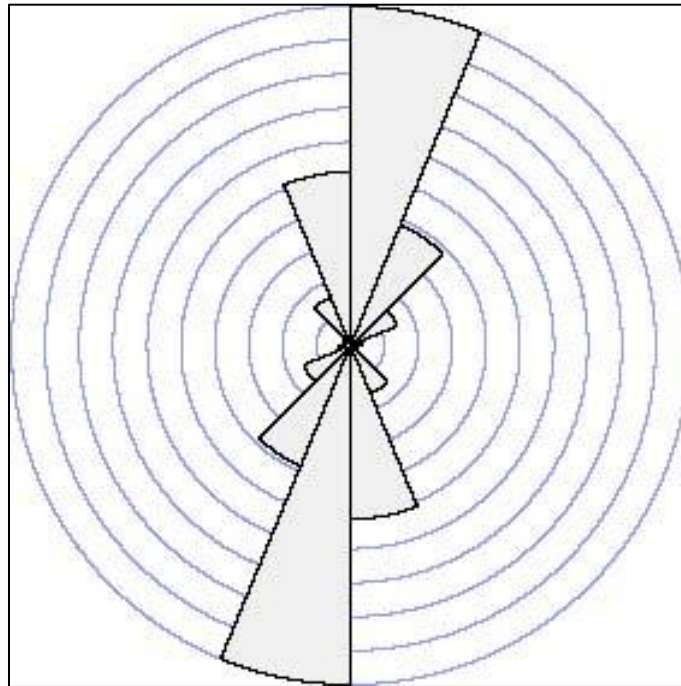


Figure 47. Rose diagram of orientations of lineaments.

Faults

The location and length of inferred faults were determined from various derivative grids (**Figure 48**). They were determined by an offset or disruption in character of the linear magnetic anomalies.

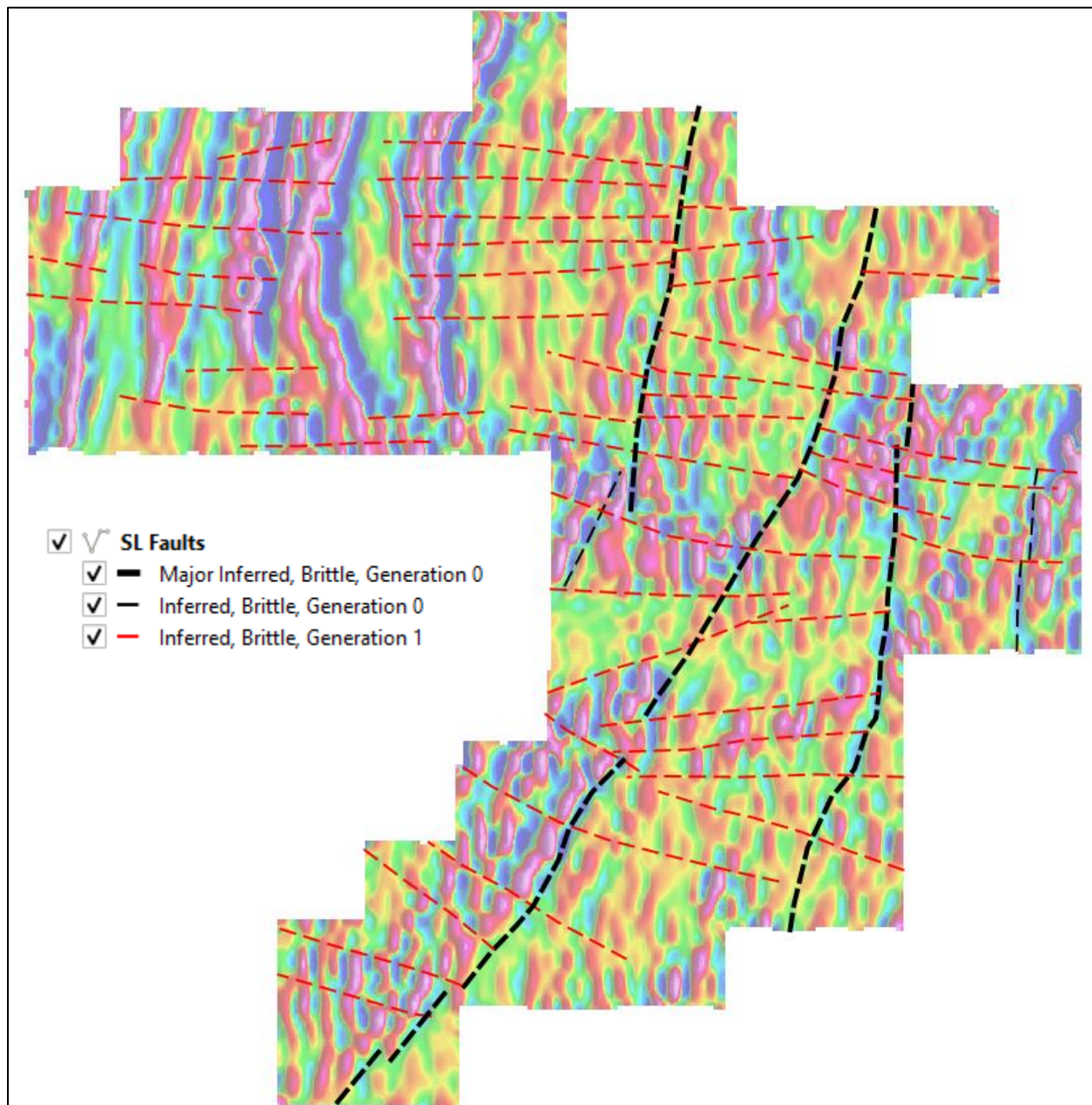


Figure 48. Interpreted faults overlain upon the second vertical derivative of the pole reduced field (50% transparency).

A Rose diagram of the fault orientations (**Figure 49**) show and majority of the interpreted faults to be between 90° (E) and 112.5° (ESE). The two fault generations are generally defined by their orientations, as follows:

- Generation 0: 0° (N) to 22.5° (NNE) are interpreted to be the oldest. Generation 0 faults are offset by faults of the other fault generation. The major inferred faults either delineate two separate lithologies or a large offset between features.
- Generation 1: 67.5° (ENE) to 112.5° (ESE) are interpreted to be younger than Generation 0. Where offsets are seen, Generation 1 faults are mostly dextral and occur throughout the study area. Note

that the flight line direction is 90° (E) so that some of the Generation 1 faults may actually be a gridding artefact, however care was taken to only interpret east-west faults that had a good degree of confidence, but still some artefacts may have been mapped.

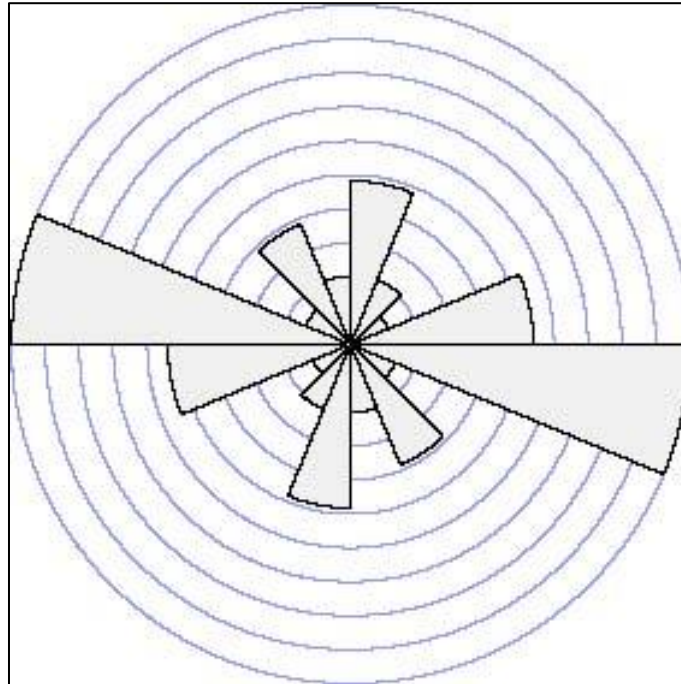


Figure 49. Rose diagram of fault orientations.

Folds

One fold axis was interpreted in the study area with the aid of the regional Separation Lake magnetic/radiometric survey (Figure 50). No other folds were identified within the study area.

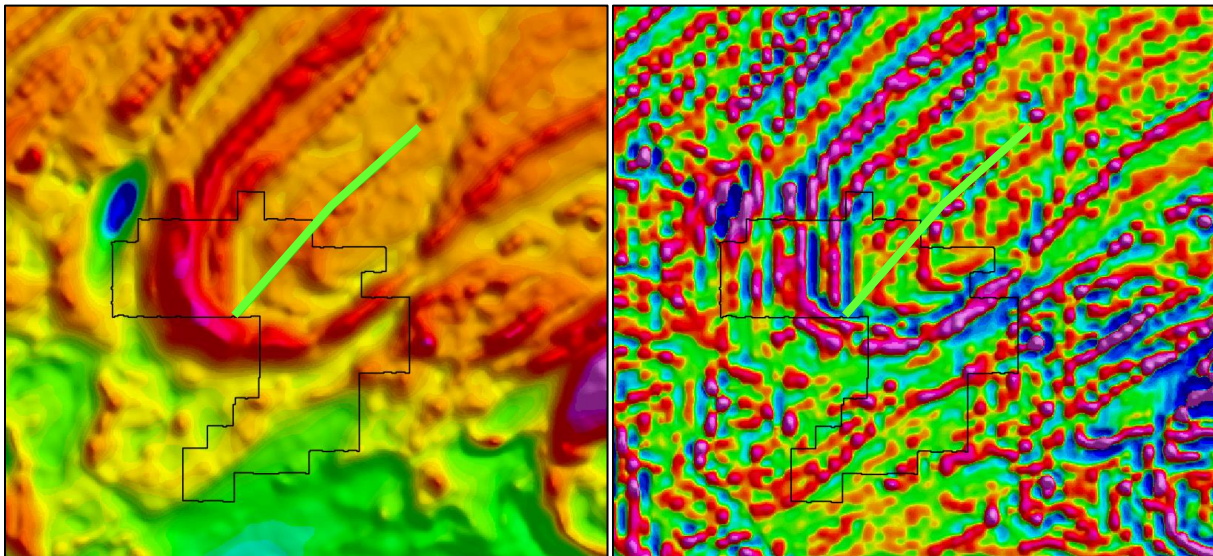


Figure 50. Fold axes (green) with the reduced to the pole (left) and 2nd vertical derivative of the pole reduced field (right).

A rose diagram of the one fold axis is shown below in Figure. It is at an orientation of 45° (NE) to 67.5° (ENE).

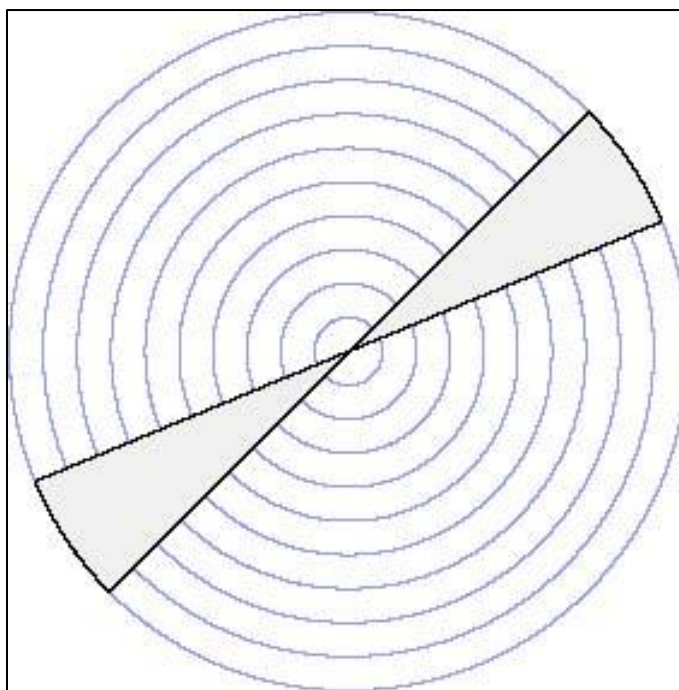


Figure 51. Rose diagram of fold orientations.

VOXI Modelling Interpretation

The VOXI 3D model of the magnetic susceptibility of the survey area is shown below in **Figure 52**. At surface the susceptibility distribution appears similar to the image of the residual magnetic intensity such as the magnetic highs from the curvilinear bands of metavolcanics in the western portion of the survey. This implies that the modelling has forced many of the magnetic sources to be near the surface. The top of the model surfaces is at 411 m above sea level. The data has been clipped to different depth slices such as 200 m, -400 m and -1,000 m above sea level (asl) or 211 m, 811 m and 1,411 m below surface, respectively (**Figure 53**, **Figure 54** and **Figure 55**).

With increasing depth these bands of mafic metavolcanics dip to the west confirming that this is a domal structure. The model shows that the metavolcanic bands remain continuous for depths of 400 below surface (approximately 0 m above sea level) at which they start to coalesce into one mafic unit (**Figure 54**).

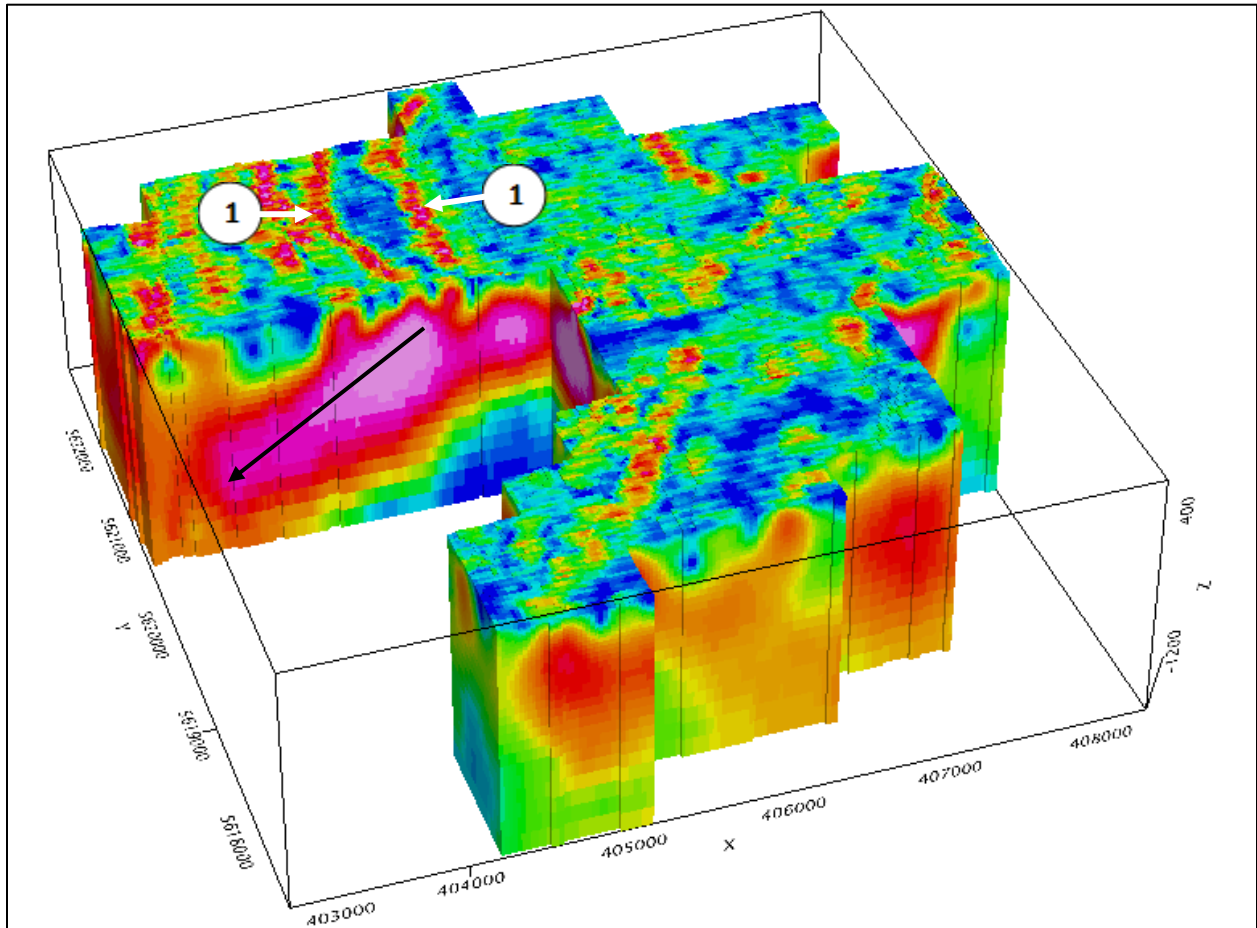


Figure 52. Magnetic susceptibility model of the survey area. The top of the model is at surface at 411 m above sea level.

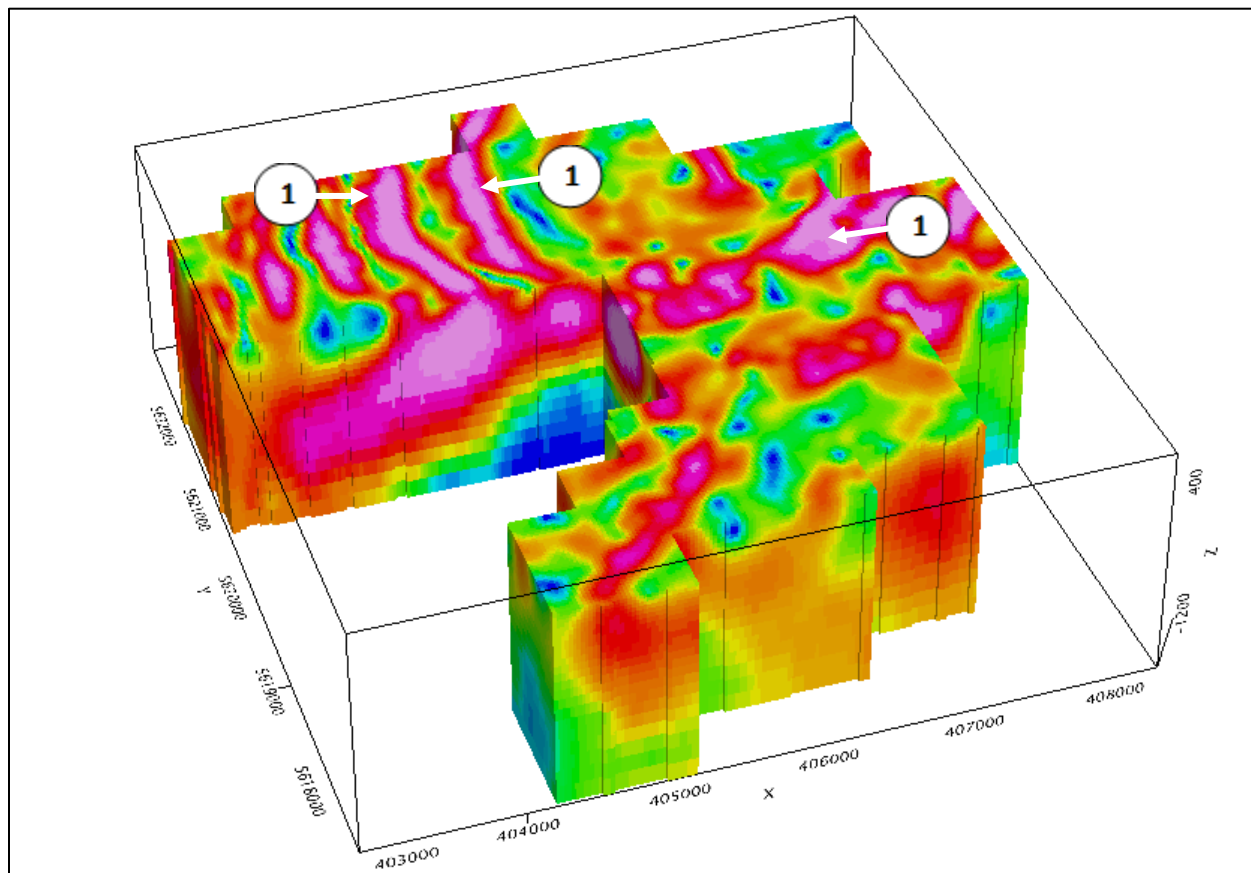


Figure 53. Magnetic susceptibility model with the top of the model is at 200 m above sea level.

By 500 m below sea level (approximately 900 below surface) the low susceptibility metasediment/migmatite units have petered out. At greater depths (1,000 m below sea level, **Figure 55**) the centre of the dome in the northeast reverts to a low susceptibility unit.

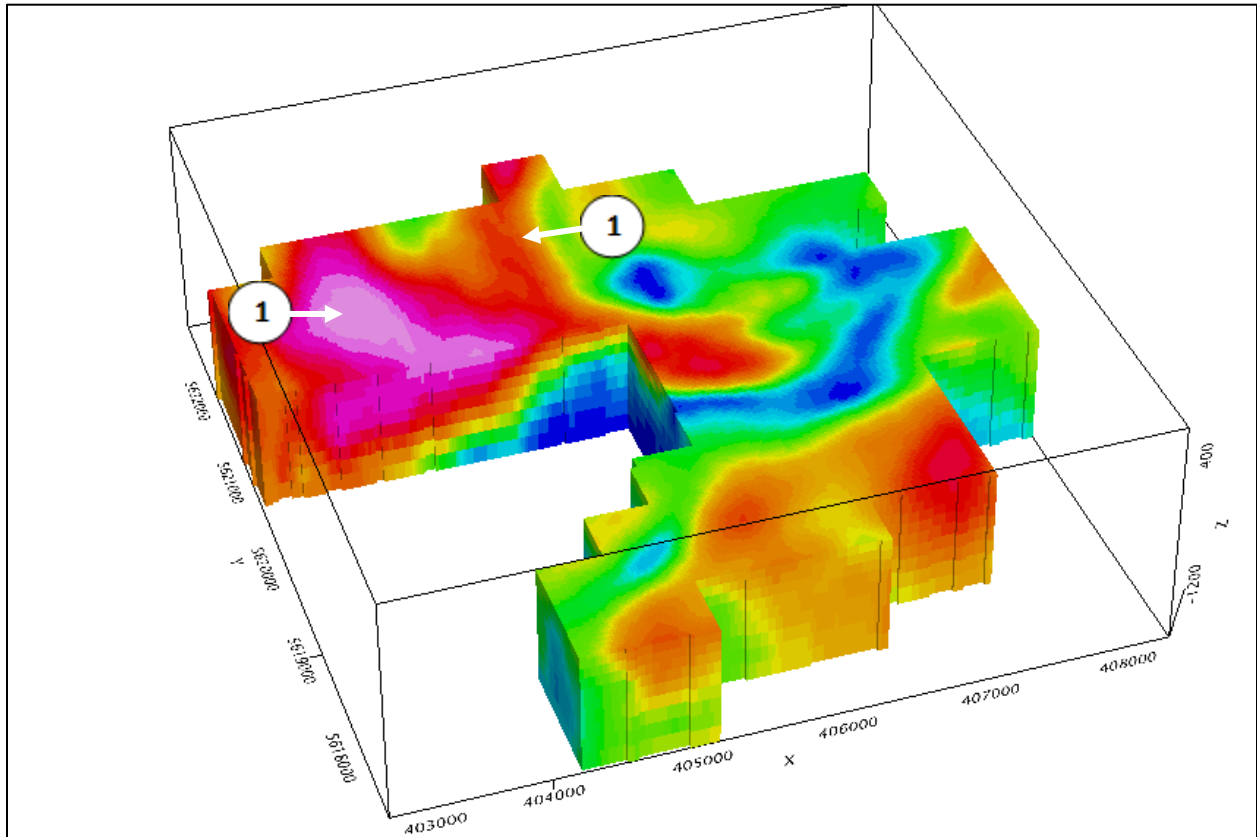


Figure 54. Magnetic susceptibility model with the top of the model is at 400 m below sea level.

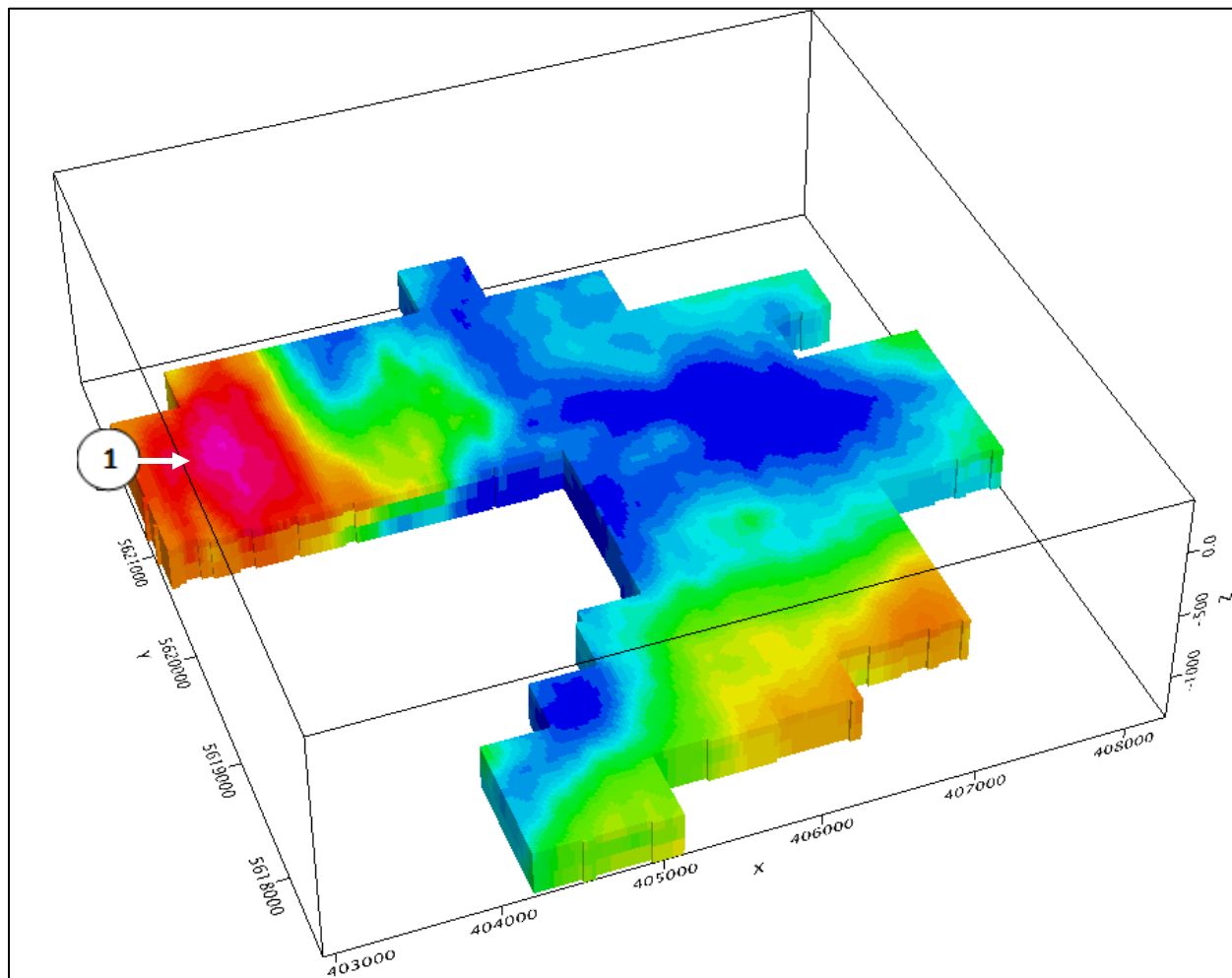










Figure 55. Magnetic susceptibility model with the top of the model is at 1000 m below sea level.

Another way to view the susceptibility models is as a series of isosurfaces or shells of constant susceptibility. The following susceptibility surfaces (legend to the right, units in SI) were imaged in **Figure 56**Figure 76 and **Figure 57** and the subsequent isosurfaces images. Rather than viewing slices or sections of the magnetic susceptibility model, an isosurface emphasises the 3-dimensional shape of the model. The isosurface of 0.001 SI was calculated but was not used in the following images since it obscures some of the finer detail.

-  SURF_SL_Ampl
-  Isosurface 0.001
-  Isosurface 0.0025
-  Isosurface 0.005
-  Isosurface 0.0075
-  Isosurface 0.01
-  Isosurface 0.02
-  Isosurface 0.05

As in the solid VOXI model, the isosurfaces show the narrow metavolcanic bands (1 as shown in **Figure 56**) at and near surface. With increasing depth, the bands coalesce into one large high susceptibility body dipping to the west as shown in **Figure 58**. The mafic metavolcanics may be divided into three separate zones dependent upon their dip (**Figure 59** and **Figure 60**). Zone “A” is in the northwestern section of the survey area with the many narrow bands of metavolcanics. The VOXI model indicates a dip to the west. The QuickMag models confirm this dip. Multiple models were inverted along the curvilinear bands and the moderate magnetic high within the dome structure. All indicate a dip to the west with varying dip angles. Zone “B” is part of the metavolcanics which form a wider band in the centre of the survey area

near the nose of the folded dome. The VOXI and QuickMag model indicate a unit with a near vertical dip. Zone "C" is the wide metavolcanic unit east of "B" separated by a major inferred fault. VOXI and QuickMag models indicate a south dipping unit.

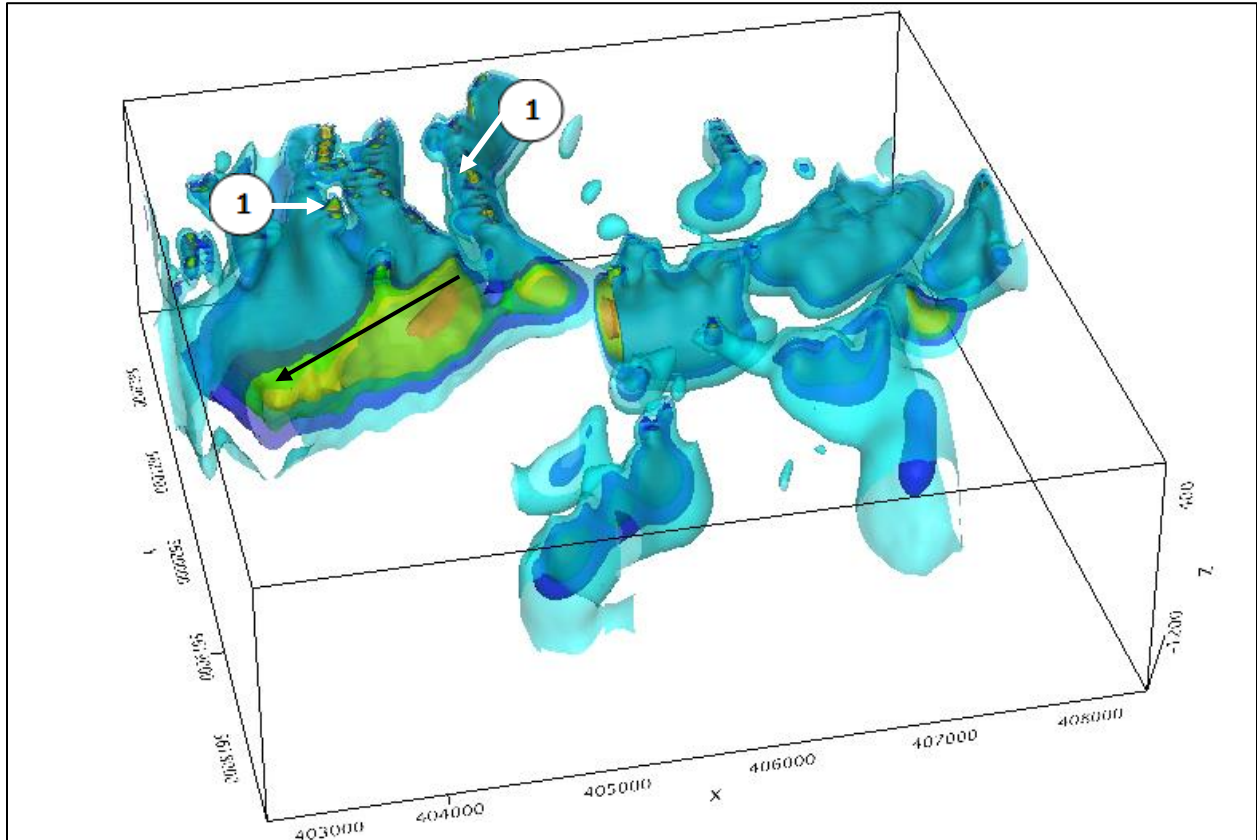


Figure 56. Multiple isosurfaces of susceptibility.

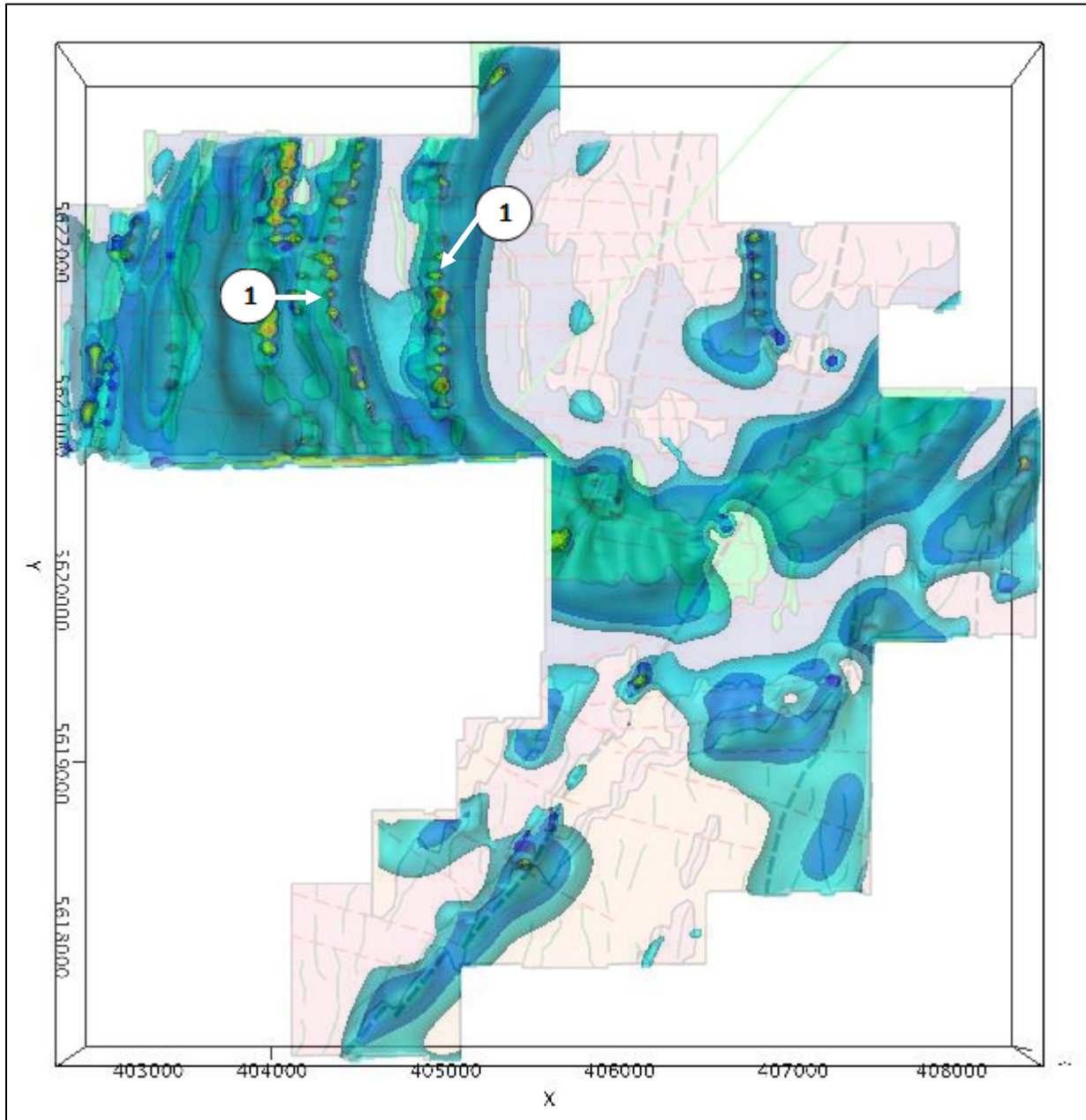


Figure 57. Multiple isosurfaces of susceptibility viewed from above with a transparency of the geophysical interpretation.

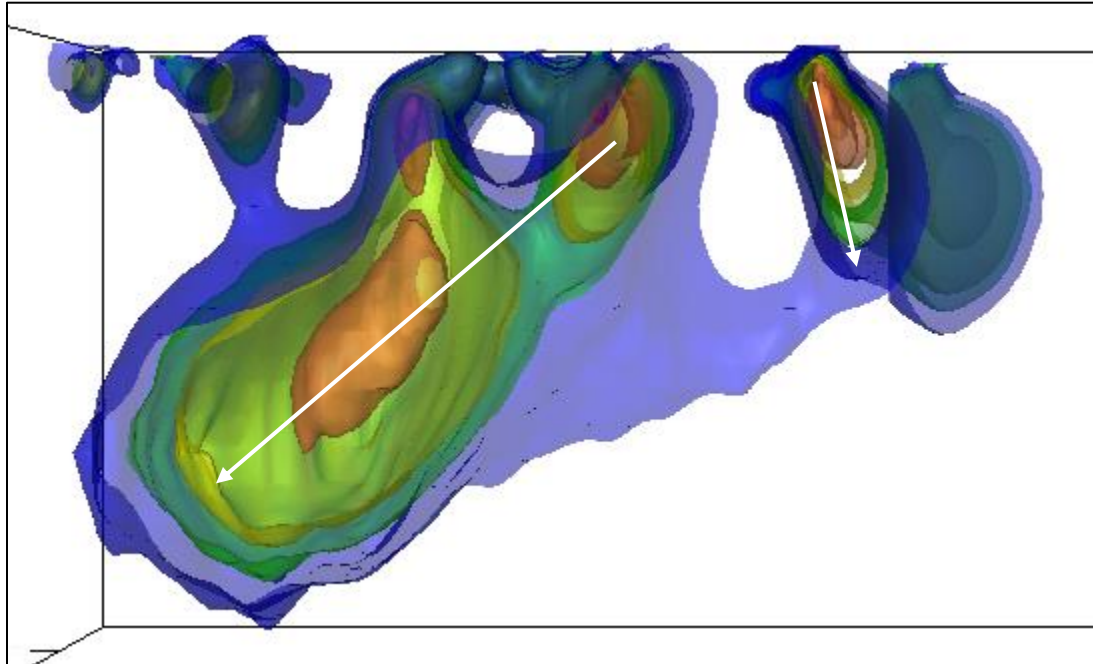


Figure 58. A cross section through multiple isosurfaces of susceptibility viewed from above towards the northwest without some of the lower isosurfaces.

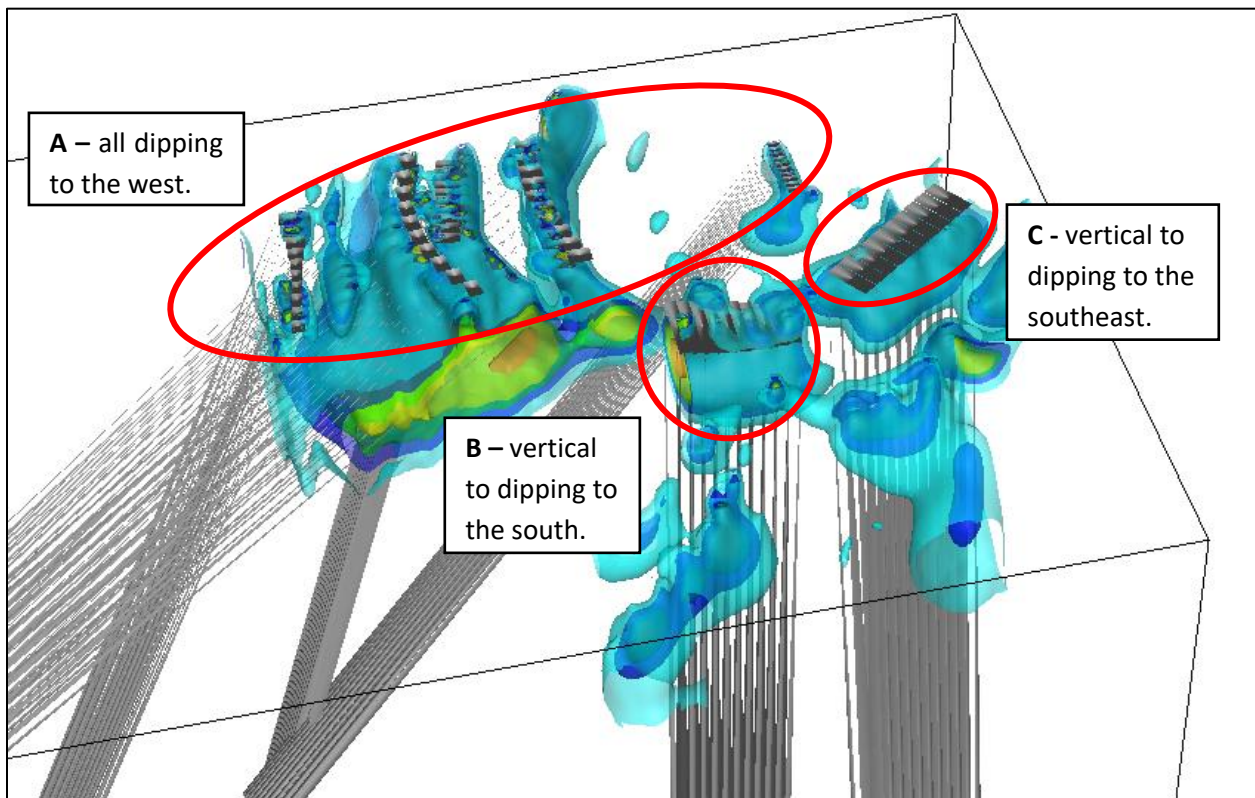


Figure 59. Higher susceptibility isosurfaces and the calculated QuickMag model with a view towards the northeast.

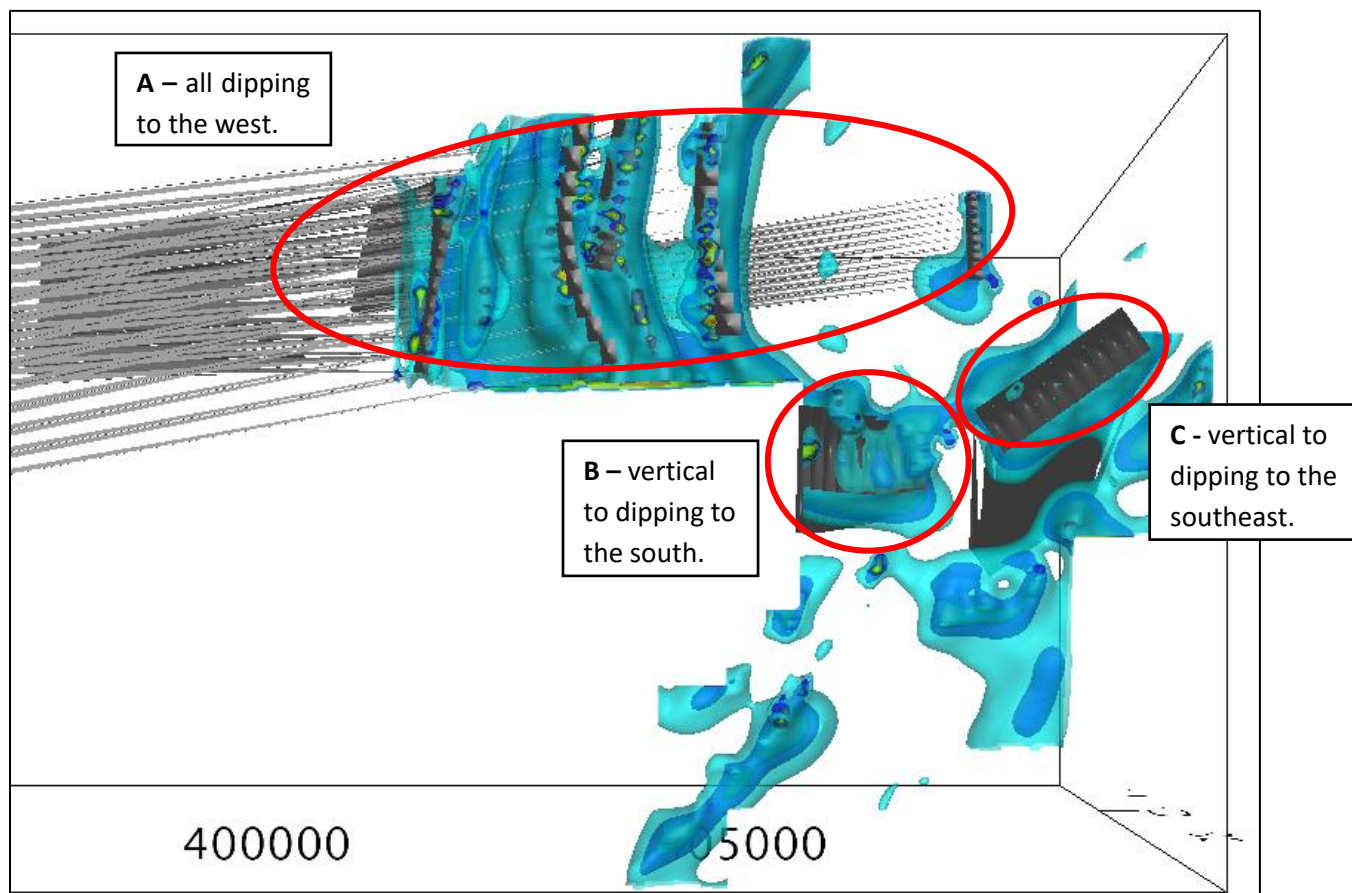


Figure 60. Higher susceptibility isosurfaces and the calculated QuickMag model with a view from overhead.

Landform Analysis

Landform analysis of the topography to delineate structures such as faults, lineaments and folds had some limited usefulness. Some faults seen in the magnetic could also be confirmed in the landform analysis and occasionally a fault would be included based on topography alone. The following landform analysis was included for completeness sakes.

SRTM and Analytic Hill Shade

The SRTM derived elevation model with a grid cell size of 30.7 m was not used as the Digital Elevation Model. The DEM was calculated from the difference of the GPS height and radar altimeter data with a grid cell size of 20 m. It was incorporated with the analytic hill shade image with an inclination of 45°, a declination of 0°, and vertical exaggeration of 36.3. The elevation varied from 337 to 410 m above sea level with a mean of 369 m.

The Generation 0 inferred faults (black dashed lines) are generally reflected in the topography as valleys or the sides of topographic highs. Some Generation 1 faults could be correlated in the same manner.

Generally, the lithographic units of mafic tonalite to granodiorite and mafic metavolcanics stand out as topographic highs and the metasediments as topographic lows.

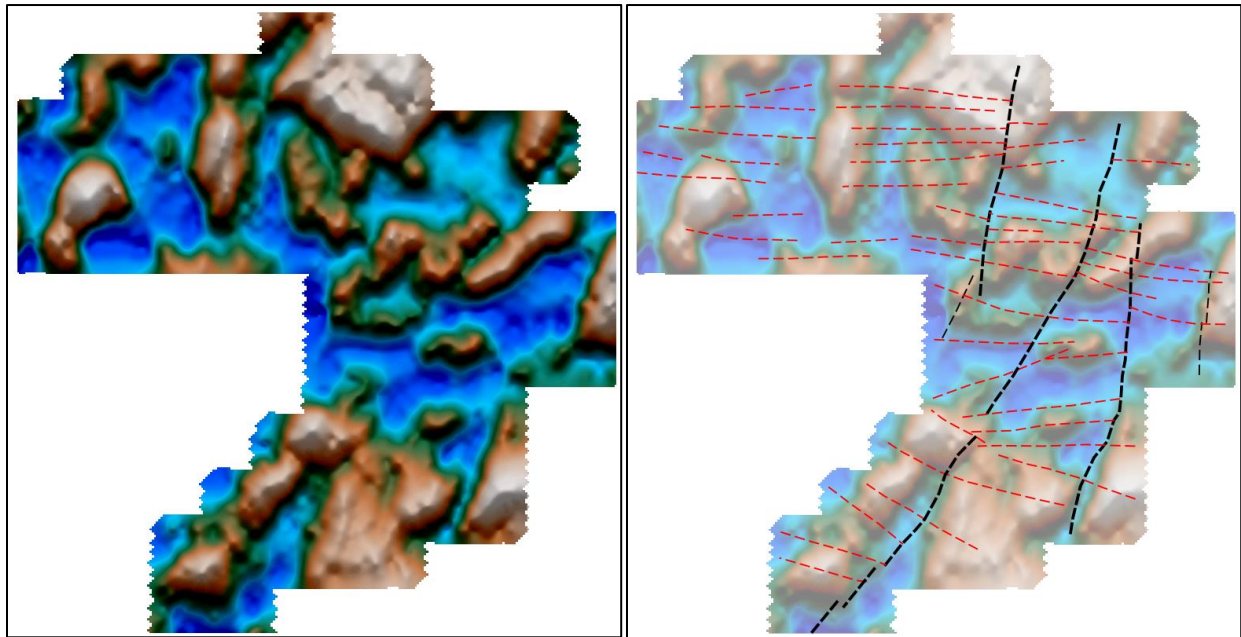


Figure 61. DEM combined with analytic hill shade (left) and with interpreted faults (right).

Slope Analysis

Again, there is not much to be gleaned from the slope analysis. As with the SRTM and Analytic Hill Shade, some Generation 0 inferred faults can be correlated with low values of slope indicating topographic valleys.

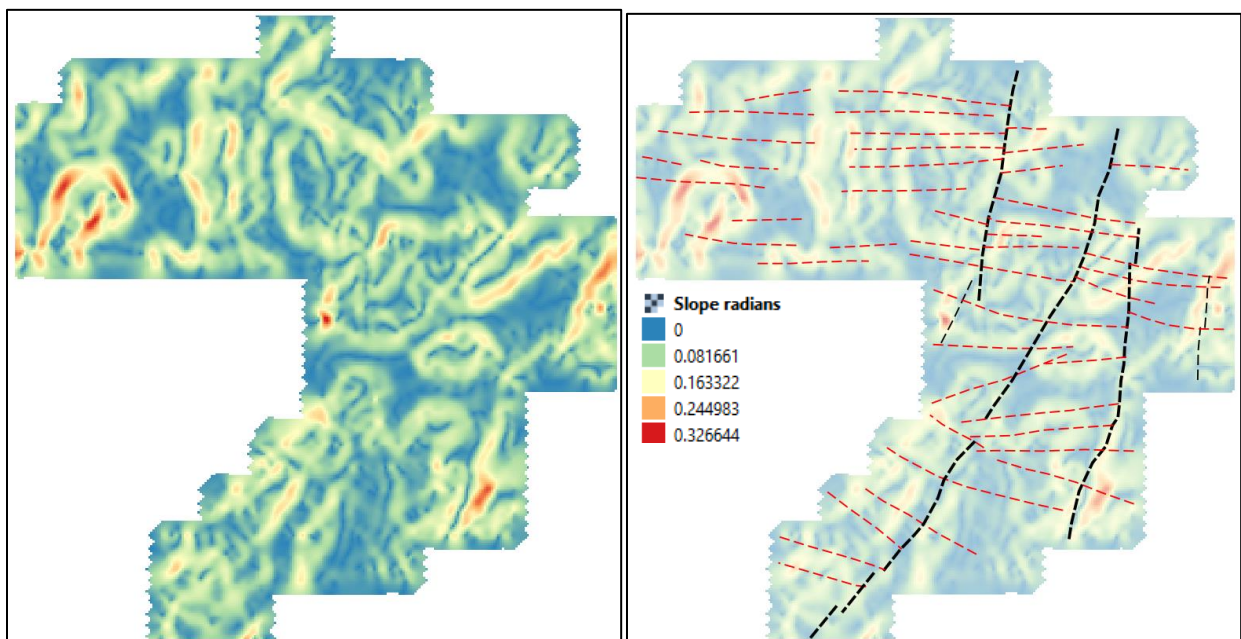


Figure 62. Slope derived from the DEM (left) and with interpreted faults (right).

Aspect Analysis

Some faults correlate with changes in slope aspect, i.e., a change in slope direction, such as the Generation 0 inferred faults. Due to the different erosional characteristics of the mafic metavolcanics and metasediments in the northwestern area, there appears to be some slight correlation in the changes of the slope aspect and the lithologies.

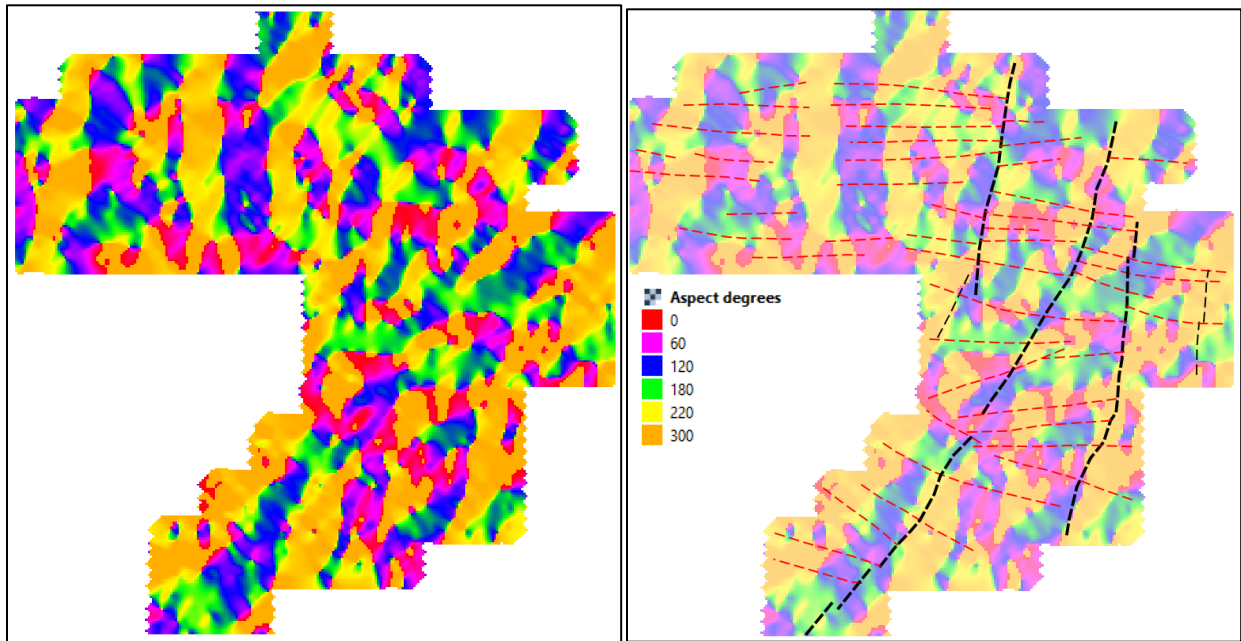


Figure 63. Aspect derived from the DEM (left) and with interpreted faults (right).

Landform Classification

Structure or lithology is very difficult to correlate with the landform classification. Generally, the Generation 0 inferred faults correlate with the various degrees of incised valleys (1 – Canyons, deeply incised streams, 2 – Midslope drainages, shallow valleys, 3 – Upland drainages, headwaters and 4 – U-shaped valleys). The metasediments tend to correlate with the “U-shaped valleys”.

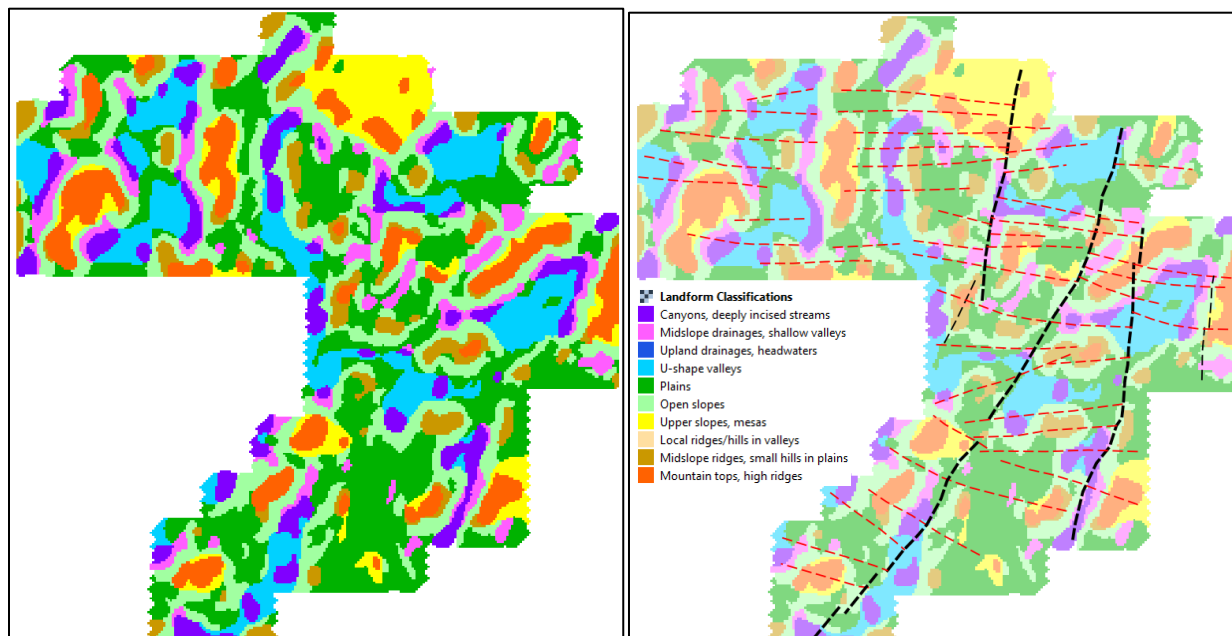


Figure 64. Landform Classification derived from the DEM (left) and with interpreted faults (right).

Western Bear

Lithological Interpretation

The central very high amplitude magnetic signal likely corresponds with a mafic to ultramafic intrusion such as a hornblendite or peridotite. Some high magnetic linear highs have been interpreted as mafic metavolcanic rocks such as been noted at outcrops as basaltic or andesitic flows. Much of the rest of the property is interpreted to be mafic tonalite to granodiorite with some felsic tonalitic gneiss with medium and low magnetic amplitudes, respectively. The following **Table 3** briefly describes the magnetic amplitude and textures that were used to assign the various interpreted lithologies.

	Lithology	Amplitude	Comments
1	Mafic to Ultramafic Intrusive Rocks	Very high – 1,000's nT	Could be a hornblendite or peridotite intrusion
2	Mafic Metavolcanic Rocks	High – low 100's nT	Tend to be narrow and linear or curvilinear
3	Mafic Tonalite to Granodiorite	Medium – 100 to 200 nT	Low magnetic background signal
4	Felsic Tonalite Gneiss	Low – 10's nT	May be just a less mafic version of unit above.

Table 3. Geophysical criteria for various lithological units.

A plan (**Figure 65**) and 3D view (**Figure 66**) of the reduced to the pole image illustrates these four units well.

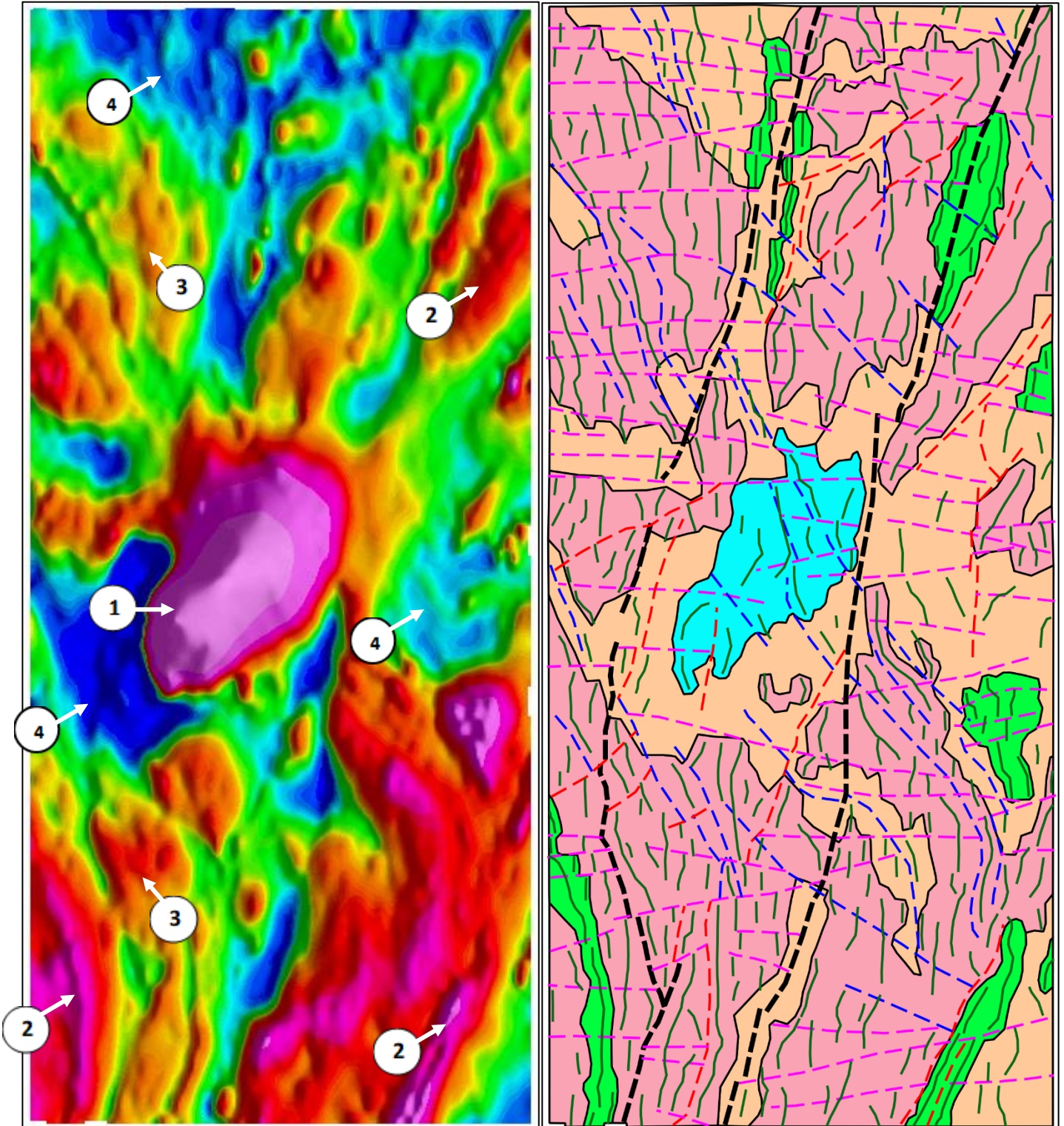


Figure 65. Residual magnetic intensity reduced to the pole (left) and the current geophysical interpretation (right).

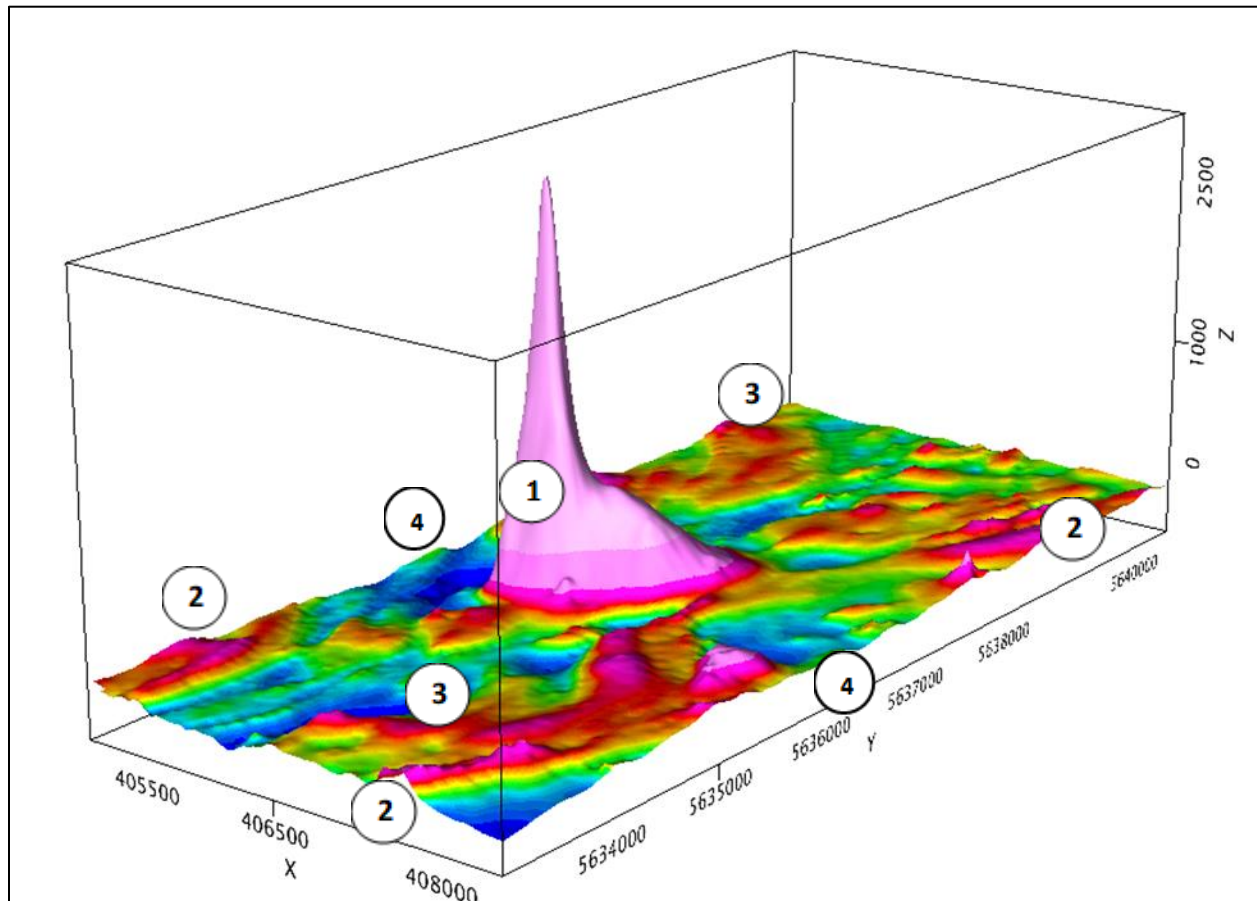


Figure 66. 3D view of the residual magnetic intensity reduced to the pole.

The Medicine Stone Lake Area geological map (P.3397, **Figure 67**)¹² and the digital bedrock geology from the Ontario Geological Survey¹³ were used as guides to assign the likely lithological units. There was good agreement in some areas and not in others due to the lack of outcrop and geological mapping detail in this region.

The major magnetic high in the center of the survey was assigned a lithology of a peridotite or hornblendite due to their high magnetic susceptibility and their mapped occurrence in small outcrops east of the survey area. The geological map implies a metavolcanic “dyke” throughout the middle of the survey area from north to south. This is not strictly seen in the magnetics other than the magnetic high in the center of the survey. The mafic metavolcanic units have a high magnetic magnitude (100’s nT) and their linear or curvilinear shape and narrow thickness. A similar feature west of the interpreted mafic metavolcanic in the southwest corner of the survey are similar in thickness and shape. There are a number of interpreted mafic metavolcanic units in the north of the survey that were identified by their linear shape, though their magnetic amplitude is much less than those in the southern portion of the survey.

¹² Atkinson, B. T. 1999. Precambrian geology, Medicine Stone lake area; Ontario Geological Survey, Preliminary Map p.3397, scale 1:50 000.

¹³ Ontario Geological Survey 2011. 1:250 000 scale bedrock geology of Ontario; Ontario Geological Survey, Miscellaneous Release–Data 126 - Revision 1.

These mafic metavolcanics may be more weakly magnetized or deeply buried. Most of the background geology has been identified as biotite tonalite to granodiorite, or more generally, mafic tonalite to granodiorite. Also seen in the survey area is a felsic tonalite gneiss which would be less magnetic than the mafic tonalite to granodiorite. As I have noted in the table, some of the interpreted felsic tonalite gneiss may just be fractured mafic tonalite to granodiorite. Fracturing and the associated hydrothermal activity can lead to magnetite destruction. As well, the low magnetic signal around the ultramafic intrusion could be a heat aureole leading to magnetite destruction.

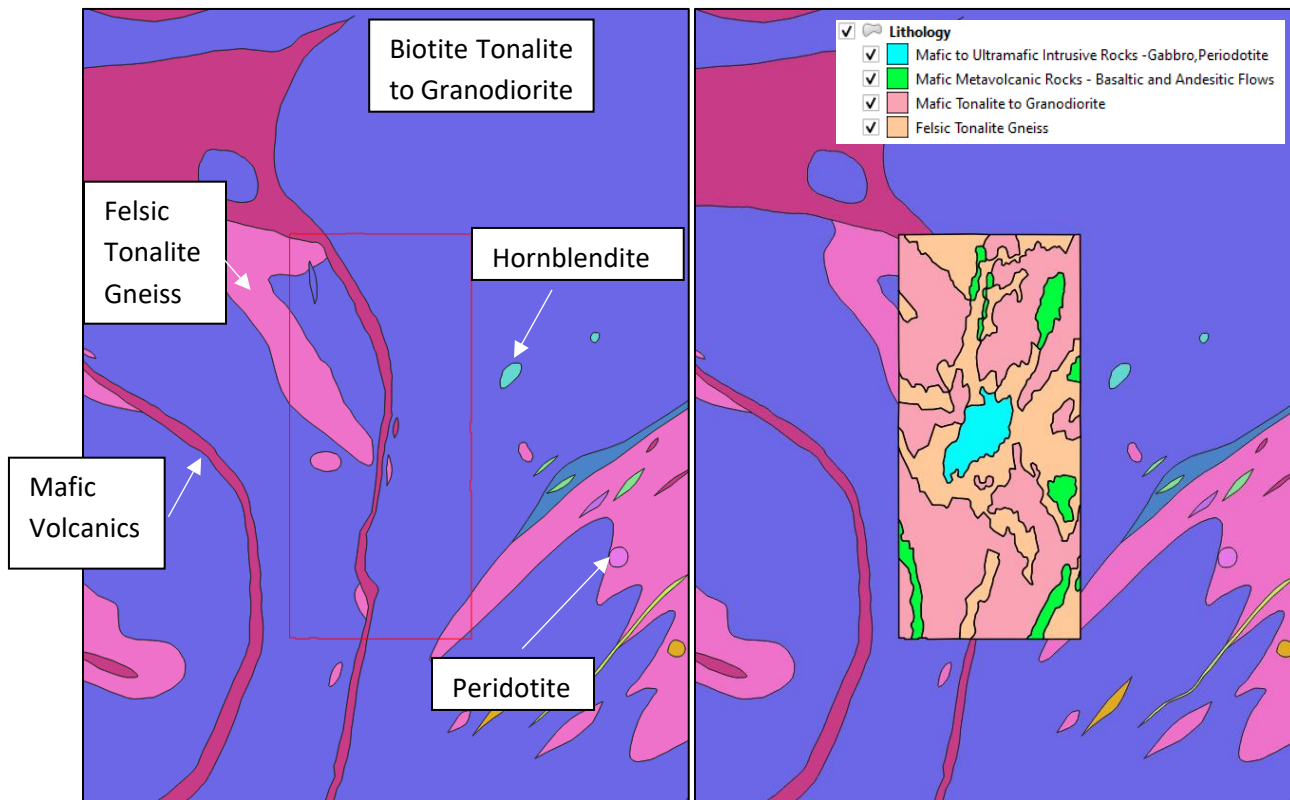


Figure 67. Published geology (left) and the current lithological interpretation (right).

Lineaments

Lineaments were traced along highs in the second vertical derivative of the pole reduced field (RTP2VD.grd), tilt derivative (TILT.grd) and total horizontal gradient (TDX.grd). The tilt derivative with lineaments is shown in the image below (**Figure 68**).

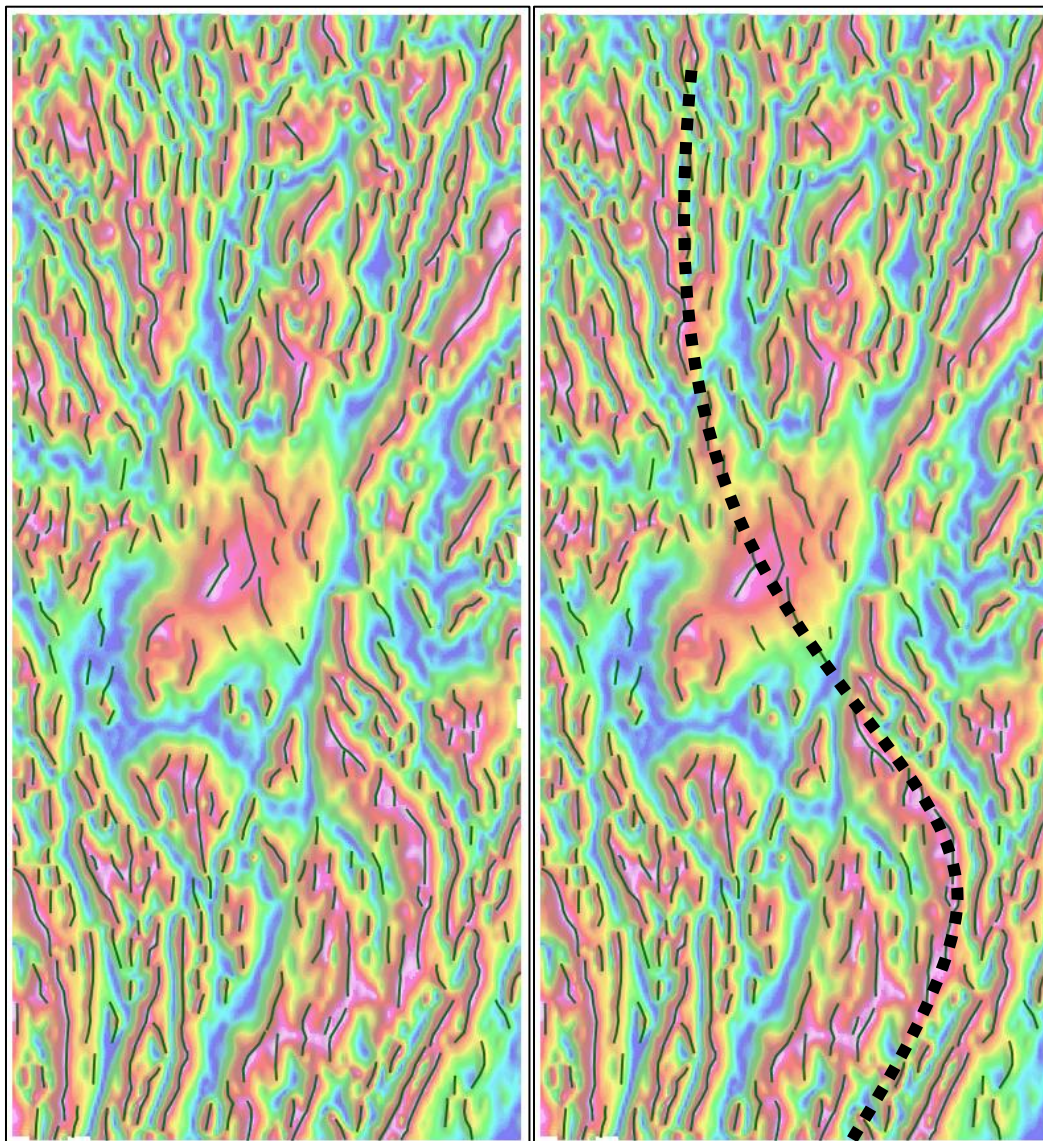


Figure 68. Lineaments or trends overlain upon the tilt derivative (50% transparency applied).

A rose diagram of the orientations of the lineaments (**Figure 69**) show a vast majority of the orientations lie within the NNW and NNE directions. Minor amounts of lineaments occur in the NNW to NW and NNE to NE directions. No lineaments are seen in other directions. These orientations are very similar to the Sydney Lake property to the south. The pattern of lineaments also shows a shearing in the centre of the survey (**Figure 68**). From south to north, the lineament direction changes from NE to NW and then generally N. The internal lineaments of the ultramafic intrusive are vague and not as well defined as in the other lithological units.

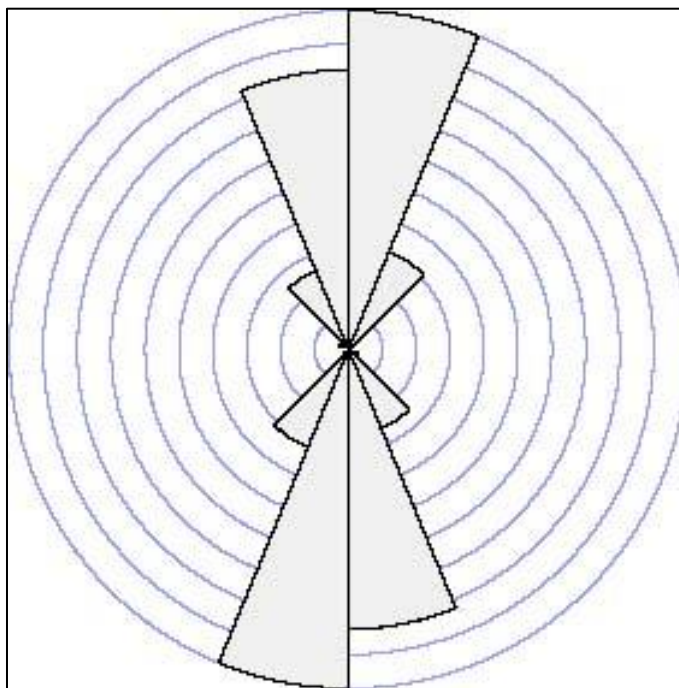


Figure 69. Rose diagram of orientations of lineaments.

Faults

The location and length of inferred faults were determined from various derivative grids (**Figure 70**). They were determined by an offset or disruption in character of the linear magnetic anomalies.

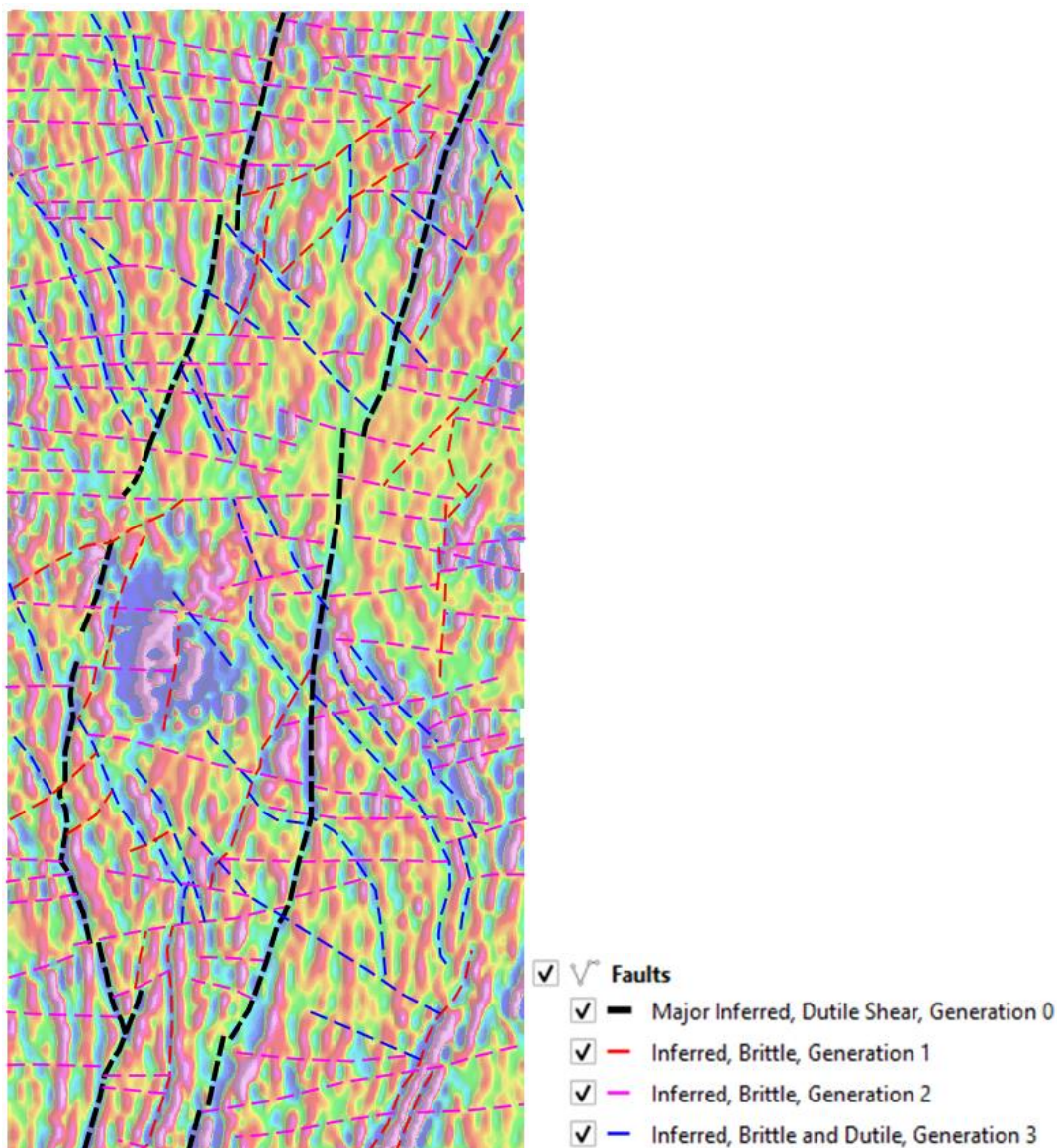


Figure 70. Interpreted faults overlain upon the second vertical derivative of the pole reduced field (50% transparency).

A Rose diagram of the fault orientations (**Figure 71**) show the majority of the interpreted faults to be between 90° (E) and 112.5° (ESE). The faults have been divided into 4 generations generally defined by their orientations, as follows:

- Generation 0: 22.5° (NNE) are interpreted to be the oldest. Generation 0 faults are offset by faults of all other fault generations. Generation 0 faults occur as two major parallel faults. There appears to be some shearing along or between these two major faults so that it has been defined as a major ductile shear.
- Generation 1: 22.5° (NNE) to 45° (NE) are interpreted to be younger than Generation 0. Generation 1 faults are mostly sinistral and occur throughout the study area. They are generally parallel to the Generation 0 faults. These faults are offset by generation 2 faults and are truncated by Generation 3 faults.

- Generation 2: 67.5° (ENE) to 112.5° (ESE) are interpreted to be younger than Generation 1 and the sense is undefined. There are some fault intersections that suggest dextral and others sinistral motions, but most intersections show no fault offset. They occur throughout the study area.
- Generation 3: 135° (SE) to 157.5° (SSE) are interpreted to be the youngest faults. Generation 3 faults are the ones that show the shearing effects. They occur throughout the study area.

Due to the lack of clear and consistent offsets of the different fault generations, I can not be confident in the absolute order of the different generations, especially that of Generations 2 and 3.

The number of faults and generations in such a small study area indicates a complex structural history. The structural interpretation of the magnetic data adds substantial information regarding possible fault locations to the geology of the Western Bear area. For a better understanding of the fault character (e.g., associated alteration, slip direction) ground truthing of the interpreted structures is necessary.

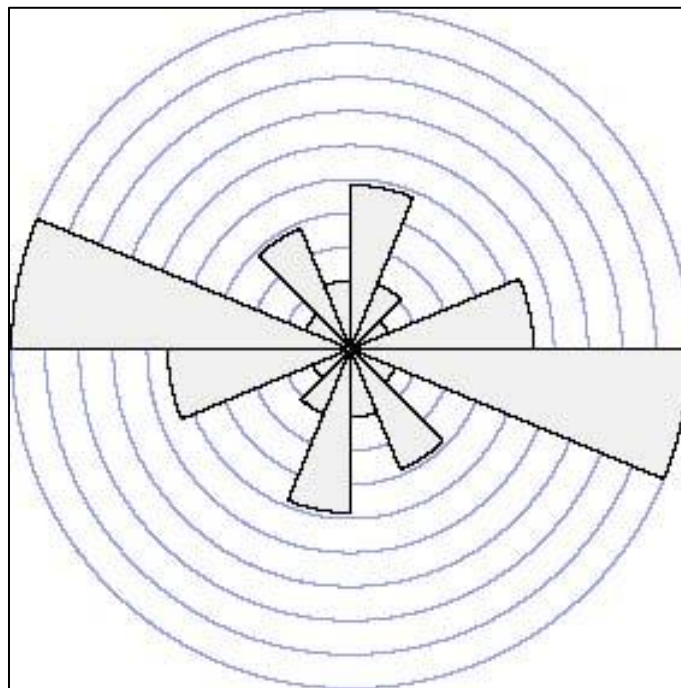


Figure 71. Rose diagram of fault orientations.

VOXI Modelling Interpretation

The VOXI 3D model of the magnetic susceptibility of the survey area is shown below in **Figure 72**. At surface the susceptibility distribution appears similar to the image of the residual magnetic intensity such as the magnetic high in the centre of the survey and some of the mafic metavolcanics in the south. This implies that the modelling has forced many of the magnetic sources to be near the surface. The top of the model surfaces is at 432 m above sea level. The data has been clipped to different depth slices such as 200 m, -400 m and -1,300 m above sea level (asl) or 232 m, 832 m and 1,732 m below surface, respectively (**Figure 73**, **Figure 74**, and **Figure 75**).

In the following figures of the VOXI model clipped to various depths, the ultramafic intrusion (labelled 1) and mafic metavolcanic units (labelled 2) are highlighted. Many of the other magnetic features seen at surface tend to dissolve and disappear at depth. The ultramafic intrusion persists from surface to at least 1,300 m below sea level or approximately 1,700 m in depth extent. Some of the mafic metavolcanics in the south tend to disappear between 400 and 1,300 m below sea level.

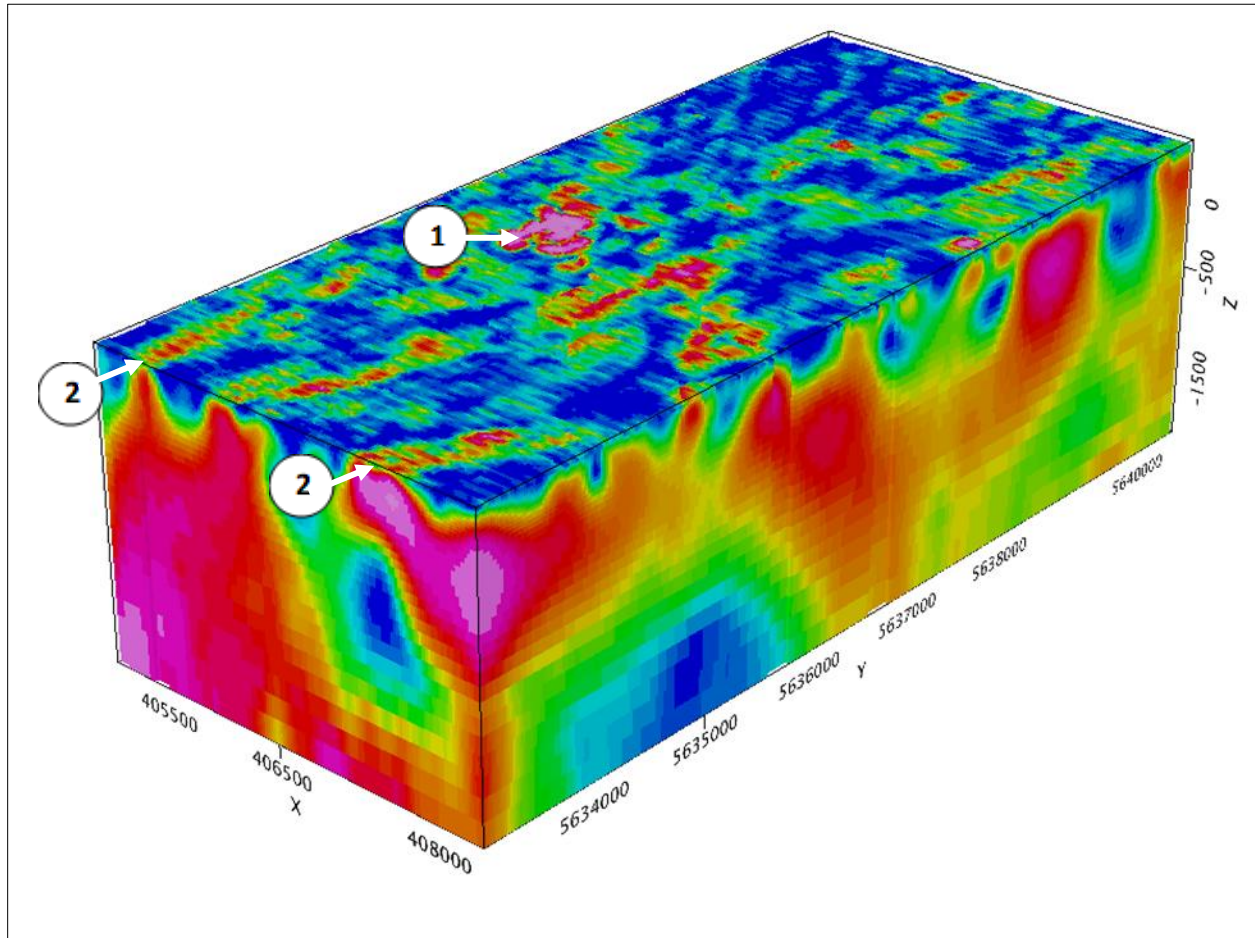


Figure 72. Magnetic susceptibility model of the survey area. The top of the model is at surface at 432 m above sea level.

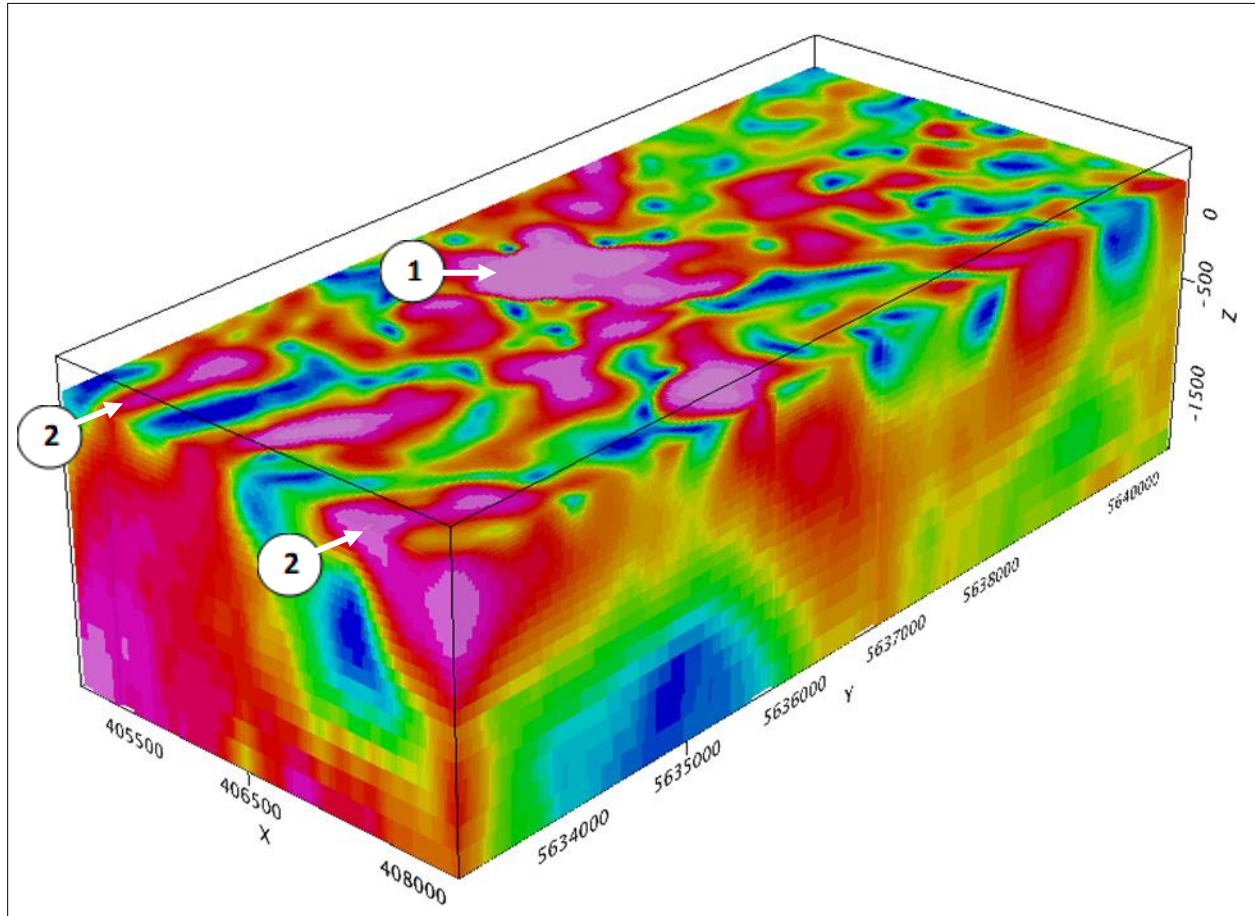


Figure 73. Magnetic susceptibility model with the top of the model is at 200 m above sea level.

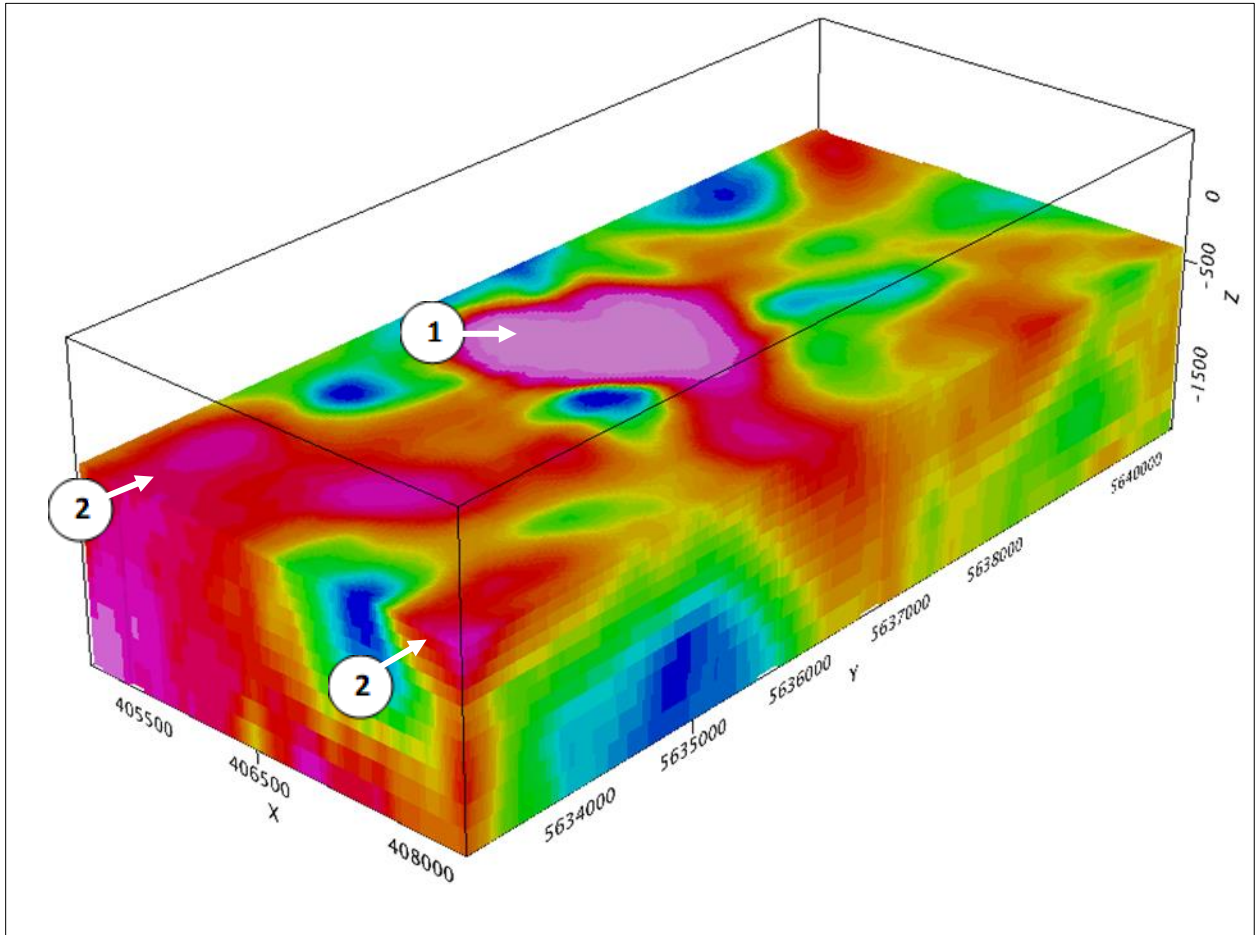


Figure 74. Magnetic susceptibility model with the top of the model is at 400 m below sea level.

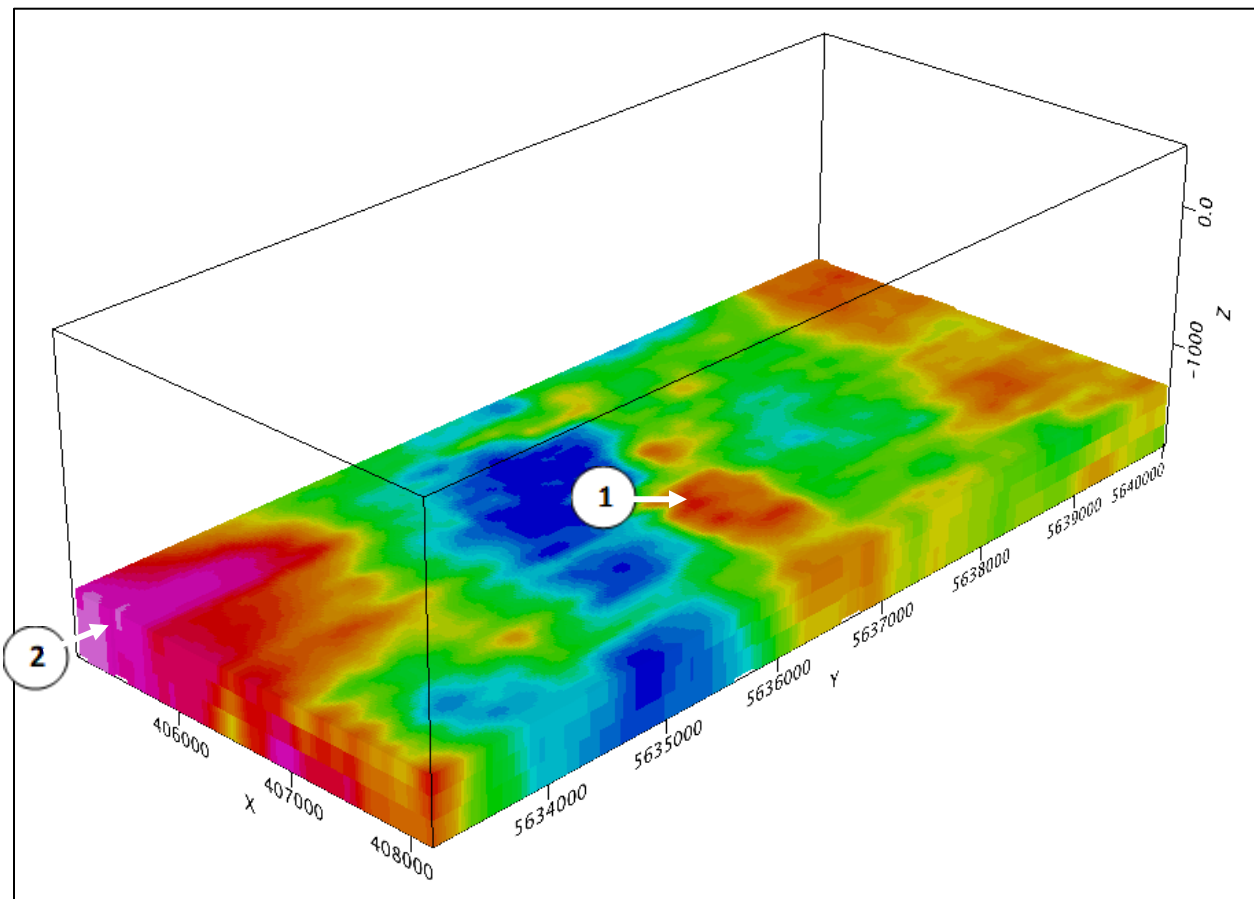


Figure 75. Magnetic susceptibility model at a depth of 1300 m below sea level.

Another way to view the susceptibility models is as a series of isosurfaces or shells of constant susceptibility. The following susceptibility surfaces (legend to the right, units in SI) were imaged in **Figure 76** and the subsequent isosurfaces images. Rather than viewing slices or sections of the magnetic susceptibility model, an isosurface emphasises the 3-dimensional shape of the model. The isosurface of 0.001 SI was calculated but was not used in the following images since it obscures some of the finer detail.

- SURF_WB_Ampl
- Isosurface 0.001
- Isosurface 0.0025
- Isosurface 0.005
- Isosurface 0.0075
- Isosurface 0.01
- Isosurface 0.02

Again, the central ultramafic intrusion dominates the voxel isosurfaces (labelled 1, **Figure 76** and **Figure 77**). The geophysical interpretation has been overlain upon the voxel isosurfaces. The VOXI model confirms that the ultramafic intrusion is bounded by the two major inferred faults. The depth extent of its 0.0025 SI isosurface is to approximately 1,100 below sea level or 1,532 m below surface. A close-up of the higher value isosurfaces (0.0075, 0.01, 0.02 and 0.05 SI) is shown in

Figure 78. A cross section through multiple isosurfaces of susceptibility viewed from above towards the northwest without some of the lower isosurfaces.

. The higher values of susceptibility are in the southwestern portion of the intrusion and this also corresponds to being close to surface. With depth the intrusion extends to the northeast. The QuickMag model implies that the intrusion dips to the northwest which is not supported by the VOXI modelling (**Figure 79**). The QuickMag model may be overly influenced by the high susceptibility material in the top 150 m. The QuickMag model does agree with the VOXI model in the sense that the top of the most susceptible portion of the intrusion deepens towards the northeast. Both models indicated that there may be outcrop of the ultramafic intrusion at the approximate UTM coordinates of 405900, 5635950 (QuickMag) at the south side of a small lake or directly north on the other shoreline at 405900, 5635330 (VOXI). These area around these locations would be worth checking in the field.

Only some of the mafic metavolcanics are represented in the voxel isosurfaces in the southern portion of the survey and the small mafic intrusion in the east central region (labelled 2). The southwestern unit appears to have a vertical dip while the southeastern unit implies an easterly dip. The small mafic intrusion in the east central region has a depth extent of 550 m.

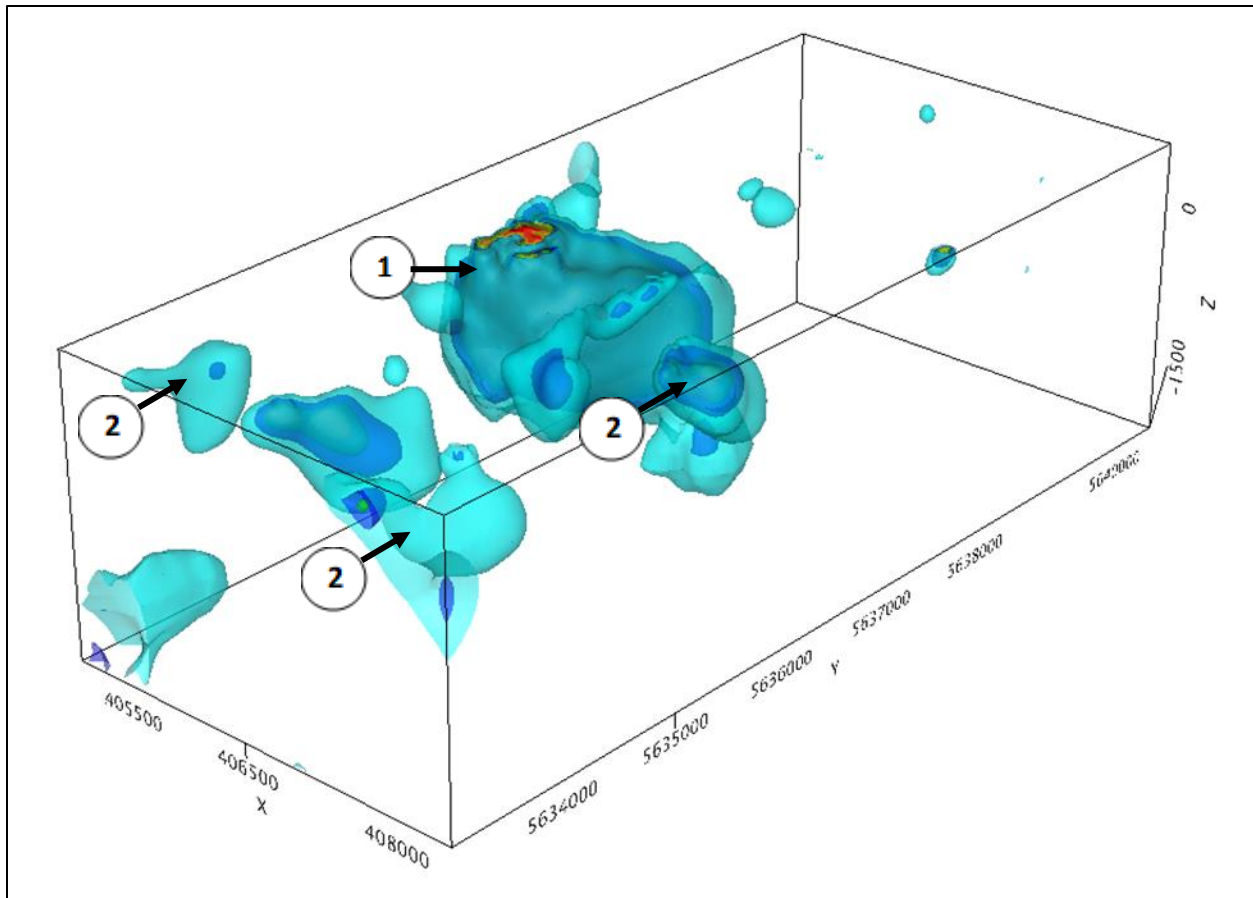


Figure 76. Multiple isosurfaces of susceptibility.

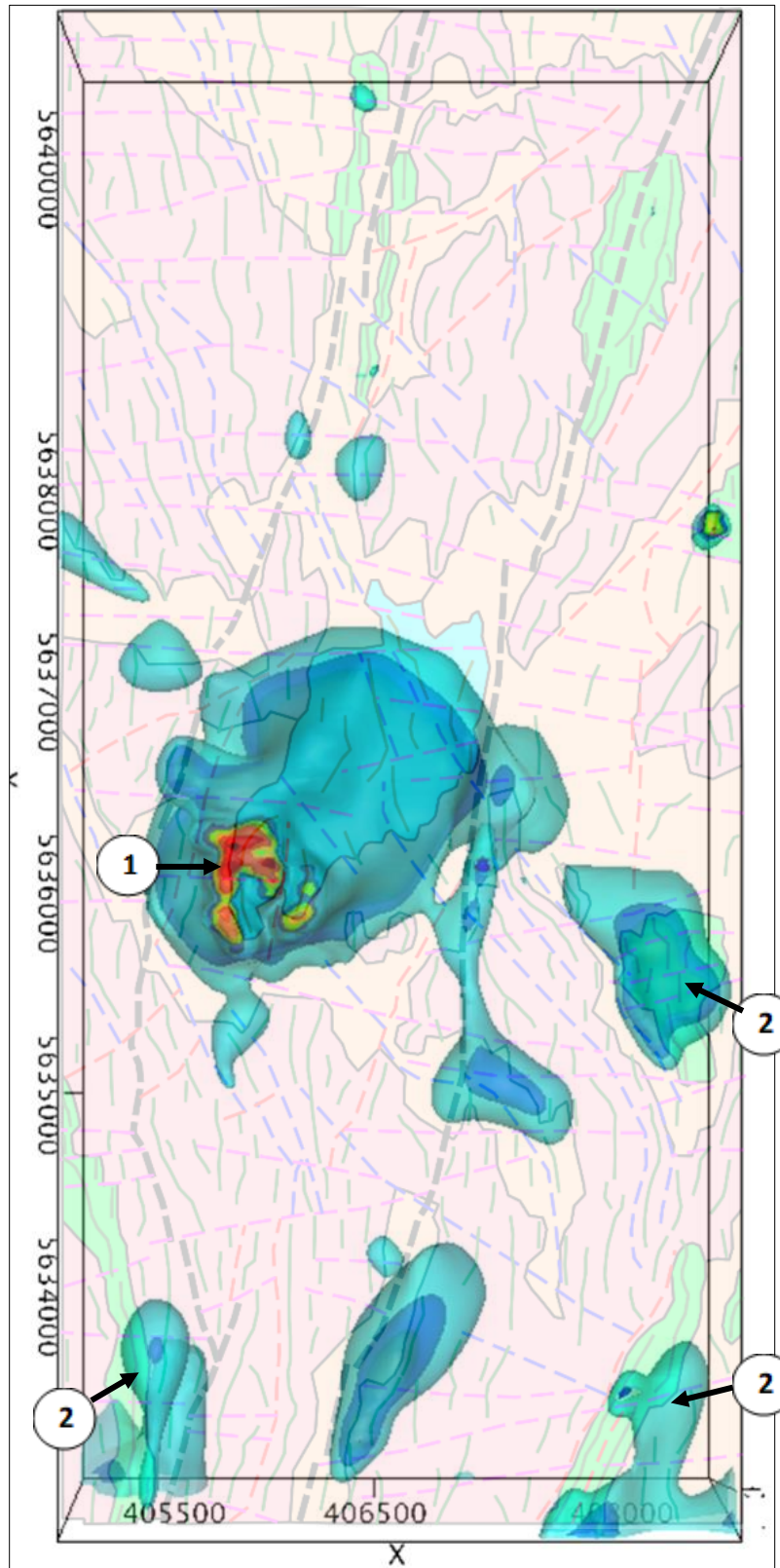


Figure 77. Multiple isosurfaces of susceptibility viewed from above with a transparency of the geophysical interpretation.

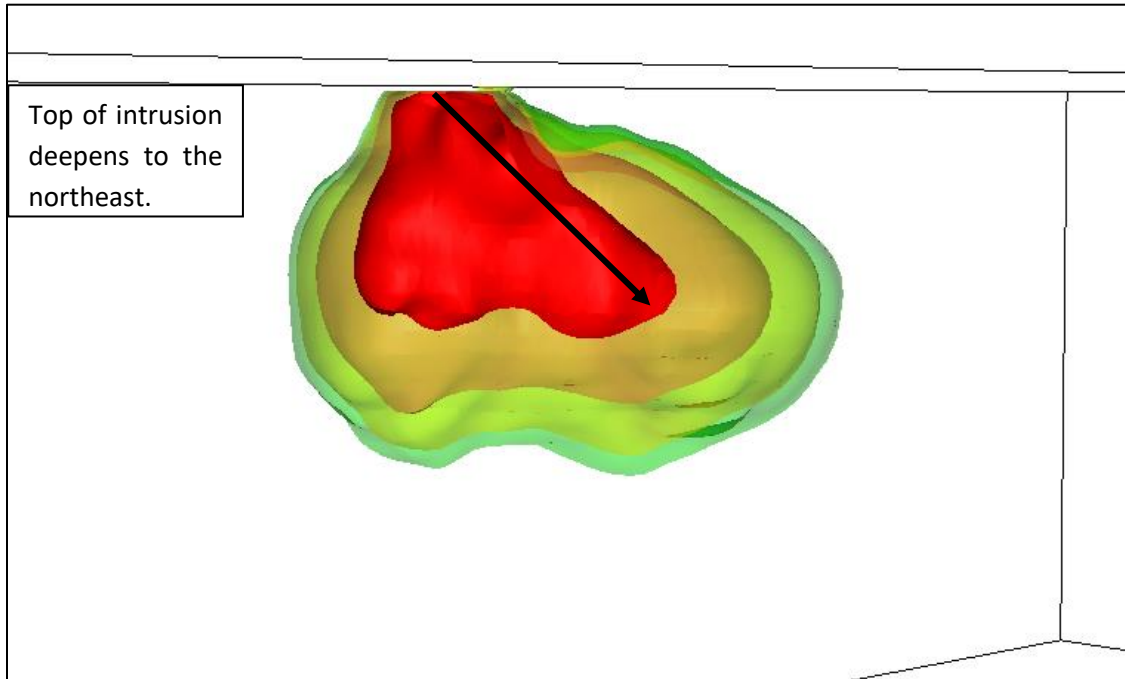


Figure 78. A cross section through multiple isosurfaces of susceptibility viewed from above towards the northwest without some of the lower isosurfaces.

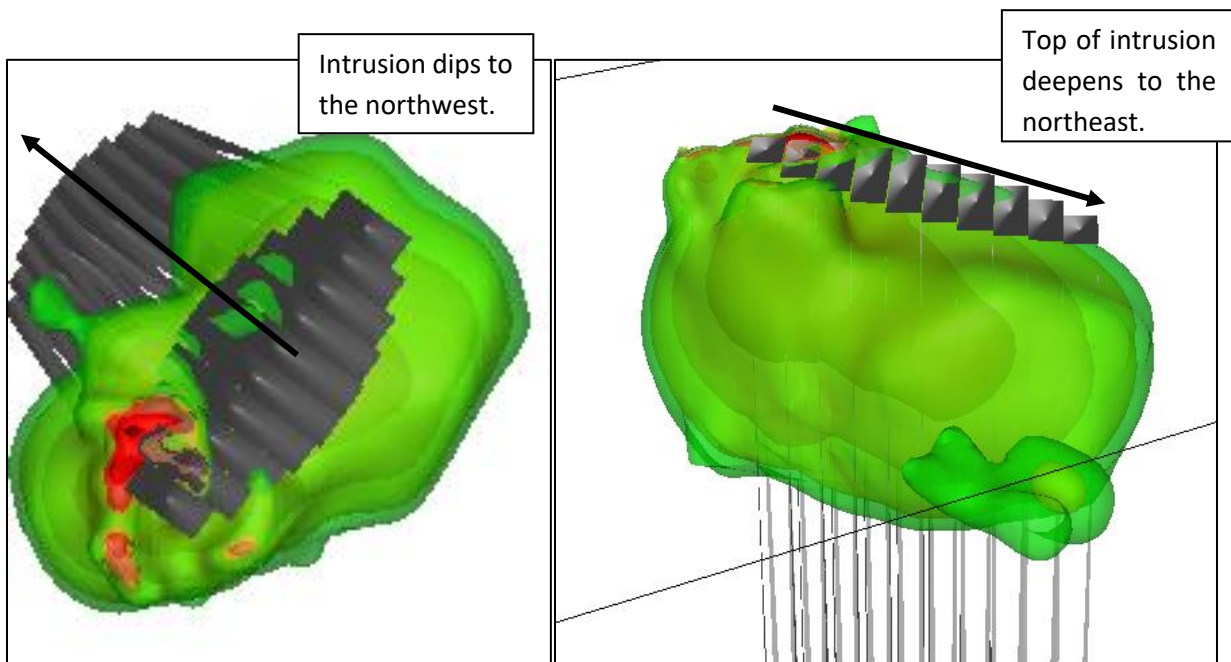


Figure 79. Higher susceptibility isosurfaces and the calculated QuickMag model with a view from the top (left) and a side view looking towards the northwest (right).

Landform Analysis

Landform analysis of the topography to delineate structures such as faults, lineaments and folds had some limited usefulness. Some faults seen in the magnetic could also be confirmed in the landform analysis and

occasionally a fault would be included based on topography alone. The following landform analysis was included for completeness sakes.

SRTM and Analytic Hill Shade

The SRTM derived elevation model with a grid cell size of 30.7 m was not used as the Digital Elevation Model. The DEM was calculated from the difference of the GPS height and radar altimeter data with a grid cell size of 20 m. It was incorporated with the analytic hill shade image with an inclination of 45°, a declination of 0°, and vertical exaggeration of 68.5. The elevation varied from 389 to 432 m above sea level with a mean of 414 m.

The Generation 0 inferred ductile shears/faults (black dashed lines) are generally reflected in the topography as valleys or the sides of topographic highs. Many of the other fault generations can also be seen to be reflected in the topography.

Generally, the mafic metavolcanics and mafic tonalite to granodiorite are topographic highs. The mafic to ultramafic intrusion reflected as a major magnetic high in the centre of the survey area, is a mix of topographic highs and lows likely mirroring multiple fault directions.

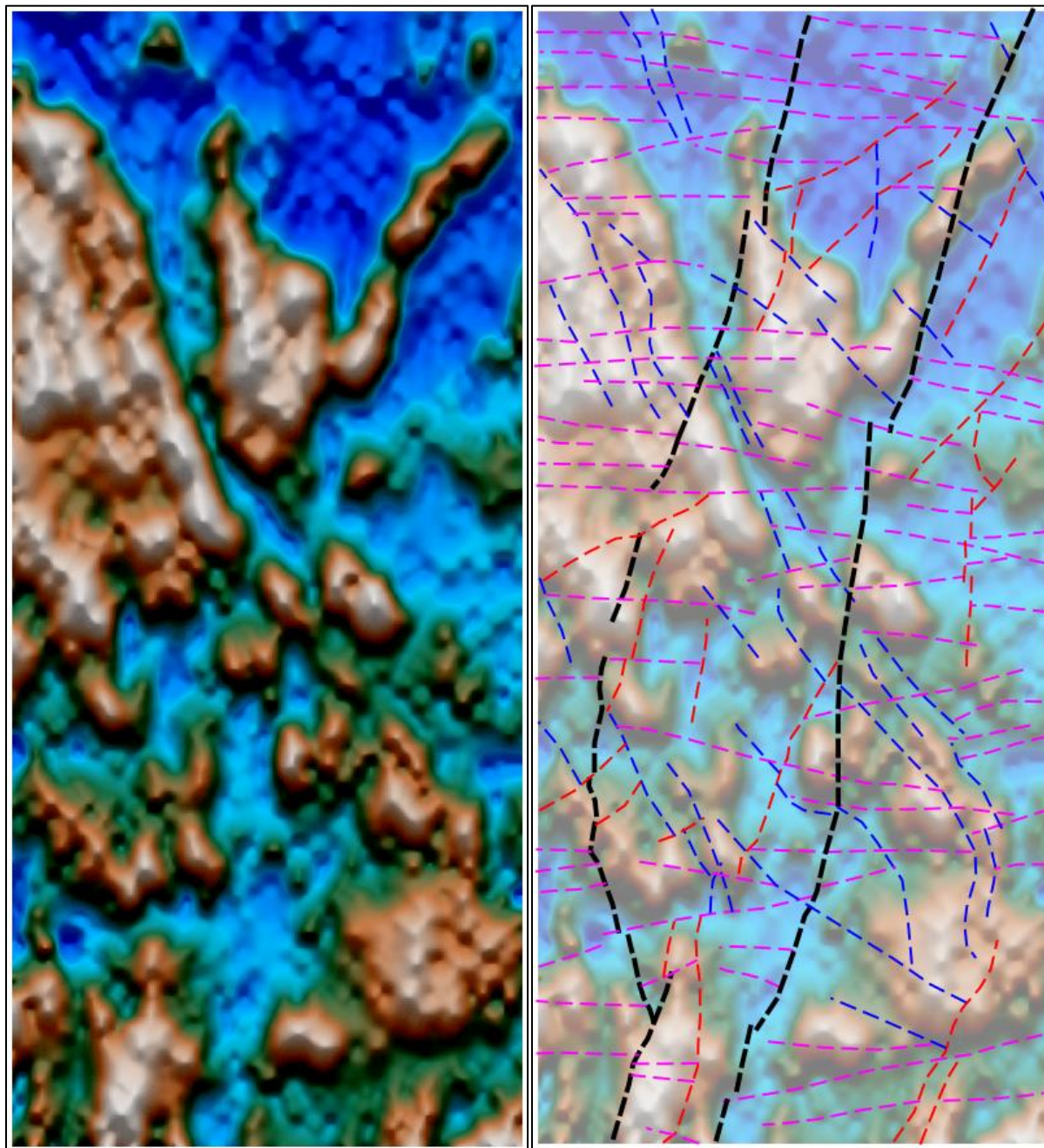


Figure 80. DEM combined with analytic hill shade (left) and with interpreted faults (right).

Slope Analysis

Again, there is not much to be gleaned from the slope analysis. As with the SRTM and Analytic Hill Shade, some fault generations can be correlated with low values of slope indicating topographic valleys.

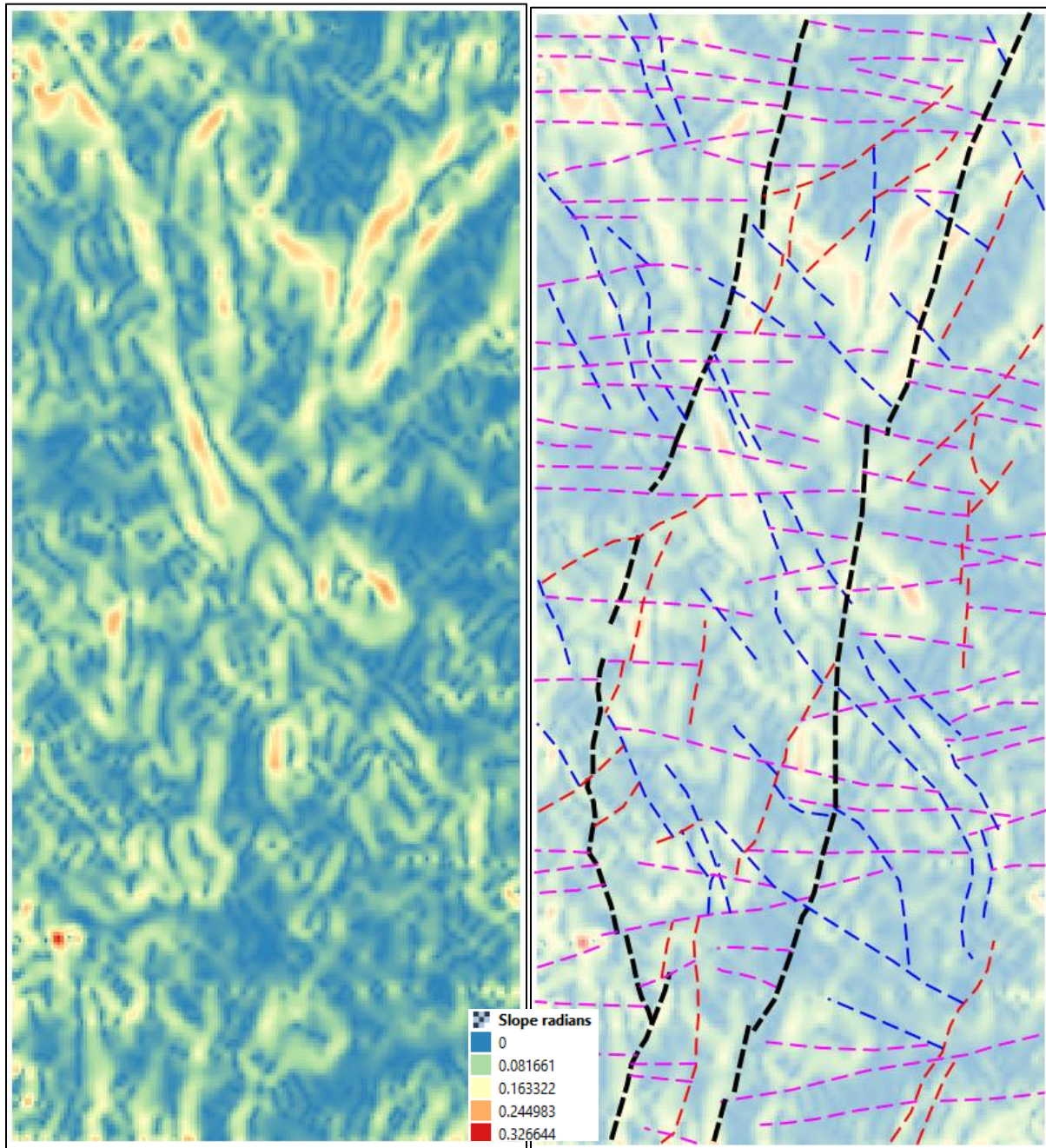


Figure 81. Slope derived from the DEM (left) and with interpreted faults (right).

Aspect Analysis

Some faults correlate with changes in slope aspect, i.e., a change in slope direction, in all fault generations. It is especially noticeable in the Generation 3 inferred faults. There seems to be little correlation between the slope aspect and lithology.

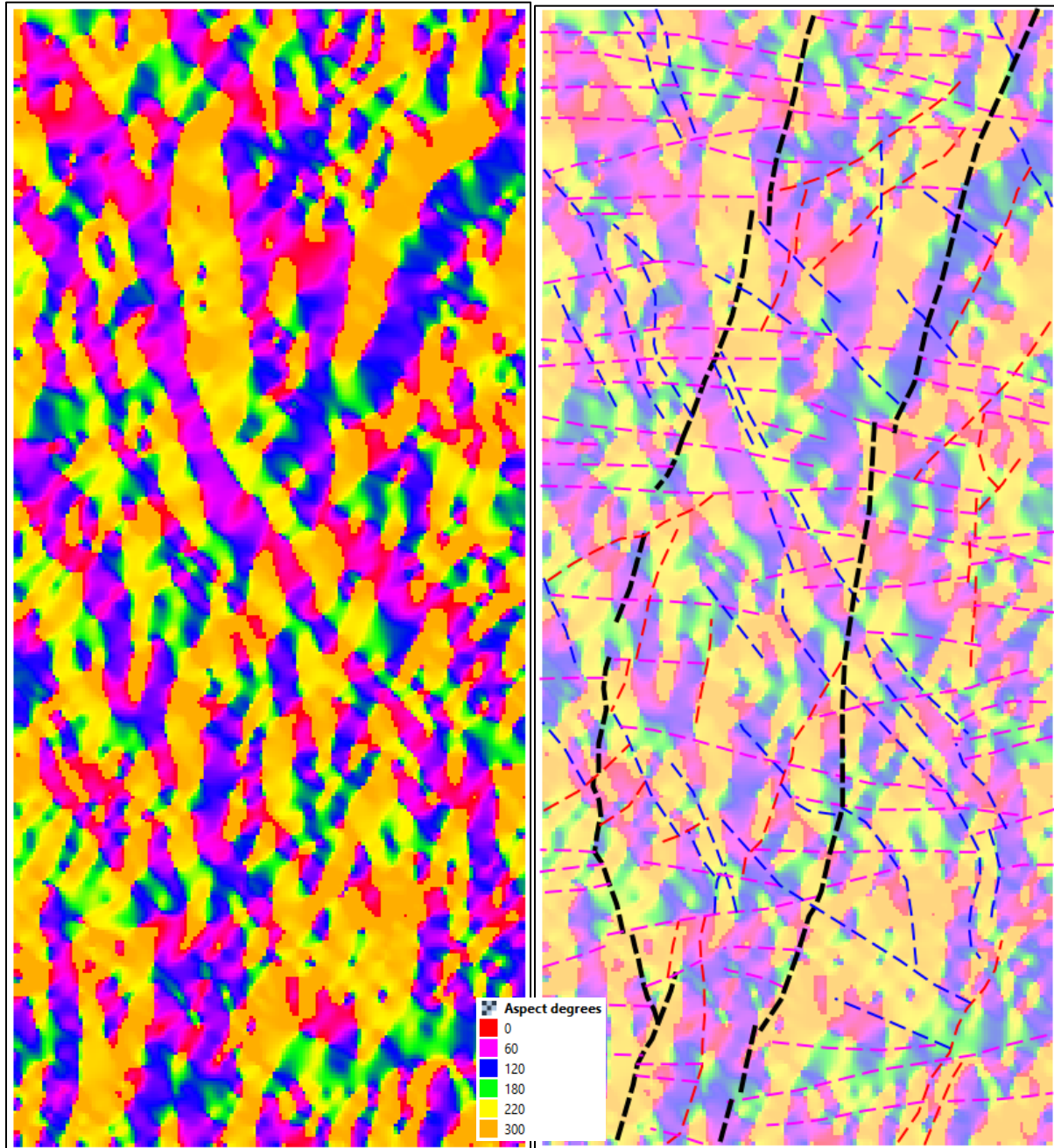


Figure 82. Aspect derived from the DEM (left) and with interpreted faults (right).

Landform Classification

Structure or lithology is very difficult to correlate with the landform classification. Most of the area is classified as “Plains” likely due to the low topographic relief of the area.

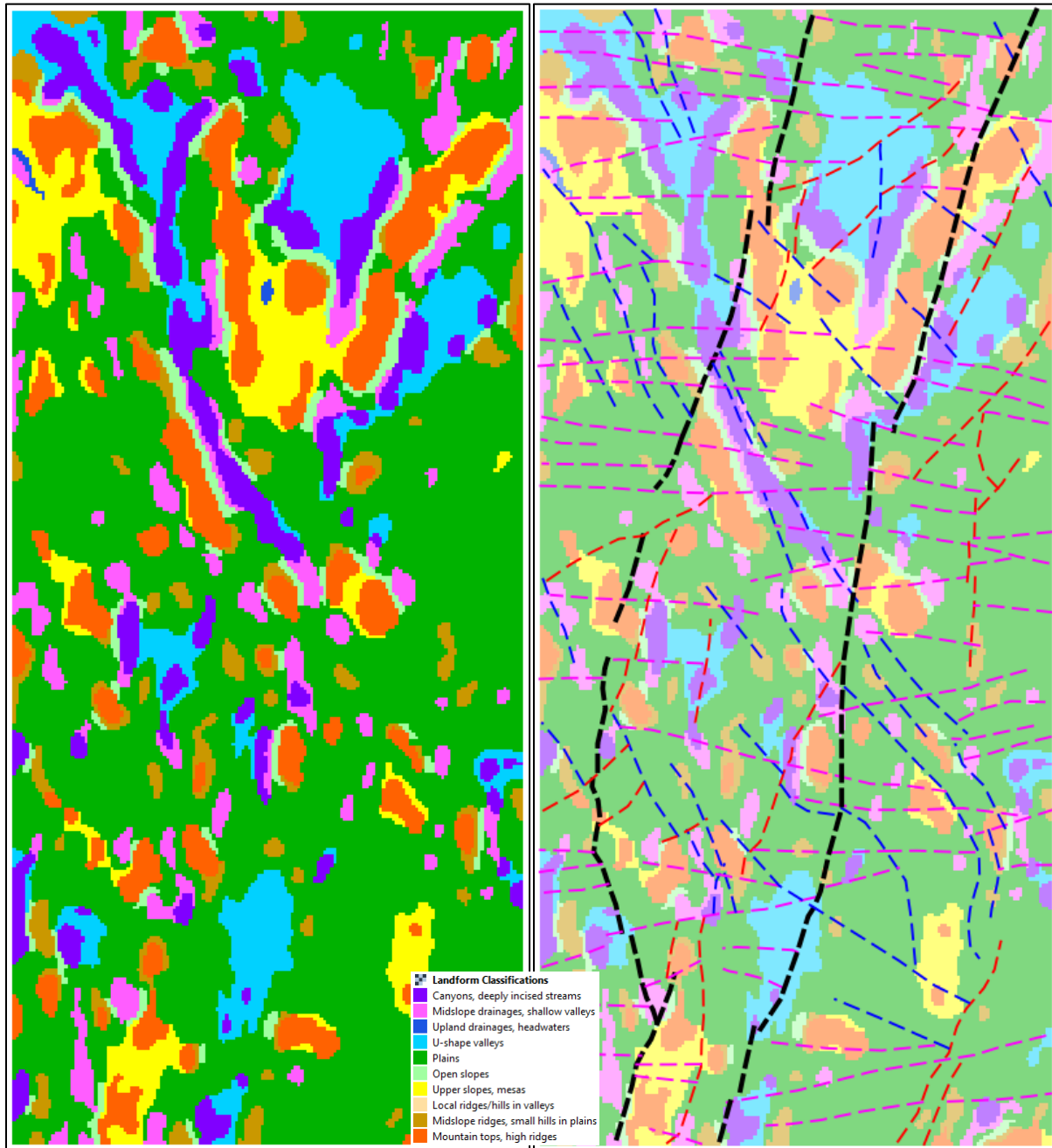


Figure 83. Landform Classification derived from the DEM (left) and with interpreted faults (right).

Recommended Target Areas

Target areas are based upon a number of geological criteria:

- Proximity to, or correlation with, a major deformation zone
- Local scale with or without semi-regional faulting/shearing
- Proximity to a local scale heat source, i.e., intrusion
- Dominant brittle fracture

GEOPHYSICAL INTERPRETATION OF WESTERN BEAR, SYDNEY LAKE AND LEO PROPERTIES

- Deep source for fluids, i.e., intrusion or regional deformation
- High Fe content with additional Fe-rich alteration
- Close to known gold occurrences.

Leo

The Pakwash-Longlegged Lake geological map (P.1027, **Figure 84**)¹⁴ does not report any mineral occurrences within or near the Leo property, however this map is from 1974. Toby Hughes’ targeting report¹⁵ indicates that the present area is underexplored and some nearby exploration has been conducted for Li pegmatite, gold and base metals. The Leo property is outlined in black. There is no coverage in this map for the eastern 20% of the property but exists on other geology maps.

A number of primary and secondary targets were selected for follow-up exploration (**Figure 85**). They are denoted by the solid and dashed ovals in the maps of West (**Figure 87**), Central (**Figure 88**) and East (**Figure 89**) areas which have been subdivided, as shown in **Figure 86**.

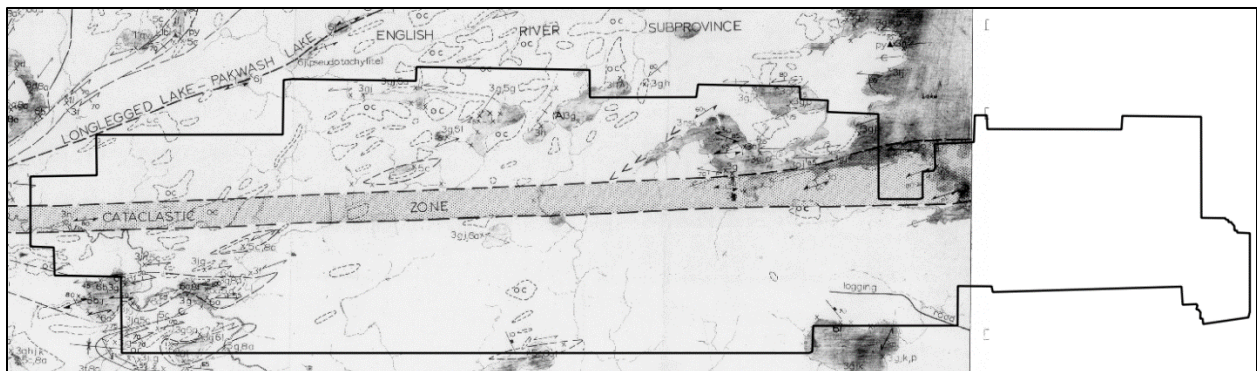


Figure 84. Local mapped geology of the Leo property.

Most of the target areas are related to the fold noses of the granodiorite intrusions where low pressure regimes exist and are suitable for the precipitation of mineralized fluids. The targets are also associated with high magnetic susceptibility (Fe rich) lithological units.

¹⁴ Breaks, F. W., Bond, W. D., McWilliams, G. H., Gower, C. F., and Stone, Denver 1975 Operation Kenora-Sydney Lake, Pakwash-Longlegged Lakes Sheet, District of Kenora; Ontario Div. Mines, Prelim. Map P.1027 Geol. Ser., scale 1 inch to 1 mile or 1:63,360. Geology 1974.

¹⁵ Hughes, T.N.J., P.Geo., 2020, Targeting in the Leo Property, English River Subprovince, Red Lake Mining Division, Ear Falls, Ontario for Trillium Gold Mines Inc.

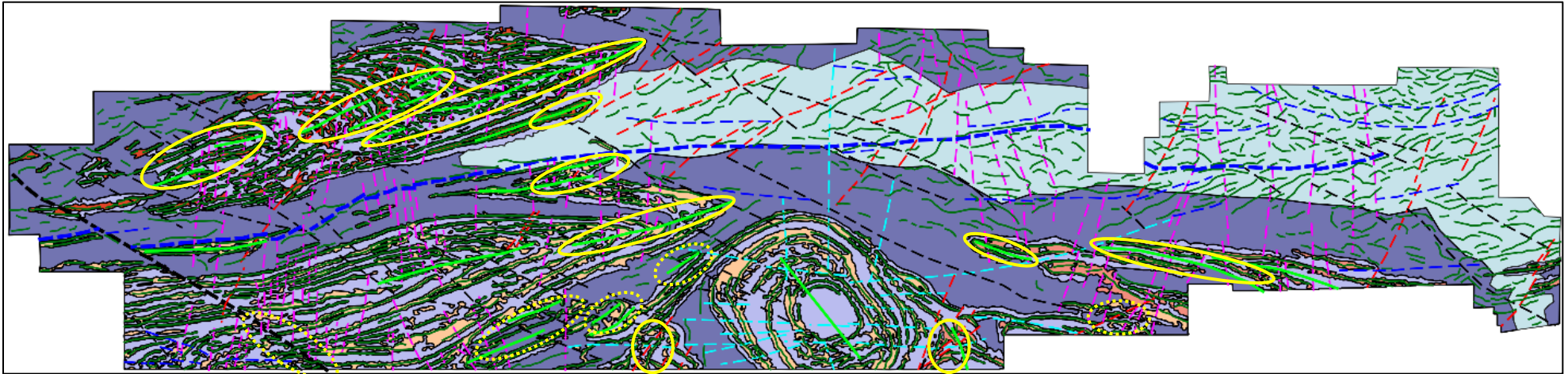


Figure 85. Recommended primary and secondary targets for follow-up for the Leo property.

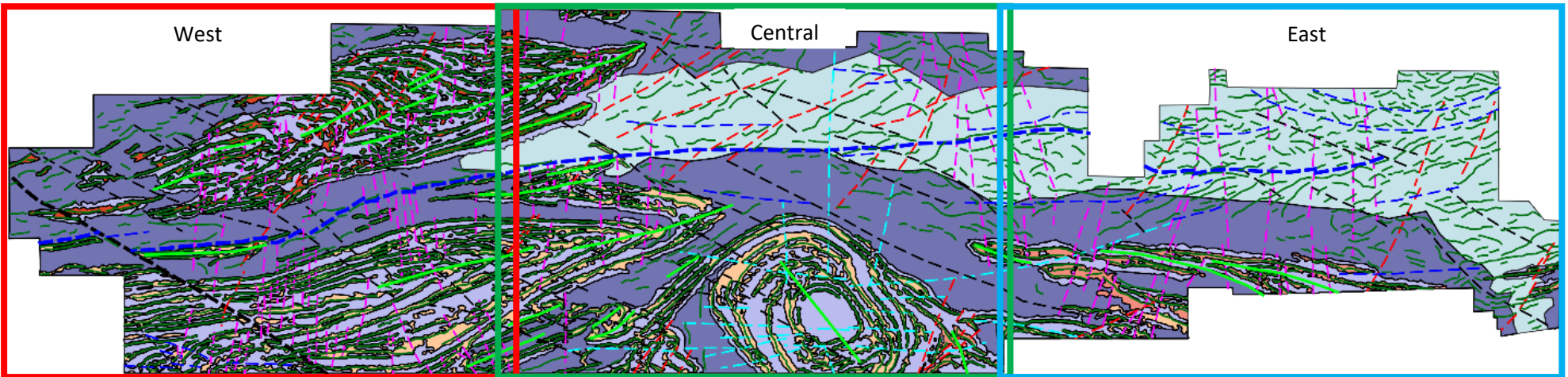


Figure 86. Subset areas of recommended targets.

West

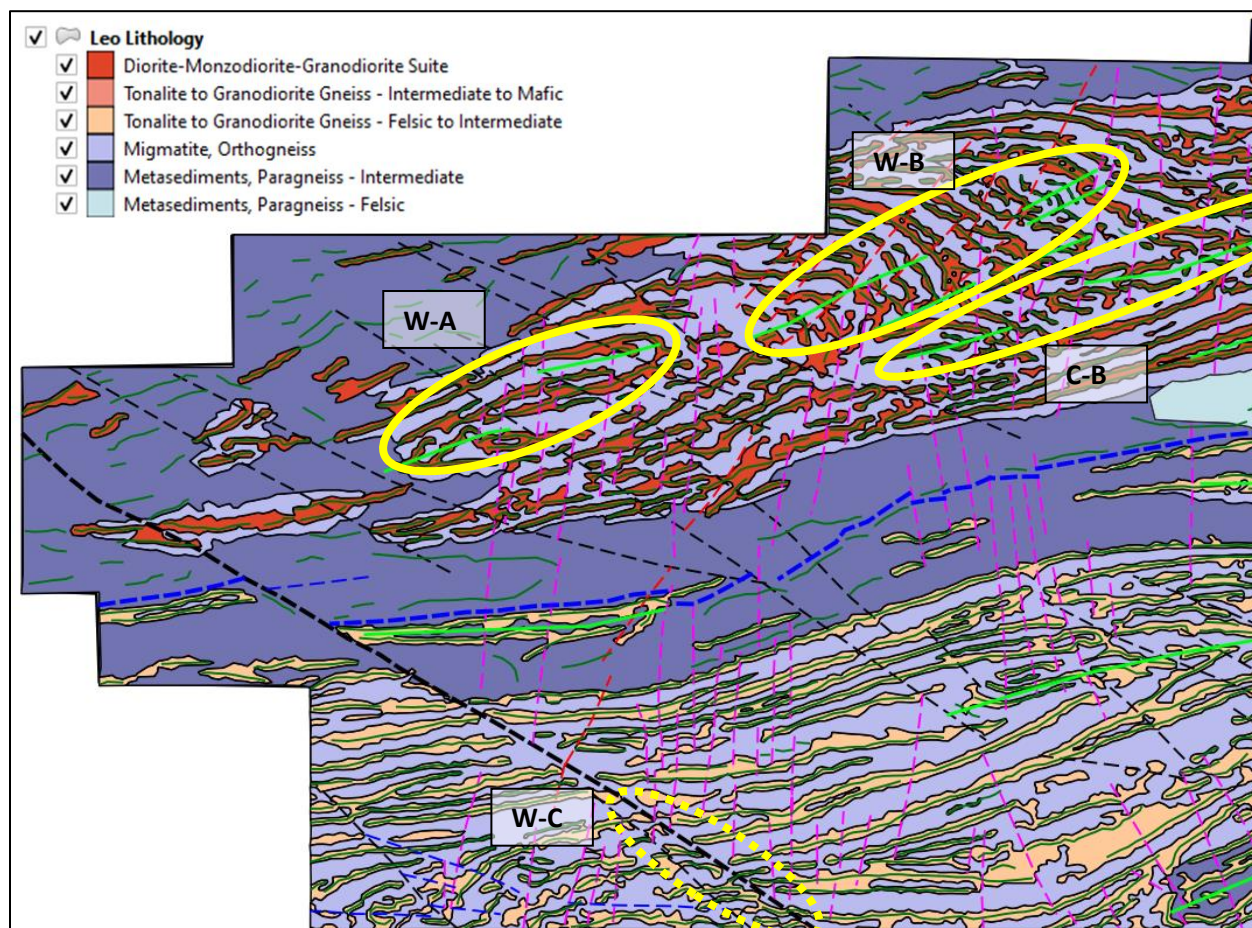


Figure 87. Recommended primary and secondary targets for follow-up for the Western Leo property.

Targets **W-A**, **W-B** and **C-B** all have about the same priority. Each target is centred along a fold axis or fold axes within the compressed diorite-monzodiorite-granodiorite suite north of the Sydney Lake fault zone. **C-B** continues into the central subset of the area.

Target **W-C** is a secondary target within the compressed tonalite to granodiorite gneiss (felsic to intermediate) south of the Sydney Lake fault zone. It lies along the southern portion of a major inferred Generation 3 fault with a dextral offset of 1.2 to 1.5 km. There is also a high concentration of Generation 1 faults intersecting the area. The southern portion of this fault overlaps the higher magnetic susceptible (Fe-rich) portion of the granodiorite.

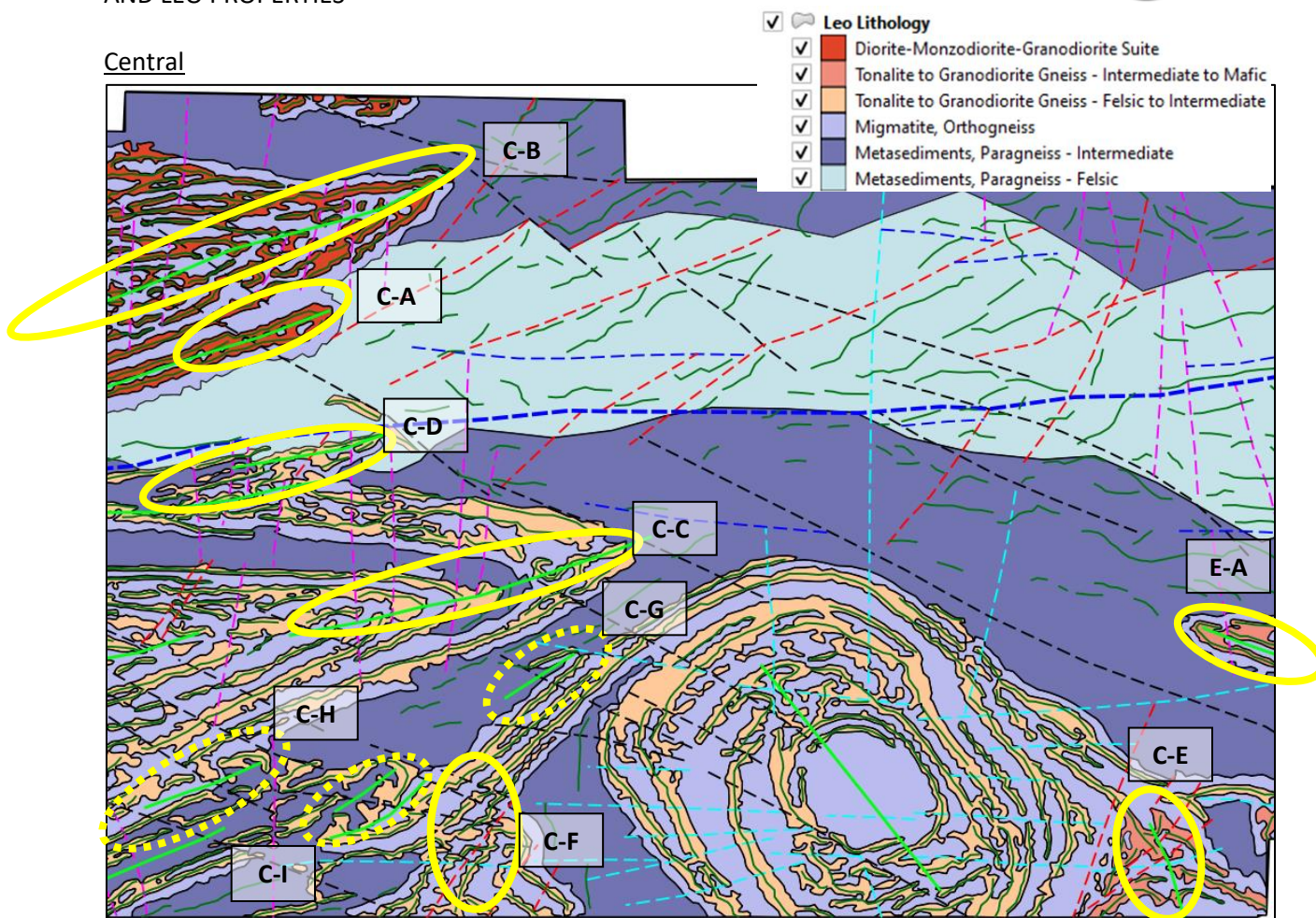


Figure 88. Recommended primary and secondary targets for follow-up for the Central Leo property.

Targets **C-A** and **C-B** are primary targets that are similar in character to that of **W-A**, **W-B** and **W-C**. Target **C-A** occurs along a very tight fold nose and very high magnetic susceptibility (Fe rich). Similarly, Targets **C-C** and **C-D** are at the fold axes of the tonalite to granodiorite gneiss (felsic to intermediate). Target **C-C** contains multiple fold nose locations while Target **C-D** contains two fold axes in opposite directions to one another. Both Targets **C-C** and **C-D** are intersected by numerous Generation 1 faults.

The uncompressed granodiorite intrusion in the centre of this area appears to have compressed the units to its east and west. Two target areas, Target **C-E** and **C-F** show complicated fold axes and orientations of the bands of magnetic material. Multiple fault orientations intersect the targets. Target **C-E** is in a higher magnetic susceptible version of the tonalite to granodiorite gneiss which has been interpreted to be more mafic to intermediate, which would make this a slightly higher priority target than **C-F**.

Multiple secondary targets were chosen in the intermediate space between the compressed tonalite to granodiorite gneiss (felsic to intermediate) in the western portion of the area and the uncompressed granodiorite intrusion in the centre of this area. Targets **C-G**, **C-H** and **C-I** host minor fold axes and multiple fault generations, but mostly Generation 3.

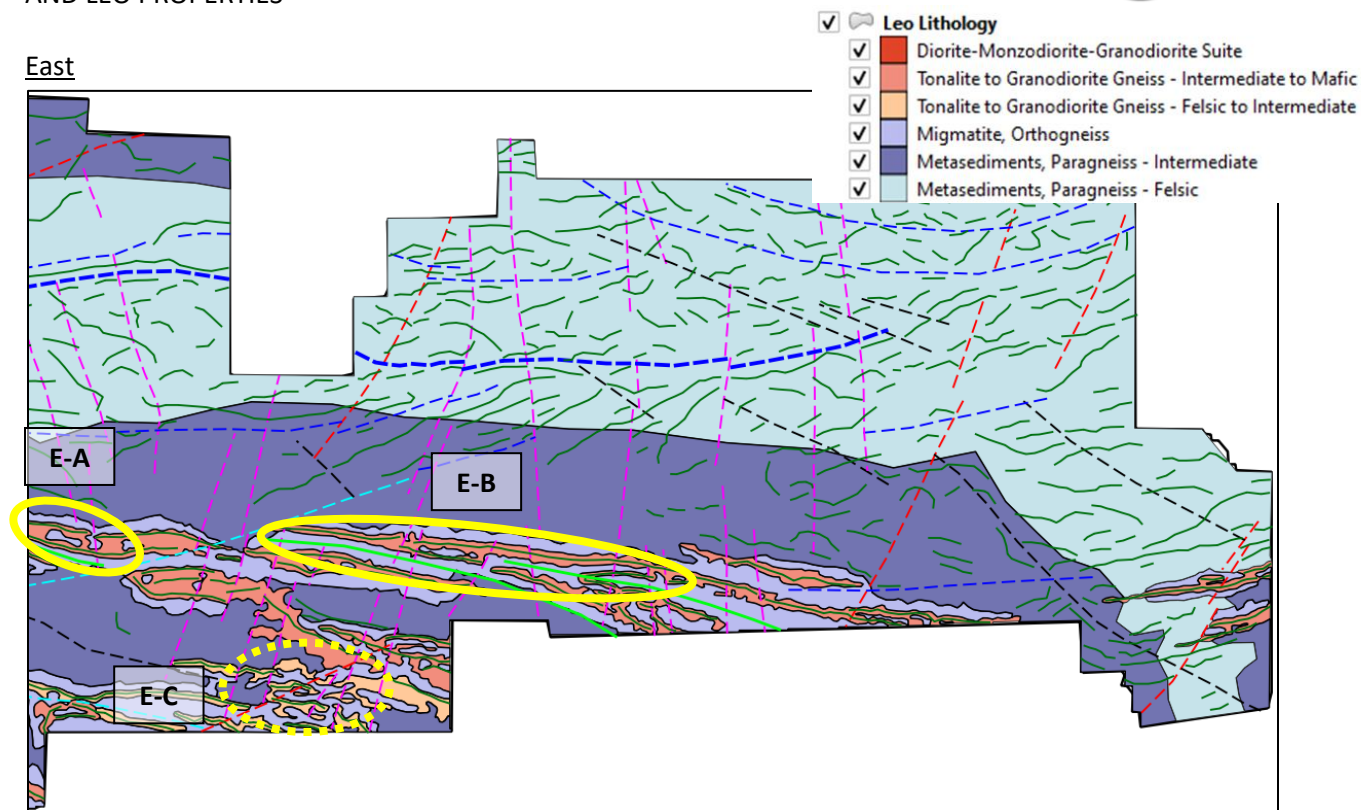


Figure 89. Recommended primary and secondary targets for follow-up for the Eastern Leo property.

The Eastern subset hosts a very tightly folded, highly magnetic susceptible unit interpreted to be a tonalite to granodiorite gneiss (mafic to intermediate). As with many of the previous primary targets in the western diorites, the targets lie along a fold axis with the nose fold. Target **E-A**'s western extent terminates at a very highly magnetic susceptible (Fe rich) fold nose. Target **E-B** lies along a longer portion of the granodiorite and has mineral potential along its length. In the eastern portion of the target area is a fold nose that would be a promising mineral host area. Target **E-C** is similar in style to that of Target **C-E** and **C-F**. That is, it is in a moderately magnetic terrain of complicated fold axes and orientations of the bands of magnetic material and crosscut by two to three generations of faults.

Sydney Lake

The Eagle-Sydney Lake geological map (P.1026, **Figure 90**)¹⁶ shows a number of mineral occurrences within the Sydney Lake property. The mineral indicators are pyrrhotite (po), pyrite (py), chalcopyrite (cp), arsenopyrite (asp), sphalerite (sp), molybdenite (mo), gold (au) and silver (ag). They are all associated with narrow bands of mafic metavolcanics. The Sydney Lake property is outlined in black.

A number of primary and secondary targets were selected for follow-up exploration. They are denoted by the solid and dashed ovals in **Figure 91**. Primary target areas **A**, **B** and **C** are located on the southern limb

¹⁶ Breaks, F. W., Bond, W. D., McWilliams, G. H., Gower, C. F., and Stone, Denver 1975 Operation Kenora-Sydney Lake, Eagle-Sydney Lakes Sheet, District of Kenora; Ontario Div. Mines, Prelim. Map P.1026 Geol. Ser., scale 1 inch to 1 mile or 1:63,360. Geology 1974.

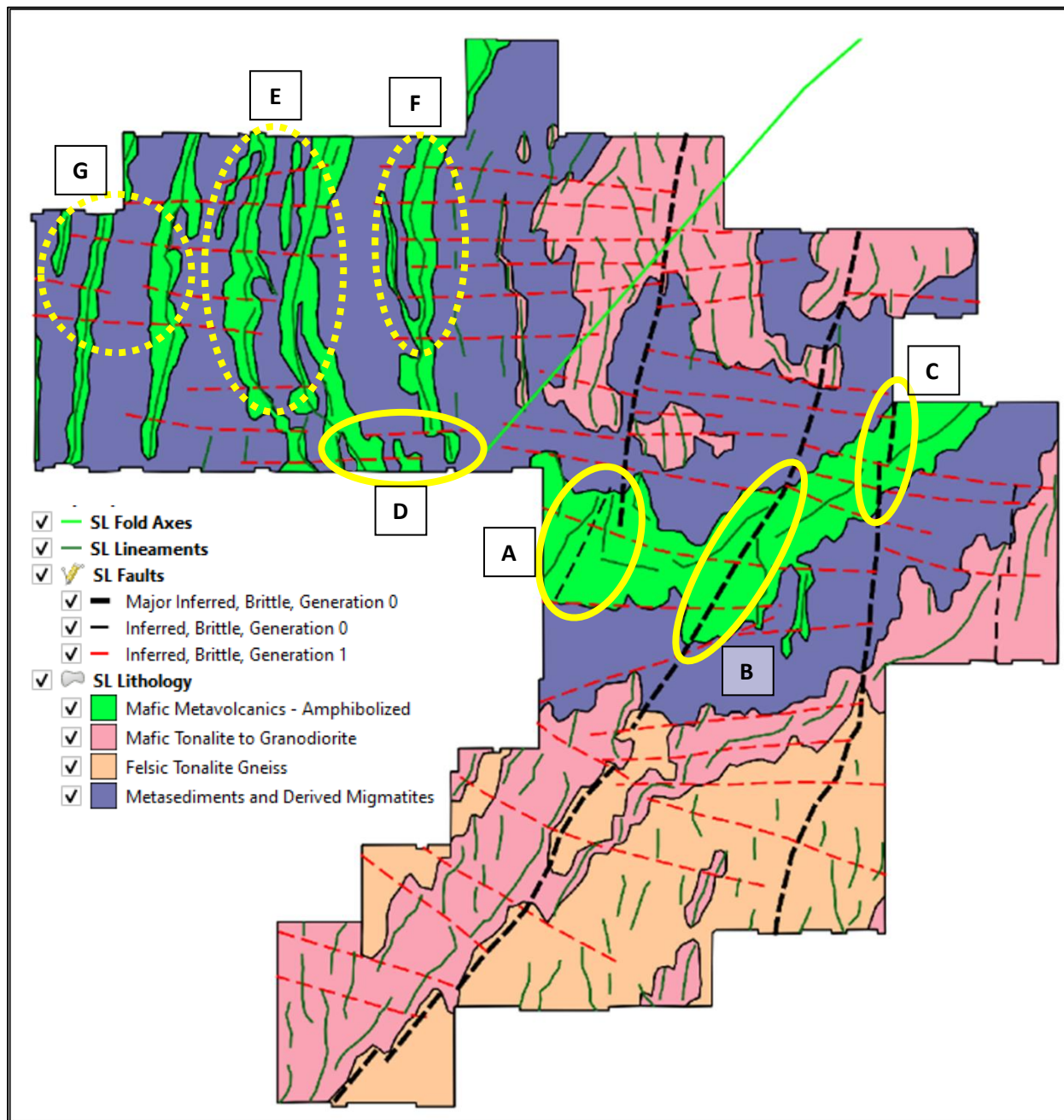


Figure 91. Recommended primary and secondary targets for follow-up for the Sydney Lake property.

Western Bear

The Medicine Stone Lake Area geological map (P.3397, **Figure 67**)¹⁷ does not report any mineral occurrences within or near the Western Bear property, however this map is from 1999.

¹⁷ Atkinson, B. T. 1999. Precambrian geology, Medicine Stone lake area; Ontario Geological Survey, Preliminary Map p.3397, scale 1:50 000.

A number of primary and secondary targets were selected for follow-up exploration. They are denoted by the solid and dashed ovals in **Figure 92**. Target **A** is the southwestern expression of the mafic to ultramafic intrusion. This portion of the intrusion was highlighted since the modelling indicates an outcrop or near surface exposure suitable for geological mapping and ground geophysics. The entire mafic to ultramafic intrusion should be further explored (Target **E**). This has been given a secondary status due to the large area covered by this target and that it is not a specific locale. Since this intrusion is located between two major faults showing a ductile or shearing character makes Targets **A**, **B** and **E** a good host for mineralized fluids. Within Target **E**, Target **B** has been designated as a primary target. This was chosen due to the multiple generations and concentrations of faults within the area despite the modelling indicating that the source is deeper than Target **A**. There is still a possibility of outcrop expressions in this target area. Targets **C** and **D** are associated with the major ductile/shear faults and mafic metavolcanics. Target **F** is also associated with mafic metavolcanics but also the Generation 3 faults that have a local S-type fold. It may be a good location for the deposition of mineralizing fluids. Target **G** and **H** were chosen as a secondary target since it covers some potential mineralized zones along the major ductile/shear and some Generation 3 faults that have a local S-type fold. The VOXI modelling indicates some magnetic susceptible material, i.e., mafics at depth, though it has not been interpreted as that in the current study.

Generally, the areas along the Generation 0 major ductile/shear faults warrant further exploration with a priority that diminishes with distance from the mafic to ultramafic intrusion. This would satisfy a number of the criteria listed above. By and large, Target **A** and its surrounding area, is the most promising.

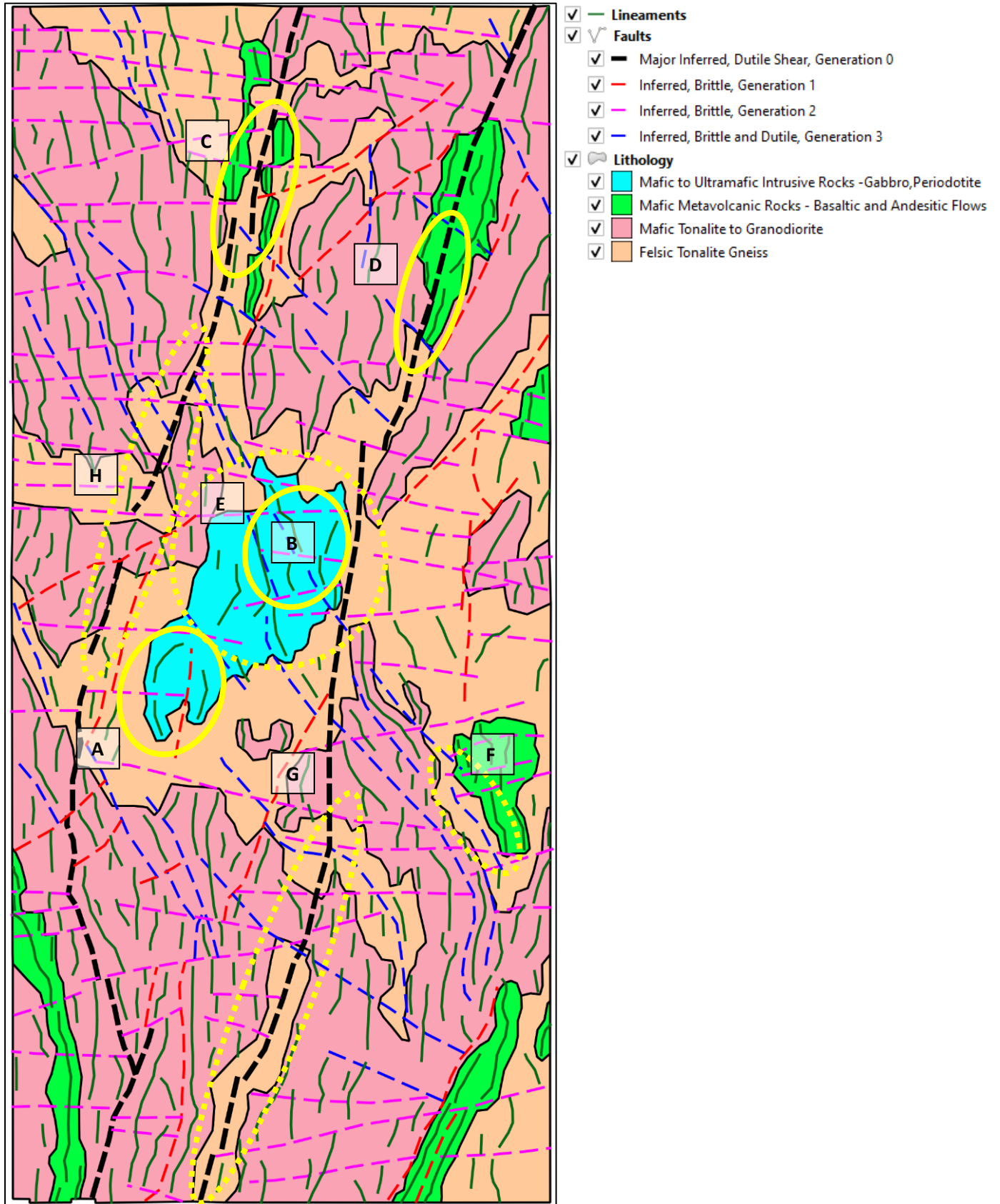


Figure 92. Recommended primary and secondary targets for follow-up for the Western Bear property.

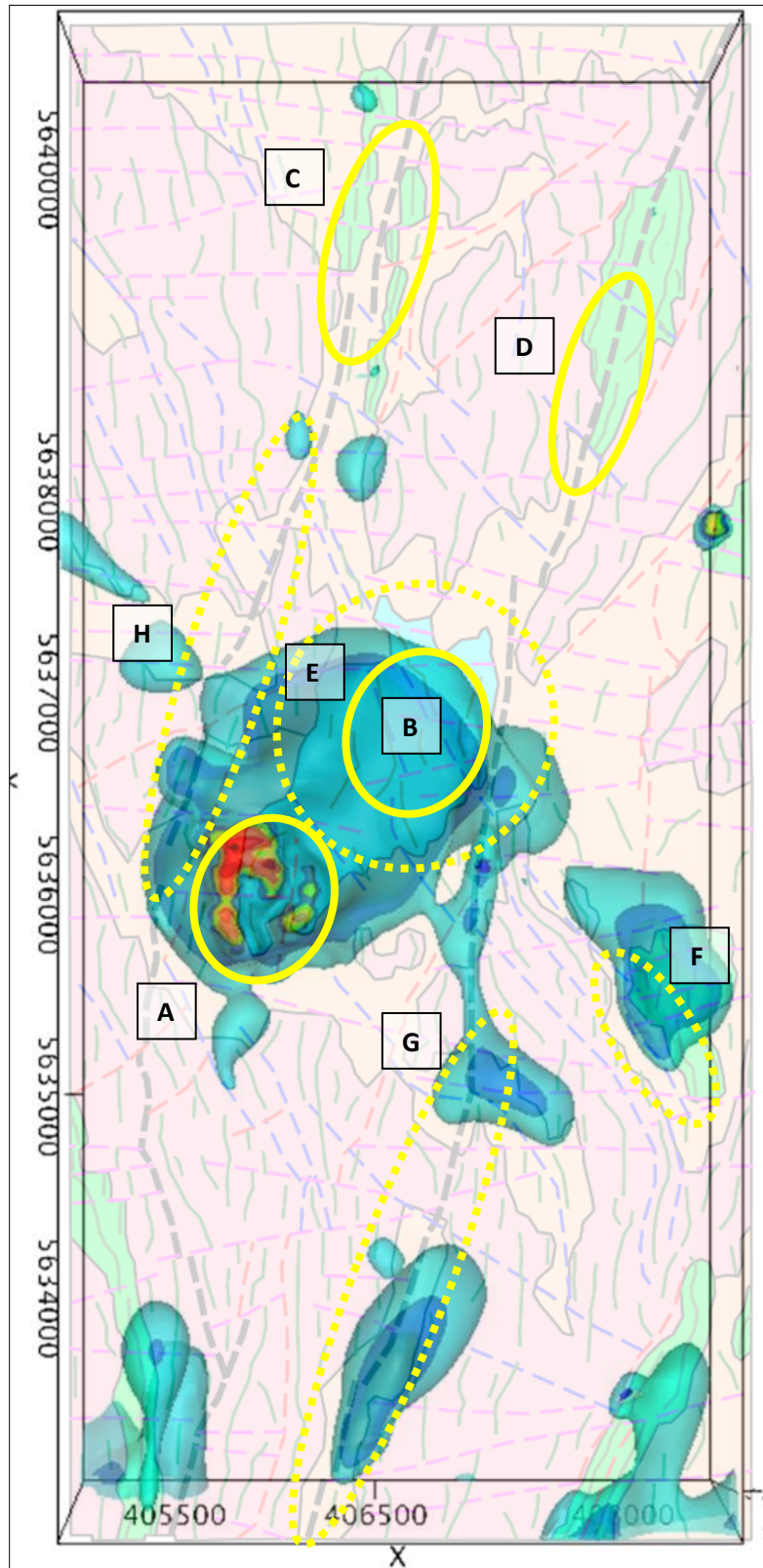


Figure 93. Recommended primary and secondary targets for follow-up for the Western Bear property with the VOXI modelling results.



Recommendations Summary

A number of target areas are recommended for ground follow-up. The central location of each target is listed below (WGS84/UTM15N) and are also provided as a ESRI shapefile in the accompanying QGIS interpretation project.

Primary Targets

Leo

W-A: 438599, 5613782
W-B: 442899, 5615317
C-A: 447346, 5614864
C-B: 447128, 5615792
C-C: 449990, 5612044
C-D: 447598, 5613290
C-E: 458153, 5609040
C-F: 450056, 5609105
E-A: 459409, 5611323
E-B: 465015, 5611127

Sydney Lake

A: 405822, 5620306
B: 406594, 5620183
C: 407380, 5620743
D: 404804, 5620770

Western Bear

A: 405976, 5636053
B: 406703, 5636878
C: 406449, 5638977
D: 407471, 5638318

Secondary Targets

Leo

W-C: 440682, 5608892
C-G: 450936, 5611017
C-H: 446603, 5609444
C-I: 449084, 5609619
E-C: 462480, 5609553

Sydney Lake

E: 404161, 5621618
F: 404947, 5621816
G: 403385, 5621637

Western Bear

E: 406571, 5636869
F: 407763, 5635345
G: 406561, 5634206
H: 405819, 5637192

Certificate of Qualification and Declaration

I, Edna Mueller-Markham, P.Geo., do hereby certify that:

1. I currently reside at 3315 – 81 Navy Wharf Court, Toronto, Ontario, M5V 3S2, Canada.
2. I am a graduate of the University of Toronto, Toronto, Ontario with a Bachelor of Science degree – Honours Physics, specialization in Geophysics, completed in 1988.
3. I am a graduate of McMaster University, Hamilton, Ontario with a Master of Science degree – Geology, completed in 1991.
4. I have worked as a geophysicist for a total of 24 years since my graduation, all of which has been with Paterson, Grant & Watson Limited.
5. I am currently Vice President and Senior Consulting Geophysicist for Paterson, Grant & Watson Limited.
6. I am a Practising Member in good standing with the Association of Professional Geoscientists of Ontario, (APGO member #2185).
7. I am responsible for all sections of the report “Geophysical Interpretation of Western Bear, Sydney Lake and Leo Properties” dated March 23, 2021.
8. I have no financial interests in Trillium Gold.

Dated this 23rd day of March 2021.



Edna Mueller-Markham, P.Geo.





Appendix A - Processing Details

Enhanced Derivative Grids

The final residual total magnetic intensity grid is RMI.grd.

Enhanced derivative grids derived from the microlevelled residual magnetic intensity were created using Geosoft Oasis montaj and Encom Discover PA software platforms. The following grids were created:

- Residual magnetic intensity reduced to the pole (RTP.grd)
- First vertical derivative of the pole reduced field (RTP1VD.grd)
- Second vertical derivative of the pole reduced field (RTP2VD.grd)
- Tilt derivative of the pole reduced field (TILT.grd)
- Horizontal gradient of the pole reduced field (RTP_HG.grd and TDX.grd)
- Analytic signal of the residual magnetic intensity (ASIG.grd)
- Depth to magnetic source using Source Parameter Imaging (SPI) (SPI_depth.grd)
- Area Filter – Encom special filter (RTP_ZS_Area.grd)
- Edge Filter – Encom special filter (RTP_ZS_Edge.grd)
- Digital elevation model from the airborne survey data (DTM.grd)

And databases of:

- Original survey database
- Source Edge Detection - a semi automated technique to detect edges
- SPI – database of derived depths to magnetic source

Each grid and database have the datum/projection of WGS84/UTM15N.

Reduction to the Magnetic Pole (RTP)

The direction (inclination and declination) of the geomagnetic field varies over the Earth and influences the shape of the magnetic responses over geological sources. At the North Magnetic Pole, the inducing magnetic field is vertical (i.e., inclination of 90° and declination of 0°), which results in the magnetic response being a symmetric positive magnetic peak over a source, in the absence of dip and magnetic remanence. Transforming the measured magnetic field to a pole reduced magnetic field simplifies the interpretation, particularly to determine the location and geometry of the sources (Baranov, 1957).¹⁸

The RTP filter, computed from the residual magnetic field after it is transformed to the Fourier domain, is defined as follows in equation 1 as:

$$L(\theta) = \frac{[\sin(I) - i \cdot \cos(I) \cdot \cos(D - \theta)]^2}{[\sin^2(I_a) + \cos^2(I_a) \cdot \cos^2(D - \theta)] \cdot [\sin^2(I) + \cos^2(I) \cdot \cos^2(D - \theta)]}$$

if ($|I_a| < |I|$), $I_a = I$ (equation 1)

¹⁸ Baranov, V. 1957. A new method for interpretation of aeromagnetic maps: pseudo-gravimetric anomalies. *Geophysics*, 22, 359-383.



where:

$L(\theta)$ = pole-reduced magnetic anomaly for wavenumber θ

I = geomagnetic inclination

I_a = inclination for amplitude correction (never less than I)

D = geomagnetic declination

i = imaginary number in the Fourier domain

Since the study area is fairly small, constant magnetic inclination and declination values of 75.6°N and 0.15°W, respectively, were used.

First Vertical Derivative of the Pole Reduced Field (1VD)

The vertical derivative is commonly applied to the RTP magnetic field grid in the Fourier domain to enhance shallower geologic sources in the data. This is particularly useful for locating contacts (e.g., the anomaly texture is revealed) and mapping structure (Telford et al., 1990).¹⁹ It is expressed in equation 2 as:

$$1VD = dRTP/dZ \quad (\text{equation 2})$$

where Z is the vertical offset.

Computing the vertical derivative enhances high frequency noise in the data which can produce ringing artefacts emanating from large amplitude, sharp magnetic anomalies. These effects were apparent in several places in the data and in order to eliminate it, a 40 m 8th order Butterworth filter was applied. This filter is equal to the length of four grid cells and was applied to all higher frequency magnetic grids.

Second Vertical Derivative of the Pole Reduced Field (2VD)

The second vertical derivative is commonly applied to the RTP magnetic field data in the Fourier domain to further enhance shallower geologic sources in the data. This is particularly useful for locating contacts (i.e., at the location of the zero contour) and mapping structure close to surface (Telford et al., 1990). It is expressed in equation 3 as:

$$2VD = d^2RTP/dZ^2 \quad (\text{equation 3})$$

where Z is the vertical offset.

Tilt Angle of the Pole Reduced Field

The tilt angle (Miller and Singh, 1994)²⁰ has been applied to the RTP magnetic field data to enhance the weaker magnetic signals in the dataset; it effectively applies an automatic gain control such that deep and shallow sources are resolved equally well. The tilt angle also transforms the magnetic data such that the tilt angle is positive over a magnetic source, passes through zero over or near the edge, and is negative outside of the body. These properties make the tilt angle particularly useful for mapping texture, structure, and edge contacts of weakly magnetic sources. It is expressed in equation 4 as:

¹⁹ Telford, W. M., Geldart, L. P., Sheriff, R. E. 1990. Applied Geophysics Second Edition. Cambridge University Press, 792 p.

²⁰ Miller, H.G. and Singh, V. 1994. Potential field tilt - a new concept for location of potential field sources, Journal of Applied Geophysics, 32, 213-217.



$$TILT = \tan^{-1} \left\{ \frac{\frac{dRTP}{dZ}}{\sqrt{\left[\frac{dRTP}{dX}\right]^2 + \left[\frac{dRTP}{dY}\right]^2}} \right\} \quad (\text{equation 4})$$

where X and Y are the horizontal offsets in the east and north directions.

The first vertical derivative is computed in the Fourier domain whereas the horizontal derivatives in the X and Y directions are computed in the space domain.

Horizontal Gradient Magnitude

The horizontal gradient magnitude of the total magnetic field reduced to the pole is applied to the magnetic dataset to aid in locating magnetic source body edges. The horizontal gradient magnitude will display a symmetric peak with maxima over the edge of a source body (Pilkington and Keating, 2000).²¹ An automated source edge detection routine is subsequently applied to the horizontal gradient magnitude to locate maxima's using the technique described by Blakley and Simpson (1986).²² The horizontal gradient magnitude is defined in equation 5 as:

$$HGRAD = \sqrt{\left[\frac{dRTP}{dX}\right]^2 + \left[\frac{dRTP}{dY}\right]^2} \quad (\text{equation 5})$$

The TDX is another version of the horizontal gradient that is sharper, especially in areas of high amplitude in the horizontal gradient. It is defined in equation 6 as:

$$TDX = \tan^{-1} \left\{ \frac{\sqrt{\left[\frac{dRTP}{dX}\right]^2 + \left[\frac{dRTP}{dY}\right]^2}}{\frac{dRTP}{dZ}} \right\} \quad (\text{equation 6})$$

Analytic Signal Amplitude

The amplitude of the analytic signal (AS) is the square root of the sum of the squares of the derivatives in the horizontal (X and Y) and vertical (Z) directions (i.e., the Fourier domain first vertical derivative and the space domain horizontal derivatives in X and Y), computed from the total magnetic field (Nabighian, 1972)²³ in equation 7 as:

$$AS = \sqrt{\left(\left[\frac{dT}{dX}\right]^2 + \left[\frac{dT}{dY}\right]^2 + \left[\frac{dT}{dZ}\right]^2\right)} \quad (\text{equation 7})$$

The analytic signal is useful in locating the edges of magnetic source bodies, particularly where magnetic remanence complicates interpretation. It is especially useful to interpret the contacts of intrusions.

²¹ Pilkington M. and Keating P. 2004. Contact mapping from gridded magnetic data? A comparison of techniques. *Exploration Geophysics* 35, 306–311.

²² Blakely, R.J., and Simpson, R.W., 1986, Approximating edges of source bodies from magnetic or gravity anomalies, *Geophysics*, v. 51, p. 1494-1498.

²³ Nabighian, M.N. 1972. The analytic signal of two-dimensional magnetic bodies with polygonal cross-section: Its properties and use for automated anomaly interpretation. *Geophysics*, 37, 507-517.



Source Parameter Imaging (SPI)

The SPI method locates the depths of edges in the gridded magnetic data (Thurston and Smith, 1997).²⁴ It assumes a 2D sloping contact or 2D dipping thin sheet model for the magnetic sources. The SPI values calculated are depths between the magnetic source and the instrument height and therefore the altitude above ground must be subtracted from the SPI value to result in a depth below surface. If the value of the depth to source is <0 , i.e., above ground, it has been set to zero. The grid was created using a minimum curvature gridding algorithm with a grid cell size of 10 m.

Source Edge Detection

The semi-automated extraction of magnetic anomaly peaks, troughs and edges is useful for delineating structure, foliation, texture and contacts. Anomaly peaks typically trace the center of a source or the more magnetic horizons within a larger source. Anomaly troughs often complement the peaks, indicating a less magnetic horizon. They also may map a remanent (i.e., reversely) magnetized source, or magnetite depletions (e.g., along a fault) which are a less magnetic source in a more magnetic host rock. Anomaly edges mark geological contacts or the boundaries of horizons within a geological unit. Offsets and orientation changes in the peaks, troughs and edges are useful for mapping faults and shears. Detection for peaks, troughs and edges was performed based on the Source Edge Detection extension in Geosoft Oasis montaj.

The process (based upon Blakely and Simpson, 1986) uses the pole reduced field and its horizontal gradient to find localised peaks in the grid. For each grid cell to be considered, the method compares its value with the eight surrounding grid cells in four directions (x-direction, y-direction, and both diagonals). There are four levels to determine whether a grid cell can be selected as a peak:

- 'all 4 directions': grid values in all adjacent grid cells are lower (i.e., a peak)
- '3/4 directions': grid values in three directions are lower
- '2/4 directions': grid values in two directions are lower (i.e., a ridge)
- '1/4 direction': grid values in any one direction are lower

The symbol plotted shows the strike direction of the edge (contact) by the direction of the long axis, and the 'down-gradient' direction by the dip indicator. When plotted over the original grid, these symbols trace the geological contacts. When plotted over the total horizontal gradient grid, these symbols trace the local peaks. The 'down-gradient' direction points away from the source which is locally more magnetized.

Encom Special Filters – Area and Edge

Encom's Discover PA software has a number of special filters used to enhance the edges of magnetic sources and to classify or zone areas that are similar in character. The method and results are described

²⁴ Thurston, J.B. and Smith, R.S., 1997. Automatic conversion of magnetic data to depth, dip, and susceptibility contrast using the SPI™ method. *Geophysics*, 62(3), pp.807-813.



in the paper by Shi and Butt (2004).²⁵ A copy of the paper is included in [Appendix B](#). The Edge filter is sharper than most edge detection filters or methods. As well, the Edge filter produces “edges that migrate down-dip towards the deepest edge of the source. This effect produces anomaly asymmetry that can assist interpretation of dip,” (Shi and Butt, 2004). Once edges have been defined the areas in between may be classified using a number of Block filters developed by Encom. The Area filter was found to be the most useful in discriminating between different lithological units. The other Encom special filtered grids (Block, Plateau, Modulus and EdgeZone) were also included in the deliverables, but not used in the interpretation.

Digital Elevation Model

The Digital Elevation Model was downloaded from the Geosoft Public DAP server (<http://dap.geosoft.com>) for the survey area with a grid cell size of 30 m. The DEM grid was sampled from the worldwide SRTM (Shuttle Radar Topographic Mission) DEM. A Digital Elevation Model was also calculated from the survey data using a minimum curvature algorithm with a grid cell size of 10 m.

VOXI Modelling

The directory of the VOXI modelling folder contains the 3D View (Madsen_Modelling_V2.geosoft_3dv) and other relevant files for various areas within the survey. The 3D views contain the surface terrain and measured residual magnetic intensity grids and a 3D voxel of the magnetic susceptibility derived from the Magnetic Vector Intensity (MVI) (IRI2_Ampl.geosoft_voxel) and isosurfaces of the magnetic susceptibility (IRI2_Ampl.geosoft_surface). There are also input grids of the digital elevation model and measured magnetic intensity.

²⁵Shi, A. and Butt, G., 2004, New enhancement filters for geological mapping. Extended Abstracts, ASEG 17th Geophysical Conference and Exhibition, Sydney 2004.



Appendix B – Selected Papers

Iwahashi, J. and Pike, R.J., 2007. Automated classifications of topography from DEMs by an unsupervised nested-means algorithm and a three-part geometric signature. *Geomorphology*, 86(3-4), pp.409-440.

MacLeod, I. and Ellis, R. (2013) Magnetic Vector Inversion, a simple approach to the challenge of varying direction of rock magnetization. 23rd International Geophysical Conference and Exhibition, 11-14 August 2013 - Melbourne, Australia

MacLeod, I. and Ellis, R. (2015) Quantitative Magnetization Vector Inversion. Extended Abstracts of the 14th SAGA Biennial Technical Meeting and Exhibition 2015.

Shi, Z. and Butt, G., (2004) New enhancement filters for geological mapping. ASEG 17th Geophysical Conference Exhibition, Sydney, Australia, Extended Abstracts.

Western Bear 2020 AMAG Survey - Total Costs

Costs associated with 2020 Airborne Magnetometer Survey on Western Bear property

<u>Inv #</u>	<u>Inv ref</u>	<u>Inv Amt</u>	<u>Pro rata</u>	<u>Applicable cost</u>	<u>Inv date</u>	<u>Inv company</u>	<u>Details</u>
1	2068	\$ 13,746.00	100%	\$ 13,746.00	7-Oct-20	Precision GeoSurveys Inc.	237 km (2140 ha) areomagnetic survey
1	2068	\$ 4,000.00	50%	\$ 2,000.00	7-Oct-20	Precision GeoSurveys Inc.	50% of mob, calibration and logistics report fee
			Total	<u>\$ 15,746.00</u>			
2	P9574EMM	\$ 25,000.00	20%	\$ 5,000.00	25-Mar-21	Paterson, Grant & Watson Limited	Interpretation report for Precision aeromagnetic survey (Job 2020-09) portion applicable to Western Bear
3	20.12.21	\$ 2,190.00	100%	\$ 2,190.00	20-Dec-21	Assessment report	TGM Geologist 3.5 days @ \$600/day
4			Total	<u>\$ 7,190.00</u>			
5			Total cost	\$ 22,936.00			

Pro Rata Calculations - Western Bear 2020 AMAG

Trillium Gold Mines Inc.
2022 Assessment Filing

Total area 2,139.90
Total costs \$ 22,936.00

Pro-rated total
\$22,936

* Pro rata factor calculated as proportion of area on each claim of the total area flown in AMAG survey

Claims surveyed	Property	Area (ha)	Pro rata factor	Pro-rata cost for AMAG	Rounded for entry
560628	Western Bear	20.368	0.95%	218.31	218
560629	Western Bear	20.367	0.95%	218.30	218
560630	Western Bear	20.367	0.95%	218.30	218
560631	Western Bear	20.367	0.95%	218.30	218
560632	Western Bear	20.367	0.95%	218.30	218
560633	Western Bear	20.367	0.95%	218.30	218
560634	Western Bear	20.367	0.95%	218.30	218
560635	Western Bear	20.369	0.95%	218.32	218
560636	Western Bear	20.369	0.95%	218.32	218
560637	Western Bear	20.369	0.95%	218.32	218
560638	Western Bear	20.369	0.95%	218.32	218
560639	Western Bear	20.369	0.95%	218.32	218
560640	Western Bear	20.369	0.95%	218.32	218
560641	Western Bear	20.369	0.95%	218.32	218
560642	Western Bear	20.371	0.95%	218.34	218
560643	Western Bear	20.371	0.95%	218.34	218
560644	Western Bear	20.371	0.95%	218.34	218
560645	Western Bear	20.371	0.95%	218.34	218
560646	Western Bear	20.371	0.95%	218.34	218
560647	Western Bear	20.371	0.95%	218.34	218
560648	Western Bear	20.371	0.95%	218.34	218
560649	Western Bear	20.373	0.95%	218.36	218
560650	Western Bear	20.373	0.95%	218.36	218
560651	Western Bear	20.373	0.95%	218.36	218
560652	Western Bear	20.373	0.95%	218.36	218
560653	Western Bear	20.373	0.95%	218.36	218
560654	Western Bear	20.373	0.95%	218.36	218
560655	Western Bear	20.373	0.95%	218.36	218
560656	Western Bear	20.375	0.95%	218.38	218
560657	Western Bear	20.375	0.95%	218.38	218
560658	Western Bear	20.375	0.95%	218.38	218
560659	Western Bear	20.375	0.95%	218.38	218
560660	Western Bear	20.375	0.95%	218.38	218
560661	Western Bear	20.375	0.95%	218.38	218
560662	Western Bear	20.375	0.95%	218.38	218
560663	Western Bear	20.377	0.95%	218.41	218
560664	Western Bear	20.376	0.95%	218.39	218
560665	Western Bear	20.376	0.95%	218.39	218
560666	Western Bear	20.376	0.95%	218.39	218
560667	Western Bear	20.376	0.95%	218.39	218
560668	Western Bear	20.376	0.95%	218.39	218
560669	Western Bear	20.376	0.95%	218.39	218
560670	Western Bear	20.378	0.95%	218.42	218

Pro Rata Calculations - Western Bear 2020 AMAG

Trillium Gold Mines Inc.
2022 Assessment Filing

Claims surveyed	Property	Area (ha)	Pro rata factor	Pro-rata cost for AMAG	Rounded for entry
560671	Western Bear	20.378	0.95%	218.42	218
560672	Western Bear	20.378	0.95%	218.42	218
560673	Western Bear	20.378	0.95%	218.42	218
560674	Western Bear	20.378	0.95%	218.42	218
560675	Western Bear	20.378	0.95%	218.42	218
560676	Western Bear	20.378	0.95%	218.42	218
560677	Western Bear	20.38	0.95%	218.44	218
560678	Western Bear	20.38	0.95%	218.44	218
560679	Western Bear	20.38	0.95%	218.44	218
560680	Western Bear	20.38	0.95%	218.44	218
560681	Western Bear	20.38	0.95%	218.44	218
560682	Western Bear	20.38	0.95%	218.44	218
560683	Western Bear	20.38	0.95%	218.44	218
560684	Western Bear	20.382	0.95%	218.46	218
560685	Western Bear	20.382	0.95%	218.46	218
560686	Western Bear	20.382	0.95%	218.46	218
560687	Western Bear	20.382	0.95%	218.46	219
560688	Western Bear	20.382	0.95%	218.46	219
560689	Western Bear	20.382	0.95%	218.46	219
560690	Western Bear	20.382	0.95%	218.46	219
560691	Western Bear	20.384	0.95%	218.48	219
560692	Western Bear	20.384	0.95%	218.48	219
560693	Western Bear	20.384	0.95%	218.48	219
560694	Western Bear	20.384	0.95%	218.48	219
560695	Western Bear	20.384	0.95%	218.48	219
560696	Western Bear	20.384	0.95%	218.48	219
560697	Western Bear	20.384	0.95%	218.48	219
560698	Western Bear	20.386	0.95%	218.50	219
560699	Western Bear	20.386	0.95%	218.50	219
560700	Western Bear	20.385	0.95%	218.49	219
560701	Western Bear	20.385	0.95%	218.49	219
560702	Western Bear	20.385	0.95%	218.49	219
560703	Western Bear	20.385	0.95%	218.49	219
560704	Western Bear	20.385	0.95%	218.49	219
560705	Western Bear	20.387	0.95%	218.51	219
560706	Western Bear	20.387	0.95%	218.51	219
560707	Western Bear	20.387	0.95%	218.51	219
560708	Western Bear	20.387	0.95%	218.51	219
560709	Western Bear	20.387	0.95%	218.51	219
560710	Western Bear	20.387	0.95%	218.51	219
560711	Western Bear	20.387	0.95%	218.51	219
560712	Western Bear	20.389	0.95%	218.53	219
560713	Western Bear	20.389	0.95%	218.53	219
560714	Western Bear	20.389	0.95%	218.53	219
560715	Western Bear	20.389	0.95%	218.53	219
560716	Western Bear	20.389	0.95%	218.53	219
560717	Western Bear	20.389	0.95%	218.53	219

Pro Rata Calculations - Western Bear 2020 AMAG

Trillium Gold Mines Inc.
2022 Assessment Filing

Claims surveyed	Property	Area (ha)	Pro rata factor	Pro-rata cost for AMAG	Rounded for entry
560718	Western Bear	20.389	0.95%	218.53	219
560719	Western Bear	20.391	0.95%	218.56	219
560720	Western Bear	20.391	0.95%	218.56	219
560721	Western Bear	20.391	0.95%	218.56	219
560722	Western Bear	20.391	0.95%	218.56	219
560723	Western Bear	20.391	0.95%	218.56	219
560724	Western Bear	20.391	0.95%	218.56	219
560725	Western Bear	20.391	0.95%	218.56	219
560726	Western Bear	20.393	0.95%	218.58	219
560727	Western Bear	20.393	0.95%	218.58	219
560728	Western Bear	20.393	0.95%	218.58	219
560729	Western Bear	20.393	0.95%	218.58	219
560730	Western Bear	20.393	0.95%	218.58	219
560731	Western Bear	20.393	0.95%	218.58	219
560732	Western Bear	20.392	0.95%	218.57	219